The George W. Woodruff School of Mechanical Engineering

Georgia Institute of Technology

Atlanta, Georgia 30332

DOCUMENTATION REPORT

FOR

KSTAB

A Computer Program to Analyze the Dynamic Stability Characteristics of Conventionally Configured Subsonic Airplanes

Prepared for

National Aeronautics and Space Administration
Langley Research Center
Hampton, Virginia 23665

by

Kohlman Aviation Corporation
2721 W. 6th Street
Lawrence, Kansas 66044

Contract No. NAS1-16695

February 1982

TABLE OF CONTENTS

CHAPTERS		PAGE
	List of Symbols	v
	List of Figures	xv
	List of Tables	xxi
1.	INTRODUCTION	1.1
	1.1 References	1.2
2.	GENERAL INFORMATION AND EXECUTIVE PROGRAM	2.1
	2.1 General Information	2.1
	2.1.1 Major Changes	2.2
	2.1.2 Input Logic	2.3
	2.2 Executive Routine	2.3
	2.2.1 Executive Program Flowchart	2.4
	2.2.2 Executive Program Listing	2.4
3.	TRIM	3.1
	3.1 Introduction	3.1
	3.2 Trim Equations	3.1
	3.3 Program Description	3.4
4.	GROUND EFFECTS	4.1
	4.1 Introduction	4.1
	4.2 Derivation of Equations	4.1
	4.3 References	4.6
5.	POWER EFFECTS	5.1
	5.1 Introduction	5.1
	5.2.1 Derivation of Equations, Effects on Lift, Propeller Engine	5.1
	5.2.1.1 Effects of Propeller Forces	5.3
	5.2.1.2 Effect of Propeller Slipstream, Increase in Dynamic Pressure	5.9
	5.2.1.3 Effect of Propeller Slipstream, Propeller Downwash ε_p	5.13
	5.2.2.1 Pitching Moment Due to Thrust Offset	5.21
	5.2.2.2 Pitching Moment Due to Propeller Normal Force	5.21
	5.2.2.3 The Zero Lift Pitching Increment	5.22
	5.2.2.4 Pitching Moment Increment Due to Change in Wing Lift	5.23
	5.2.2.5 Pitching Moment Due to Effect of Slipstream on Nacelle	5.24
	5.2.2.6 Pitching Moment Due to Effect of Power on Tail	5.27
	5.2.3 Derivation of Equations, Effect on Lateral-Directional Derivatives, Propeller Engine	5.27

CHAPTERS PAGE

5.2.4 Effect of Power on Speed-Derivatives. 5.29
5.3 Derivation of Equations, Effects of Power, Jet Engine. 5.29
5.3.1 Effect of Jet Engine Thrust on Stability Derivatives. 5.30
5.3.1.1 Effect on Lift. 5.30
5.3.1.2 Effect on Pitching Moment Coefficient C_{m_α} 5.30
5.3.1.3 Effect on C_{L_o} and C_{m_o} 5.31
5.3.1.4 Effect on Speed Derivatives, $C_{M_{T_u}}$ and $C_{T_{X_u}}$ 5.31
5.3.1.5 Effect on Lateral Directional Derivatives. 5.32
5.4 Description of Program. 5.32
5.5 References. 5.33

6. STATIC LONGITUDINAL STABILITY. 6.1
6.1 Introduction. 6.1
6.2 Derivation of Equations. 6.1
6.3 Function "ACEM". 6.7
6.4 Subroutine "MULTOP". 6.8
6.5 Subroutine "CONSHP". 6.9
6.6 References. 6.10

7. DIRECTIONAL STABILITY. 7.1
7.1 Introduction. 7.1
7.2 Discussion of Design Criteria. 7.1
7.3 References. 7.2

8. VMC ROUTINE. 8.1
8.1 Introduction. 8.1
8.2 Single-Degree-of-Freedom Approximation. 8.1
8.3 Three-Degree-of-Freedom Method. 8.2
8.4 References. 8.5

9. ROTATION SPEED. 9.1
9.1 Introduction. 9.1
9.2 Derivation of Equations. 9.1
9.2.1 Rotation Phase. 9.2
9.2.2 Airborne Phase. 9.3
9.3 References. 9.6

10. INERTIA ROUTINE. 10.1
10.1 Introduction. 10.1
10.2 Discussion of Method. 10.2
10.3 Check Calculations. 10.18
10.4 Program Description. 10.21
10.5 References. 10.39

CHAPTERS PAGE

11. 11.1 Variation of Drag Coefficient with Angle of Attack, C_{D_α} 11.1.1

11.2 Lift-Curve Slope. 11.2.1

11.3 Downwash Behind the Wing. 11.3.1

11.4 Variation of Pitching Moment With Angle of Attack, C_{m_α} 11.4.1

11.5 Variation of Drag Coefficient With Forward Speed, C_{D_U} 11.4.1

11.6 C_{L_u}, Variation of Lift Coefficient With Speed Perturbations. 11.6.1

11.7 C_{m_u}; Variation of Pitching Moment Coefficient Due to Speed Perturbations, C_{m_u} 11.7.1

11.8 C_{D_q}, Variation of Drag Coefficient With Pitch Rate. . 11.8.1

11.9 C_{L_q}, Variation of Lift Coefficient With Pitch Rate. . 11.9.1

11.10 C_{m_q}, Variation of Pitching Moment Coefficient With Pitch Rate. 11.10.1

11.11 $C_{D_{\dot{\alpha}}}$, Variation of Drag Coefficient With Angle of Attack Rate. 11.11.1

11.12 $C_{L_{\dot{\alpha}}}$, Variation of Lift Coefficient With Angle of Attack Rate. 11.12.1

11.13 $C_{m_{\dot{\alpha}}}$, Variation of Pitching Moment Coefficient With Angle of Attack Rates. 11.13.1

11.14 Variation of Side Force Coefficient With Sideslip Angle, C_{Y_β} 11.14.1

11.15 C_{ℓ_β}, Variation of Rolling Moment Coefficient With Sideslip Angle. 11.15.1

11.16 Variation of Yawing Moment Coefficient With Sideslip Angle C_{n_β} 11.16.1

11.17 C_{y_p}, Variation of Side Force Due to Roll Rate Perturbations. 11.17.1

11.18 C_{ℓ_p}, Variation of Rolling Moment Coefficient With Roll Rate. 11.18.1

11.19 C_{n_p}; Variation of Yawing Moment Coefficient With Roll Rate. 11.19.1

11.20 Variation of Side Force Coefficient With Yaw Rate, C_{y_r} 11.20.1

11.21 Subroutine "CLARE" (CLR), Variation of Rolling Moment With Yaw Rate. 11.21.1

11.22 Variation of Yawing Moment Coefficient With Yaw Rate, C_{n_r} 11.22.1

11.23 Longitudinal Control Derivatives. 11.23.1

CHAPTERS PAGE

11.24 Aileron Stability Derivatives $C_{\ell_{\delta_A}}$, $C_{n_{\delta_A}}$, $C_{y_{\delta_A}}$ . . . 11.24.1

11.25 Directional Control Derivatives $C_{y_{\delta_R}}$, $C_{\ell_{\delta_R}}$ and $C_{n_{\delta_R}}$ 11.25.1

11.26 Hinge Moments of Control Surfaces C_{h_α}, C_{h_δ} 11.26.1

11.27 C_{L_o}, C_{m_o} Lift and Pitching Moment Coefficients at $\alpha = i_H = \delta_E = 0$. 11.27.1

12. DYNAMIC STABILITY ROUTINE. 12.1

13. INPUT ROUTINE. 13.1

14. SUMMARY. 14.1

APPENDICES

A. Comparison of Methods for Computation of Ground Effect

B. Function RDP - A Function Sub-Program For Interpolating Curves and Graphs

C. Data For Test-Airplanes

D. Derivation of Correction For the Polhamus Formula

LIST OF SYMBOLS

SYMBOL	DEFINITION	DIMENSION
A_i	Aspect ratio defined in Eqn. (5.3)	
a.c.	Aerodynamic Center	
AR , A	Aspect ratio	
b	Span	ft
B	Compressibility correction factor	
b_c	Distance defined in Fig. 5.3.b	ft
b_{i_e}	Distance defined in Fig. 5.3.b (single engine) or Fig. 5.3.c (twin engine)	ft
B_L	Number of propeller blades	
c	Chord	ft
$\bar{c}$	Mean aerodynamic chord	ft
C_D	Drag coefficient	
$C_{D_\alpha} = \frac{\partial C_D}{\partial \alpha}$	Variation of drag coefficient with angle of attack	rad^{-1}
$C_{D_u} = \frac{\partial C_D}{\partial u/U_1}$	Variation of drag coefficient with speed	
$C_{D_{\dot{\alpha}}} = \frac{\partial C_D}{\partial \frac{\dot{\alpha}\bar{c}}{2U_1}}$	Variation of drag coefficient with rate of change of angle of attack	rad^{-1}
$C_{D_q} = \frac{\partial C_D}{\partial \frac{q\bar{c}}{2U_1}}$	Variation of drag coefficient with pitch rate	rad^{-1}
c.g.	Center of Gravity	
$\bar{c}_i$	Distance defined in Fig. 5.3.b (single engine) or in Fig. 5.3.c (twin engine)	ft
C_ℓ	Section lift coefficient	
$C_L = \frac{L}{\bar{q}S}$	Lift coefficient	
$C_{L_\alpha} = \frac{\partial C_L}{\partial \alpha}$	Lift curve slope	rad^{-1}

SYMBOL	DEFINITION	DIMENSION
$C_{\ell_\alpha} = \frac{\partial C_\ell}{\partial \alpha}$	Section lift curve slope	rad^{-1}
C_{L_0}	Lift coefficient at zero angle of attack	
$C_{L_{i_H}} = \frac{\partial C_L}{\partial i_H}$	Nondimensional variation of lift coefficient with stabilizer angle of incidence	rad^{-1}
$C_{L_{\delta_E}} = \frac{\partial C_L}{\partial \delta_E}$	Variation of lift coefficient with elevator deflection	rad^{-1}
$C_{L_u} = \frac{\partial C_D}{\partial u/U_1}$	Variation of lift coefficient with speed	
$C_{L_q} = \frac{\partial C_L}{\partial \frac{q\bar{c}}{2U_1}}$	Variation of lift coefficient with pitch rate	rad^{-1}
$C_{L_{\dot{\alpha}}} = \frac{\partial C_D}{\partial \frac{\dot{\alpha}\bar{c}}{2U_1}}$	Variation of lift coefficient with rate of change of angle of attack	rad^{-1}
$C_{L_{\delta_F}} = \frac{\partial C_L}{\partial \delta_F}$	Variation of lift coefficient with flap deflection angle	rad^{-1}
$C_{L_{\delta_E}} = \frac{\partial C_L}{\partial \delta_E}$	Variation of lift coefficient with elevator deflection angle	rad^{-1}
$C_{L_{i_H}} = \frac{\partial C_L}{\partial i_H}$	Variation of lift coefficient with stabilizer incidence angle	rad^{-1}
$C_{\ell_{\delta_A}} = \frac{\partial C_\ell}{\partial \delta_A}$	Variation of rolling moment coefficient with aileron angle	rad^{-1}
$C_{\ell_{\delta_R}} = \frac{\partial C_\ell}{\partial \delta_R}$	Variation of rolling moment coefficient with rudder angle	rad^{-1}

SYMBOL	DEFINITION	DIMENSION
$C_{\ell_r} = \frac{\partial C_\ell}{\partial \frac{rb}{2U_1}}$	Variation of rolling moment coefficient with yaw rate	rad^{-1}
$C_{\ell_\beta} = \frac{\partial C_\ell}{\partial \beta}$	Variation of rolling moment coefficient with sideslip angle	rad^{-1}
$C_{\ell_p} = \frac{\partial C_\ell}{\partial \frac{pb}{2U_1}}$	Variation of rolling moment coefficient with roll rate	rad^{-1}
C_m	Pitching moment coefficient	
$C_{m_\alpha} = \frac{\partial C_m}{\partial \alpha}$	Variation of pitching moment coefficient with angle of attack	rad^{-1}
C_{m_o}	Pitching moment coefficient at zero angle of attack	
$C_{m_{\delta_E}} = \frac{\partial C_m}{\partial \delta_E}$	Variation of pitching moment coefficient with elevator deflection	rad^{-1}
$C_{m_q} = \frac{\partial C_m}{\partial \frac{q\bar{c}}{2U_1}}$	Variation of pitching moment coefficient with pitch rate	rad^{-1}
$C_{m_{\dot{\alpha}}} = \frac{\partial C_m}{\partial \frac{\dot{\alpha}\bar{c}}{2U_1}}$	Variations of pitching moment coefficient with rate of change of angle of attack	rad^{-1}
$C_{m_{\delta_F}} = \frac{\partial C_m}{\partial \delta_F}$	Variation of pitching moment coefficient with flap deflection angle	rad^{-1}
$C_{m_{\delta_E}} = \frac{\partial C_m}{\partial \delta_E}$	Variation of pitching moment coefficient with elevator deflection angle	rad^{-1}
$C_{m_{i_H}} = \frac{\partial C_m}{\partial i_H}$	Variation of pitching moment coefficient with stabilizer incidence angle	rad^{-1}

SYMBOL	DEFINITION	DIMENSION
C_N	Normal force coefficient	
$C_{n_\beta} = \frac{\partial C_n}{\partial \beta}$	Variation of yawing moment coefficient with sideslip angle	rad^{-1}
$C_{n_p} = \frac{\partial C_n}{\partial \frac{pb}{2U_1}}$	Variation of yawing moment coefficient with roll rate	rad^{-1}
$C_{n_r} = \frac{\partial C_n}{\partial \frac{rb}{2U_1}}$	Variation of yawing moment coefficient with yaw rate	rad^{-1}
$C_{n_{\delta_A}} = \frac{\partial C_n}{\partial \delta_A}$	Variation of yawing moment coefficient with aileron angle	rad^{-1}
$C_{n_{\delta_R}} = \frac{\partial C_n}{\partial \delta_R}$	Variation of yawing moment coefficient with rudder angle	rad^{-1}
$C_{r_{C_L}}$	Root chord at centerline	ft
$(c_{r_i})_e$	Distance defined in Fig. 5.3.b	ft
C_R	Root chord	ft
C_t	Tip chord	ft
C_{t_i}	Distance defined in Fig. 5.3.b	ft
$C_{y'_{\psi_o}}$	Factor obtained from Fig. 5.5	
$C_{y_\beta} = \frac{\partial C_y}{\partial \beta}$	Variation of side force coefficient with sideslip angle	rad^{-1}

SYMBOL	DEFINITION	DIMENSION
$C_{y_p} = \frac{\partial C_y}{\partial \frac{pb}{2U_1}}$	Variation of sideforce coefficient with roll rate	rad^{-1}
$C_{y_r} = \frac{\partial C_y}{\partial \frac{rb}{2U_1}}$	Variation of side force coefficient with yaw rate	rad^{-1}
$C_{y_{\delta_A}} = \frac{\partial C_y}{\partial \delta_A}$	Variation of side force coefficient with aileron angle	rad^{-1}
$C_{y_{\delta_R}} = \frac{\partial C_y}{\partial \delta_R}$	Variation of side force coefficient with rudder angle	rad^{-1}
D	Diameter	ft
D	Drag	lbf
d	Fuselage diameter at the wing root chord	ft
e	Oswald's efficiency factor	
f	Propeller in flow factor, see Fig. 5.4	
g	Gravitational acceleration	ft/sec^2
h	Height	ft
h_{ac}	Height of wing aerodynamic center above ground	ft
h_c	Height defined in Fig. 4.4	ft
h_{eff}	Effective height above ground, defined in Fig. 4.2 (no flap deflection) or in Eqn. (4.13) (with flap deflection)	ft
h_f	Height defined in Fig. 4.4	ft
h_H	Height from wing root chord to horizontal tail aerodynamic center	ft
h_{TE}	Height of wing trailing edge above ground	ft

LIST OF SYMBOLS (Cont'd)

SYMBOL	DEFINITION	DIMENSION
i_H	Stabilizer angle of incidence	deg,rad
i_T	Thrust inclination angle	deg,rad
i_w	Wing angle of incidence	deg, rad
K_A	Correction factor for aspect ratio	
K_H	Correction factor for horizontal tail position	
$K_{H_{power}}$	Factor defined in Eqn. (5.36)	
K_{WB}	Empirical factor to correct for body effect on wing lift curve slope	
K_λ	Correction factor for taper ratio	
K 1	Empirical correlation factor in Fig. 5.8	
K 2	Correction factor for maximum lift in Fig. 5.11	
L	Lift	lbf
ℓ_b	Length of fuselage	ft
$\ell_{\bar{c}/4_w}$	Distance defined in Fig. 5.15	ft
ℓ_{cg}	Distance from the nose of the airplane to the center of gravity	ft
ℓ_H	Distance defined in Fig. 5.3.a	ft
ℓ'_H	Distance defined in Fig. 5.3.a	ft
ℓ_n	Distance defined in Fig. 5.16	ft
ℓ_{no}	Distance defined in Fig. 5.18	ft
M	Mach number	
m	Airplane mass	lb
N_p	Propeller normal force	lbf
N	Normal force	lbf
N	Number of engines	
N_{pax}	Number of passengers	

LIST OF SYMBOLS (Cont'd)

SYMBOL	DEFINITION	DIMENSION
q	Pitch rate	rad/sec
$\bar{q}$	Dynamic pressure	lbf/ft^2
R_p	Propeller radius	ft
S	Area	ft^2
S_i	Area defined in Eqn. (5.3b)	ft^2
S_{H_i}	Area defined in Eqn. (5.37) (single engine) or in Eqn. (5.38) (multi-engine)	ft^2
SO	Area defined in section 5	
T	Thrust	lbf
$T_c' = \frac{T}{\bar{q}_\infty S_w}$	Thrust coefficient	
$T_c = \frac{T}{\rho V^2 D^2}$	Thrust coefficient	
V, U_1	Airspeed	ft/sec, knots
V_{mu}	Minimum unstick speed	ft/sec, mph
V_s	Stall speed	ft/sec, mph
V_{ROT}	Rotation speed	ft/sec, mph
W	Weight	lb
w_{aisle}	Width of aisle	ft
w_c	Cabin width	
w_n	Nacelle width	ft
w_{seat}	Width of seat	ft
X	X-axis, positive forward from the center of gravity	
$\bar{X}_{ac}$	Distance from leading edge of the wing to the aerodynamic center in tenths of $\bar{c}$	
$\bar{X}_{cg}$	Distance from the leading edge of the wing m.g.c. to the airplane in tenths of $\bar{c}$	

SYMBOL	DEFINITION	DIMENSION
X_H	Distance from airplane c.g. to the horizontal tail a.c.	ft
X_{pilot}	Distance defined in Fig. 10.12	ft
x'_p	Distance defined in Fig. 5.3.a	ft
x_p	Distance defined in Fig. 5.3.a	ft
X_w	Distance defined in Eqn. (5.49)	ft
$y_{\bar{c}_i}$	Distance defined in Fig. 5.3.b	ft
Z_H	Distance defined in Fig. 5.3.a	ft
$Z_{H_{eff}}$	Distance defined in Fig. 5.3.a	ft
Z_{H_T}	Distance defined in Fig. 5.3.a	ft
Z_s	Distance defined in Fig. 5.3.a	ft
Z_T	Distance defined in Fig. 5.3.a	ft
Z_w	Distance defined in Fig. 5.3.a	ft

GREEK SYMBOLS

$\Lambda_{\bar{c}/4}$	Quarter chord sweep angle	deg, rad
λ	Taper ratio	
Δ	Change of a quantity	
α	Angle of attack	deg, rad
α_o	Angle of attack for zero lift	deg, rad
β	Factor defined in Equation (4.4)	
σ	Factor defined in Equation (4.8)	
α_i	Induced angle of attack	deg,rad

GREEK SYMBOLS (Cont'd)		DIMENSION
$\Lambda_{c/2}$	Half chord sweep angle	deg, rad
δ	Control surface deflection	deg, rad
γ	Flight path angle	deg, rad
$\tau_E = \frac{\partial \alpha_H}{\partial \delta_E}$	Elevator effectiveness	
ϵ	Downwash angle	deg, rad
$\alpha_T = \alpha_b + i_T$	Thrust angle of attack	deg, rad
ϵ_{pow}	Total downwash angle at horizontal tail	deg, rad
λ_{i_e}	Taper ratio of immersed wing (see Fig. 5.3.b)	
α_p	Local angle of attack of the propeller plane	deg, rad
ϵ_u	Upwash angle	deg, rad
$\eta_H = \frac{\bar{q}_H}{\bar{q}_\infty}$	Ratio of dynamic pressures at the horizontal tail	
$\kappa = \frac{C_{\ell_\beta}}{2\pi}$	Ratio of section lift-curve slope to 2π	

SUBSCRIPTS	
ac	Aerodynamic center
A	Aileron
b	Body
B	Body axis
cg	Center of gravity
C	Cabin
E	Elevator
e	Elevator
eng	Engine
fus	Fuselage

SUBSCRIPTS (Cont'd)

F	Flaps
f	Flaps
FUS	Fuselage
GE	Ground effect
H	Horizontal tail
L	Landing
LE	Leading edge
LAND	Landing
MIN	Minimum
MAX	Maximum
NAC	Nacelle
P	Power
P	Propeller
prop	Propeller
PROP	Propeller
R	Rudder
R	Root
S	Stability axis
t	tip
TE	Trailing edge
TO	Takeoff
V	Vertical tail
W	Wing
∞	Infinitely far away
1	Steady state

LIST OF FIGURES

NUMBER	DESCRIPTION	PAGE
2.1	Flowchart for Executive Program	2.5
4.1	Image Vortex System .	4.1
4.2	Definition of Effective Height	4.3
4.3	Total Effect of Ground-Proximity on Wing Lift	4.4
4.4	Definition of Geometry Parameters	4.5
5.1	Direct Effect of Power	5.2
5.2	Indirect Effects of Power	5.2
5.3a	Definition of Geometric Parameters	5.3
5.3b	Definition of Geometric Parameters, Single Engine	5.4
5.3c	Definition of Geometric Parameters, Multi Engine	5.5
5.4	Variation of f with T_C (Ref. 5.1)	5.6
5.5	Propeller Side Force Coefficient (Ref. 5.1)	5.7
5.6	Propeller Side Force Coefficient (Ref. 5.1)	5.7
5.7	Upwash Gradient at Plane of Symmetry for Unswept Wings (Ref. 5.2)	5.9
5.8	Empirical Correlation Factor for Additional Lift Due to Slipstream (Ref. 5.2)	5.11
5.9	Propeller induced downwash (Ref. 5.2)	5.12
5.10	Effect of Power on Maximum Lift	5.14
5.11	Correction Factor for Maximum Lift (Ref. 5.2)	5.14
5.12	Effect of Power on Downwash for Single Engine Airplanes (Ref. 5.2)	5.16
5.13	Effect of Power on Downwash for Multiengine Airplanes (Ref. 5.2)	5.16
5.14	Effect of Power on the Dynamic Pressure Ratio at the Tail (Ref. 5.2)	5.19
5.15	Geometry of the Wing	5.24

LIST OF FIGURES (Cont'd)

NUMBER	DESCRIPTION	PAGE
5.16	Shape of Nacelle (Twin Engine)	5.25
5.17	Nacelle Shape Parameter, Twin Engine Airplanes	5.26
5.18	Shape of Nacelle (Single Engine)	5.27
5.19	Nacelle Shape Parameter, Single Engine Airplane	5.28
6.1	Definition of Dimensional and Nondimensional Aerodynamic Center Locations	6.4
6.2	Aerodynamic Center Locations of Lifting Surfaces	6.4
6.3	Geometric Parameters for the Computation of the Effect of Body or Nacelles on a.c. Location	6.6
6.4	Upwash Ahead of the Wing	6.6
6.5	Ellipse Parameter Definitions	6.10
8.1	V_{mc} Variable Geometric Definitions	8.4
9.1	Takeoff Parameters	9.2
9.2	The Functions F(h) and F(α) Used in Perry's Method for the Analysis of the Airborne Path. (Derived from Ref. 9.2)	9.5
10.1	Statistical Data for Pitching Moment of Inertia	10.3
10.2	Statistical Data for Rolling Moment of Inertia	10.4
10.3	Statistical Data for Yawing Moment of Inertia	10.5
10.4	Airplane Geometry	10.7
10.5	Parameter for Wing Rolling Moment of Inertia, I_{ox}	10.8
10.6	Parameter for Fuselage Pitching Moment of Inertia, I_{oy}	10.9
10.7	Parameter for Fuselage Rolling Moment of Inertia, I_{ox}	10.10
10.8	Parameter for Horizontal Tail Rolling Moment of Inertia, I_{ox}	10.11

LIST OF FIGURES (Cont'd)

NUMBER	DESCRIPTION	PAGE
10.9	Parameter for Vertical Tail Rolling Moment of Inertia, I_{ox}	10.12
10.10	Fuel Tank Geometry	10.15
10.11	Tip Tank Geometry	10.16
10.12	Passenger Compartment	10.17
10.13	Flowchart of Subroutine "INERTA"	10.32
10.14	Listing of Subroutine "INERTA"	10.35
11.1.1	Method for Estimating the Oswald Efficiency Factor	11.1.2
11.3.1	Geometric Parameters for Horizontal Tail Location	11.3.2
11.7.1	Wing Geometry	11.7.2
11.10.1	Correction Constant K for Wing Contribution	11.10.2
11.14.1	Wing-Body Interference Factor for Wing-Body Sideslip Derivative C_{y_β}	11.14.2
11.14.2	Empirical Factor for Estimating Sideslip Derivative for Single Vertical Tails	11.14.3
11.14.3	Effect of Body Interference on Aspect-Ratio, Used for Estimating Sideslip Derivative for Single Vertical Tails	11.14.5
11.14.4	Effect of Horizontal Tail Interference on Aspect Ratio, Used for Estimating the Sideslip Derivative for Single Vertical Tails	11.14.5
11.14.5	Factor Accounting for Relative Size of Horizontal and Vertical Tail	11.14.6
11.15.1	Wing Sweep Contribution to C_{ℓ_β}	11.15.2
11.15.2	Compressibility Correction Factor to Sweep Contribution to Wing C_{ℓ_β}	11.15.3
11.15.3	Fuselage Correction Factor	11.15.3
11.15.4		11.15.5
11.15.5	Effect of Uniform Geometric Dihedral on Wing C_{ℓ_β}	11.15.5

LIST OF FIGURES (Cont'd)

NUMBER	DESCRIPTION	PAGE
11.15.6	Compressibility Correction to Dihedral Effect on Wing C_{ℓ_β}	11.15.6
11.15.7	Effect of Wing Twist on Wing C_{ℓ_β}	11.15.6
11.16.1	Definition of Geometric Parameters	11.16.2
11.16.2	Empirical Factor for Wing + Wing-Body Interference	11.16.3
11.16.3	Effect of Fuselage Reynolds Number on Wing-Body Combinations	11.16.3
11.18.1	Roll Damping Parameter, Used for Computation of C_{ℓ_p}	11.18.2
11.18.2	Geometry for Determining Distance from Vertical Tail A.C. to Body X-axis	11.18.4
11.19.2	Effect of Flap Deflection of Wing Rolling Derivative C_{n_p}	11.19.3
11.19.2a	Definition of Geometric Parameters	11.19.4
11.19.3	Influence of Flap Chord on Flap Effectiveness	11.19.4
11.21.1	Wing Yawing Derivative, C_{ℓ_r}	11.21.2
11.21.2	Effect of Wing Twist on C_{ℓ_r}	11.21.2
11.21.3	Effect of Flaps on C_{ℓ_r}	11.21.4
11.23.1	Geometric Parameters for Control Surface Flap	11.23.1
11.23.2	Influence of Flap Chord on Flap Effectiveness	11.23.3
11.23.3	Span Factor of Inboard Flaps	11.23.4
11.23.4	Theoretical Lift Effectiveness of Plain Trailing Edge Control Flap	11.23.4
11.23.5	Empirical Correction for Lift Effectiveness of Trailing Edge Control Flaps	11.23.5
11.23.6	Empirical Correction for Lift Effectiveness of Plain Trailing Edge Control Flaps at High Control Deflections	11.23.6
11.24.1	Determination of C_{ℓ_δ}/k	11.24.2
11.24.2	Correction for Flap-Span Effect	11.24.3

LIST OF FIGURES (Cont'd)

NUMBER	DESCRIPTION	PAGE
11.24.3	Correlation Constant for $C_{n_{\delta_A}}$	11.24.4
11.26.1	Geometry of Aileron	11.26.1
11.26.2	Rate of Change of Section Hinge Moment C'_{h_α}	11.26.2
11.26.3	Theoretical Hinge Moment Derivative	11.26.2
11.26.4	Effect of Nose Balance on Section Hinge Moment Derivatives	11.26.4
11.26.5	Geometry of Control Surface	11.26.4
11.26.6	Various Types of Nose Shapes	11.26.4
11.26.7	Correction for Induced Camber	11.26.5
11.26.8	Effect of Control Surface Span	11.26.6
11.26.9	Control Surface Span Parameters	11.26.6
11.26.10	Correction for Chord Ratio	11.26.7
11.26.11	Effect of Open Gap on Section Hinge Moment Coefficient for a .35$\bar{c}$ Flap	11.26.8
11.26.12	Effect of Bevel Angle on Hinge Moment Coefficient for a .2$\bar{c}$ Flap	11.26.9
11.26.13	Correction for Flap-Chord Ratio	11.26.9
11.26.14	Ratio of Actual to Theoretical Hinge Moment	11.26.11
11.26.15	Theoretical Hinge Moment Derivative	11.26.11
11.26.16	Effect of Nose Balance on Section Hinge Moment Derivative	11.26.12
11.26.17	Listing Surface Correction for Hinge Moment Derivative	11.26.14
11.26.18	Correction Factor for Control Surface Span	11.26.15
11.26.19	Effect of Horn Balance	11.26.15
13.1	Flowchart of Subroutine INPUT	13.4
13.2	Planform Parameters	13.6

LIST OF FIGURES (Cont'd)

NUMBER	DESCRIPTION	PAGE
A.1	Effect of Ground Proximity on Wing Lift-Curve Slope	A.3
A.2	Ground Effect on Lift-Curve	A.4
A.3	Effect of Trailing Vortex on Lift in Ground Effect	A.6
A.4	Effect of Bound Vortex on Lift in Ground Effect	A.6
A.5	Effect of Finite Span on Lift in Ground Effect	A.7
A.6	Effect of Flaps on Lift in Ground Effect	A.7
A.7	Comparison of Ground Effect Methods	A.10
C.1	Threeview of Airplane A	C.2
C.2	Threeview of Airplane B	C.3
C.3	Threeview of Airplane C	C.4
D.1	Correction Factor for Lift-Curve Slope	D.2

LIST OF TABLES

NUMBER	DESCRIPTION	PAGE
10.1	Variable Names in Subroutine "INERTA"	10.21
10.2	Comparison of Inertia Computations	10.29
10.3	Inertia Calculations, Comparison	10.31
A.1	Calculation of Ground Effect for Corning Method	A.2
A.2	Calculation of Ground Effect by Perkins and Hage Method	A.4
A.3	Calculation of Datcom Method	A.8
A.4	Calculation of Torenbeek Method	A.9
C.1	Airplane Data	C.5

CHAPTER 1

INTRODUCTION

This report presents work performed to correct and modify a stability and control computer program which was produced by the University of Kansas Flight Research Laboratory. The original program was written between May 16, 1976 and May 31, 1978 under NASA grant NSG 2145. (Reference 1)

The present effort was aimed specifically at correcting deficiencies in:

1. The executive program, including documentation.
2. The C_{L_α} computation.
3. The downwash and trim computations.
4. The power effect computation.
5. The output of nonstandard transfer functions.
6. The dynamic stability routine switches to allow for sensitivity analyses.
7. The input methods where C_{L_o} and C_{M_o} may be calculated internally instead of being supplied as inputs.
8. The overall input logic in an attempt to streamline the input format.
9. The User's Manual, including rewriting the manual to increase program utility.

Furthermore, the program was to be thoroughly scrutinized in an effort to detect and correct errors not previously identified. This latter task proved to be monumental and, eventually, every routine (64) was examined in detail with changes eventually being made in all of them. In certain cases, entire subroutines were rewritten in order to comply with existing methods of stability derivative prediction. A problem which eventually surfaced as

a result of this investigation was that, while the original routines were checked individually, the integrated program was plagued with inconsistencies in variable definition. For example, common blocks added as part of the integration process were found to be of different size in different routines or had variables listed in the wrong order. The impact of these errors can be better appreciated when one realizes that, in one case, the wing mean aerodynamic chord was being used as the tail arm in the horizontal tail volume coefficient. In another case, the vertical tail sweep was not accounted for, and in still another case the same variable was being specified both in the formal argument list of the subroutine call as well as in a common block. To complicate matters, the calling routine presumed different definitions for this variable with attendant errors in the final output.

Having discovered the nature of the predominant error in the existing program, a major effort was directed at tracing each variable in each common block. As may be expected, changes accordingly resulted in almost every one of the 64 subroutines and functions included in this program.

The final computer program resulting from this study also includes major changes to the input methodology whereby formatted input via the main program and different subroutines based on 37 read statements was changed to namelist input using 3 read statements in a newly created INPUT subroutine.

The results of the present study are embodied in this basic documentation manual, a new User's Manual, and a separate Fortran cross reference listing of the program.

add COSMIC note

1.1 REFERENCES

1.1 Van Keppel, Bob, et al — A Computer Program for the Analysis of the Dynamic Stability Characteristics of Airplanes. University of Kansas Flight Research Laboratory, December 1978.

CHAPTER 2

GENERAL INFORMATION AND EXECUTIVE PROGRAM

2.1 GENERAL INFORMATION

This chapter briefly describes the more significant changes to the program and then discusses the main (executive) program in detail. While major changes in logic were made to the principal routines such as subroutines TRIM, POWER, CMALPA, VMCE, ROTSPD, CYBETA, LIFCRV, MULTOP, CLBETA, CNBETA, ACEM, and CONSUR, most of these changes involved the realignment of program logic to agree with the (original) basic documents. Changes made to the original document were for the most part cosmetic in nature, where variables were redefined for clarity or to more accurately represent source document (references) data, and equations were corrected or redefined. An example of redefining an equation is the case where a curve fit which was developed to represent graphical data was replaced by the closed form equation which originally generated the graphical data.

For completeness, all of the theoretical developments of the original documents have been included in this report as corrected. As such, Chapters 3 through 12 of this report retain a one-for-one alignment with the original documentation. However, most of the difficulties of the original computer program stemmed from the fact that subroutines were predominantly checked in isolation without adequate regard for the large number of common blocks which eventually permeated the program upon integration of the separate routines. As such, all of the computer program "descriptions" and "verifications" of the original documentation are omitted in this report except those of Chapter 10. Furthermore, section 11.27 has been added to describe

the new subroutine CLOCMO and Chapter 13 to describe the new subroutines INPUT, PLANFM, and ATMOS.

2.1.1 Major Changes

A major effort of this study was to streamlines the utility of the program by making it easier to use. Hence, the input format of the program was changed from one based on formatted input where 220 variables were input on 41 cards in 109 combinations, to one where 193 variables are input via 3 namelists. While several original variables were deleted, several others were added. The net effect of these changes may be summarized as follows:

1. Data entry is simplified immensely. While the original method required detailed attention to the column location of numbers (particularly for integer variables), field width and location for different operations on each data line, and proper combinations of data line entries, the present method requires only that 1 data line and 3 namelists be entered in the correct order.
2. Fifteen variables were found to be overspecified. These were eliminated as inputs and are computed internally within the program. However, they are echoed together with other input variables.
3. Forty-one variables specifically associated only with the computation of moments and products of inertias were identified. When the moments and products of inertia are input (preferred method), the variable list drops to 152. These, in turn, are clearly identified by operation. Due to Fortran namelist features, only those variables required for a specific analysis need be input.
4. Multiple cases may be easily analyzed for different flight conditions since only those variables which change need be input. The original method required that a complete data set be re-entered

for successive runs.

5. Data input is concentrated at only 2 points in the program. A single plain-language identification line is read in the main program and also acts as an end-of-file locator, and 3 namelists are read in an input subroutine. This is to be contrasted with 37 read statements dispersed throughout the original executive routine with 1 read statement in the rotation speed routine and 2 in the dynamic stability routine.

2.1.2 Input Logic

The main program reads and echos a single, plain language, 78 character string, identification line. If an end-of-file marker is not encountered, program execution proceeds with data entry accomplished through an input routine. Subroutines INPUT (section 11.27) and ATMOS (section 11.29) have been added to facilitate data entry and echo.

2.2 EXECUTIVE ROUTINE

The executive routine (main program) ultimately manages 64 subroutines and functions. While most of the subroutine calls never proceed beyond 2 levels, calls to CLOCMO, CMALPA, POWER, VMCE, and ROTSPD result in 4 levels of calls. (e.g. MAIN→CLOCMO→LIFCRV→DOWNWS→SLOPE)

Only 1 computational loop exists in the executive routine where 3 passes are made over subroutines LCDER, CMALPHA, and TRIM. Here LCDER establishes the control derivatives $C_{L_{\delta_e}}$, $C_{m_{\delta_e}}$, $C_{D_{\delta_e}}$, and TRIM obtains δ_e to balance the longitudinal moment equation. Successive calls to LCDER and TRIM are accomplished to account for possible changes in the control derivatives resulting

from elevator deflection.

2.2.1 Executive Program Flow Chart

A flowchart of the executive program is presented in Figure 2.1. The only escape provided is the end-of-file (EOF) mark after the (only) read statement in the executive program. Hence, the program is provided with an automatic capability for consecutive runs where one or more variables may be changed.

2.2.2 Executive Program Listing

The executive program listing is provided under separate cover as part of a complete Fortran cross reference listing.

Figure 2.1 Flowchart For Executive Program

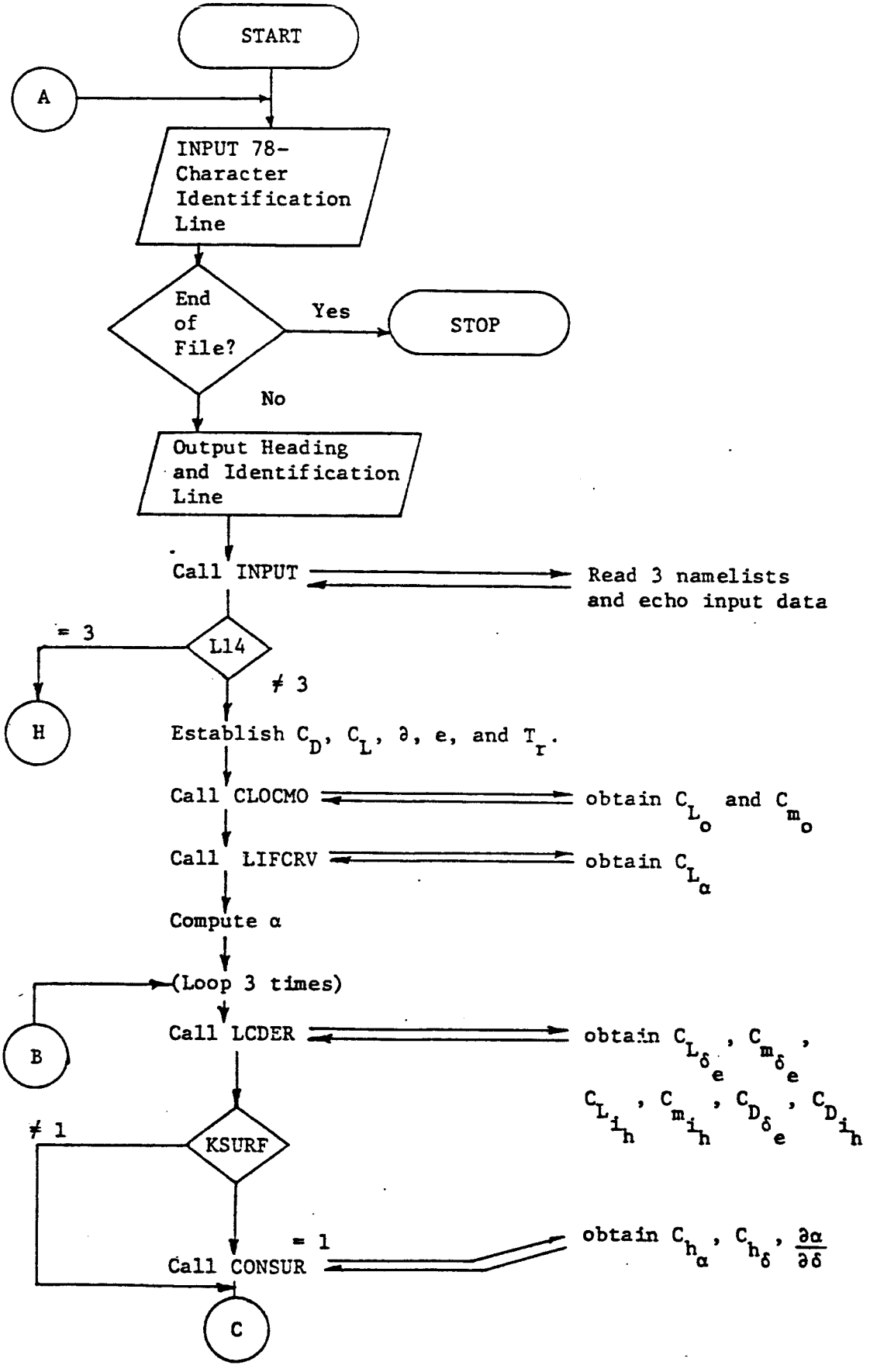

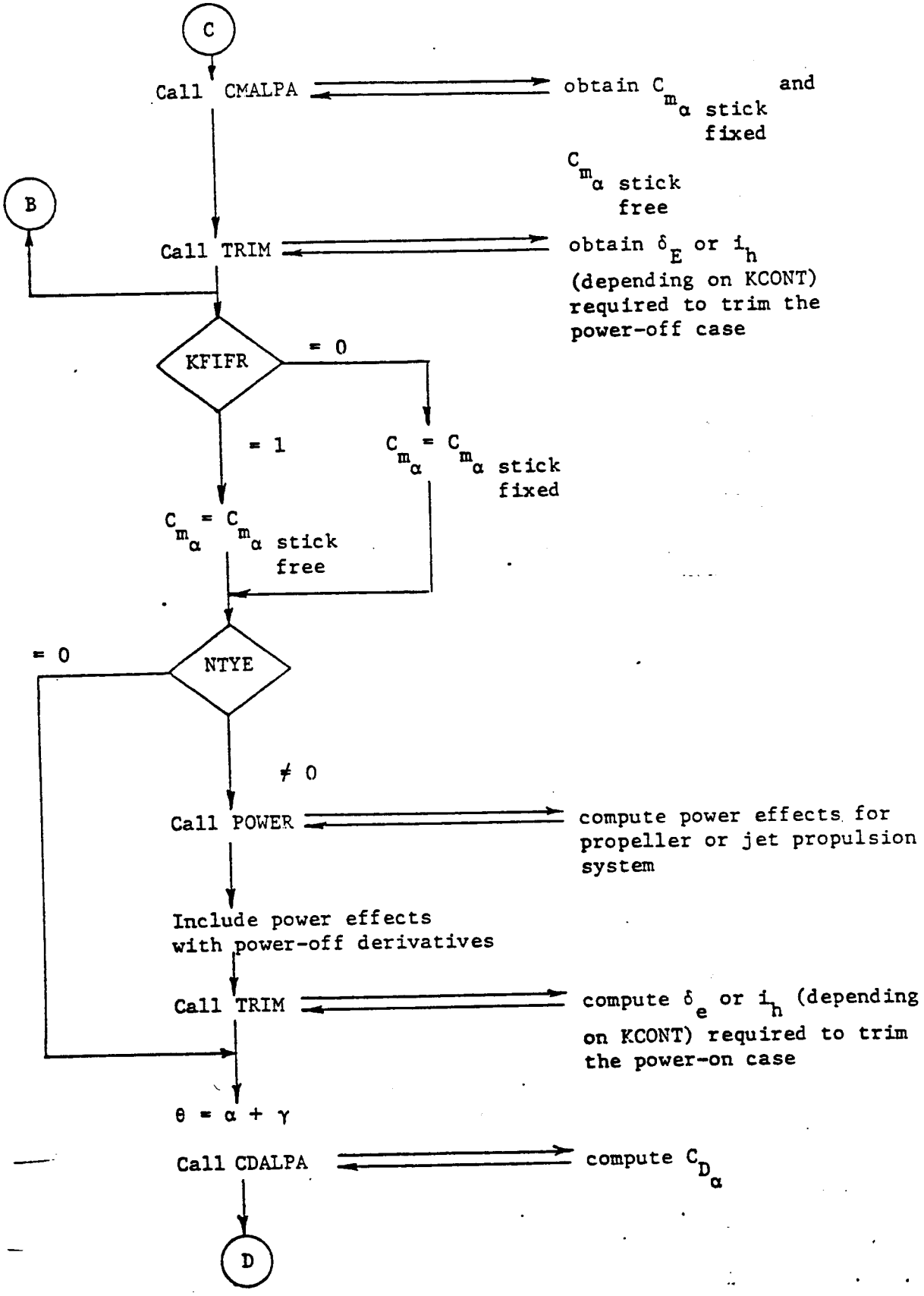
C
Call CMALPA
obtain C_{m_α} stick fixed and
C_{m_α} stick free
B
Call TRIM
obtain δ_E or i_h (depending on KCONT) required to trim the power-off case
KFIFR
= 0
= 1
$C_{m_\alpha} = C_{m_\alpha}$ stick fixed
$C_{m_\alpha} = C_{m_\alpha}$ stick free
= 0
NTYE
≠ 0
Call POWER
compute power effects for propeller or jet propulsion system
Include power effects with power-off derivatives
Call TRIM
compute δ_e or i_h (depending on KCONT) required to trim the power-on case
$\theta = \alpha + \gamma$
Call CDALPA
compute C_{D_α}
D

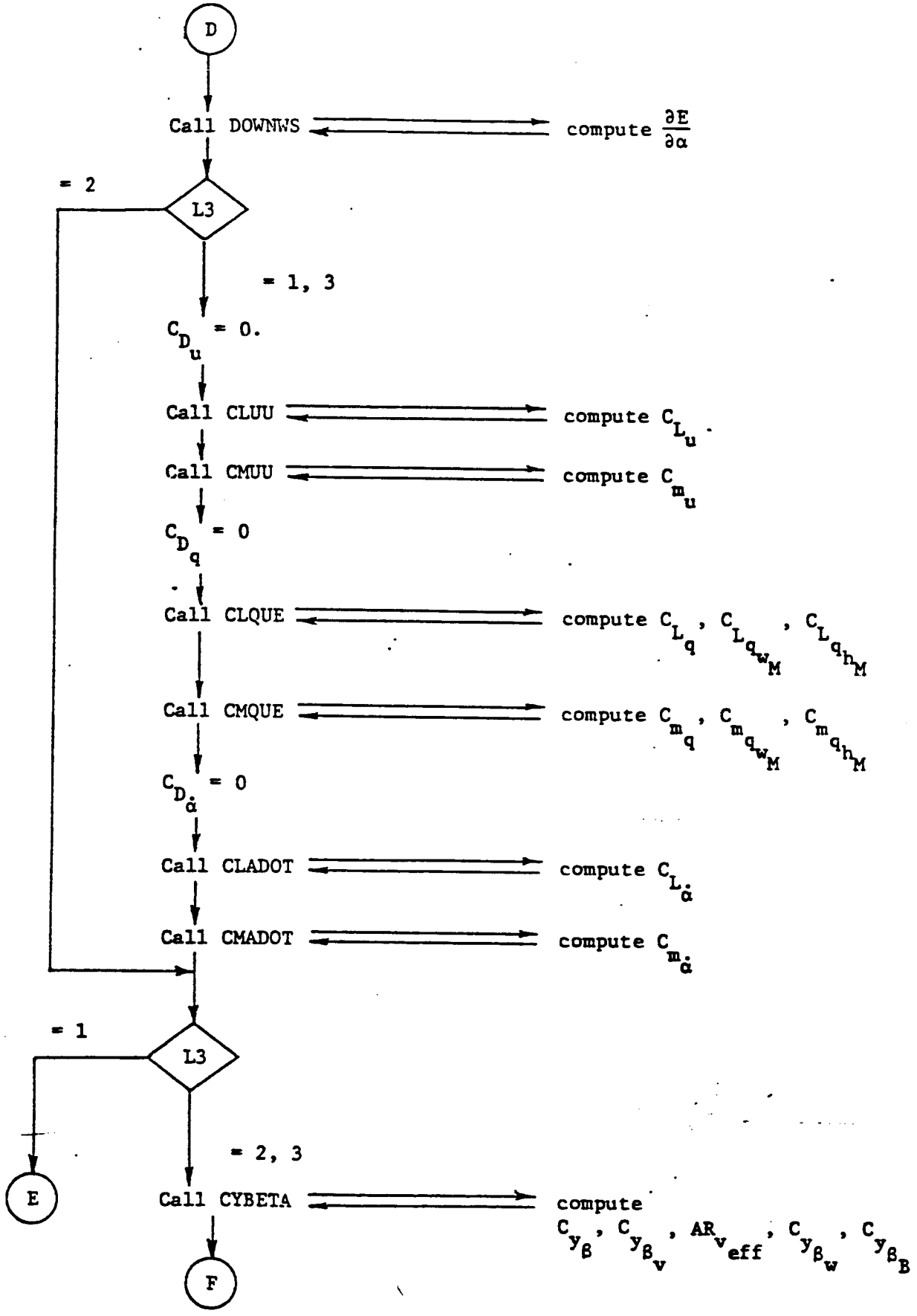
D
Call DOWNWS
compute $\frac{\partial E}{\partial \alpha}$
= 2
L3
= 1, 3
C_{D_u} = 0.
Call CLUU
compute C_{L_u}
Call CMUU
compute C_{m_u}
C_{D_q} = 0
Call CLQUE
compute C_{L_q}, $C_{L_{q_{w_M}}}$, $C_{L_{q_{h_M}}}$
Call CMQUE
compute C_{m_q}, $C_{m_{q_{w_M}}}$, $C_{m_{q_{h_M}}}$
$C_{D_{\dot{\alpha}}}$ = 0
Call CLADOT
compute $C_{L_{\dot{\alpha}}}$
Call CMADOT
compute $C_{m_{\dot{\alpha}}}$
= 1
L3
= 2, 3
E
Call CYBETA
compute
C_{y_β}, $C_{y_{\beta_v}}$, $AR_{v_{eff}}$, $C_{y_{\beta_w}}$, $C_{y_{\beta_B}}$
F

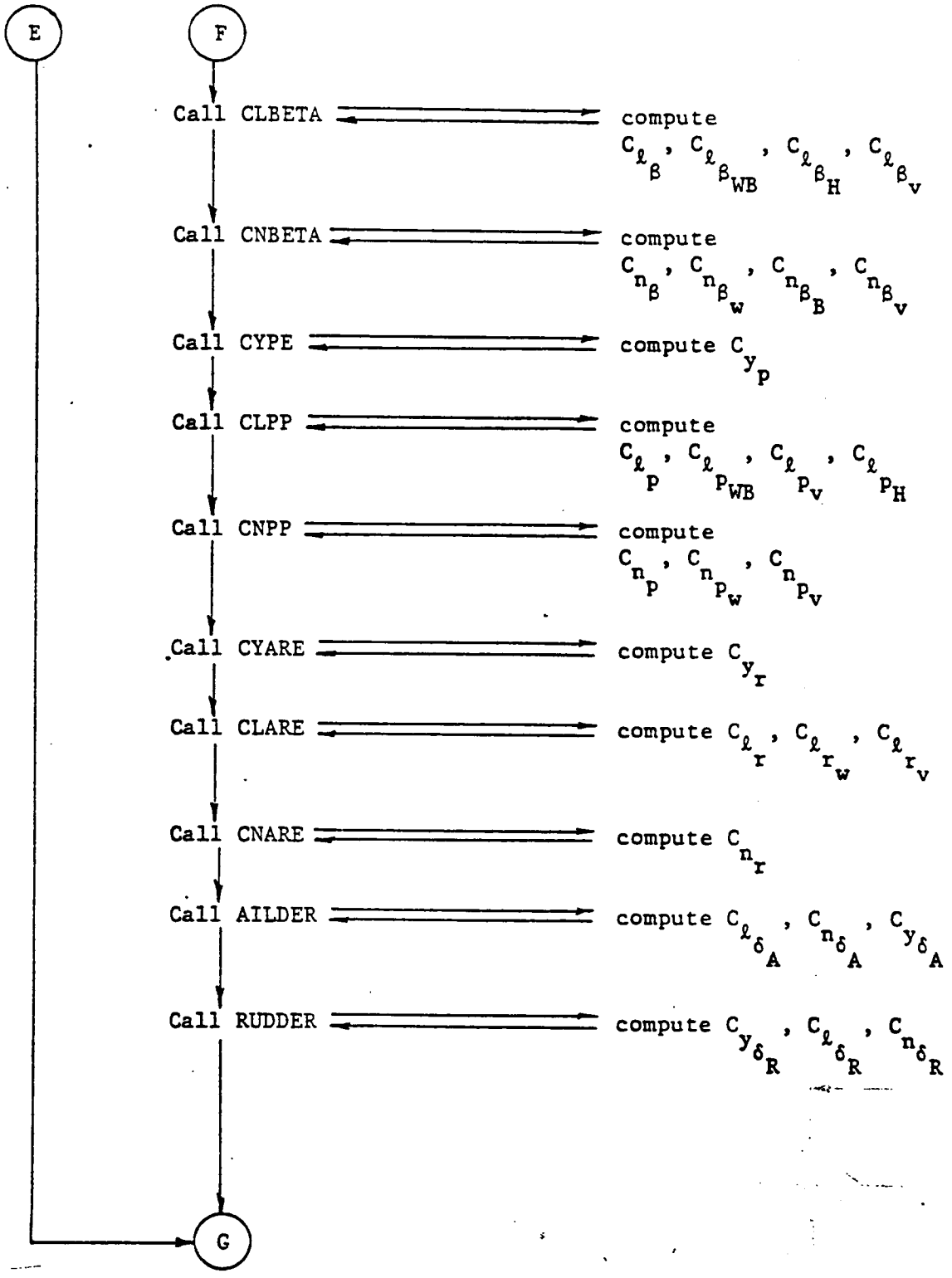
E
F
Call CLBETA
compute C_{ℓ_β}, $C_{\ell_{\beta_{WB}}}$, $C_{\ell_{\beta_H}}$, $C_{\ell_{\beta_v}}$
Call CNBETA
compute C_{n_β}, $C_{n_{\beta_w}}$, $C_{n_{\beta_B}}$, $C_{n_{\beta_v}}$
Call CYPE
compute C_{y_p}
Call CLPP
compute C_{ℓ_p}, $C_{\ell_{p_{WB}}}$, $C_{\ell_{p_v}}$, $C_{\ell_{p_H}}$
Call CNPP
compute C_{n_p}, $C_{n_{p_w}}$, $C_{n_{p_v}}$
Call CYARE
compute C_{y_r}
Call CLARE
compute C_{ℓ_r}, $C_{\ell_{r_w}}$, $C_{\ell_{r_v}}$
Call CNARE
compute C_{n_r}
Call AILDER
compute $C_{\ell_{\delta_A}}$, $C_{n_{\delta_A}}$, $C_{y_{\delta_A}}$
Call RUDDER
compute $C_{y_{\delta_R}}$, $C_{\ell_{\delta_R}}$, $C_{n_{\delta_R}}$
G

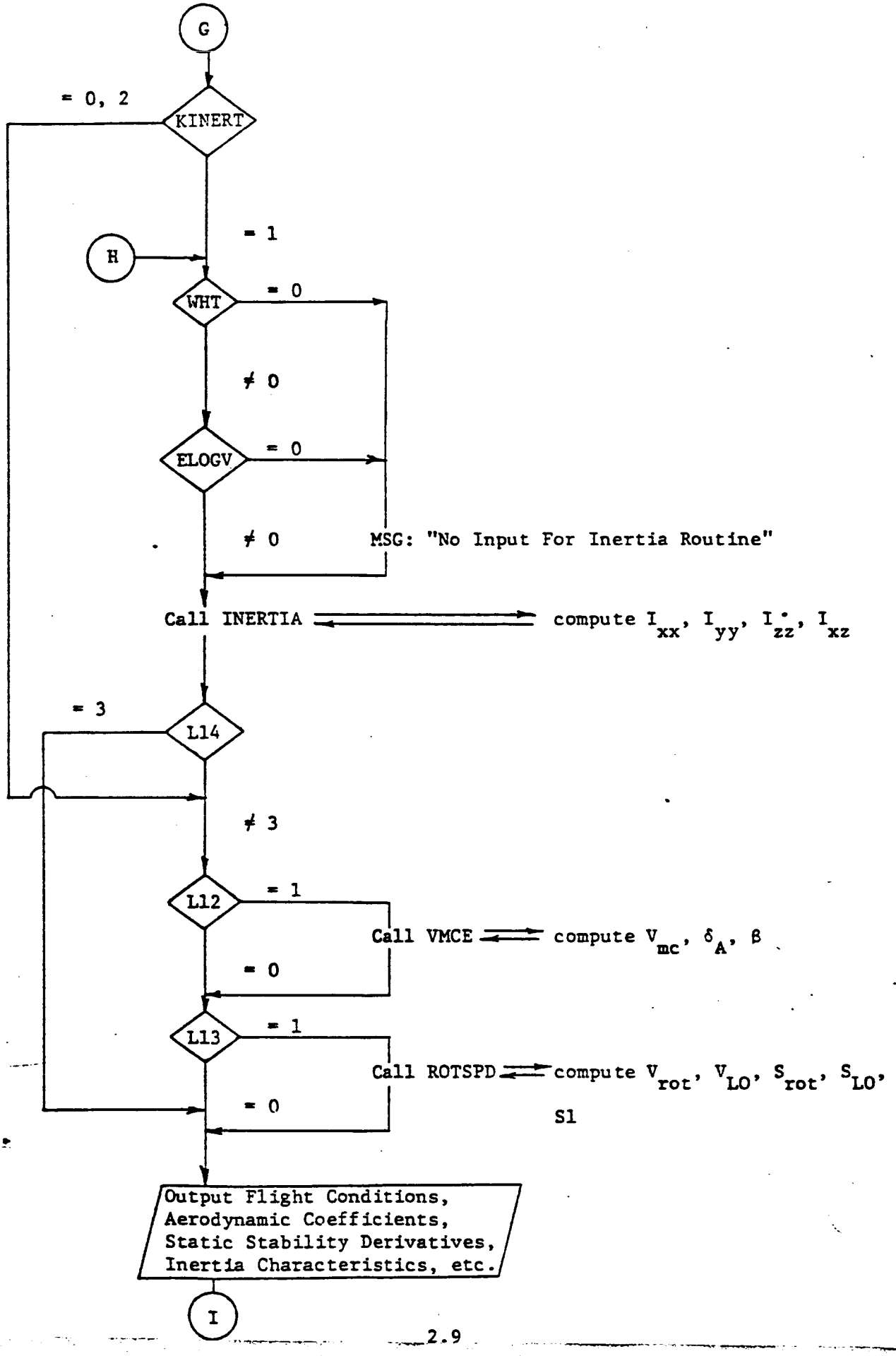
G
= 0, 2
KINERT
= 1
H
WHT
= 0
≠ 0
ELOGV
= 0
≠ 0
MSG: "No Input For Inertia Routine"
Call INERTIA
compute I_{xx}, I_{yy}, I_{zz}, I_{xz}
= 3
L14
≠ 3
L12
= 1
Call VMCE
compute V_{mc}, δ_A, β
= 0
L13
= 1
Call ROTSPD
compute V_{rot}, V_{LO}, S_{rot}, S_{LO}, S1
= 0
Output Flight Conditions,
Aerodynamic Coefficients,
Static Stability Derivatives,
Inertia Characteristics, etc.
I

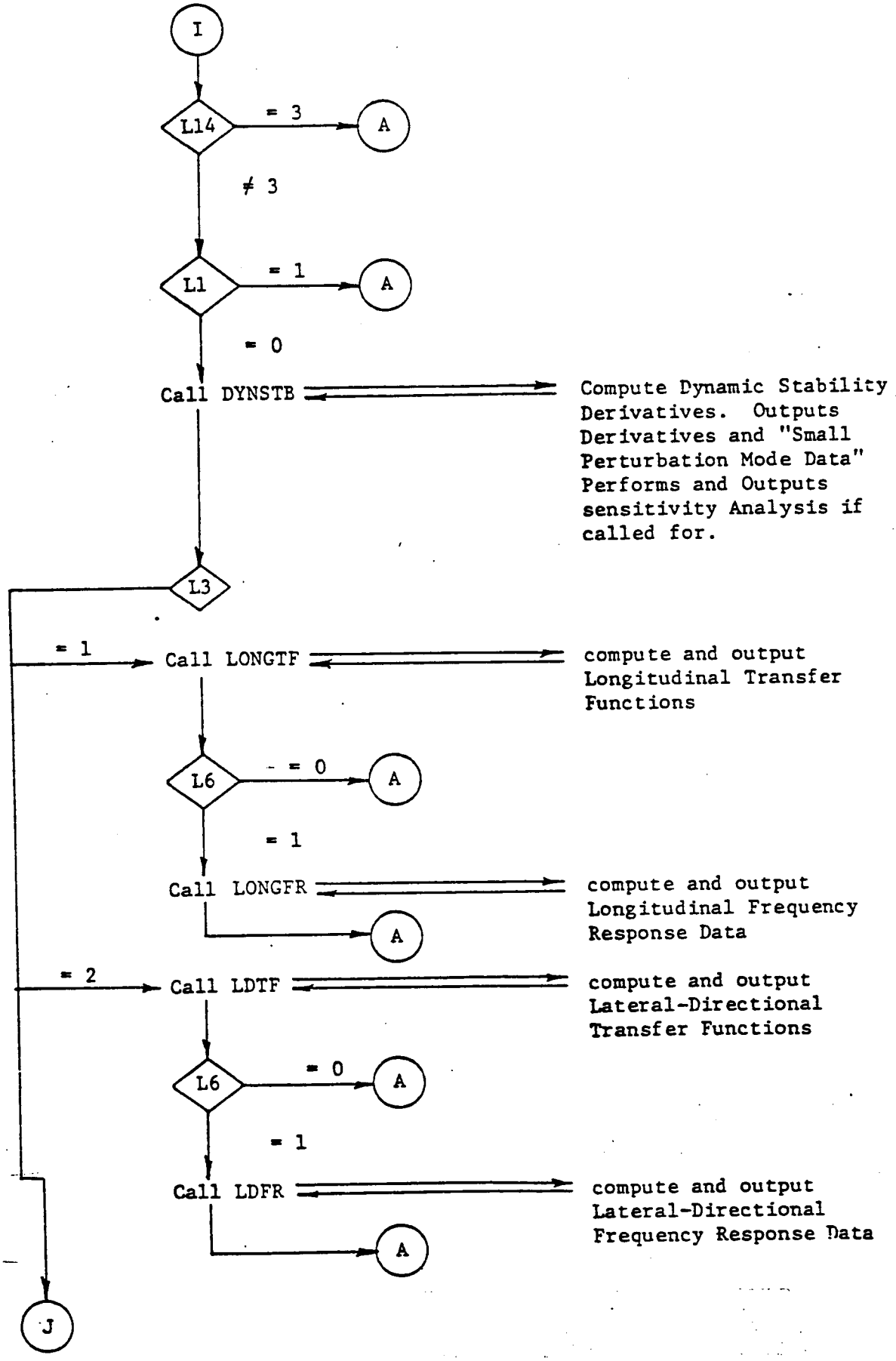
I
L14
= 3
A
≠ 3
L1
= 1
A
= 0
Call DYNSTB
Compute Dynamic Stability Derivatives. Outputs Derivatives and "Small Perturbation Mode Data" Performs and Outputs sensitivity Analysis if called for.
L3
= 1
Call LONGTF
compute and output Longitudinal Transfer Functions
L6
= 0
A
= 1
Call LONGFR
compute and output Longitudinal Frequency Response Data
A
= 2
Call LDTF
compute and output Lateral-Directional Transfer Functions
L6
= 0
A
= 1
Call LDFR
compute and output Lateral-Directional Frequency Response Data
A
J

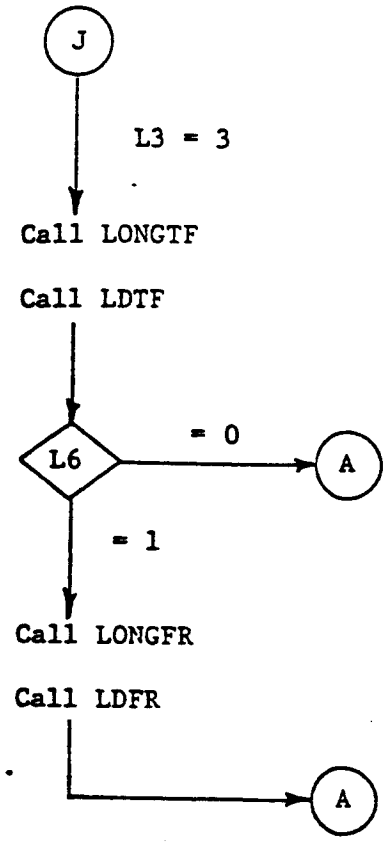
J
L3 = 3
Call LONGTF
Call LDTF
L6
= 0
A
= 1
Call LONGFR
Call LDFR
A

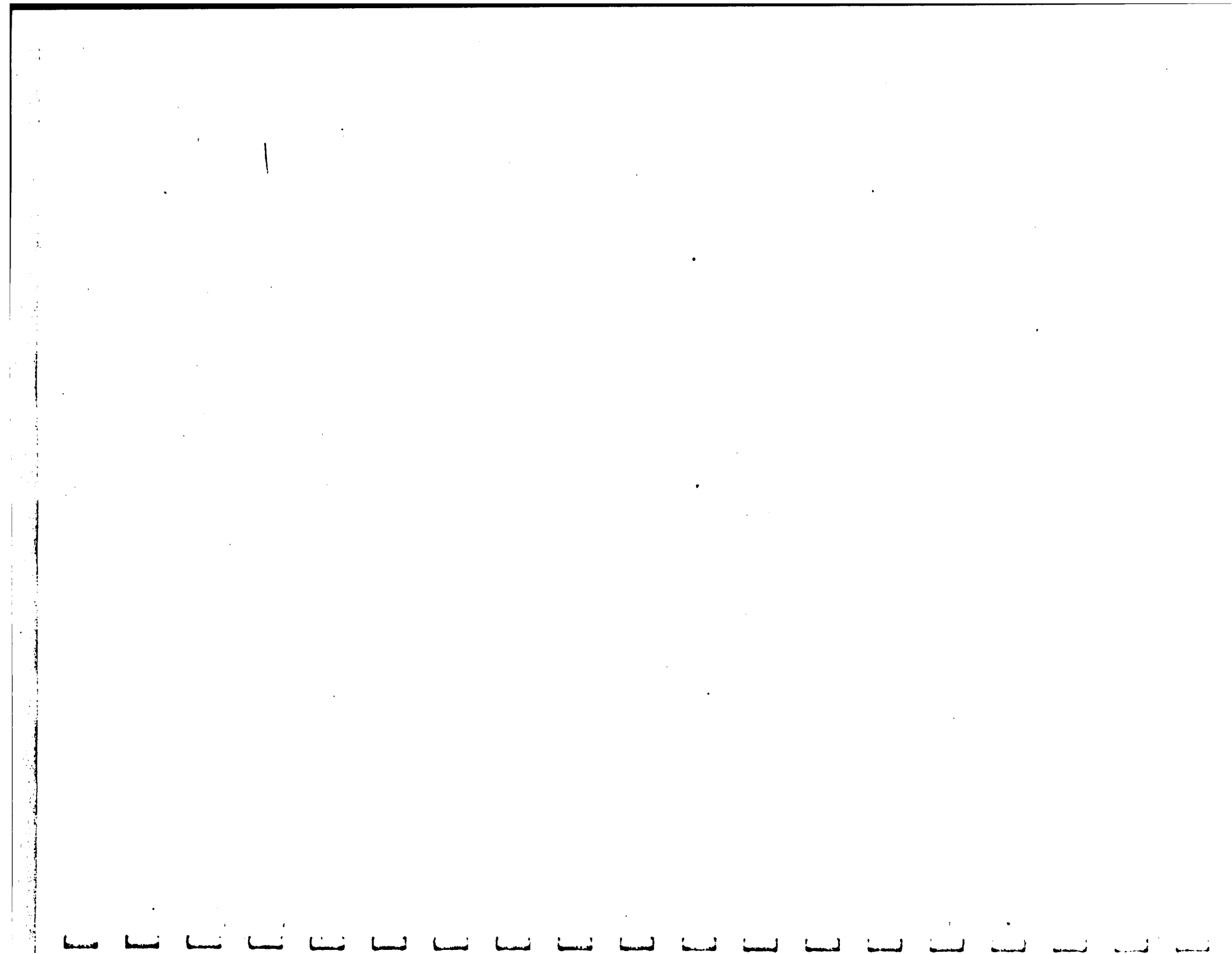

CHAPTER 3

TRIM

3.1 INTRODUCTION

This subroutine calculates stabilizer angle of incidence, elevator deflection and lift coefficient of the horizontal tail needed for moment equilibrium in cruise. The program distinguishes two cases: one in which there is a fixed stabilizer with an elevator and one in which there is an adjustable stabilizer with an elevator. In the first case the airplane is trimmed with the elevator; in the second case, with the stabilizer while elevator deflection is zero. The resulting stick force is not calculated.

3.2 TRIM EQUATIONS

There are two unknowns to be calculated: angle of attack and either elevator deflection or stabilizer incidence. Therefore, two equations are needed: the lift equation and the pitching moment equation.

$$mg \cos \gamma = (C_{L_0} + C_{L_\alpha} \alpha + C_{L_{i_H}} i_H + C_{L_{\delta_E}} \delta_E) \bar{q} S \qquad (3.1)$$

$$0 = C_{m_0} + C_{m_\alpha} \alpha + C_{m_{i_H}} i_H + C_{m_{\delta_E}} \delta_E \qquad (3.2)$$

Since the airplane is considered to be in level flight, the flight path angle is either zero or very shallow, so $\cos \gamma = 1$. The zero on the left hand side of Equation (3.2) represents the moment equilibrium condition.

All possible power effects are assumed to be included in the above equations. These effects are calculated in the subroutine POWER (see

Chapter 5) and can be added to the stability derivatives as determined by the shape of the airplane.

The above equations can also be written in matrix form. For the case in which the airplane is trimmed with the elevator, they become:

$$\begin{bmatrix} C_{L_\alpha} & C_{L_{\delta_E}} \\ C_{m_\alpha} & C_{m_{\delta_E}} \end{bmatrix} \begin{Bmatrix} \alpha \\ \delta_E \end{Bmatrix} = \begin{Bmatrix} C_{L_1} - C_{L_0} - C_{L_{i_H}} i_H \\ -C_{m_0} - C_{m_{i_H}} i_H \end{Bmatrix} \tag{3.3}$$

in which:

$$C_{L_1} = \frac{mg}{\bar{q}S} \tag{3.4}$$

The value of i_H is fixed, e.g. at a value which yields minimum trim drag in cruise.

If the airplane is trimmed with i_H, the matrix form of Equations (3.1) and (3.2) becomes:

$$\begin{bmatrix} C_{L_\alpha} & C_{L_{i_H}} \\ C_{m_\alpha} & C_{m_{i_H}} \end{bmatrix} \begin{Bmatrix} \alpha \\ i_H \end{Bmatrix} = \begin{Bmatrix} C_{L_1} - C_{L_0} - C_{L_{\delta_E}} \delta_E \\ -C_{m_0} - C_{m_{\delta_E}} \delta_E \end{Bmatrix} \tag{3.5}$$

The value of δ_E will be taken as zero because it is not necessary to have two deflections at a time for moment trim (for force trim, i.e. zero stick force, it is different). This means that the right hand side of Equation (3.5) is reduced to:

$$\begin{Bmatrix} C_{L_1} - C_{L_0} \\ -C_{m_0} \end{Bmatrix} \tag{3.6}$$

The solution of the matrix equations (3.3) and (3.5) can be written as follows:

If one or more of the calculated values fall outside the limits, appropriate action must be taken.

3.3 PROGRAM DESCRIPTION

Subroutine TRIM calculates values of i_H, δ_E and C_{L_H} according to the equations described in the previous section. To let the computer know which case it has to consider, there is a control parameter KCONT. For KCONT = 10 the airplane is trimmed with the elevator, and for KCONT = 12 the airplane is trimmed with stabilizer incidence.

To make the program as efficient as possible, the dummy variables PEA, CUE, ARE and ESS are used. Values of these variables depend on the value of KCONT. They are put into a matrix equation; the solution vector of this equation consists of α and another dummy variable, CS, which is either i_H or δ_E, depending on the value of KCONT.

$$\{\underline{x}\}=[A]^{-1}\{\underline{b}\} \tag{3.7}$$

If the airplane is elevator trimmed, the solution becomes:

$$\begin{Bmatrix} \alpha \\ \delta_E \end{Bmatrix} = \frac{\begin{bmatrix} C_{m_{\delta_E}} & -C_{L_{\delta_E}} \\ -C_{m_\alpha} & C_{L_\alpha} \end{bmatrix}}{\begin{vmatrix} C_{L_\alpha} & C_{L_{\delta_E}} \\ C_{m_\alpha} & C_{m_{\delta_E}} \end{vmatrix}} \begin{Bmatrix} C_{L_1} & -C_{L_0} & -C_{L_{i_H}} i_H \\ -C_{m_0} & -C_{m_{i_H}} i_H & \end{Bmatrix} \tag{3.8}$$

In the case of trim with stabilizer incidence, the solution becomes, with the reduced right hand side of Equation (3.5):

$$\begin{Bmatrix} \alpha \\ i_H \end{Bmatrix} = \frac{\begin{bmatrix} C_{m_{i_H}} & -C_{L_{i_H}} \\ -C_{m_\alpha} & C_{L_\alpha} \end{bmatrix}}{\begin{vmatrix} C_{L_\alpha} & C_{L_{i_H}} \\ C_{m_\alpha} & C_{m_{i_H}} \end{vmatrix}} \begin{Bmatrix} C_{L_1} & -C_{L_0} \\ -C_{m_0} & \end{Bmatrix} \tag{3.9}$$

Once the airplane is trimmed, the horizontal tail load can be calculated according to:

$$C_{L_H} = C_{L_{\alpha_H}} (\alpha + i_H - \varepsilon + \tau_E \delta_E - \alpha_{0_H}) \tag{3.10}$$

Power effects are assumed to be included in $C_{L_{\alpha_H}}$ and in ε.

Checks are made on the limits of control surface deflections and on the maximum lift coefficient of the horizontal tail.

CHAPTER 4

GROUND EFFECT

4.1 INTRODUCTION

A method often used to compute ground effect is a simple one from Reference 4.1. This method uses only height above ground and aspect ratio as variables. However, References 4.2 and 4.3 indicate that, among other things, the lift coefficient generated by the wing is of great importance in determining the ground effect. Several methods for calculation of the ground effect were compared, and the method provided by Reference 4.5 was finally chosen for its completeness and relative simplicity.

4.2 DERIVATION OF EQUATIONS

In this chapter the method of Reference 4.5 will be described. Appendix A describes the other methods used in the evaluation. The method used in Reference 4.5 is based on a lifting line theory. In a situation where the wing is within a wingspan distance of the ground, a system of image vortices may be set up to account for the effect of ground proximity on the wing. The image vortex system is set up such that the boundary condition is met: i.e., the normal velocity on the ground plane is zero. Figure 4.1 depicts the situation.

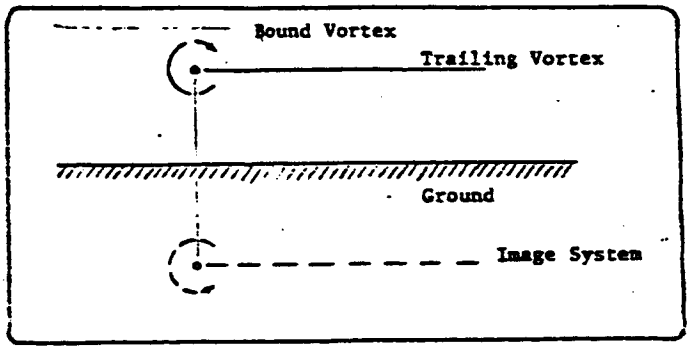

Figure 4.1: Image Vortex System

The effects of the image vortex system may be summarized as follows:

1. The image vortex of the bound vortex induces a velocity distribution in the opposite direction to the free stream velocity, thus reducing the lift. Also the camber and incidence of the wing airfoil are increased, thereby increasing the lift.
2. The image vortices of the trailing vortex system induce upwash at the wing which may be seen as an increase in wing angle of attack.

The effect of the bound image vortex may be found by applying Helmholtz's law which gives the decrease in speed at the airfoil:

$$\frac{\Delta V}{V_\infty} = \frac{-C_L}{8\pi\ h/c} \tag{4.1}$$

From this the increase in angle of attack to maintain C_ℓ may be found as:

$$\Delta\alpha = \frac{C_L^{\,2}}{4\pi\ h/c\ C_{L_\alpha}} \tag{4.2}$$

The effective increase in camber is proportional to $\Delta V/V_\infty$ and the chord length, inversely proportional to the height. By assuming that the average upwash induced by the image trailing vortex is equal to the upwash at the mid chord point, the decrease in angle of attack to maintain C_L constant may be found as:

$$\Delta\alpha = -.25\ \frac{\Delta V}{V_\infty}\ \frac{c}{2h} = -\frac{C_L}{64\pi\ (h/c)^2} \tag{4.3}$$

For finite wings the effects described above are less due to the finite length of the vortices. A correction factor β takes this into account. The total effect of the bound image vortex may now be found from:

$$\Delta_i\alpha = \beta \frac{C_L}{4\pi\ h/c_g} \left(\frac{C_L}{C_{L_\alpha}} - \frac{1}{16\ h/c_g} \right) \tag{4.4}$$

where:

$$\beta = \sqrt{1 + (2\ h_{eff}/b)^2} - 2\ h_{eff}/b \tag{4.5}$$

The effective height h_{eff} is as defined in Figure 4.2.

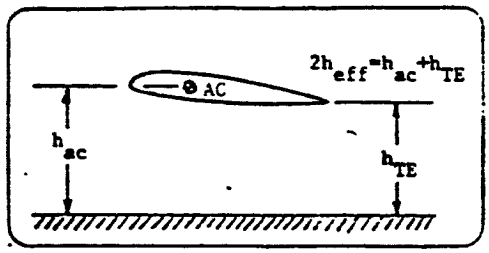

Figure 4.2: Definition of Effective Height

The induced upwash due to the images of the trailing vortex may be seen as a reduction in angle of attack to maintain C_ℓ constant:

$$\Delta_2\alpha = -\ \sigma\alpha_i \tag{4.6}$$

$$\text{where:}\quad \alpha_i = C_L/\pi AR \tag{4.7}$$

$$\sigma = \text{EXP}\left[-\ 2.48\ (2\ h_{eff}/b)^{.768} \right] \tag{4.8}$$

Again, σ is a correction factor which takes the finite length of the vortices into account. A general expression for swept wings of arbitrary aspect ratio is:

$$\Delta_2\alpha = -\ \sigma C_L\ (\ 1/C_{L_\alpha} - 1/C_{\ell_\alpha}\ ) \tag{4.9}$$

The total effect of the ground on the wing lift is as seen in Figure 4.3.

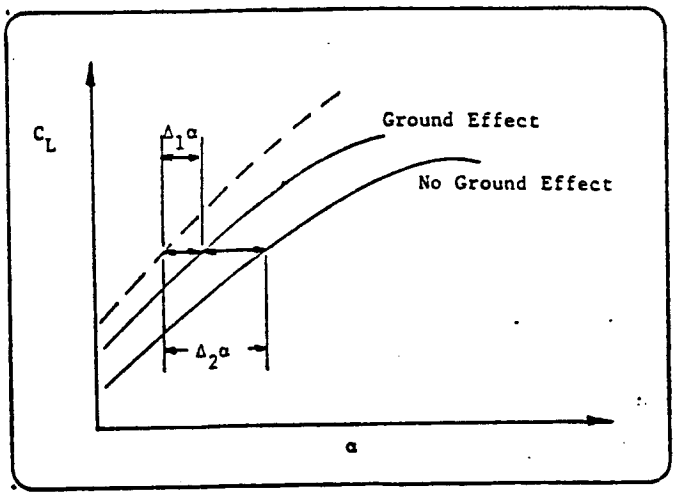

Figure 4.3: Total Effect of Ground-Proximity on Wing Lift

There are several other effects of ground proximity on the lift of the complete aircraft, generally of lesser importance than the effects described above. They are the following:

1. The image vortex system induces an upwash at the horizontal tailplane, thereby changing the lift. Also ground effect causes a shift in the wing center of pressure which causes a moment to be counteracted by elevator deflection. Furthermore, the image vortices of the tailplane itself causes upwash or downwash. All these effects are not easily calculated and of relatively small magnitude and therefore will be disregarded.

2. The pressure distribution around the airfoil changes considerably within ground proximity. The attainable $C_{L_{MAX}}$ usually will be decreased, which can have an important influence on V_{MU}. Again these effects cannot be expressed in a readily usable format.

Summarizing, the total effect of the ground proximity on the airplane lift may be expressed as:

$$\frac{C_L}{C_{L_\infty}} = 1+\sigma-\left[\frac{\sigma AR \cos\Lambda_{1/2}}{2\cos\Lambda_{1/2}+\sqrt{AR^2+(2\cos\Lambda_{1/2})^2}}\right]-\left[\frac{\beta}{4\pi h/\bar{c}}\left(C_{L_\infty}-\frac{C_{L_\alpha}}{16h/\bar{c}}\right)\right] \quad (4.10)$$

This expression provides the lift increase at constant angle of attack.

To account for the effect of flap deflection on height above the ground, the following expression was derived (see Figure 4.4):

The height of the trailing edge is:

$$h_{TE} \cong h_{ac} - h_f \quad \text{(disregarding } h_c\text{)} \quad (4.11)$$

$$\text{or: } h_{TE} \cong h_{ac} - \text{SIN } \delta_f \left(\frac{c_f}{c}\right)(c) \quad (4.12)$$

For the effective height, h_{eff}, it is seen that:

$$h_{eff} \cong 2\, h_{ac} - \text{SIN } \delta_f \left(\frac{c_f}{c}\right)(c) \quad (4.13)$$

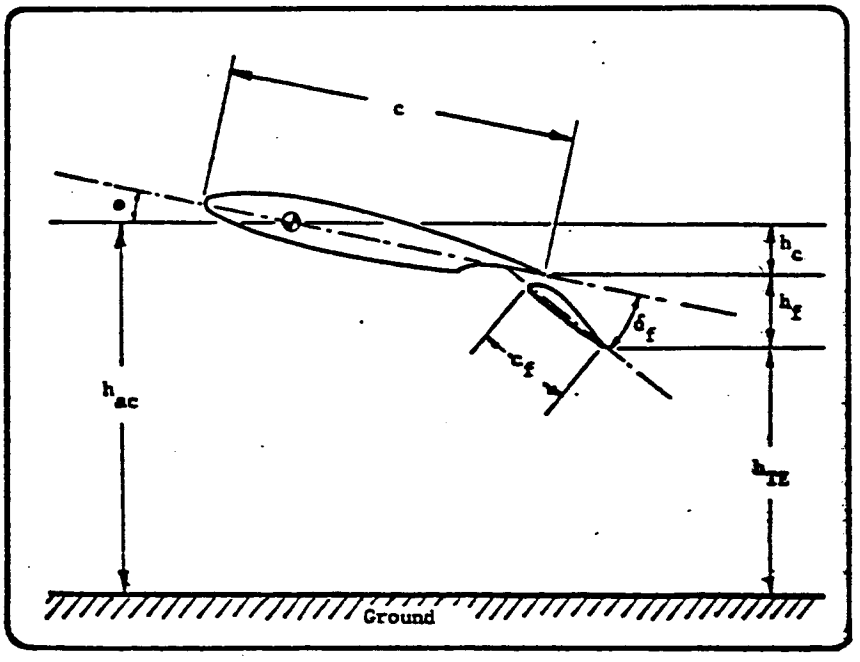

Figure 4.4: Definition of Geometry Parameters

4.3 REFERENCES

4.1 Perkins, C.D.
Hage, C.D.
Airplane Performance, Stability and Control, New York, John Wiley & Sons, 1949.

4.2 Corning, G.
Supersonic and Subsonic Airplane Design, Published by the author, 1953.

4.3 Baker, P.A.
Schweikhard, W.G.
Flight Evaluation of Ground Effect on Several Low-Aspect-Ratio Airplanes. NASA TN D-6053, 1970.

4.4 Hoak, D.E.
Ellison, D.E.
USAF Stability and Control Datcom. Air Force Flight Dynamics Laboratory, Wright Patterson Air Force Base, Ohio, 44533.

4.5 Torenbeek, E.
Synthesis of Subsonic Airplane Design. Delft University of Technology, Delft University Press, Delft, The Netherlands, 1976.

CHAPTER 5

POWER EFFECTS

5.1 INTRODUCTION

This chapter describes the subroutine that calculates the effect of power on various coefficients and stability derivatives. The program uses formulas and empirical data compiled from several references. The effects of propeller as well as jet thrust is computed for single- and twin-engine configurations.

5.2.1 DERIVATION OF EQUATIONS, EFFECTS ON LIFT, PROPELLER ENGINE

The effect of power on the aircraft characteristics may be split into two parts:

- Direct effect due to propeller forces
- Indirect effect due to propeller slipstream

The direct effects are the following (see Figure 5.1):

1. The propeller normal force adds to the total lift force and moment.
2. The propeller thrust force adds to the total lift force and moment.

The indirect forces are the following (see Figure 5.2):

3. Due to the slipstream over the wing (increased velocity), there will be an increase in wing normal force.
4. The propeller slipstream will act as a form of boundary layer control, thereby influencing the maximum attainable lift coefficient.
5. Due to the increase in velocity at the tail location, there will be a change in tail-lift.

6. The downwash at the tail will be influenced.

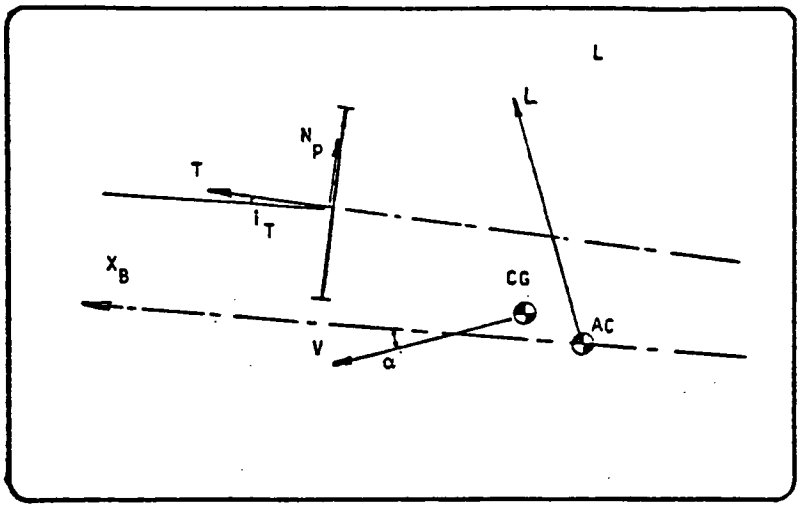

Figure 5.1: Direct effect of power

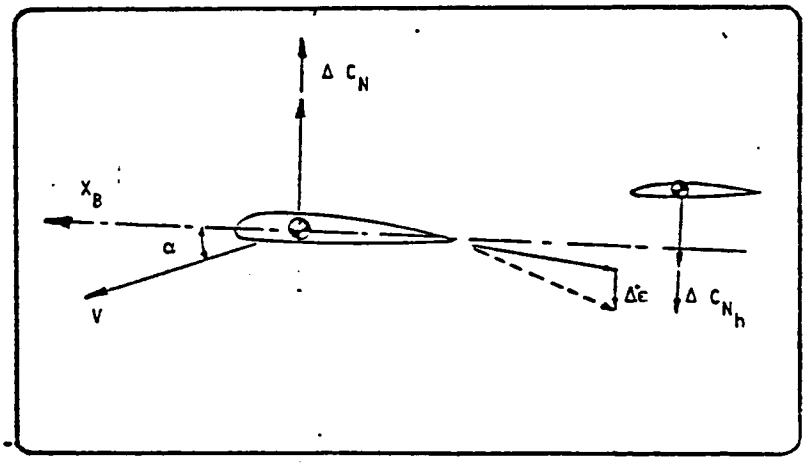

Figure 5.2; Indirect effects of power

The total lift coefficient of the airplane may now be expressed as:

$$C_L = C_{L_{Prop\text{-}off}} + (\Delta C_L)_T + (\Delta C_L)_{NP} + (\Delta C_L)_{\Delta\bar{q}_W} + (\Delta C_L)_{\varepsilon_p} + (\Delta C_{L_H})_{\Delta\bar{q}_H} + (\Delta C_{L_H})_{\Delta\varepsilon_H}$$

Propeller Forces — Propeller Slipstream Effects (Wing, Horizontal Tail)

(5.1)

5.2.1.1 EFFECT OF PROPELLER FORCES

The definition of the geometric parameters is as given in Figure 5.3.

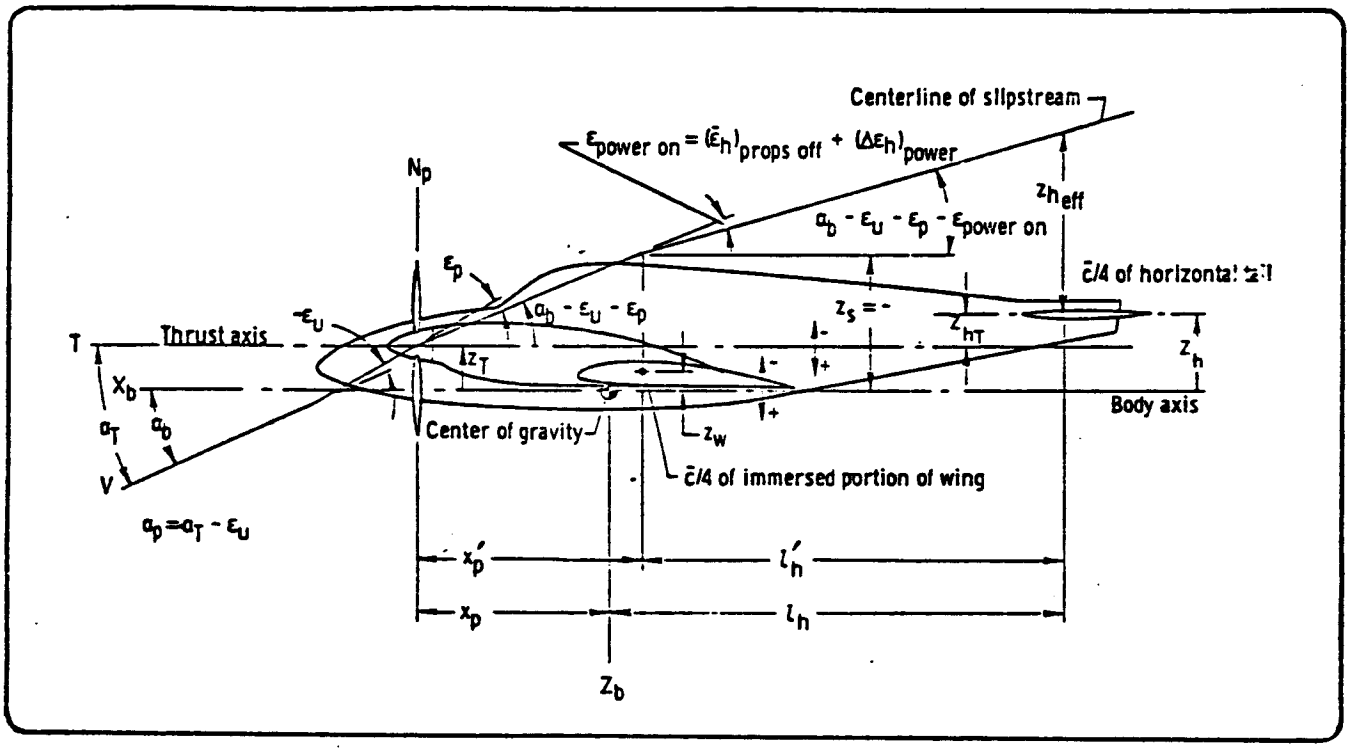

Figure 5.3.a: Definition of geometric parameters

The contribution of the thrust vector to lift is obtained from:

$$(\Delta C_L)_T = N\ (T_c'/prop)\ \sin \alpha_T \qquad (5.2)$$

where:

N is the number of engines

$$T_c'/prop = \frac{Thrust/prop}{\bar{q}_\infty S_W} \qquad (5.2.a)$$

$$\alpha_T = \alpha_b + i_T \qquad (5.2.b)$$

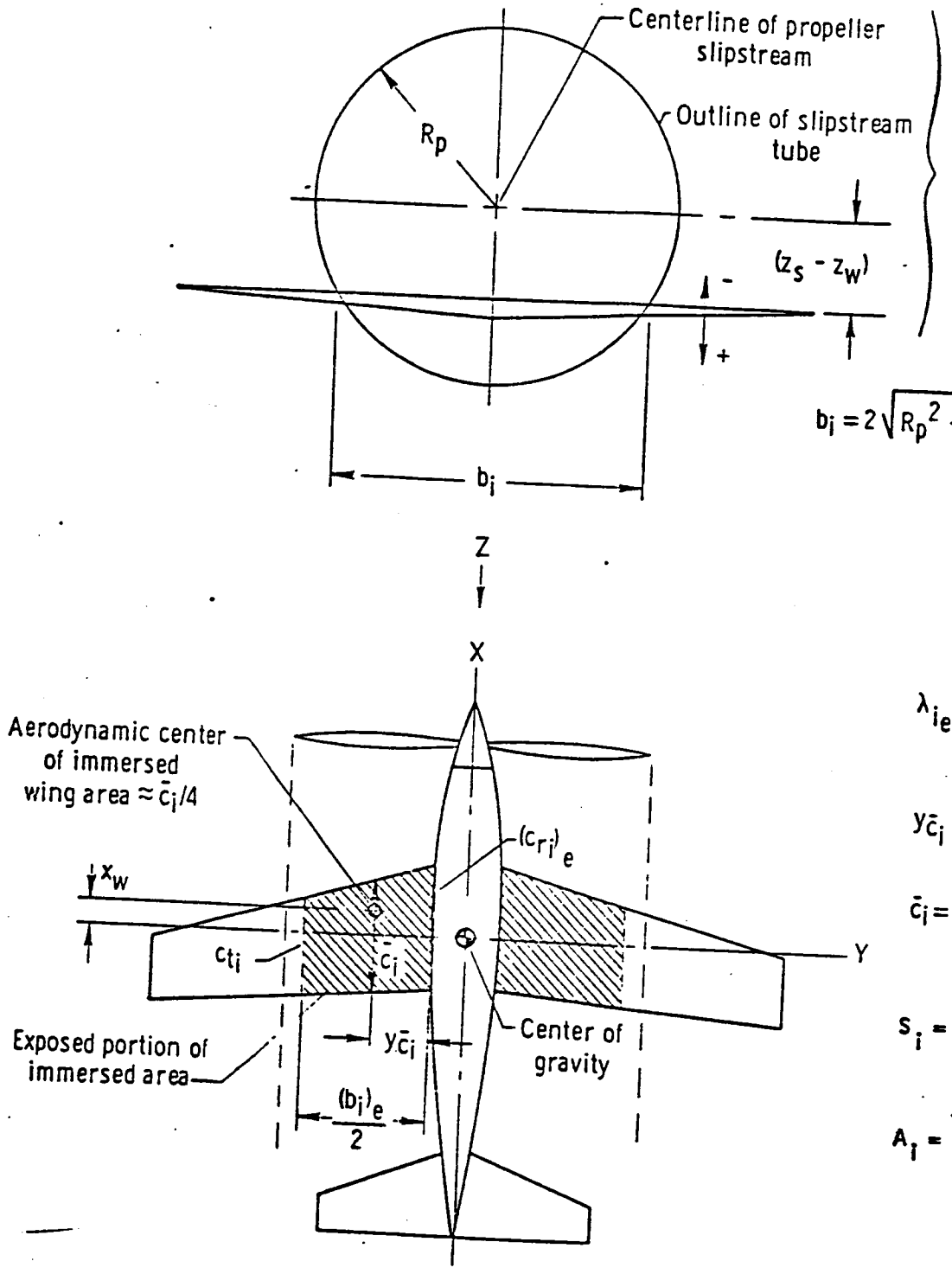

Figure 5.3.b: Definition of geometric parameters, single engine

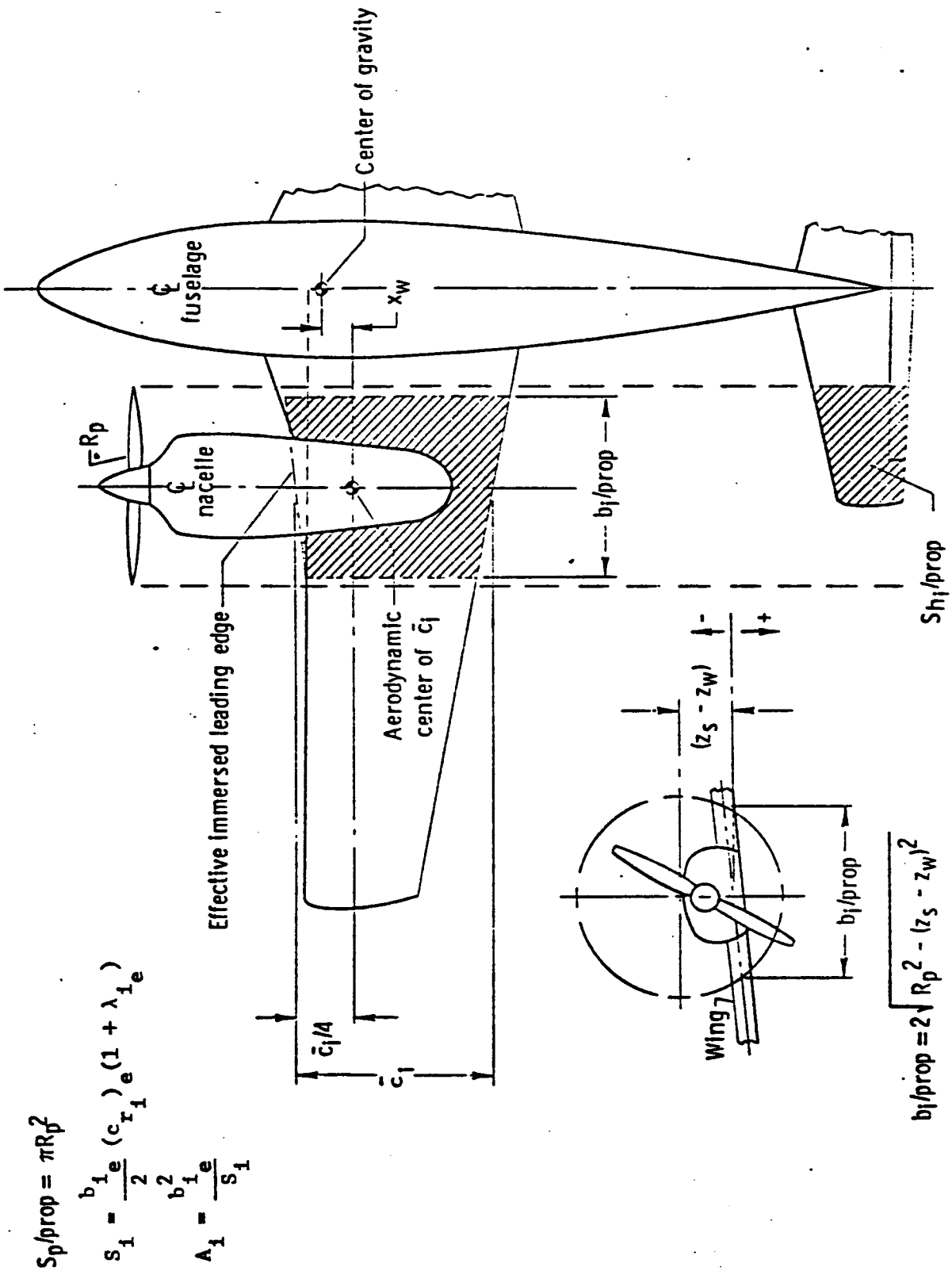

Figure 5.3.c: Definition of geometric parameters, multi engine

The contribution of the propeller normal force to the lift is obtained from the following equation from Reference 5.1:

$$(\Delta C_L)_{N_p} = N\, f\, C_{y'_{\psi_0}}\, \alpha_p \cos\alpha_T \frac{S_p/\text{prop}}{S_W} \qquad (5.3)$$

where:

f is the propeller inflow factor from Figure 5.4 as a function of

$$T_c = (T/\text{prop})/\rho V^2 D^2 \qquad (5.3.a)$$

$C_{y'_{\psi_0}}$ is a function of propeller type and operating condition. The values for a particular propeller family are given in Figure 5.5. Extrapolation to other propellers can be made by means of Figure 5.6 on the basis of the "side-force factor", SFF. This is a geometrical propeller parameter, approximated by Equation (5.4.)

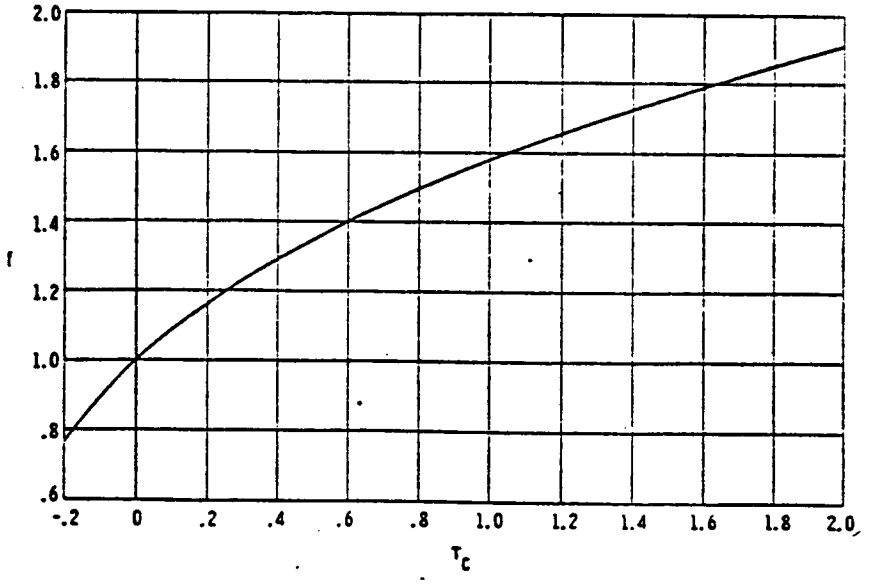

Figure 5.4: Variation of f with T_c (ref 5.1)

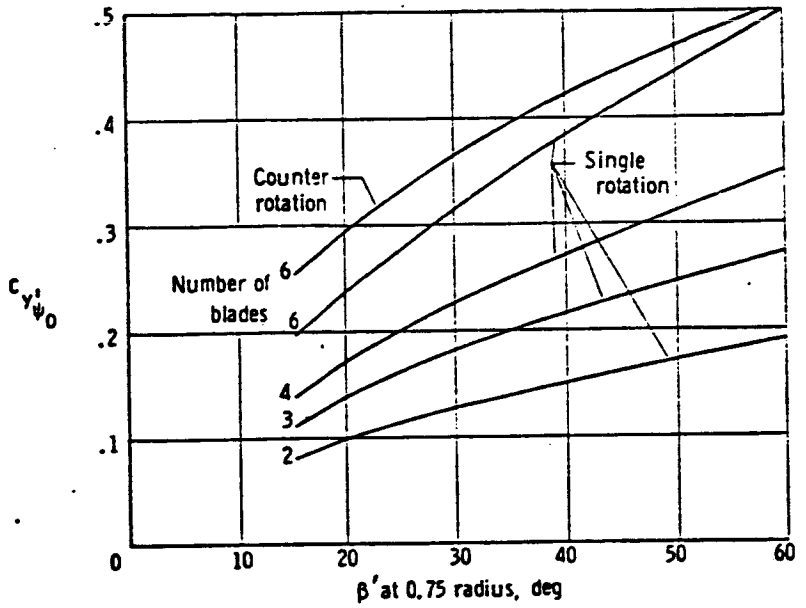

Figure 5.5: Propeller side-force coefficient (ref 5.1)

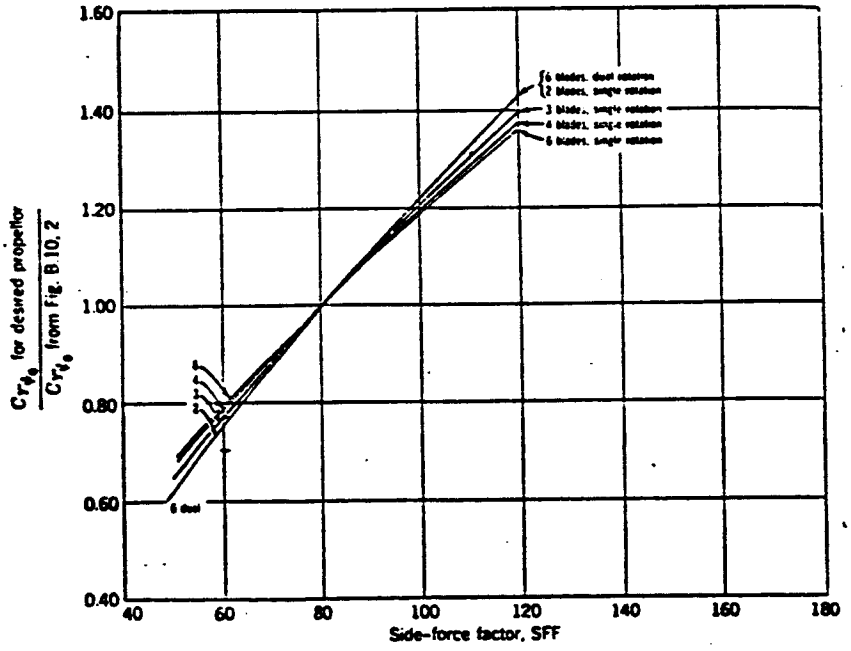

Figure 5.6: Propeller side-force coefficient as function of SFF (ref 5.1)

The propeller side force factor is given by:

$$SFF = 525\ [(b/D)_{0.3} + (b/D)_{0.6}] + 270\ (b/D)_{0.9} \qquad (5.4)$$

where:

b/D is the ratio of blade width to propeller diameter and the subscript is the relative radius at which the ratio is measured.

The local angle of attack of the propeller plane, α_p, may be obtained from:

$$\alpha_p = \alpha_T - \frac{\partial \varepsilon_u}{\partial_\alpha} (\alpha_W - \alpha_0) \qquad (5.5)$$

where:

$-\frac{\partial \varepsilon_u}{\partial_\alpha}$ is the upwash gradient at the propeller, obtained from Figure 5.7.

α_W is the wing angle of attack:

$$\alpha_W = \alpha_b + i_W$$

α_0 is the zero lift angle of the wing

The total effect of propeller side force on lift may now be calculated as follows:

$$(\Delta C_L)_{N_p} = N\ f\ C_{y'_{\psi_0}} \left[\frac{C_{y'_{\psi_0}} \text{ for desired prop}}{C_{y'_{\psi_0}} \text{ from Figure 5.5}}\right] \left\{\alpha_T - \frac{\partial \varepsilon_u}{\partial_\alpha}(\alpha_W - \alpha_0)\right\} \left(\frac{(S_p/\text{prop})}{S_W}\right) \cos \alpha_T \qquad (5.6)$$

Using HP 65 curve fitting routines, the following approximations were found:

$$f = 0.652 + 1.183\ LN\ (T_c + 1.3) \qquad (5.7)$$

$$C_{y'_{\psi_0}} = 0.013 \beta_{0.75}^{.657} + \{0.0125 + 0.001125\ \beta_{0.75}\}\ (B_L - 2) \qquad (5.8)$$

where:

$\beta_{0.75}$ is the blade angle at 75% of the propeller radius (in degrees)

$$\frac{C_{y'_{\psi_0}} \text{ actual prop}}{C_{y'_{\psi_0}} \text{ ref prop}} = -2.938 + 0.901 \, Ln(SFF) \qquad (5.9)$$

$$\frac{\partial \varepsilon_u}{\partial \alpha} = -0.1136 \left(\frac{X'_p}{C_i}\right)^{-1.8141} - 0.027 \, (AR - 4) \qquad (5.10)$$

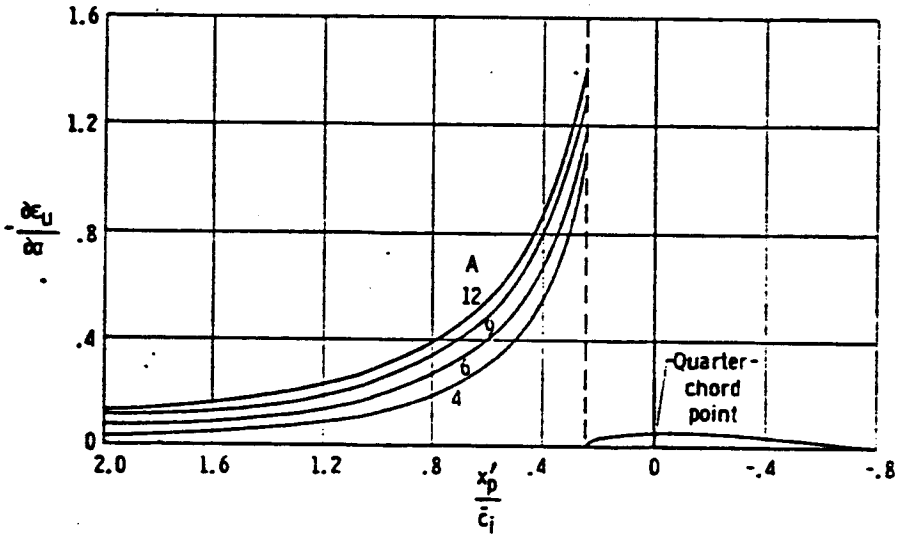

Figure 5.7: Upwash gradient at plane of symmetry for unswept wings (ref 5.2)

5.2.1.2 EFFECT OF PROPELLER SLIPSTREAM, INCREASE IN DYNAMIC PRESSURE

The contribution of power to lift due to change in dynamic pressure on the immersed portion of the wing is obtained from the following equation from Reference 5.2:

$$(\Delta C_L)_{\Delta \bar{q}_W} = N \, K_1 \left(\frac{\Delta \bar{q}_W}{\bar{q}_\infty}\right) \left(C_{L_W}\right)_{\text{prop off}} \left(\frac{(S_i/\text{prop})}{S_W}\right) \qquad (5.11)$$

where:

K_1 is an empirical correlation parameter for additional wing lift due to the power effects. May be obtained from Figure 5.8.

$\frac{\Delta\bar{q}_W}{\bar{q}_\infty}$ is the increase in dynamic pressure due to propeller slipstream on the immersed portion of the wing, as given by Equation 5.12:

$$\frac{\Delta\bar{q}_W}{\bar{q}_\infty} = \frac{S_W\ (T_c'/\text{prop})}{\pi\ R_p^2} \tag{5.12}$$

S_i/prop is the portion of the wing immersed in the propeller slipstream (per propeller), obtained from Figure 5.3 with:

$$S_i/\text{prop} = \frac{b_i/\text{prop}}{2}\ (c_{r_{i_e}})\ (1 + \lambda_{i_e}) \tag{5.13}$$

where:

$$b_i/\text{prop} = 2\sqrt{R_p^2 - (Z_S - Z_W)^2} \tag{5.14}$$

$$Z_S = -X_p' \tan(\alpha_b - \varepsilon_u - \varepsilon_p) - Z_T \tag{5.15}$$

The upwash at the propeller plane is obtained from Equation (5.10) and:

$$-\varepsilon_u = -\frac{\partial\varepsilon_u}{\partial_\alpha}\ (\alpha_W - \alpha_0) \tag{5.16}$$

The propeller-induced downwash is given by:

$$\varepsilon_p = \frac{\partial\varepsilon_p}{\partial\alpha_p}\ \alpha_p \tag{5.17}$$

The derivative $\partial\varepsilon_p/\partial\alpha_p$ follows from Reference 5.2:

$$\frac{\partial\varepsilon_p}{\partial\alpha_p} = C_1 + C_2\left(C_{y'_{\psi_0}}\right)_p \tag{5.18}$$

where:

C_1 and C_2 follow from Figure 5.9, and

$\left(C_{y_{\psi_0}} \right)_P$ follows from section 5.2.1.

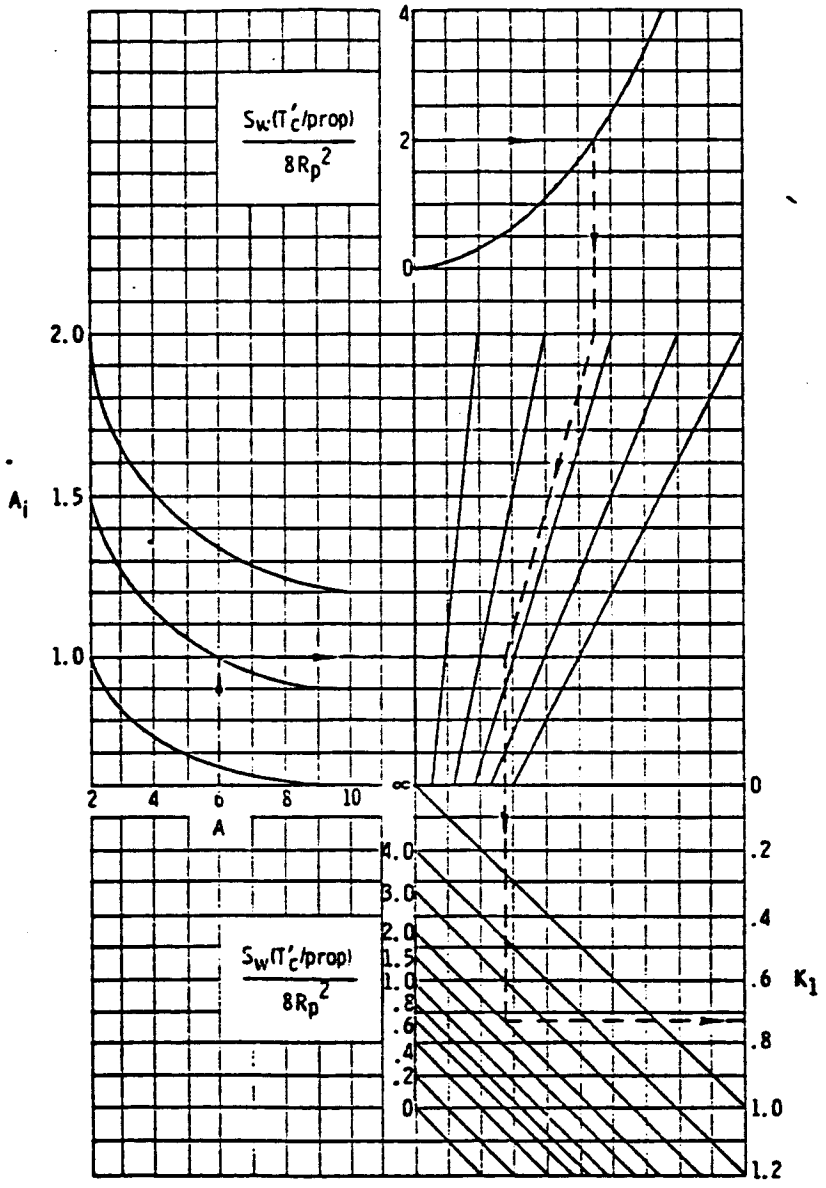

Figure 5.8: Empirical correlation factor for additional lift due to slipstream (ref 5.2)

Propeller angle of attack is given by Equation (5.5). Using curve fitting routines, it may be found for Figure 5.8:

$$X_1 = 2.6384\ A_i^{2.0312} + (-3.8116 + 4.2237\ A_i - 1.6186\ A_i^2)\ A + \\ + (0.0418\ A_i^{1.3383})\ A^2 \qquad (5.19)$$

$$X_2 = 1.9938 + 1.2194\ LN\left(\frac{S_W(T_c'/prop)}{8\ R_p^{\ 2}}\right) \qquad (5.20)$$

$$X_3 = \frac{X_2(X_1 + 3)}{10} \qquad (5.21)$$

$$K_1 = + 0.9191\ e^{\left(-0.3663\ \frac{S_W\ (T_c'/prop)}{8\ R_p^{\ 2}}\right)} + \frac{X_3}{5} \qquad (5.22)$$

The equation for the propeller induced downwash was found to be:

$$\frac{\partial \varepsilon_p}{\partial \alpha_p} = 0.3732 + 0.1703\ LN\left(\frac{S_W\ (T_c'/prop)}{8\ R_p^{\ 2}}\right) + \\ + \left[0.2115 - 0.0504\left(\frac{S_W(T_c'/prop)}{8\ R_p^{\ 2}}\right)\right]\left(C_{y'_{\psi_0}}\right)_p \qquad (5.23)$$

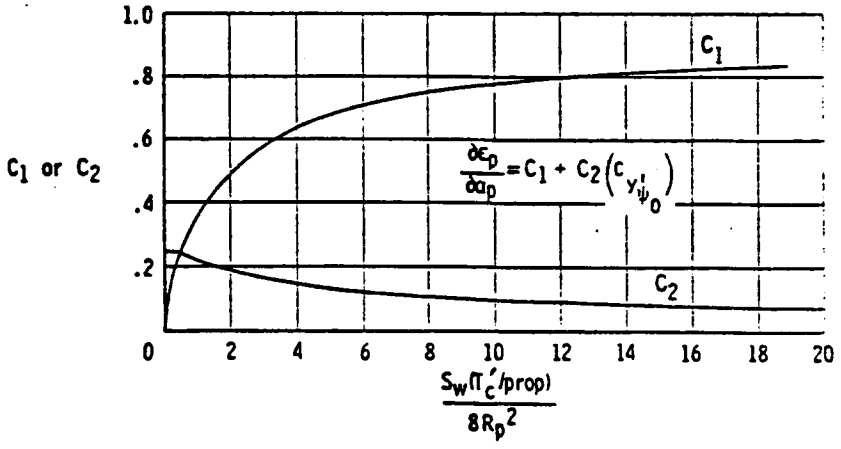

Figure 5.9: Propeller Induced downwash (ref 5.2)

5.2.1.3 EFFECT OF PROPELLER SLIPSTREAM, PROPELLER DOWNWASH ε_p

The contribution of power to lift due to a change in angle of attack as a result of propeller downwash, ε_p, may be obtained from:

$$(\Delta C_L)_{\varepsilon_p} = N\left(1 + \frac{\Delta \bar{q}_W}{\bar{q}_\infty}\right)\left(C_{L_\alpha}\right)_{\text{prop off}} (\Delta\alpha)_{S_i} \frac{(S_i/\text{prop})}{S_W} \qquad (5.24)$$

(Ref. 5.2)

where:

$\frac{\Delta \bar{q}_W}{\bar{q}_\infty}$ is defined by Equation (5.12)

S_i/prop is defined by Equation (5.13)

and

$$(\Delta\alpha)_{S_i} = -\frac{\varepsilon_p}{1 - \frac{\partial \varepsilon_u}{\partial \alpha}}$$ is the change in angle of attack (5.25)

5.2.1.4 EFFECT OF POWER ON MAXIMUM LIFT

Thus far, the effect of power on lift at discrete angles of attack has been calculated. Power also has an effect on maximum attainable lift, since the angle of attack at which stall occurs first will be increased with power. This depends primarily on the ratio of immersed wing area to total wing area. Figure 5.10 illustrates the effect.

The increment in maximum lift due to power may be obtained from the following empirical equation:

$$\Delta C_{L_{MAX}} = K_2 \, (\Delta C_L')_{\text{Power}} \qquad (5.26)$$

where:

$(\Delta C_L')_{\text{Power}}$ is the increment in tail-off lift due to power at power-off maximum lift angle of attack.

K_2 is a correction for immersed wing area, obtained from Figure 5.11.

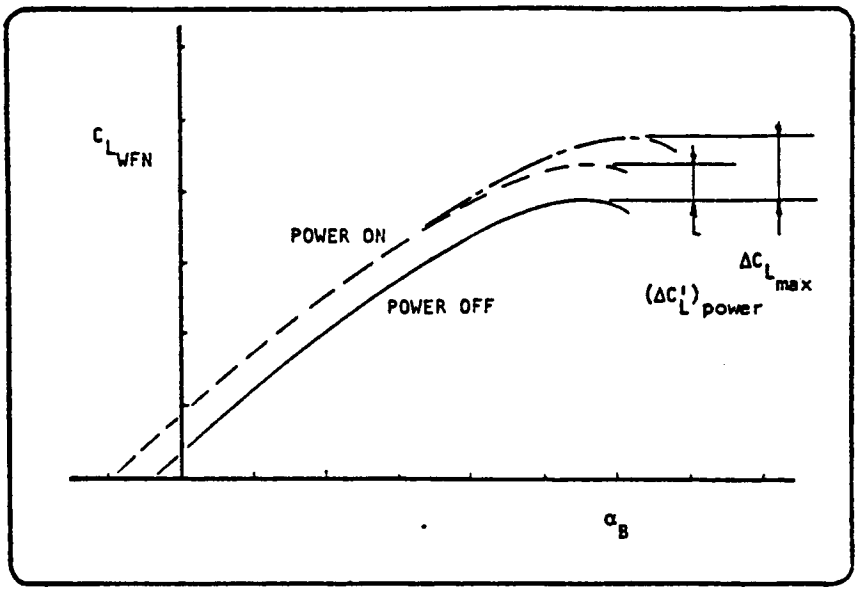

Figure 5.10: Effect of power on maximum lift

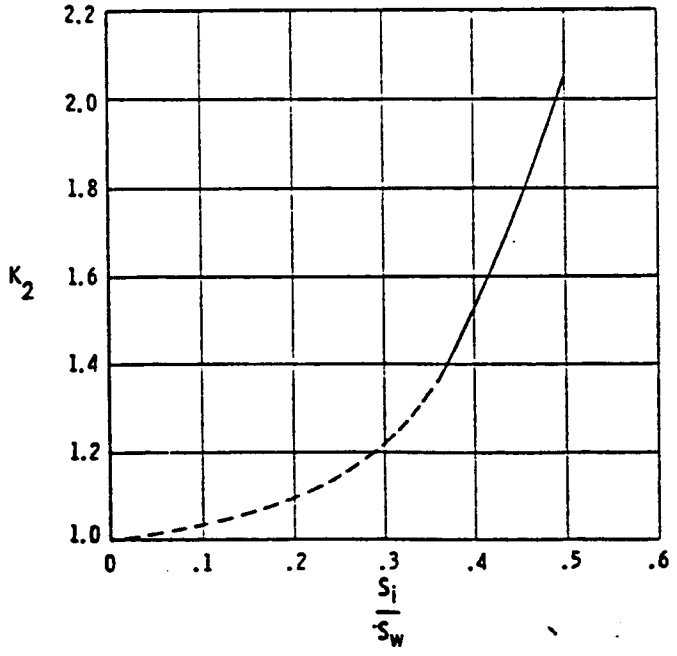

Figure 5.11: Correction factor for maximum lift (ref 5.2)

Using curve-fitting methods, it was found that the Factor K_2 may be represented by:

$$K_2 = 1.1854 - 2.1129 \frac{S_i}{S_W} + 7.6104 \left(\frac{S_i}{S_W}\right)^2 \qquad (5.27)$$

By using the foregoing procedures, the tail-off lift characteristics of the airplane can be calculated. Now the effect of power on tail-plane lift will be calculated. The effect of the change in lift of the horizontal tail on the total lift of the airplane is small. However, the effect on pitching moment is significant.

5.2.1.5 EFFECT OF POWER INDUCED DOWNWASH ON HORIZONTAL TAIL-LIFT

The power induced change in downwash at the tail, $(\Delta\varepsilon_H)_{Power}$, may be estimated for single engine airplanes by using Figure 5.12 or for multiengine airplanes by using Figure 5.13. These figures are from Reference 5.2. The variables involved are:

$(\bar{\varepsilon}_H)_{props\ off}$	Propeller-off downwash angle calculated in subroutine DOWNWS.
$T_c'/prop$	Propeller thrust coefficient.
S_W	Wing area.
R_p	Propeller radius.
Z_{H_T}	Distance from thrust axis to horizontal tail (see Figure 5.3a).

Curve-fitting methods yielded the following approximations for Figures 5.12 and 5.13. The effect of power on downwash for single engine airplanes may be calculated with:

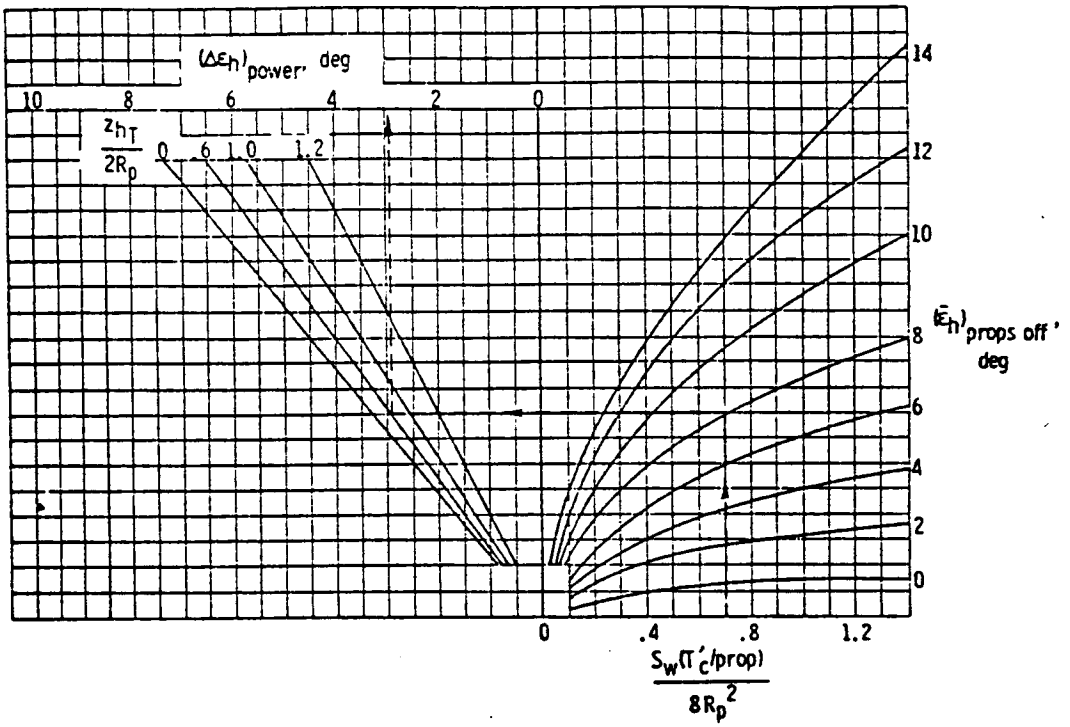

Figure 5.12: Effect of power on downwash for single engine airplanes (ref 5.2)

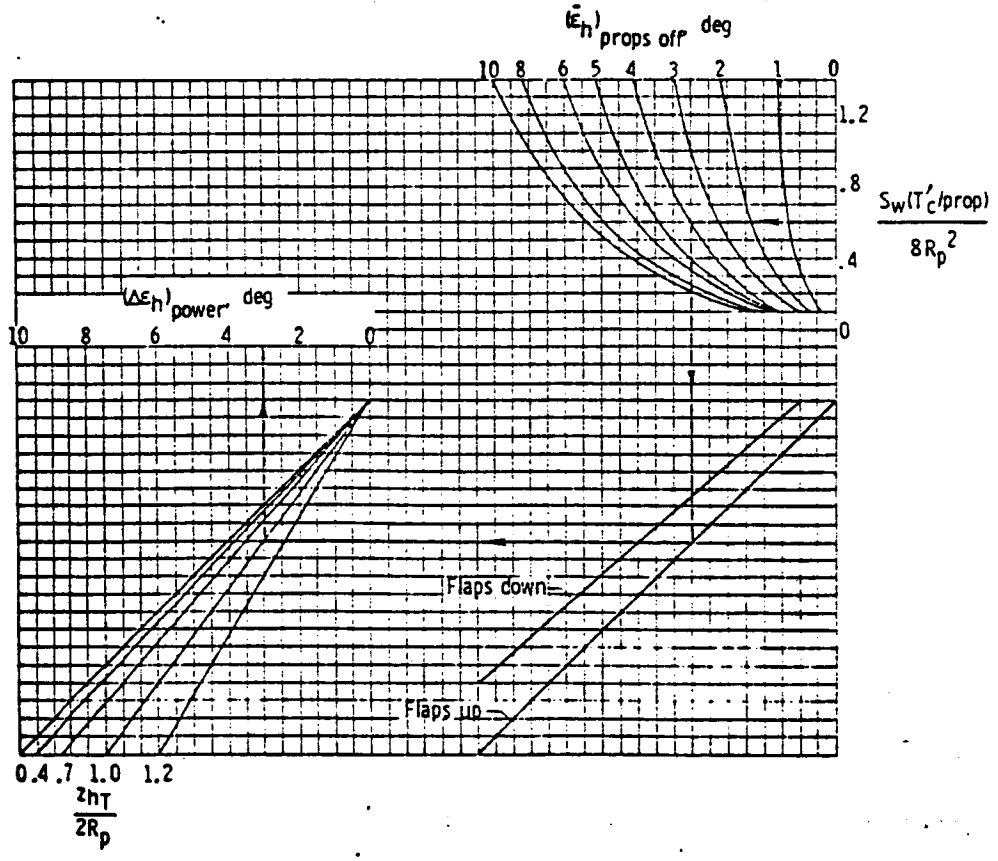

Figure 5.13: Effect of power on downwash for multiengine airplanes (ref 5.2)

$$X_4 = 0.5376e^{0.0688(\bar{\varepsilon}_h)_{\text{props off}}} + 0.4366(\bar{\varepsilon}_h)^{1.2345}_{\text{props off}} \left(\frac{S_W(T_c'/\text{prop})}{8\,R_p^2}\right) - \left\{0.1091(\bar{\varepsilon}_h)^{1.3152}_{\text{props off}}\right\}\left(\frac{S_W(T_c'/\text{prop})}{8\,R_p^2}\right)^2 \quad (5.28)$$

$$(\Delta\varepsilon_H)_{\text{Power}} = X_4\left\{0.8189 - 0.0185\,\frac{Z_{H_T}}{2R_p} - 0.1953\left(\frac{Z_{H_T}}{2R_p}\right)^2\right\} \quad (5.29)$$

For multiengine airplanes the following equations can be used:

$$X_5 = -1.0234 + 0.9775(\bar{\varepsilon}_H)_{\text{prop off}} - 0.1032(\bar{\varepsilon}_H)^2_{\text{prop off}} + \left\{3.5191 - 0.2409(\bar{\varepsilon}_H)_{\text{prop off}} + 0.2025(\bar{\varepsilon}_H)^2_{\text{prop off}}\right\}\left(\frac{S_W(T_c'/\text{prop})}{8\,R_p^2}\right) - \left\{0.8738e^{0.2253(\bar{\varepsilon}_H)_{\text{prop off}}}\right\}\left(\frac{S_W(T_c'/\text{prop})}{8\,R_p^2}\right)^2 \quad (5.30)$$

$X_6 = X_5$(No Flaps) (5.31.a) OR $X_6 = -0.5 + 0.889\,X_5$ (Flaps) (5.31.b)

where: $(\varepsilon_H)_{\text{power off}}$ in degrees.

$$(\Delta\varepsilon_H)_{\text{power}} = \left\{0.9951 + 0.0419\,\frac{Z_{H_T}}{2R_p} - 0.3021\left(\frac{Z_{H_T}}{2R_p}\right)^2\right\} X_6 \quad (5.32)$$

where the height of the horizontal tail above the thrust line, Z_{H_T}, is given by the following equation, see Figure 5.3.a,

$$Z_{H_T} = Z_H - Z_T - \left(\tan(i_T)\right)\left(X_p + \ell_H\right) \quad (5.32.a)$$

To calculate the effect of power on dynamic pressure ratio at the tail, $\frac{\Delta\bar{q}_h}{\bar{q}_\infty}$, use can be made of Figure 5.14 (from Reference 5.2). For low values of T_c' (close to zero), use should be made of the free-flight value for the tail.

$$X_7 = \left\{0.34 + \frac{S_W(T_c'/\text{prop})}{8\,R_p^{\,2}}\right\}\left\{0.865\left(\frac{S_{h_i}}{S_h}\right)\right\} \tag{5.33}$$

$$\frac{\Delta\bar{q}_H}{\bar{q}_\infty} = \left\{1.0102 - 0.1438\,\frac{Z_{H_{eff}}}{R_p} - 0.3904\left(\frac{Z_{H_{eff}}}{R_p}\right)^2\right\} X_7 \tag{5.34}$$

The effective height of the propeller slipstream, $Z_{H_{eff}}$, at the tail, may be calculated as follows (see Figure 5.3a):

$$Z_{H_{eff}} = Z_S - \ell'_H\left\{\tan\ \alpha_b - \varepsilon_u - (\varepsilon_H)_{\text{power off}} - (\Delta\varepsilon_H)_{\text{power}}\right\} - Z_H \tag{5.34.a}$$

where:

Z_S is the vertical distance from X - body axis to slipstream centerline at 1/4 c_i:

$$Z_S = -X'_p \tan(\alpha_b - \varepsilon_u - \varepsilon_p) - Z_T \tag{5.34.b}$$

The change in lift due to above effects may be obtained from the following relation:

$$C_{L_{H(hf)}} = \left[\left(C_{L_{H(hf)}}\right)_{S_H,\ \bar{q}_H/\bar{q}_\infty = 1}\right]\frac{S_H}{S_W}\,\frac{\Delta\bar{q}_H}{\bar{q}_\infty} \tag{5.35}$$

$$- C_{L_{\alpha_H}}\,\Delta E_{H_{power}}\,\frac{S_H}{S_W}\left(\frac{\bar{q}_H}{\bar{q}_\infty} + \frac{\Delta\bar{q}_H}{\bar{q}_\infty}\right) \tag{5.36}$$

$\left(C_{L_{H(hf)}}\right)_{S_H,\ \bar{q}_H/\bar{q}_\infty=1}$ is the lift of the tail, referenced to the tail area and a dynamic pressure ratio of one.

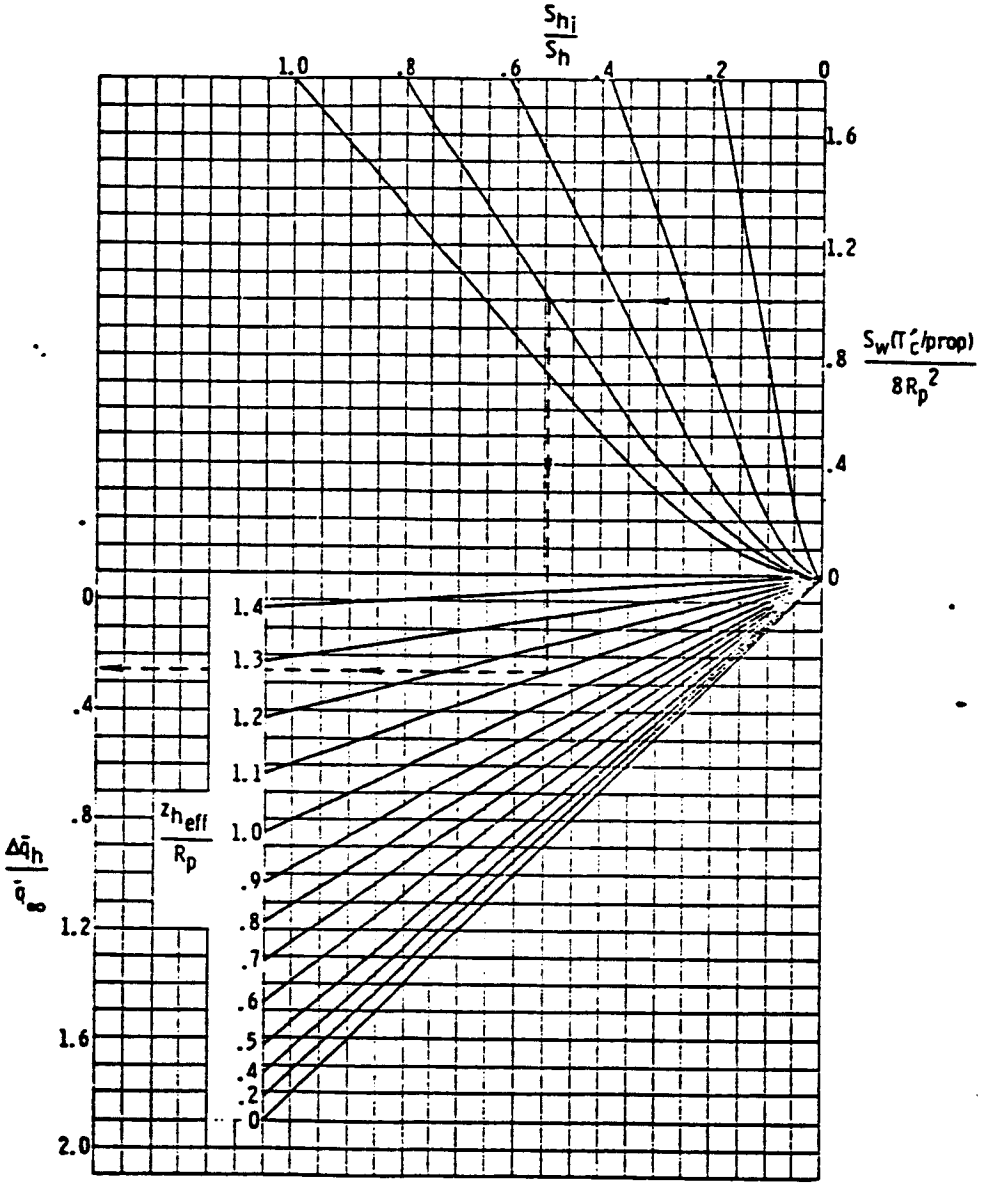

Figure 5.14: Effect of power on the dynamic pressure ratio at the tail (ref 5.2)

The tail lift may be obtained from:

$$C_{L_{H(hf)_{S_H,\ \bar{q}_u/\bar{q}_\infty=1}}} = C_{L_{\alpha_H}} (\alpha_H - \alpha_{0_H}) \qquad (5.36.a)$$

where:

$$\alpha_H = \alpha_b - (\varepsilon_H)_{\text{power off}} - \Delta\varepsilon_{H_{\text{power}}} + i_H + \frac{\partial\alpha}{\partial\delta}\delta_E \qquad (5.36.b)$$

The area of the horizontal tail, immersed in the slipstream, may be calculated as follows (see Figure 5.3c):

Single-engine airplanes:

$$S_{H_i} = \left(2\sqrt{R_p^2 - Z_{H_{eff}}^2}\ / b_{H_T}\right) S_{H_T} \qquad (5.37)$$

Multi-engine airplanes:

$$S_{H_i} = \left[\frac{(b_{H_T}/2 - Y_T) + \sqrt{R_p^2 - Z_{H_{eff}}^2}}{b_H/2}\right] S_{H_T} \qquad (5.38)$$

The total effect of power on lift may now be calculated as indicated by Equation (5.1.)

Now that the effects of power on the lift force of the airplane are known, the effects on moment about the Y-axis may be calculated.

5.2.2 DERIVATION OF EQUATIONS, EFFECT ON PITCHING MOMENT, PROPELLER ENGINE

The total effect of power on pitching moment may be summarized as in Equation (5.39):

$$C_m = (C_{m_{wfn}})_{\text{Power off}} + (\Delta C_m)_T + (\Delta C_m)_{NP} + (\Delta C_{m_0})_{\Delta\bar{q}_W} + (\Delta C_m)_{WL} + (\Delta C_m)_{np} + \bar{C}_{m_{H(hf)}} \qquad (5.39)$$

where:

$(C_{m_{wfn}})_{\text{power off}}$ is the power-off, tail-off pitching moment

$(\Delta C_m)_T$ is the pitching moment due to offset thrust.

$(\Delta C_m)_{N_p}$ is the pitching moment due to offset propeller normal force.

$(\Delta C_{m_0})_{\Delta \bar{q}_W}$ is the effect of propeller slipstream dynamic pressure increment on zero lift pitching moment.

$(\Delta C_m)_{WL}$ is the total effect on pitching moment due to slipstream dynamic pressure and angle of attack changes.

$(\Delta C_m)_{np}$ is the effect of propeller slipstream on nacelle pitching moment.

$(\Delta C_m)_h$ is the effect of dynamic pressure and downwash on pitching moment due to tail-lift.

$(\overline{C_{m_H}})_{hf}$ is the power-on pitching moment of the tail.

5.2.2.1 PITCHING MOMENT DUE TO THRUST OFFSET

The pitching moment due to thrust offset may be obtained from:

$$(\Delta C_m)_T = N\ (T'_c/\text{prop})\left(\frac{Z_T}{\bar{c}_W}\right) \qquad (5.40)$$

where the geometric parameters are defined in Figure 5.3a.

5.2.2.2 PITCHING MOMENT DUE TO PROPELLER NORMAL FORCE

This effect may be calculated with:

$$(\Delta C_m)_{N_p} = (\Delta C_L)_{N_p} \left(\frac{X_p}{\bar{c}_W}\right)\left(\frac{1}{\cos\alpha_T}\right) \tag{5.41}$$

where:

$(\Delta C_L)_{N_p}$ is the propeller normal force, to be obtained from Equation (5.3).

The geometric parameters are defined in Figure 5.3a.

5.2.2.3 THE ZERO LIFT PITCHING INCREMENT

Due to the effect of slipstream on the wing and nacelles at zero lift, there will be a change in zero lift pitching moment:

$$(\Delta C_{m_0})_{\Delta\bar{q}_W} = K_{\Delta\bar{q}_W} (C_{m_0})_{i_{prop\ off}} \quad \text{(Ref. 5.2)} \tag{5.42}$$

where:

$K_{\Delta\bar{q}_W}$ is the factor that takes the power effect into account, to be calculated from Equation (5.43).

$$K_{\Delta\bar{q}_W} = \left(\frac{\Delta\bar{q}_W}{\bar{q}_\infty}\right)\left(\frac{S_i}{S_W}\right)\left(\frac{\bar{c}_i}{\bar{c}_W}\right) \quad \text{(Ref. 5.2)} \tag{5.43}$$

where:

$\frac{\Delta\bar{q}_W}{\bar{q}_\infty}$ is the increase in dynamic pressure ratio, to be calculated with Equation 5.12.

S_i is the immersed portion of the wing area (see Figure 5.3b and c):

$$S_i = \frac{b_{i_e}}{2} (C_{r_i})_e (1 + \lambda_{ie}) \tag{5.44}$$

The zero lift pitching moment $(C_{m_0})_{i_{prop\ off}}$ may be determined as follows:

For twin-engine airplanes:

$$(C_{m_0})_{i_{prop\ off}} = (C_{m_0})_{wn_{prop\ off}} - (C_{m_0})_{\text{Area not immersed}} \tag{5.45}$$

where:

$(C_{m_0})_{wn_{prop\ off}}$ is the propeller-off C_{m_0} of the wing and nacelles, obtained elsewhere.

and:

$$(C_{m_0})_{\text{Area not immersed}} = (C_{m_0})_{W_{prop\ off}} \left[\frac{S_W - S_i}{S_W}\right]\left[\frac{\bar{c}_{\text{not immersed}}}{\bar{c}_W}\right] \tag{5.46}$$

where:

$(C_{m_0})_{W_{prop\ off}}$ is the propeller-off C_{m_0} of the wing

$$\bar{c}_{\text{not immersed}} = \frac{S_W - S_i}{b_W - b_i} \tag{5.47}$$

For a single-engine airplane:

Replace $(C_{m_0})_{wn_{prop\ off}}$ with $(C_{m_0})_{wf_{prop\ off}}$ which is the propeller-off C_{m_0} of the wing and fuselage

5.2.2.4 PITCHING MOMENT INCREMENT DUE TO CHANGE IN WING LIFT

This power effect may simply be obtained from:

$$(\Delta C_m)_{WL} = -\left\{(\Delta C_L)_{\Delta \bar{q}_w} + (\Delta C_L)_{\epsilon_r}\right\}\frac{X_W}{\bar{c}_W} \tag{5.48}$$

where:

X_W is the distance between aerodynamic center of the immersed wing and the center of gravity.

$$X_W = \ell_{cg} - \left\{ \ell_{l/4\bar{c}_W} + (Y_{\bar{c}_i} + b_c/2) \tan \Lambda_{l/4\bar{c}} \right\} \qquad (5.49)$$

See Figure 5.15 for geometry definition.

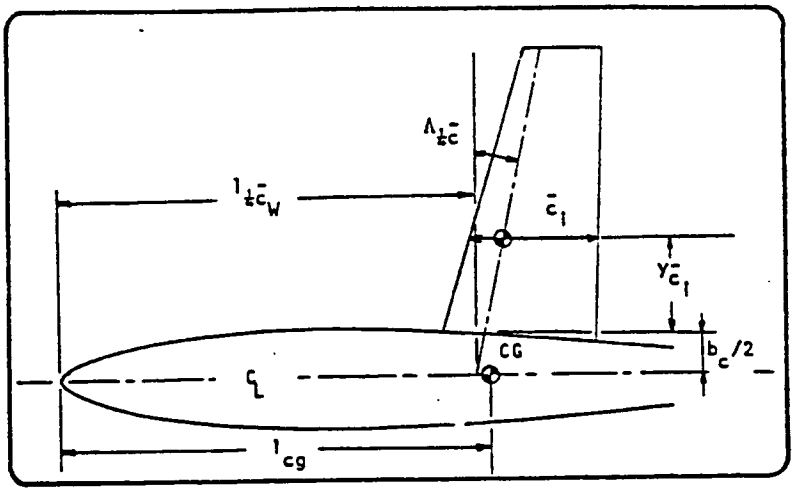

Figure 5.15: Geometry of the wing

The increments in lift due to power, $(\Delta C_L)_{\Delta\bar{q}_w}$ and $(\Delta C_L)_{\varepsilon_p}$, may be found from Equations (5.11) and (5.24), respectively.

5.2.2.5 PITCHING MOMENT DUE TO EFFECT OF SLIPSTREAM ON NACELLE

For multi-engine installations the effect of the propeller slipstream on nacelle pitching moments may be calculated with Equation (5.50)(from Reference 5.2):

$$(\Delta C_m)_{n_p} = - \frac{N}{36.5\ S_W \bar{c}_W} \int w_n^2 (\varepsilon_p + \varepsilon_u) \left(1 + \frac{\Delta\bar{q}_w}{\bar{q}_\infty}\right) dx \qquad (5.50)$$

OR:

$$(\Delta C_m)_{n_p} = \left[- \frac{N(\varepsilon_p + \varepsilon_u)}{36.5\ S_W \bar{c}_W} \left(1 + \frac{\Delta\bar{q}_w}{\bar{q}_\infty}\right) \int w_n^2 dx \right] \qquad (5.51)$$

where:

ε_p and ε_u are obtained from Equations (5.16) and (5.17).

$\frac{\Delta \bar{q}_w}{\bar{q}_\infty}$ is obtained from Equation (5.12).

$\int w_n^2 dx$ is a function of the shape of the nacelle (see Figures 5.16 and 5.18).

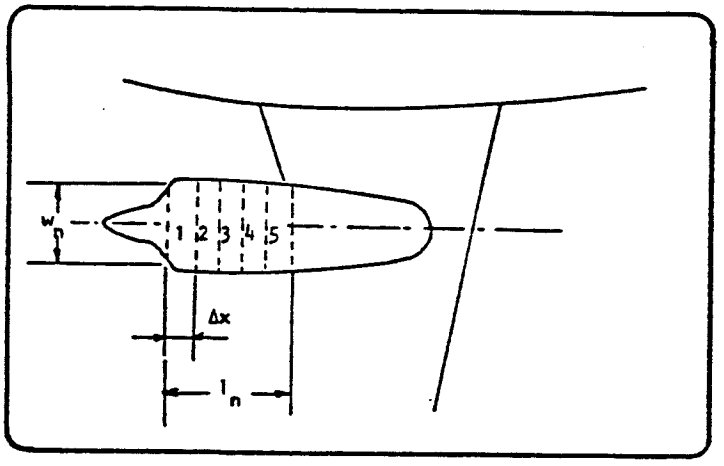

Figure 5.16: Shape of nacelle (twin engine)

To see if there is a general trend in the shape of nacelles, some research was done. A distinction was made between turbine engines and reciprocating engines. The nacelle was divided into five equal parts, as shown in Figure 5.16. Then the parameter $w_n^2 \Delta x$ was determined as a function of nacelle length, ℓ_n. The results are shown in Figures 5.17 and 5.19. Also included in this figure are two straight-line approximations. The equations for the nacelle shape parameter $w_n^2 \Delta x$ thus found for twin engine aircraft are:

Reciprocating engines:

$$w_n^2 \Delta x = -3.07 + 10.51\ \ell_n \tag{5.52}$$

Turbine engines:

$$w_n^2 \Delta x = -6.84 + 6.90\ \ell_n \tag{5.53}$$

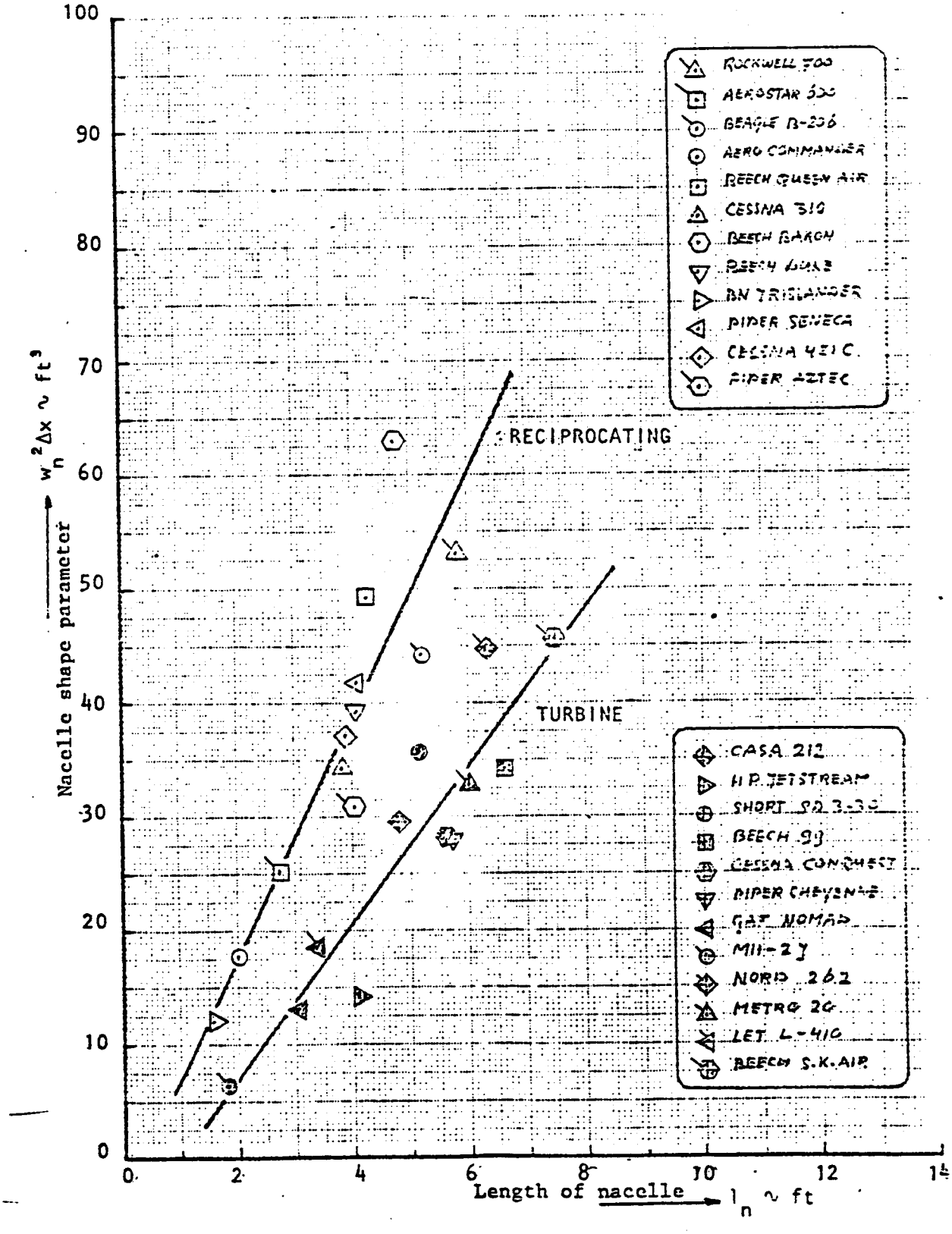

Figure 5.17: Nacelle shape parameter, twin engine airplanes

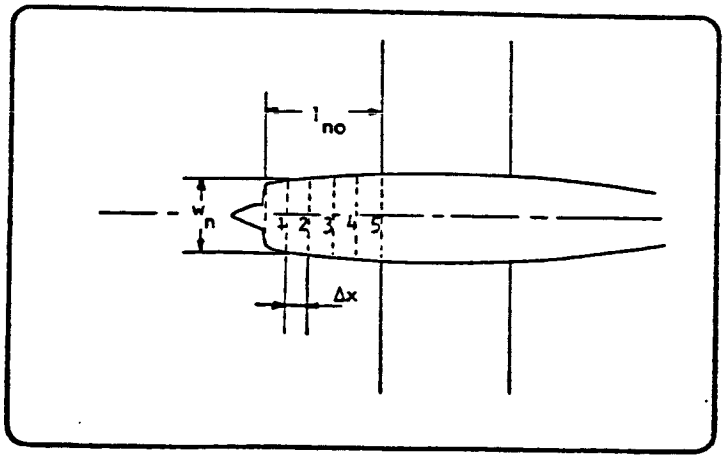

Figure 5.18: Shape of nacelle (single engine)

For single engine aircraft the following approximation was found:

$$w_n^2 \Delta x = -28.06 + 16.59\ l_{no} \tag{5.54a}$$

5.2.2.6 PITCHING MOMENT DUE TO EFFECT OF POWER ON TAIL

The effect of power on the pitching moment contribution of the tail will be the increment in lift of the tail, $C_{L_{H(hf)}}$, computed in Equation (5.35), multiplied by the normalized moment arm, $l_H/\bar{c}$. The result is given as:

$$(\Delta C_m)_h = C_{L_{H(hf)}} \frac{l_H}{\bar{c}} \tag{5.54b}$$

5.2.3 DERIVATION OF EQUATIONS, EFFECT ON LATERAL-DIRECTIONAL DERIVATIVES, PROPELLER ENGINE

With the above derived equations it is now possible to derive equations for the effect of power on the lateral-directional derivatives. The effect of power on the C_{Y_β} derivative is essentially the same as the effect on C_{L_α}:

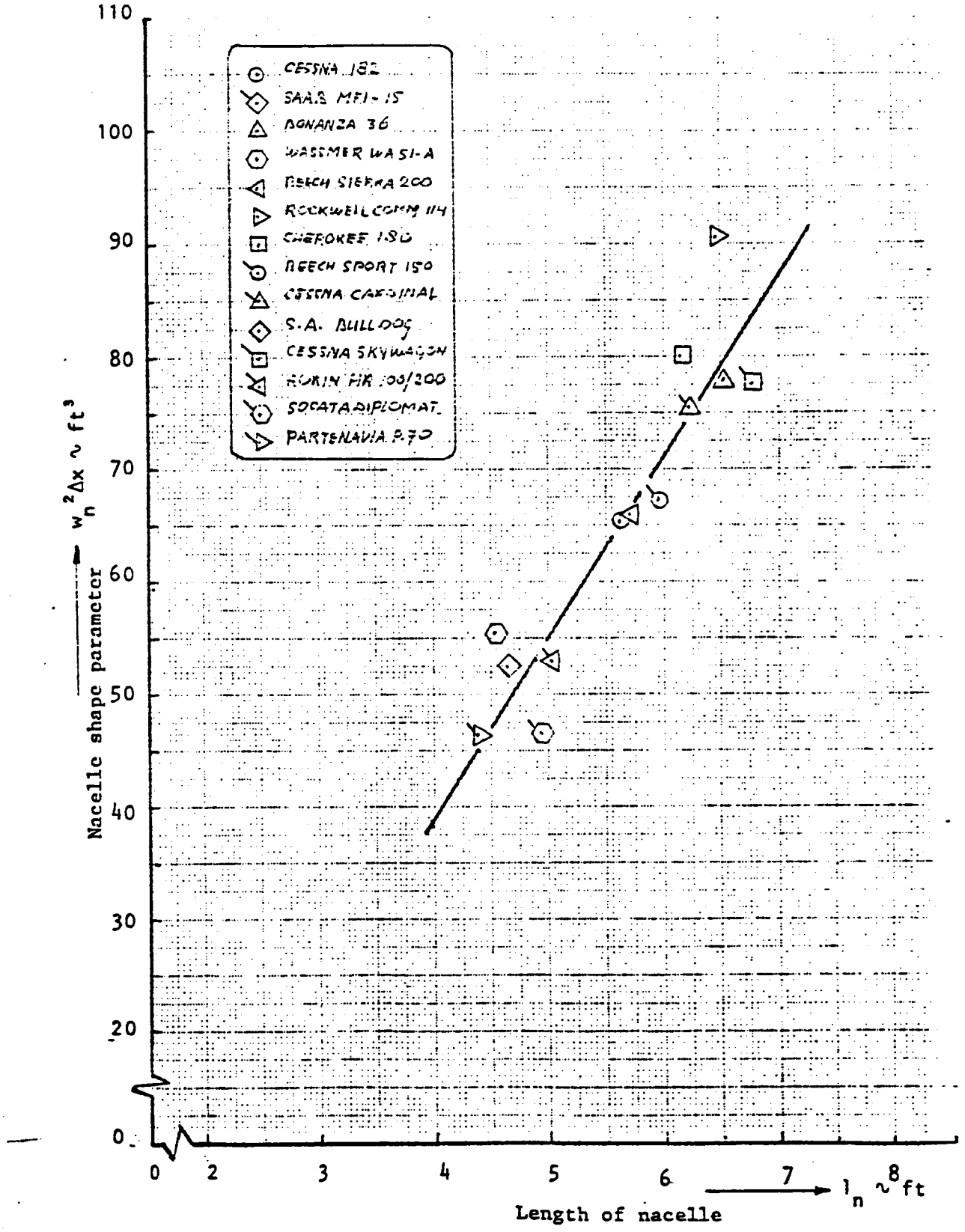

Figure 5.19: Nacelle shape parameter, single engine airplane

$$\Delta C_{Y_{\beta_p}} = -N\ f\ C_{Y'_{\psi_0}} \left(\frac{C_{Y'_{\psi_0}} \text{ for desired prop}}{C_{Y'_{\psi_0}} \text{ Figure 5.5}} \right) \left(\frac{S_p/\text{prop}}{S_W} \right) \qquad (5.55)$$

where the various variables are defined and calculated in Section 5.2.1.1.

The effect of power on the C_{n_β} derivative may be computed with the following equation:

$$\Delta C_{n_{\beta_p}} = \Delta C_{Y_{\beta_p}} \left\{ \frac{(X_p \cos \alpha_b + Z_T \sin \alpha_b)}{b} \right\} \qquad (5.56)$$

The effect of power on the C_{ℓ_β} derivative may be computed with the following equation:

$$\Delta C_{\ell_{\beta_p}} = \Delta C_{Y_{\beta_p}} \left\{ \frac{(-Z_T \cos \alpha_b + X_p \sin \alpha_b)}{b} \right\} \qquad (5.57)$$

5.2.4 EFFECT OF POWER ON SPEED-DERIVATIVES

Reference 5.5 provides the following formulas for the effect of propeller-power on the speed-derivatives:

$$\Delta C_{T_{X_u}} = -3.\ T'_c \qquad (5.58)$$

and

$$\Delta C_{M_{T_u}} = -\Delta C_{T_{X_u}} \frac{Z_T}{\bar{c}_W} \qquad (5.59)$$

5.3 DERIVATION OF EQUATIONS, EFFECTS OF POWER, JET ENGINE

The effects of jet engine thrust may again be divided into:

1). Direct effects on forces acting on aircraft.

2). Indirect effects due to jet efflux and influx.

The direct effects are easily calculated; the indirect effect, especially the influence of the jet exhaust on the flow field, are

more complicated. It was felt that the complexity of the latter computations did not warrant the inclusion of these indirect effects into the program.

5.3.1 EFFECT OF JET ENGINE THRUST ON STABILITY DERIVATIVES

5.3.1.1 EFFECT ON LIFT

The effect of thrust on lift may be accounted for by $\Delta L = T\sin\alpha_T$. It then follows that

$$\Delta C_{L_T} = N(T_c'/\text{engine})\sin\alpha_T \tag{5.60}$$

$$\Delta C_{L_{\alpha_T}} = N(T_c'/\text{engine})\cos\alpha_T \tag{5.61}$$

where $\alpha_T = \alpha + i_T$.

5.3.1.2 EFFECT ON PITCHING MOMENT COEFFICIENT C_{m_α}

Reference 5.5 provides the following formula for the computation of this effect:

$$\Delta C_{m_{\alpha_p}} = \left\{ \frac{N \dot{m}^2}{A_i \rho \, 1/2 \, \rho \, V^2 \, S \, \bar{c}} \right\} \left\{ X_j \left(1 - \frac{d\varepsilon}{d\alpha}\right) \right\} \tag{5.62}$$

where: $\dot{m}$ is mass flow through the engine in slugs-ft^3.

A_i is the jet-engine inlet area (ft^2)

X_j is the distance along the X body axis between the aircraft center of gravity and the first fan of the jet engine, forward taken as positive.

Note: If the engine is mounted forward of the wing, i.e. if X_j is positive, then the variable $d\varepsilon/d\alpha$ in Equation 5.62 should be replaced with $d\varepsilon_u/d\alpha$, upwash

ahead of the wing. This variable may be computed from:

$$\frac{d\varepsilon_u}{d\alpha} = \left[-.1136 \left\{ \frac{(X_j - X_W)}{\bar{c}_W} \right\}^{-1.8141} - .027\ (AR - 4.) \right] \quad (5.63)$$

where X_W is the distance from the wing a.c. to the c.g., positive when the c.g. is aft of the wing a.c.

5.3.1.3 EFFECT ON C_{L_o} and C_{m_o}

The effect of jet thrust at α = o on lift and longitudinal moments may be described by

$$\Delta C_{L_o} = N(T_c'/\text{engine})*\sin(i_T) \quad (5.64)$$

$$\Delta C_{m_o} = N(T_c'/\text{engine})*\cos(i_T)\ z_T/\bar{c} \quad (5.65)$$

5.3.1.4 EFFECT ON SPEED DERIVATIVES, $C_{M_{T_u}}$ AND $C_{T_{X_u}}$

Reference 5.5 provides the following formulas to approximate the effects of jet-engine thrust on the speed derivatives $C_{M_{T_u}}$ and $C_{T_{X_u}}$:

$$\Delta C_{T_{X_u}} = M \frac{\partial F_N}{\partial M} / (1/2\ \rho\ V^2\ S) - 2.\ T_c' \quad (5.66)$$

where: M is the flight Mach number.

$\frac{\partial F_N}{\partial M}$ is the change in thrust with change in Mach number, in lbs.

$$\Delta C_{M_{T_u}} = -\Delta C_{T_{X_u}} \frac{Z_T}{\bar{c}_W} \quad (5.67)$$

5.3.1.5 EFFECT ON LATERAL DIRECTIONAL DERIVATIVES

Reference 5.5 provides the following formulas for jet effects on lateral-directional derivatives.

$$C_{y_{\beta_T}} = 0. \tag{5.68}$$

$$C_{\ell_{\beta_T}} = 0. \tag{5.69}$$

$$C_{n_{\beta_T}} = -N \frac{\dot{m}^2}{A_i \zeta} \frac{X_j}{\frac{1}{2}\zeta V^2 Sb} \tag{5.70}$$

where the terms are defined as for equation (5.60).

This concludes the derivation of the effects of thrust on the aerodynamic derivatives.

5.4 DESCRIPTION OF PROGRAM

The program is divided to treat the propeller-powered and jet-powered vehicle separately, and the integer variable ENP is used to distinguish between single engine (ENP=1) and twin engine (ENP=2) aircraft. Propeller computations are performed over four angles-of-attack in the following order: $\alpha - 1°$, α, $\alpha + 1°$, and $\alpha = 0°$. Results for α and $\alpha = 0$ are then obtained directly, while $\Delta C_{L_{\alpha_p}}$ and $\Delta C_{m_{\alpha_p}}$ results are computed as $(\Delta C_{L_{\alpha_{p_{\alpha+1}}}} - \Delta C_{L_{\alpha_{p_{\alpha-1}}}})/2$ and $(\Delta C_{m_{\alpha_{p_{\alpha+1}}}} - \Delta C_{m_{\alpha_{p_{\alpha-1}}}})/2$.

Immersed areas behind the propellers of both single and twin engine airplanes are computed based on a slipstream height Z_S. Z_S is initially assumed equal to the thrust-line height Z_T and then is iterated to an approximate height over three computational loops at each of the four angles of attack.

Computations for the jet powered vehicle are very straight forward and do not involve iterative loops.

5.5 REFERENCES

5.1	Hoak, D.E. & Ellison, D.E.	USAF Stability and Control DATCOM; Air Force Flight Dynamics Lab., Wright-Patterson Air Force Base, Ohio
5.2	Wolowicz, C.H. & Yancey, R.B.	Longitudinal Aerodynamic Characteristics of Light, Twin-engine Propeller Driven Airplanes. NASA TN D-6800
5.3	Fink, M.P. & Freeman, D.C.	Full-scale Wind-tunnel Investigation of Static Longitudinal and Lateral Characteristics of a Light Twin-engine Airplane. NASA TN D-4983
5.4	Greer, H.D. & Shivers, J.P. & Fink, M.P.	Wind-tunnel Investigation of Static Longitudinal and Lateral Characteristics of a Full-scale Mockup of a Light Single-engine High-wing Airplane. NASA TN D-7149
5.5	Roskam, J.	Airplane Flight Dynamics and Automatic Flight Controls, Part I. Roskam Aviation and Engineering Corporation. 1979.

CHAPTER 6

STATIC LONGITUDINAL STABILITY

6.1 INTRODUCTION

This chapter describes the computation of static stability, C_{M_α}, static margin, dC_M/dC_L, and neutral point, $\bar{X}_{AC}$, for both stick fixed and stick free cases. Power effects accounted for in subroutine "POWER" (Chapter 5) are integrated in the MAIN program. Here, C_{m_α}, dC_m/dC_L, and $\bar{X}_{AC}$, are all obtained in subroutine "CMALPA" according to methods described in Reference 6.1. The center of gravity location is assumed to be known.

6.2 DERIVATION OF EQUATIONS

The static stability parameter, C_{M_α}, may be computed from:

$$C_{M_\alpha} = \left(\frac{dC_M}{dC_L}\right) \cdot C_{L_\alpha} \qquad (rad^{-1}) \tag{6.1}$$

where: C_{L_α} is the lift-curve slope of the complete airplane, as computed in subroutine "LIFCRV". See Section 11.2.

$\frac{dC_M}{dC_L}$ is the static margin which may be found from:

$$\frac{dC_M}{dC_L} = \bar{X}_{cg} - \bar{X}_{ac} \tag{6.2}$$

The airplane aerodynamic center location, $\bar{X}_{ac}$, may be obtained from:

$$\bar{X}_{ac_{Fixed}} = \frac{\bar{X}_{ac_{WB}} + \frac{C_{L_{\alpha_H}}}{C_{L_{\alpha_{WB}}}} \eta_H \left(\frac{S_H}{S}\right) \bar{X}_{ac_H} \left(1 - \frac{d\varepsilon}{d\alpha}\right)}{1 + \frac{C_{L_{\alpha_H}}}{C_{L_{\alpha_{WB}}}} \eta_H \left(\frac{S_H}{S}\right) \left(1 - \frac{d\varepsilon}{d\alpha}\right)} \tag{6.3}$$

Equation (6.3) is for the stick fixed case. For the stick free case the following equation should be used:

$$\bar{X}_{ac_{Free}} = \frac{\bar{X}_{ac_{WB}} + \frac{C_{L_{\alpha_H}}}{C_{L_{\alpha_{WB}}}} \eta_H \left(\frac{S_H}{S}\right) \bar{X}_{ac_H} \left(1 - \frac{d\varepsilon}{d\alpha}\right) \left(1 - \frac{C_{h_\alpha} \tau_E}{C_{h_{\delta_e}}}\right)}{1 + \frac{C_{L_{\alpha_H}}}{C_{L_{\alpha_{WB}}}} \eta_H \left(\frac{S_H}{S}\right) \left(1 - \frac{d\varepsilon}{d\alpha}\right) \left(1 - \frac{C_{h_\alpha} \tau_E}{C_{h_{\delta_e}}}\right)} \tag{6.4}$$

The various variables in Equations (6.3) and (6.4) are calculated as follows:

The lift-curve slope of the horizontal tail angle of the wing body combination, $C_{L_{\alpha_H}}$ and $C_{L_{\alpha_{WB}}}$, respectively, are computed in subroutine "LIFCRV". Section 11.2.

The downwash $d\varepsilon/d\alpha$ is calculated in subroutine "DOWNWS".

The control-surface parameters C_{h_α}, τ_E and $C_{h_{\delta_e}}$ are computed in subroutine "CONSUR". See Section 11.26.

The aerodynamic center of the horizontal tail plane and of the wing, $\bar{X}_{ac_H}$ and $\bar{X}_{ac_W}$, respectively, are defined in Figure 6.1. They may be computed with reference to Figure 6.2.

To convert the value of X'_{ac}/C_R, from Figure 6.2, to the nondimensional value $\bar{X}_{ac}$, use is made of Equation (6.5):

$$\bar{X}_{ac} = K1 \quad (X'_{ac}/C_R - K2) \tag{6.5}$$

where K1 and K2 are given as:

$$K1 = \frac{3(1 + \lambda)}{2(1 + \lambda + \lambda^2)} \tag{6.6}$$

$$K2 = \frac{(1 + 2\lambda)}{12} A \tan \Lambda_{LE} \tag{6.7}$$

and $\lambda = c_{tip}/c_{root}$

NOTE: K1 and K2 follow directly from the geometry of Figure 6.1.

$\bar{X}_{AC_w}$ and $\bar{X}_{AC_H}$ are obtained from function "ACEM".

The wing-body aerodynamic center may be computed from:

$$\bar{X}_{ac_{WB}} = \bar{X}_{ac_W} + \Delta\bar{X}_{ac_B} \tag{6.8}$$

The body-induced aerodynamic center shift $\Delta\bar{X}_{ac_B}$ in Equation (6.8) follows from:

$$\Delta \bar{X}_{ac_B} = \frac{-dM/d\alpha \text{ (Body and/or Nacelles, Tailboom)}}{\bar{q}S\bar{C}C_{L_{\alpha_W}}} \tag{6.9}$$

where:

$$\frac{dM}{d\alpha} = \frac{\bar{q}}{36.5} \sum_{i=i}^{i=h} W_f^2 (X_i) \left.\frac{d\varepsilon}{d\alpha}\right|_i \Delta X_i \tag{6.10}$$

The geometric variables in Equation (6.10) are defined in Figure 6.3 and the downwash ahead of the wing may be found from Figure 6.4. Note the different curves for different parts of the body forward of the wing.

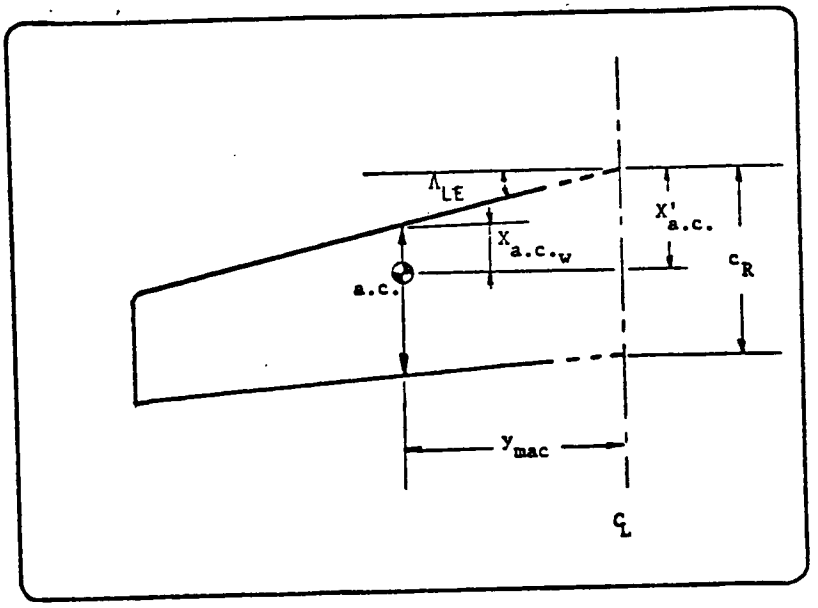

Figure 6.1: Definition of dimensional and non-dimensional aerodynamic center locations

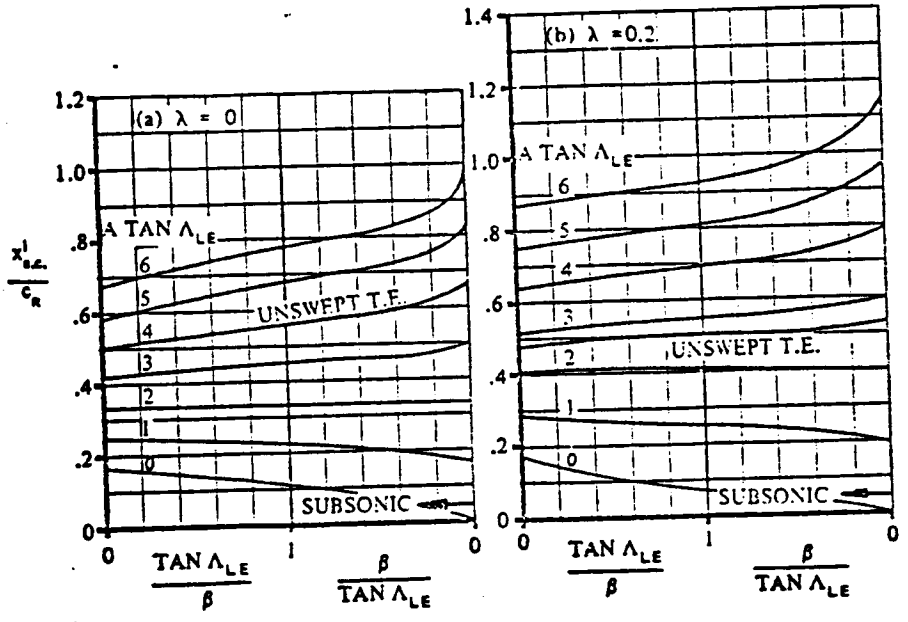

Figure 6.2: Aerodynamic center locations of lifting surfaces

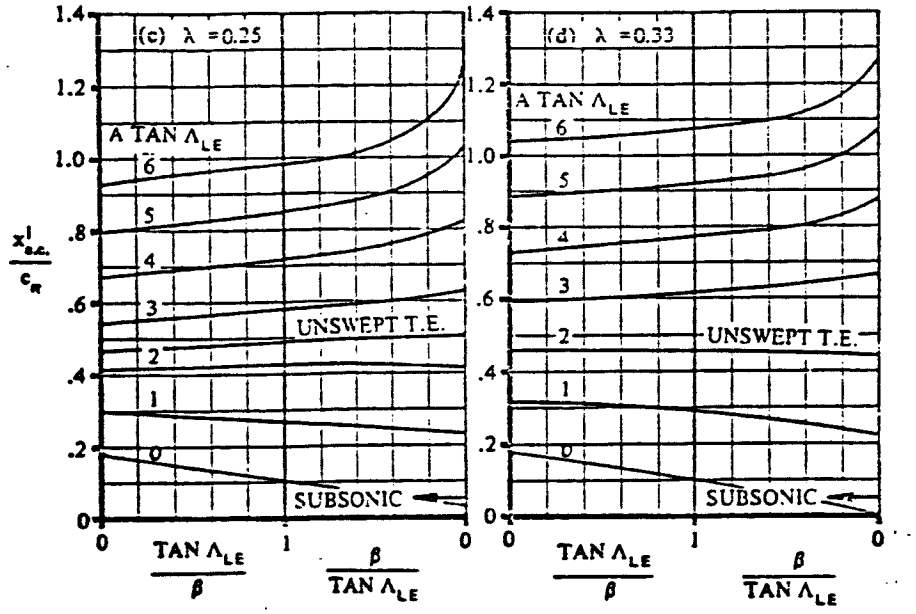

Figure 6.2: Continued

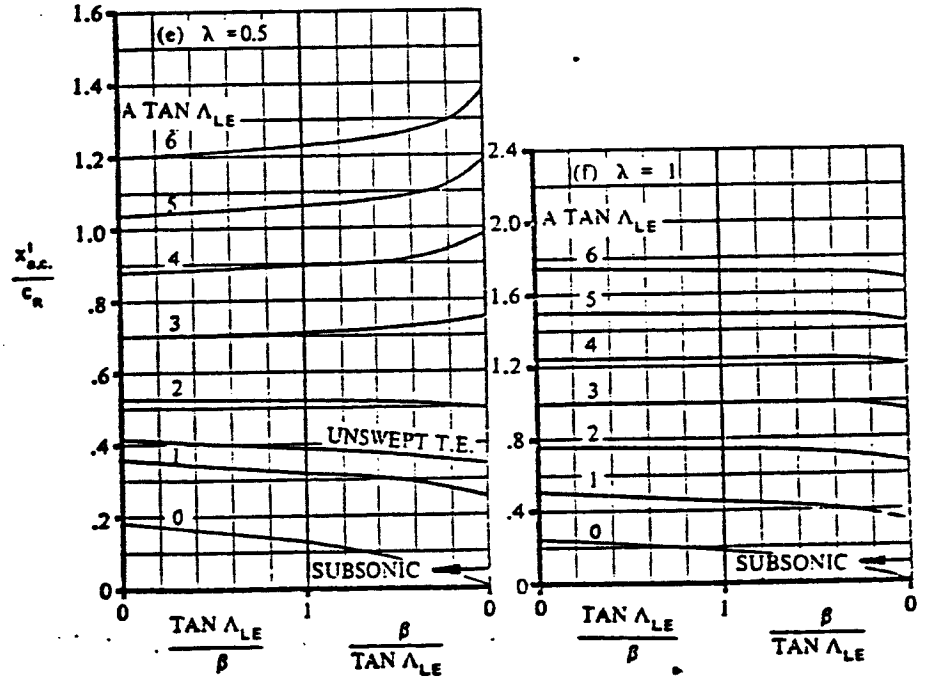

Figure 6.2: continued

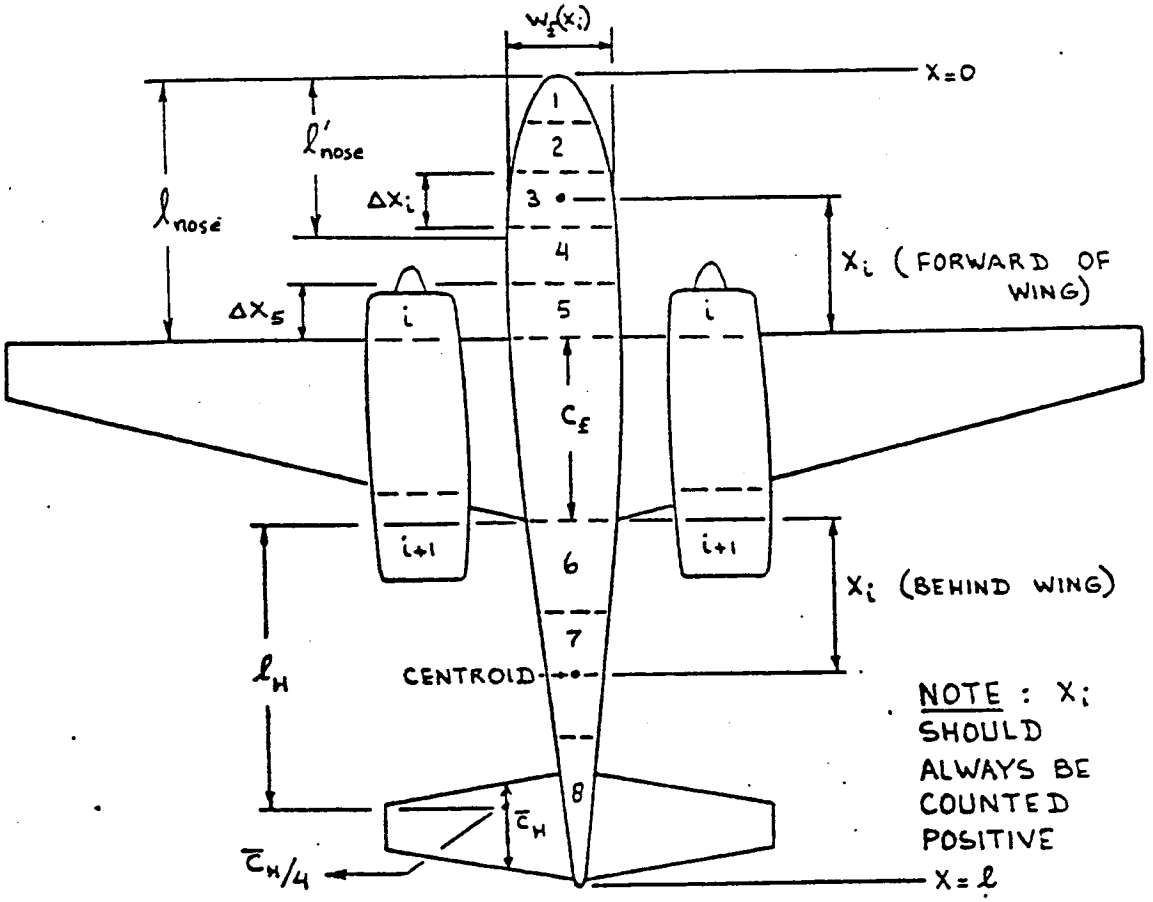

Figure 6.3: Geometric parameters for the computation of the effect of body or nacelles on a.c. location

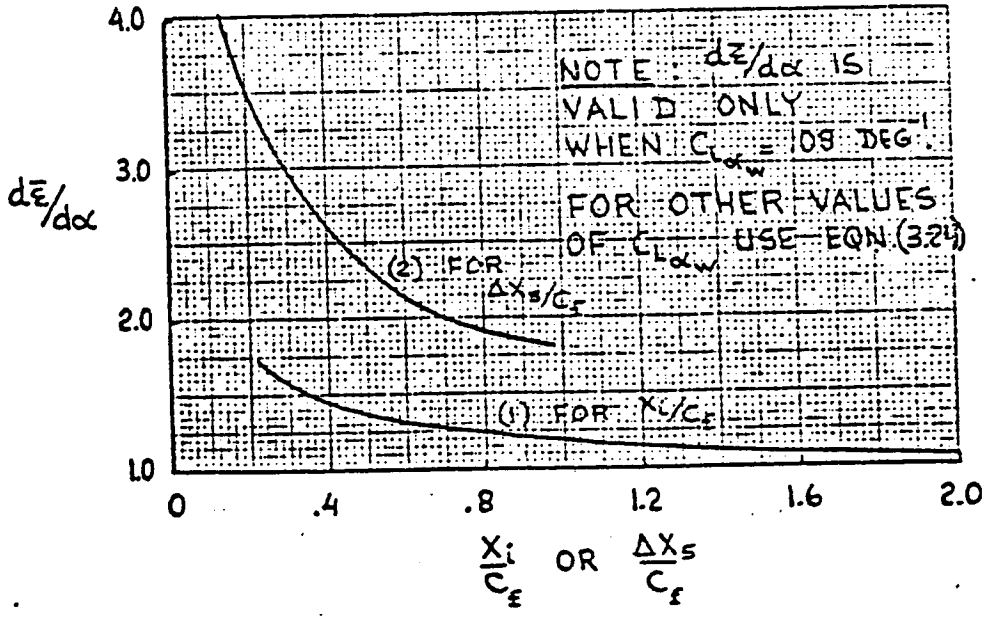

Figure 6.4: Upwash ahead of the wing

The downwash behind the wing may be found from the methods of Section 11.3, Equation 11.3.1. Here, the ℓ_H of Figure 11.3.1 is corrected for each x_i and the h_H is corrected to the x-y plant of the body axes. $\Delta\bar{X}_{AC_B}$ is obtained from subroutine "MULTOP".

This concludes the derivation of equations for the Static Longitudinal Stability.

6.3 FUNCTION "ACEM"

$\bar{X}_{AC}$ for the wing or horizontal tail is obtained through Function ACEM where this routine employs the data of Figure 6.2 to obtain X'_{AC}/C_R and then converts this result to $\bar{X}_{AC}$ in accordance with Equation 6.5

The curves of Figure 6.2 are input as straight lines where the right hand sides of the figures (for low values of $\frac{\beta}{\tan\Lambda_{LE}}$) pertain only to combinations of high Mach numbers and high sweep angles. For example, $\Lambda_{LE} = 40°$ with M = .8 results in $\frac{\beta}{\tan\Lambda_{LE}} = .715$ (which is well within the linear range), and $\Lambda_{LE} = 30°$ with M = .8 results in $\frac{\tan\Lambda_{LE}}{\beta} = .9622$ (which is in the left half of the figure). The discontinous horizontal axis can be accommodated conveniently by allowing the right half of the horizontal axis to be an extension of the left half with

$$\frac{\mathrm{Tan}\Lambda_{LE}}{\beta} = 2 - \frac{\beta}{\mathrm{Tan}\Lambda_{LE}} \qquad (6.11)$$

Since Figure 6.2 returns $\frac{X'_{AC}}{c_{root}}$, Figure 6.1 is used to convert this result as

$$\bar{X}_{AC} = \frac{X_{AC}}{\bar{c}} = \left(\frac{X'_{AC}}{c_{root}} - c_{root} - y_{mac}\tan\Lambda_{LE}\right)\frac{1}{\bar{c}} \qquad (6.12)$$

The variables K1 and K2 of Equations 6.5, 6.6, and 6.7 are defined as

$$K1 = \frac{c_{root}}{\bar{c}} = \frac{3(1 + \lambda)}{2(1 + \lambda + \lambda^2)} \qquad (6.6)$$

$$K2 = \frac{y_{mac} \tan\Lambda_{LE}}{c_{root}} = \frac{(1 + 2\lambda)}{12} \left(A \right)\left(\tan\Lambda_{LE} \right) \qquad (6.7)$$

ACEM also returns X'_{AC} (named XPACW) as the last variable in the formal argreement list. This is the longitudinal dimensional distance from the wing apex to the wing aerodynamic center.

6.4 SUBROUTINE "MULTOP"

This routine is a modified version of a routine described in Reference 6.2. It performs the summation indicated in Equation 6.10 to arrive at the aerodynamic center shift caused by the body, $\Delta\bar{X}_{AC_B}$ (named DXACB), and returns this variable for use in subroutine CMALPA. The modification consists of the addition of a similar calculation to account for the discrete contributions of wing-mounted engine nacelles to aerodynamic center shift, $\Delta\bar{X}_{AC_N}$ (named DXACN).

When called by "CMALPA," only DXACB is used. However, when called by subroutine "CLOCMO," DXACB is used to evaluate the wing-body-tail C_{m_o}, and DXACN is used to establish $C_{m_{o_{wn}}}$, the C_{m_o} of the wing-nacelle. This latter variable is passed from subroutine "CLOCMO" to subroutine "POWER" in a common AERDAI as variable CMWFN. CMWFN is not used by subroutine "CMALPA."

"MULTOP" calculates the $W_f(X_i)$ of equation 6.10 according to

$$W_f(X_i) = 1. - \frac{\ell'_{nose} + X_i - \ell_{nose}}{\ell'_{nose}}^{N\ \frac{1}{M}} \qquad (6.13)$$

where $W_f(X_i)$ = the width of the nose at X_i

ℓ'_{nose} = the input length of the elliptical nose planform

ℓ_{nose} = the length of the nose measured to the leading edge of the wing

M, N = shape parameters obtained from subroutine CONSHP.

See Figure 6.3 for a clarification of $W_f(X_i)$, ℓ'_{nose}, and ℓ_{nose}.

6.5 SUBROUTINE "CONSHP"

This subroutine is called only by subroutine "MULTOP" and iterates over N to obtain M where convergence in M is presently specified via a tolerance of

$$\Delta M = M_1 - M_2 \leq .001 \tag{6.14}$$

where $M_1 = \dfrac{\ell n\ (1. - \phi_1^N)}{\ell n(\phi_1)}$ (6.15)

and $M_2 = \dfrac{\ell n\ (1. - \phi_2^N)}{\ell n(\phi_2/2.)}$ (6.16)

N is incremented as

$$N_i = N_{i-1} + \Delta N \tag{6.17}$$

and ΔN is selectively varied in magnitude by the subroutine until convergence is achieved. ϕ_1 and ϕ_2 are normalized longitudinal distances as depicted in Figure 6.5.

When convergence is achieved, subroutine "CONSHP" returns M and N to subroutine "MULTOP" where M is defined as

$$M = \frac{M_1 + M_2}{2} \tag{6.18}$$

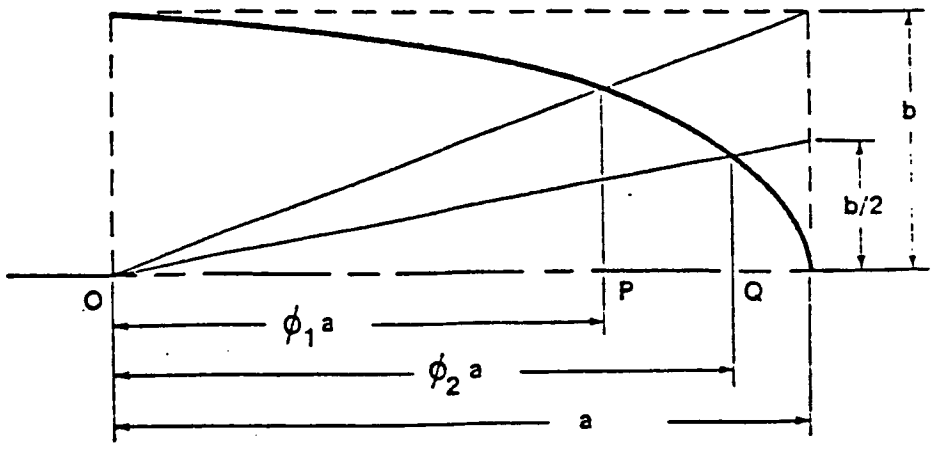

Figure 6.5 Ellipse Parameter Definitions

Two error messages may result from CONSHP if convergence is not achieved. The first results when $M_{1_i} > M_{2_i}$ and $(M_1 - M_2)_i > (M_1 - M_2)_{i-1}$ and yields the following message:

```
*** ITERATION FOR M AND N DIVERGES ***
    SET M = 1.0 AND N = 1.0
*** (MESSAGE FROM SUBROUTINE CONSHP) ***
```

The second message results when CONSHP does not yield a converged value of M within 100 increments in N. This case is signaled by:

```
*** 100 STEPS COMPLETE - DID NOT CONVERGE ***
*** (MESSAGE FROM SUBROUTINE CONSHP) ***
```

6.6 REFERENCES

6.1 Roskam, J. Methods for Estimating Stability and control Derivatives of Conventional Subsonic Aircraft (Roskam Aviation and Engineering Corp., Lawrence, Ks.)

6.2 Wyatt, R. D., Griswold, D. A., & Hammer, J. L. A Study of Commuter Airplane Design Optimization (KU-FRL 313-4/1977)

CHAPTER 7

DIRECTIONAL STABILITY

7.1 INTRODUCTION

Generally it is quite difficult to calculate the lateral-directional aerodynamic characteristics. The vertical tail plane is the dominant factor and this surface is situated in a complex asymmetrical flow field behind the wing/fuselage combination. This chapter will describe some of the criteria important for the preliminary design phase.

7.2 DISCUSSION OF DESIGN CRITERIA

The primary preliminary design criteria for the vertical tail are the following:

(1) The aircraft must possess positive directional static stability and the short-period lateral/directional oscillation must be well damped.

(2) After failure of the critical engine, the aircraft must remain controllable in the case of multi-engine aircraft.

To assure compliance with criterion (1), an adequate value for C_{n_β}, the static directional stability parameter, has to be provided. For single-engine subsonic airplanes, the value for C_{n_β} is often found to lie between .04 and .10 (Ref. 7.1). A method for the estimation of the parameter C_{n_β} is discussed in section 11.16.

To comply with criterion (2), the vertical tail has to be able to produce a certain minimum sideforce C_{y_V} to counteract the disturbing yawing moment of a stopped engine. In this case, also, the control-surface (i.e. rudder) parameters are important. A discussion of a method to compute these parameters is given in section 11.25 as well as in 11.14. A method to derive the minimum control speed, V_{MC}, is given in section 8.

7.3 REFERENCES

7.1 Torenbeek, E. Synthesis of Subsonic Airplane Design, Delft University Press, Delft, The Netherlands. 1976.

CHAPTER 8

VMC ROUTINE

8.1 INTRODUCTION

V_{MC} will be defined in this chapter as the minimum speed at which level or slightly climbing flight is maintained with one engine out and the remaining engine at maximum thrust, in a steady state flight condition.

Three methods for determining V_{MC} were evaluated: the method of Torenbeek (Ref. 8.2), and single-degree-of-freedom and three-degree-of-freedom methods from Ref. 8.1.

The method of Torenbeek was found to be similar to the first method from Ref. 8.1

8.2 SINGLE-DEGREE-OF-FREEDOM APPROXIMATION

From Ref. 8.1, p. 5.37, the moment equation about the aircraft Z axis is given by:

$$C_{n_\beta}\,\beta + C_{n_{\delta_R}}\,\delta_R + \frac{N_T}{\bar{q}Sb} = 0 \tag{8.1}$$

$$\delta_R = \frac{-C_{n_\beta}\,\beta - \dfrac{N_T}{\bar{q}Sb}}{C_{n_{\delta_R}}} \tag{8.2}$$

To check the roll axis, the maximum sideslip angle reached if the pilot does nothing is given by:

$$\beta_{max} = \frac{-N_T}{C_{n_\beta}\bar{q}Sb} \tag{8.3}$$

and the aileron deflection required for this condition is given by:

$$\delta_A = \frac{- C_{\ell_\beta} \beta_{max}}{C_{\ell_{\delta_A}}} \qquad (8.4)$$

A short computer routine was written to allow a quick check of methods. The routine finds rudder deflection as a function of flight speed V, where V is incremented by 0.5 mph after each iteration. Input values were taken from Ref. 8.3, and runs were made for two values fo sideslip angle, 0 deg. and 5 deg. (in a helpful direction). Bank angle is not taken into account by this method.

Results by this method appear to be quite high. Maximum rudder deflection for the airplane is 22 degrees, yielding a V_{MC} of about 103 mph at $\beta = 5°$. This is 1.5 (V_{Stall}), and much higher than the 1.2 V_{Stall} requirement. From Ref. 8.4, V_{MC} for the airplane investigated is 80.6 mph. This large a prediction error is unacceptable for preliminary design, leading to the use of the three-degree-of-freedom method.

8.3 THREE-DEGREE-OF-FREEDOM METHOD

From Ref. 8.1, p. 5.38, if a fixed bank angle is assumed, the three remaining variables are β, δ_A, and δ_R; these may be found by using equations 8.5, 8.6 and 8.7.

Examining these equations, it is seen that in addition to the stability derivatives of the delta matrix, the necessary input variables are weight, flight path angle γ, bank angle ϕ_1, wing span and area, dynamic pressure $\bar{q}$, rolling moment due to thrust L_{T_1}, and yawing moment due to thrust N_{T_1}.

Bank angle ϕ is the independent variable. Yawing moment due to thrust, N_{T_1}, is found by adding the thrust of the remaining engine to the drag of the feathered propeller and multiplying by the engine moment arm, which is the lateral distance from the c.g. The rolling moment due to thrust is a function of

$$\beta_1 = \frac{\begin{vmatrix} -\dfrac{\left[mg \sin \phi, \cos \gamma, + F_{T_{Y_1}}\right]}{\bar{q}_1 S} & C_{Y_{\delta_A}} & C_{Y_{\delta_R}} \\ -L_{T_{1/\bar{q}_1 Sb}} & C_{\ell_{\delta_A}} & C_{\ell_{\delta_R}} \\ -N_{T_{1/\bar{q}_1 Sb}} & C_{n_{\delta_A}} & C_{n_{\delta_R}} \end{vmatrix}}{\begin{vmatrix} C_{Y_\beta} & C_{Y_{\delta_A}} & C_{Y_{\delta_R}} \\ C_{\ell_\beta} & C_{\ell_{\delta_A}} & C_{\ell_{\delta_R}} \\ C_{n_\beta} & C_{n_{\delta_A}} & C_{n_{\delta_R}} \end{vmatrix}} \qquad (8.5)$$

$$\delta_{A_1} = \frac{\begin{vmatrix} C_{Y_\beta} & -\dfrac{\left[mg \sin \phi, \cos \gamma, + F_{T_{Y_1}}\right]}{\bar{q}_1 S} & C_{Y_{\delta_R}} \\ C_{\ell_\beta} & -L_{T_{1/\bar{q}_1 Sb}} & C_{\ell_{\delta_R}} \\ C_{n_\beta} & -N_{T_{1/\bar{q}_1 Sb}} & C_{n_{\delta_R}} \end{vmatrix}}{[\Delta]} \qquad (8.6)$$

$$\delta_{R_1} = \frac{\begin{vmatrix} C_{Y_\beta} & C_{Y_{\delta_A}} & -\dfrac{\left[mg \sin \phi, \cos \gamma, + F_{T_{Y_1}}\right]}{\bar{q}_1 S} \\ C_{\ell_\beta} & C_{\ell_{\delta_A}} & -L_{T_{1/\bar{q}_1 Sb}} \\ C_{n_\beta} & C_{n_{\delta_A}} & -N_{T_{1/\bar{q}_1 Sb}} \end{vmatrix}}{[\Delta]} \qquad (8.7)$$

the thrust inclination angle and the aircraft angle of attack; at the angles of attack typical of low speed flight, the components of asymmetrical thrust and drag in the Z direction produce an appreciable rolling moment in a direction which requires more aileron deflection and increases V_{MC}. An additional rolling moment is produced by lift due to the slipstream for propeller aircraft.

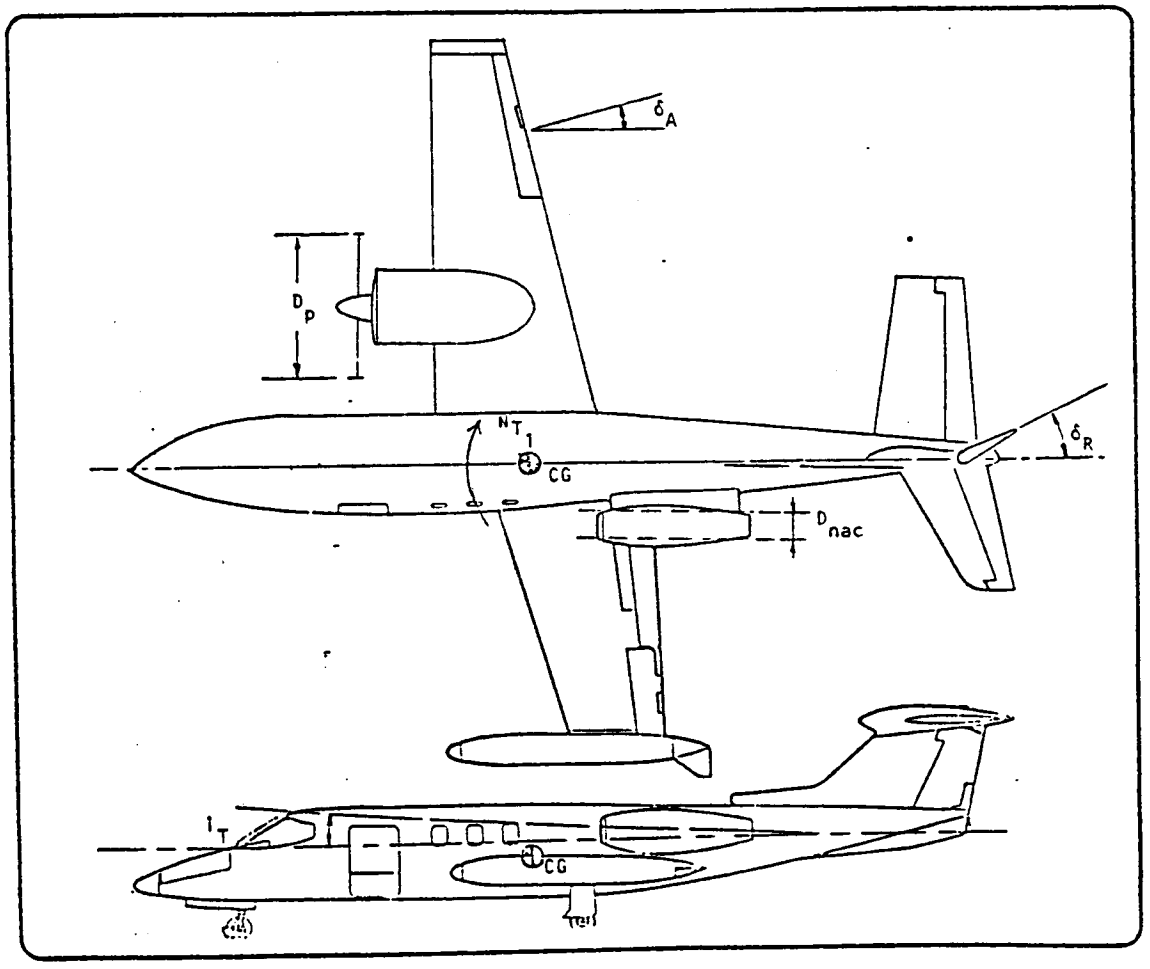

Figure 8.1 V_{mc} Variable Geometric Definitions

8.4 REFERENCES

8.1: Roskam, J. — Flight Dynamics of Rigid and Elastic Airplanes. Roskam Aviation & Engineering Corp. Lawrence, Kansas. 1972.

8.2: Torenbeek, E. — Synthesis of Subsonic Airplane Design, Delft University Press, Delft, The Netherlands, 1976

8.3: Wolowicz, C.H.& Yancey, R.B. — Longitudinal Aerodynamic Characteristics of Light, Twin-engine, Propeller-driven Airplanes. NASA TN D-6800

8.4: Anon. — Business and Commercial Aviation. April 1977, page 58 & 59.

CHAPTER 9

ROTATION SPEED

9.1 INTRODUCTION

The speed at which the aircraft rotates at takeoff, V_R, is calculated using a method from Reference 9.1. This method was originally developed by Perry (Ref. 9.2) and is based on a constant rate of pitch-up after lift-off. The advantage of the method is that it is representative of piloting techniques used in civil aviation since pitch angle can be directly observed, contrary to lift coefficient. The equations of motion are linearized by assuming V = constant and (T - D) = constant.

9.2 DERIVATION OF EQUATIONS

There are certain criteria concerning the speed during the takeoff (Ref. 9.3). The most important are the following:

- V_R — The rotation speed is the speed at which the pilot raises the nose wheel.
- $V_R \geq V_1$ — Where V_1 is the decision speed.
- $V_R \geq 1.05V_{MCG}$ — Where V_{MCG} is the minimum speed for control during engine out cases.
- V_R — Should be chosen such that V_2 is reached at 35 ft, taking into account the speed increment, ΔV, between V_R and V_1.
- $V_2 = 1.2V_S$ — V_S is the 1-g stall speed.
- V_{LOF} — Is the speed at which the landing gear leaves the ground.

$V_{LOF} \geq 1.1 V_{MU}$ All engines or:

$V_{LOF} \geq 1.05 V_{MU}$ For engine out conditions, where V_{MU} is the minimum unstick speed, or the minimum speed at which the aircraft is still controllable when it leaves the ground.

For low T/W ratios, V_R and V_{LOF} may be increased to ensure positive climb gradient.

Figure 9.1 shows a schematic diagram of the takeoff.

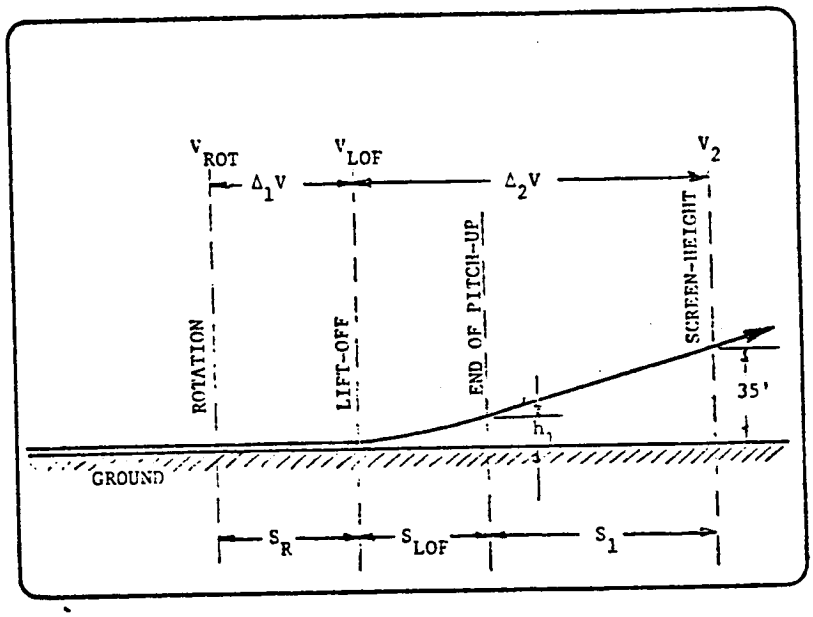

Figure 9.1: Take-off parameters.

9.2.1 ROTATION PHASE

Assuming that the acceleration along the X-axis during the rotation phase is equal to the value at lift-off and assuming a mean rate of rotation about the Y-axis $(d\theta/dt)_R$, it may be found

for the rotation distance:

$$S_R = 1/2\ (V_R + V_{LOF})\ \frac{\alpha_{LOF} - \alpha_g}{(d\theta/dt)_R} \qquad (9.1)$$

where: α_{LOF}: The angle of attack at which lift-off occurs; this follows from the $C_L - \alpha$ curve in ground effect.

The speed at lift-off may be calculated as follows:

$$V_{LOF} = V_R + \Delta_1 V = V_R + g\{\frac{T-D}{W}\}_{LOF}\ \frac{\alpha_{LOF} - \alpha_g}{(d\theta/dt)_R} \qquad (9.2)$$

The rotation rate $(d\theta/dt)_R$ depends mainly on elevator power and moment of inertia about the Y-axis. As an average value 4.6 deg/sec may be taken (Ref. 9.1).

9.2.2 AIRBORNE PHASE

The speed increment from lift-off speed to the speed at 35' may be obtained from the energy equation:

$$\Delta_2 V = \frac{g(S_{LOF} + S_1)}{V_{LOF}}\ \{\frac{T-D}{W} - \frac{35}{S_{LOF} + S_1}\} \qquad (9.3)$$

The airborne distance is composed of two phases:

- A flare-up, where the flight path angle increases from zero during the ground run to γ_2 at V_2.
- A phase with constant climb angle γ_2.

The calculations for this part of the takeoff are based on Perry's method (Ref. 9.2). Perry based his method on numerous observations of takeoffs concerning light as well as heavy aircraft. From these observations functions were derived that describe the path of the aircraft after lift-off. Using these functions, it is possible to

calculate the gain in height and the flight path angle during flare-up.

The gain in height after lift-off is given by:

$$h = \frac{V_{LOF}^2}{g} \frac{T - D}{W} F(\dot{\theta}) \; F(h) \tag{9.4}$$

where:

$$F(\dot{\theta}) = 1 + \frac{V_{LOF}}{2g} \frac{W}{T - D} \eta_\alpha \left(\frac{d\theta}{dt}\right)_A \tag{9.5}$$

$$\eta_\alpha = \frac{dC_{L/d\alpha}}{C_{L_{LOF}}} \tag{9.6}$$

$F(h)$ is a non-dimensional function of height; may be determined from Figure 9.2.

The rotation rate during flare-up may be approximated by using a value of $(d\theta/dt)_A$ of 2-3°/sec for the engine failure case and 5°/sec for the all-engine case.

The climb-angle during flare-up is given by:

$$\gamma = \frac{dh}{ds} = \frac{T - D}{W} F(\dot{\theta}) \; F(\gamma) \tag{9.7}$$

where: $F(\gamma)$ is a non-dimensional flight-path angle function depicted in Figure 9.2.

The end of the flare-up is reached when $\gamma = \gamma_2$ (for the engine out case) or $\gamma = \gamma_3$ (for the all-engine case).

It should be noted that γ_2 can only be calculated when V_2 is known. Also, the functions $F(h)$ and $F(\gamma)$ are a function of the distance traveled after lift-off. The calculations are therefore iterative.

By using curve-fitting routines, the following set of formulas was found to fit the curves in Figure 9.2:

$$F(h) = (-.01867 - .02682\ X_f + .21233\ X_f^2) +$$
$$+ \{(3 - n_\alpha)\ (.0023 + .0543[X_f - .5])\} \qquad (9.8)$$

$$F(\gamma) = (-.09813 + .56022\ X_f - .06661\ X_f^2) +$$
$$+ \{(3 - n_\alpha)\ (.009 + .0468\ [X_f - .4])\} \qquad (9.9)$$

where: $$X_f = \frac{g \cdot s}{V_{LOF}^2} \qquad (9.10)$$

and s is the total distance from lift-off.

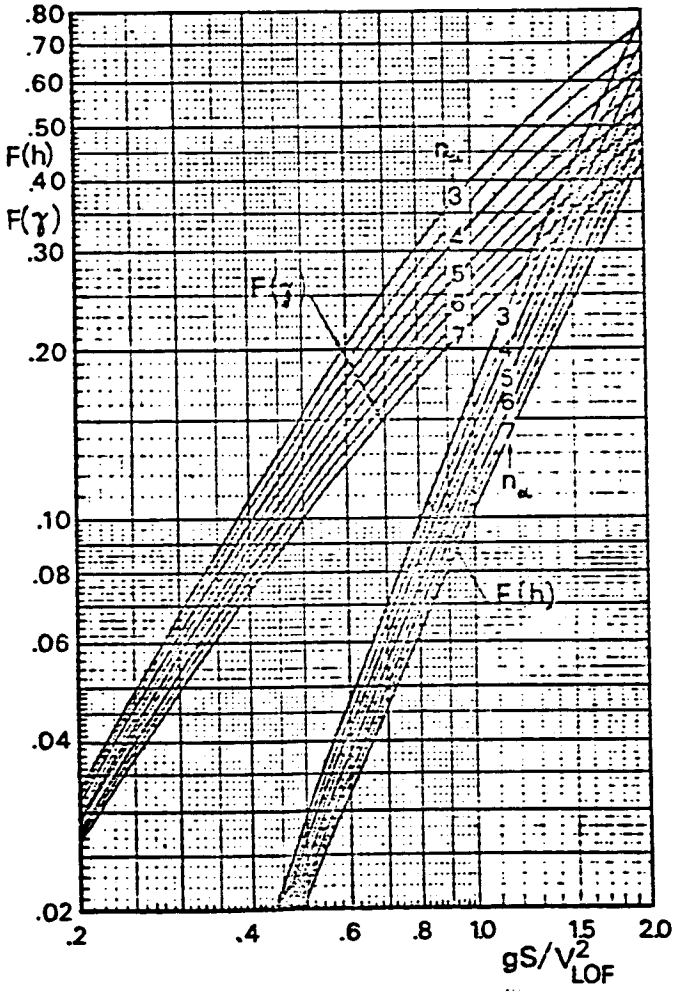

Figure 9.2: The functions F(h) and F(γ) used in Perry's method for the analysis of the airborne path (Derived from ref. 9.2)

9.3 REFERENCES

9.1	Torenbeek, E.	Synthesis of Subsonic Airplane Design, Delft University Press, Delft, The Netherlands, 1976.
9.2	Perry, D.H.	The Airborne Path During Take-off for Constant Rate of Pitch Maneuvres, ARC CP # 1042, 1969.
9.3	Anon	Federal Aviation Regulations, FAR Part 25.
9.4	Anon	Confidential Report.
9.5	Anon	Confidential Report.

CHAPTER 10

INERTIA ROUTINE

10.1 INTRODUCTION

It should be noted that the methods in this chapter were not within the scope of work for the latest revision so the remainder of this chapter, and the computer routine for determining moments of inertia, are identical with what was presented in the original documentation report. The user is advised that independently determined inertia data should be used as an input if it is available. Doing so will greatly reduce the number of input parameters required and thus simplify the use of this program considerably. The methods in Chapter 10 are only approximate, intended for general preliminary design use, and have not been independently verified.

Moments of inertia are used in the determination of the dynamic stability characteristics of an aircraft. The specific values needed for input into the dynamic stability routine are I_{XX}, I_{YY}, I_{ZZ}, and I_{XZ}, representing moments of inertai in roll, pitch, and yaw, respectively, and the XZ cross product. It was decided that the ideal routine should be able to compute inertias within $\pm$10%.

Inertia data were solicited from a number of airframe manufacturers to provide baseline data. Data for 18 aircraft were graphed and examined for trends, in the hope that a modified statistical method could be derived. These are presented as Figure 10.1-3. This method did not produce the desired results.

A trial run was made with a method from Reference 10.1. This method is relatively simple and provides the required accuracy. A description of the method and results follows.

10.2 DISCUSSION OF METHOD

The moment of inertia of a body about its own axis of rotation is given by:

$$I = \int r^2 \rho_A \, dV \qquad (10.1)$$

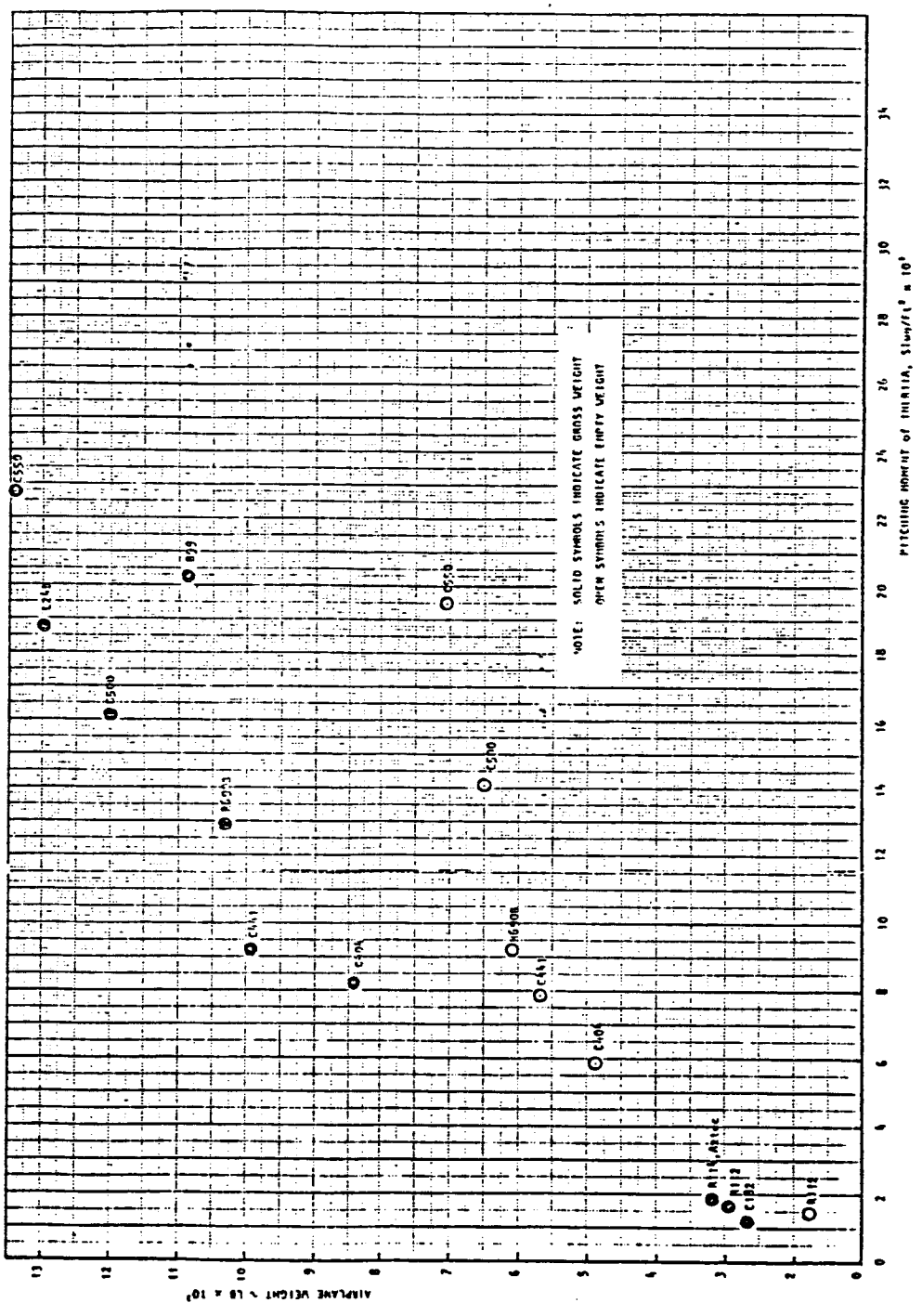

Figure 10.1: Statistical data for pitching moment of inertia

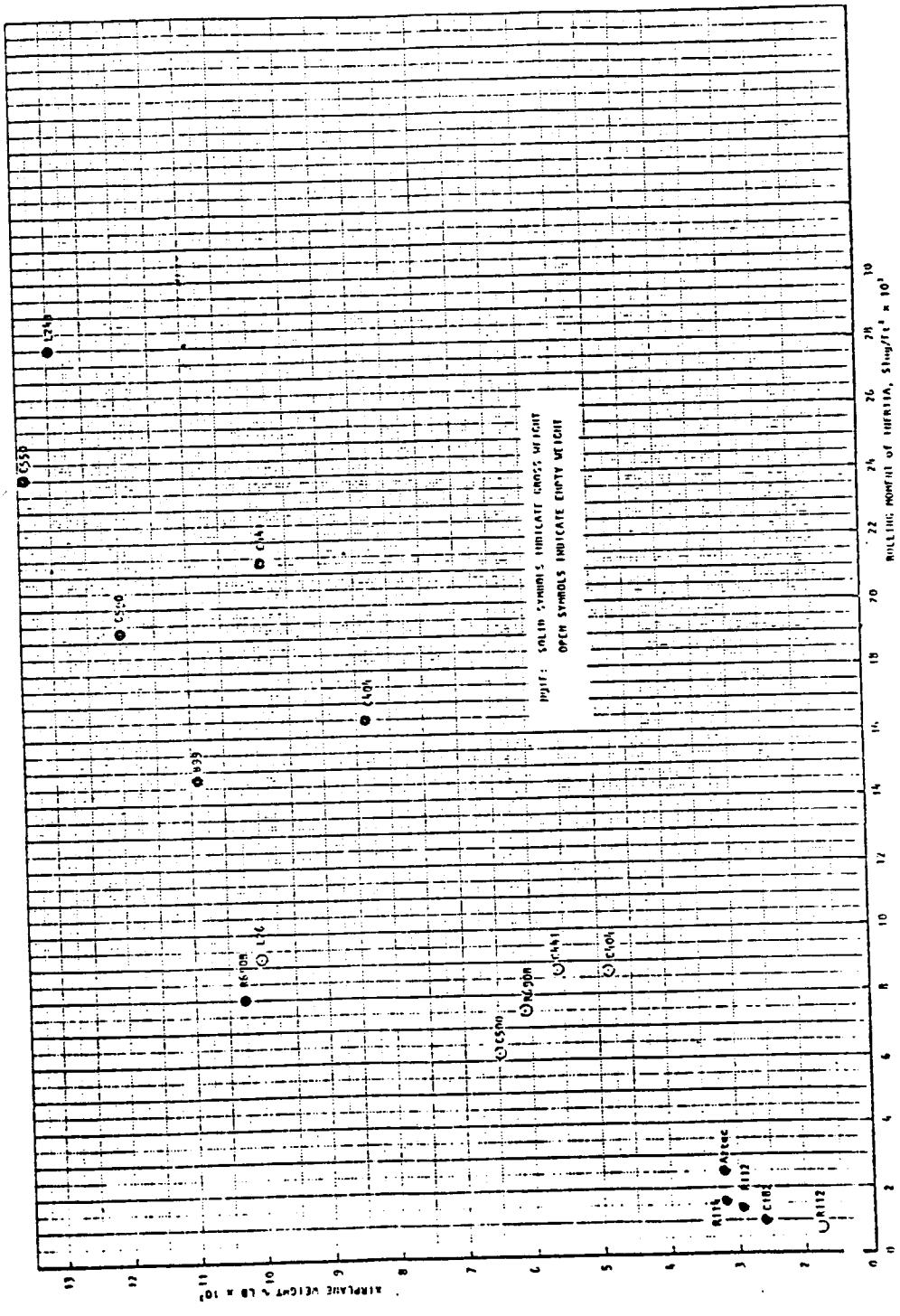

Figure 10.2: Statistical data for rolling moment of inertia

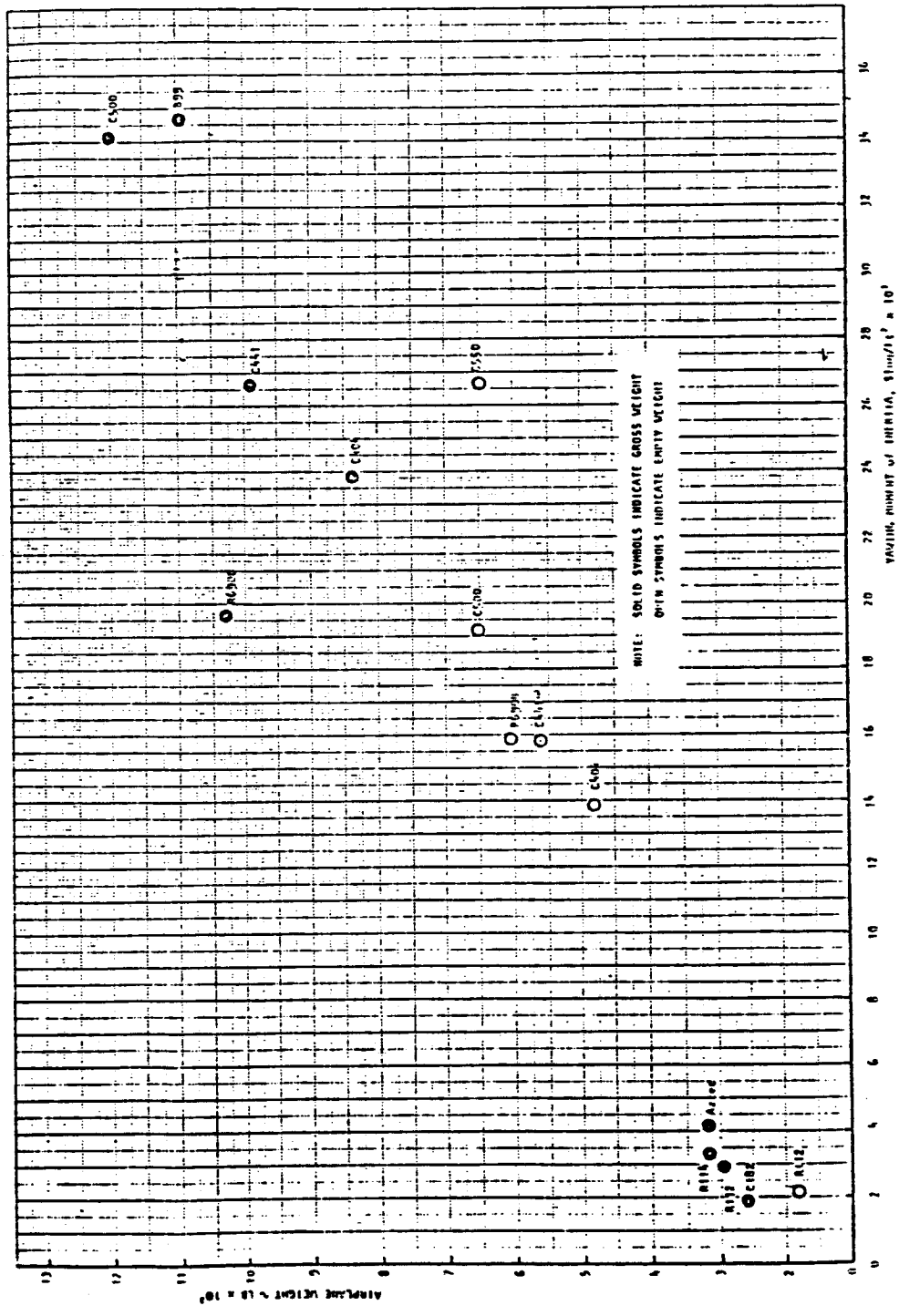

Figure 10.3: Statistical data for yawing moment of inertia

where: r is the distance to a point from the rotation axis, and

$\int \rho_A dV$ is the mass.

The inertia thus obtained will be refered to as I_0, for a body about its own axis. This inertia may be transformed to a remote axis by the parallel axis theorem:

$$I = I_0 + mr_2^2 \tag{10.2}$$

where:

r_2 is the radius to the remote axis.

In the detail design phase the aircraft may be broken up into several hundred sections to determine inertias. This is not practical in preliminary design. From the graphs of inertia data (Figures 10.1 through 10.3) it is apparent that a purely statistical approach would be difficult. The method of Reference 10.1 combines some aspects of weight breakdown and statistical methods to produce relatively rapid results.

The method of Reference 10.1 divides the empty aircraft into five major sections:

1) Wing
2) Fuselage
3) Horizontal Stabilizer
4) Vertical Stabilizer
5) Power Plant (Engine and Nacelle)

Mass and distance from the rotation axis are determined for each section, resulting in the mr^2 term of Equation (10.2); I_0's for each section are given by statistically based equations.

The inertias thus obtained are for the empty aircraft, gear up. Variable item inertias are estimated with formulas for standard geometric shapes.

Formulas for the various I_0's are presented below. Figure 10.4 illustrates geometric variables.

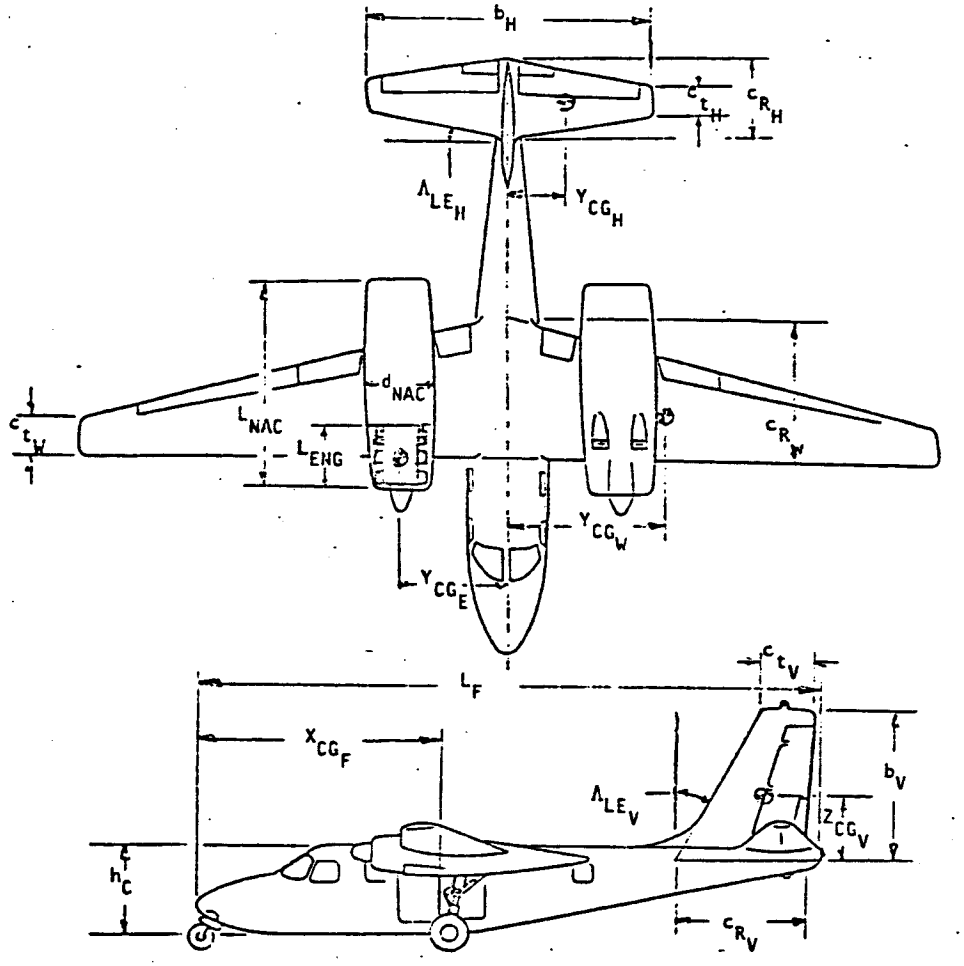

Figure 10.4: Airplane geometry

a. Wing Pitching Moment of Inertia, I_{0Y}

$$\text{if:} \quad (1) = \frac{\rho}{6}\left(-C_a^{\,2} + C_b^{\,2} + C_c\, C_b + C_c^{\,2}\right)$$

$$\text{and:} \quad (2) = \frac{\rho}{12}\left(-C_a^{\,3} + C_b^{\,3} + C_c^{\,2}\, C_b + C_c\, C_b^{\,2} + C_c^{\,3}\right) \qquad (10.3)$$

then: $(3) = (2) - \frac{(1)^2}{M_W}$

where:

$$\rho = \frac{M_W}{.5\ (-C_a + C_b + C_c)} \tag{10.4}$$

C_a is the smallest of the following values:

$$c_{R_W};\ \frac{b_W \tan\Lambda_{LE_W}}{2};\ c_{t_W} + \frac{b_W \tan\Lambda_{LE_W}}{2} \tag{10.5}$$

C_b is the intermediate value

C_c is the largest of these values

then:

$$I_{OY} = .703\,[(3)] \tag{10.6}$$

b. Wing Rolling Moment of Inertia, I_{OX}

$$I_{OX} = \frac{M_W b_W^2 K_1}{24}\left(\frac{c_{R_W} + 3c_{t_W}}{c_{R_W} + c_{t_W}}\right) \tag{10.7}$$

(For value of K_1, see Figure 10.5.)

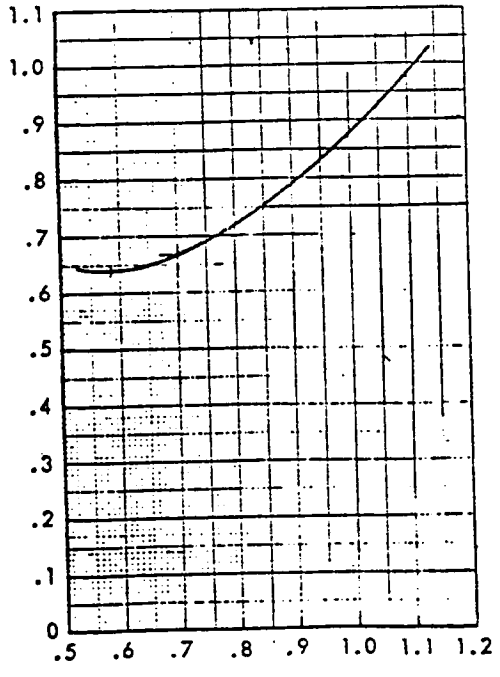

Note: X-axis parameter: $\dfrac{Y_{CG_W}}{\frac{b_W}{6}\left(\frac{c_{R_W} + 2c_{t_W}}{c_{R_W} + c_{t_W}}\right)}$

Figure 10.5: Parameter for Wing Rolling Moment of Inertia, I_{O_X}

c. Wing Yawing Moment of Inertia, I_{0Z}

$$I_{0Z} = I_{0X} + I_{0Y} \tag{10.8}$$

d. Fuselage Pitching Moment of Inertia, I_{0Y}

$$I_{0Y} = \frac{M_{fus} S K_2}{37.68} \left(\frac{3h_C}{2L_{fus}} + \frac{L_{fus}}{h_C} \right) \tag{10.9}$$

(For value of K_2, see Figure 10.6.)

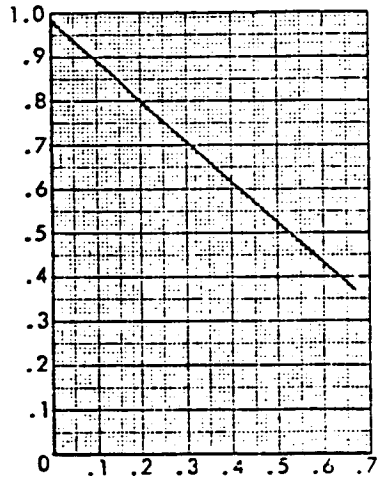

Note: X-axis parameter: $\frac{L_F/2 - X_{CG_F}}{L_F/2}$

Figure 10.6: Parameter for Fuselage Pitching Moment of Inertia, I_{o_Y}

e. Fuselage Rolling Moment of Inertia, I_{0X}

$$I_{0X} = \frac{M_f K_3}{4} \left(\frac{S_{fus}}{\pi L_{fus}} \right)^2 \tag{10.10}$$

(For value of K_3, see Figure 10.7.)

f. Fuselage Yawing Moment of Inertia, I_{0Z}

$$I_{0Z} = I_{0Y} \tag{10.11}$$

g. Horizontal Stabilizer Pitching Moment of Inertia, I_{0Y}

if:

$$(1) = \frac{\rho}{6} (-C_a^2 + C_b^2 + C_c C_b + C_c^2)$$

$$(2) = \frac{\rho}{12} (-C_a^3 + C_b^3 + C_c^2 C_b + C_c C_b^2 + C_c^3) \tag{10.12}$$

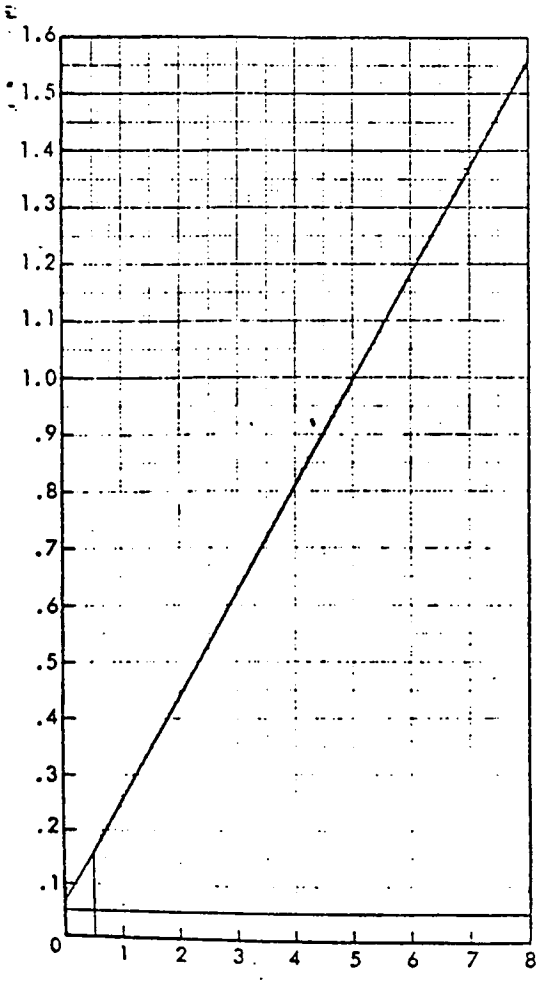

Figure 10.7: Parameter for Fuselage Rolling Moment of Inertia, I_{o_X}

$$(3) = (2) - \frac{(1)^2}{M_H} \tag{10.13}$$

where:

$$\rho = \frac{M_H}{.5\ (-C_a + C_b + C_c)} \tag{10.14}$$

C_a is the smallest of the following values:

$$c_{R_H};\quad \frac{b_H \tan\Lambda_{LE_H}}{2};\quad c_{t_H} + \frac{b_H \tan\Lambda_{LE_H}}{2} \tag{10.15}$$

C_b is the intermediate value

C_c is the largest of these values

then:

$$I_{OY} = .771 \quad (3) \tag{10.16}$$

h. Horizontal Stabilizer Rolling Moment of Inertia, I_{OX}

$$I_{OX} = \frac{M_H \, b_H^{\,2} \, K_4}{24} \left(\frac{c_{R_H} + 3c_{t_H}}{c_{R_H} + c_{t_H}} \right) \tag{10.17}$$

(For value of K_4, see Figure 10.8.)

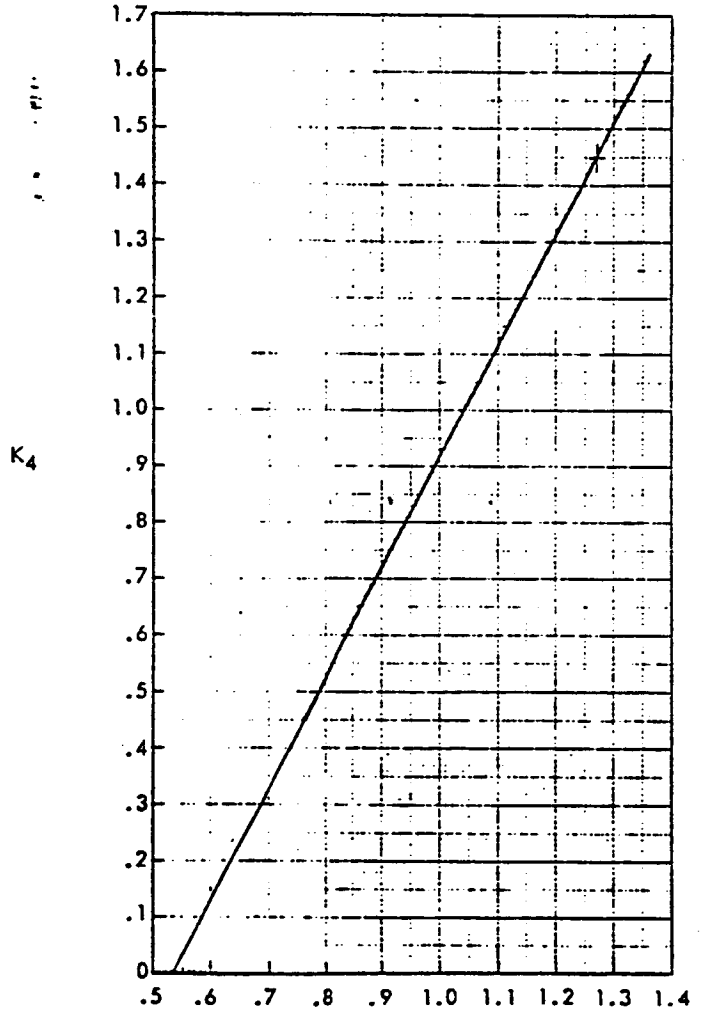

Note: X-axis parameter: $\dfrac{Y_{CG_H}}{\frac{b_H}{6}\left(\frac{c_{R_H} + 2c_{t_H}}{c_{R_H} + c_{t_H}}\right)}$

Figure 10.8: Parameter for Horizontal Tail Rolling Moment of Inertia, I_{O_X}

i. Horizontal Stabilizer Yawing Moment of Inertia, I_{OZ}

$$I_{OZ} = I_{OY} + I_{OX} \tag{10.18}$$

j. Vertical Stabilizer Pitching Moment of Inertia, I_{OY}

$$I_{OY} = I_{OX} + I_{OZ} \tag{10.19}$$

k. Vertical Stabilizer Rolling Moment of Inertia, I_{OX}

$$I_{OX} = \frac{M_V \, b_V^2 \, K_5}{18} \left[1 + \frac{2 c_{R_V} c_{t_V}}{(c_{R_V} + c_{t_V})^2} \right] \tag{10.20}$$

(For value of K_5, see Figure 10.9.)

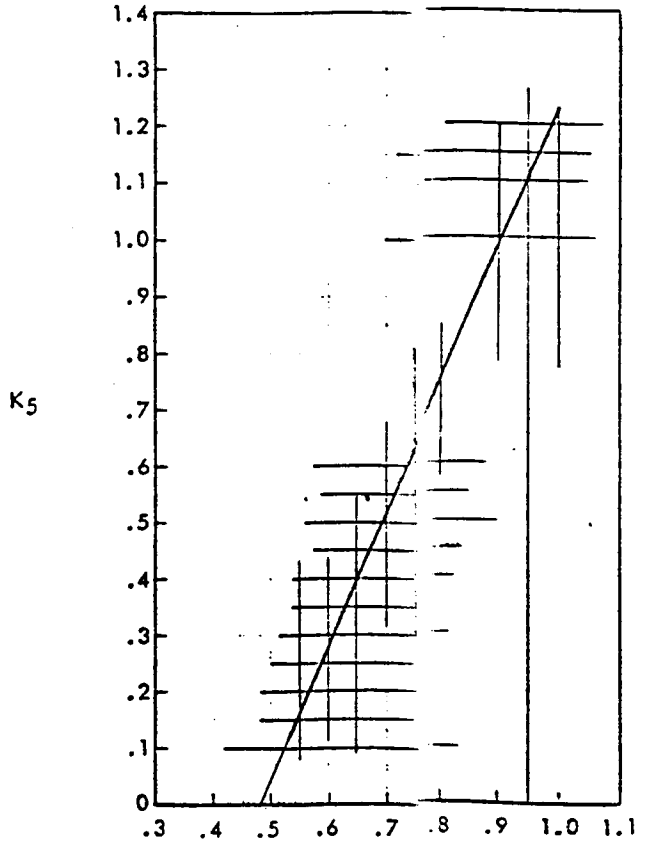

Note: X-axis parameter: $\dfrac{Z_{CG_V}}{\frac{b_V}{3}\left(\frac{c_{R_V} + 2\,c_{t_V}}{c_{R_V} + c_{t_V}}\right)}$

Figure 10.9: Parameter for Vertical Tail Rolling Moment of Inertia I_{O_X}

l. Vertical Stabilizer Yawing Moment of Inertia, I_{0Z}

if: $$(1) = \frac{\rho}{6} \left(-C_a^{\,2} + C_b^{\,2} + C_c\, C_b + C_c^{\,2}\right) \tag{10.21}$$

$$(2) = \frac{\rho}{12} \left(-C_a^{\,3} + C_b^{\,3} + C_c^{\,2}\, C_b + C_c\, C_b^{\,2} + C_c^{\,3}\right) \tag{10.22}$$

$$(3) = (2) - \frac{(1)^2}{M_V} \tag{10.23}$$

where:

$$\rho = \frac{M_V}{.5\ (-C_a + C_b + C_c)} \tag{10.24}$$

C_a is the smallest of the following values:

$$c_{R_V};\quad b_V \tan\Lambda_{LE_V};\quad c_{t_V} + b_V \tan\Lambda_{LE_V} \tag{10.25}$$

C_b is the largest of these values

then:

$$I_{0Z} = .771\ \ (3) \tag{10.26}$$

m. Power Plant Pitching Moment of Inertia, I_{0Y}

$$I_{0Y} = .061 \left[\frac{3}{4} M_p d_{Nac}^{\,2} + M_e L_{Eng}^{\,2} + (M_p - M_e)\ L_{Nac}^{\,2}\right] \tag{10.27}$$

n. Power Plant Rolling Moment of Inertia, I_{0X}

$$I_{0X} = .083\ M_p d_{Nac}^{\,2} \tag{10.28}$$

o. Power Plant Yawing Moment of Inertia, I_{0Z}

$$I_{0Z} = I_{0Y} \tag{10.29}$$

K values are statistically based and presented in graphic form as Figures 10.5 - 10.9, reproduced from Reference 10.1. An equation was fitted to the K1 line with a power curve fit. K2 - K5 are linear

equations of the form y = mx + b.

$$K1 = 1.2454\ (X1 - .585)^{1.8438} + .64 \tag{10.30}$$

where:

$$X1 = Y_{cg_W}/\{B \cdot 0.1667 \cdot (c_{R_{C_L}} + 2 \cdot c_t)/(c_R + c_t)\} \tag{10.30a}$$

$$K2 = .98 - .915\{(.5\ell_f - X_{cg_{fus}})/(.5\ell_f)\} \tag{10.31}$$

$$K3 = .07 + .186\sqrt{H_C}\ (W_{f_s}/W_f) \tag{10.32}$$

$$K4 = 1.97 \cdot X2 - 1.055 \tag{10.33}$$

where:

$$X2 = Y_{cg_{HT}}/\{b_{HT} \cdot 0.1667(c_{R_{HT}} + 2c_{t_{HT}})/(c_{R_{HT}} + c_{t_{HT}})\} \tag{10.33a}$$

$$K5 = 2.362 \cdot X3 - 1.134 \tag{10.34}$$

where:

$$X3 = Z_{cg_{VT}}/\{b_{VT} \cdot 0.3333(c_{R_{VT}} + 2c_{t_{VT}})/(c_{R_{VT}} + c_{t_{VT}})\} \tag{10.34a}$$

Fuel and passenger inertias are not accounted for by the method of Reference 10.1.

Assuming that all fuel is carried in the wing and tip tanks, fuel inertias may be approximated as follows:

Referring to Figure 10.11, the fuel tank is assumed to start at the fuselage and continue a distance, $b_{fuel}/2$, to a station, R. The fraction of the wing chord filled with fuel is given by C_{fuel}.

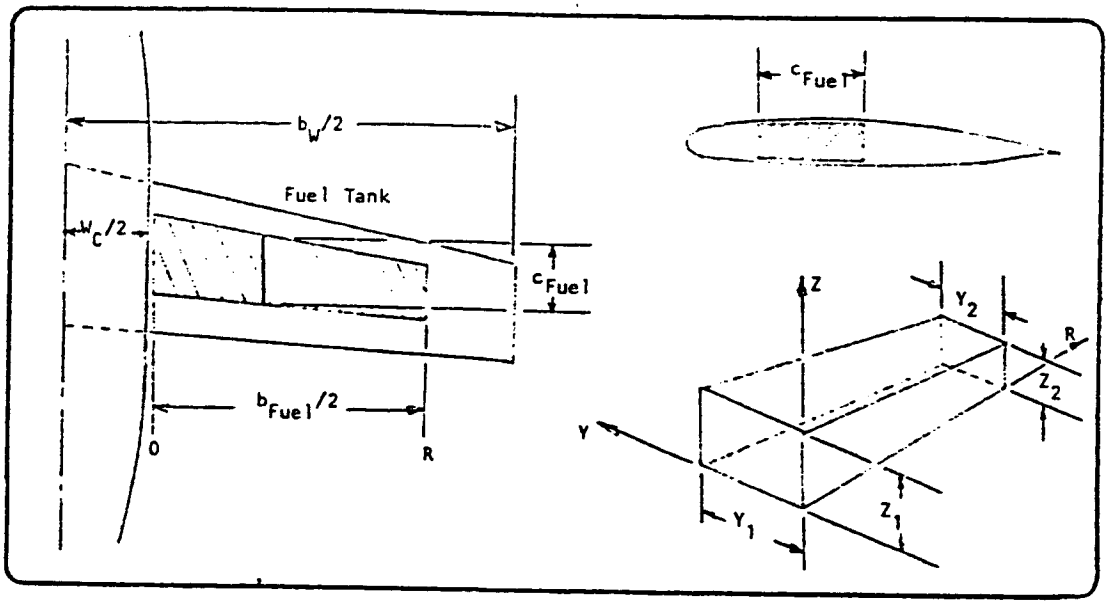

Figure 10.10: Fuel tank geometry

Fuel volume is assumed trapezoidal. Integrating over the trapezoidal volume with z, y, and r coordinates as shown, the inertia about the r = 0 plane is given by:

$$I_{0XX} = 2X \int_0^R r^2 \rho dM dr$$

$$= 2X \int_0^R r^2 \rho (Z_1 - Z_1 r + Z_2 r)(Y_1 - Y_1 r + Y_2 r) dr \qquad (10.35)$$

Z_1, Z_2, Y_1, Y_2, and ρ are constants, allowing integration of the equation to yield:

$$I_{0XX} = R^3 (0.0333\rho Z_1 Y_1 + 0.05\rho Z_2 Y_1 + 0.05\rho Z_1 Y_2 + 0.2\rho Z_2 Y_2) \qquad (10.36)$$

The variables Z_1, Z_2, Y_1, and Y_2 are functions of known variables:

$$Z_1 = \left\{(t/c_r - t/c_t)(1 - W_C/b_W) + t/c_t\right\} C_1 \qquad (10.37)$$

where:

$$C_1 = \left\{(c_{R_{C_L}} - c_t)(1 - W_C/b_W)\right\} + c_t$$

$$Z_2 = \left\{(t/c_r - t/c_t)(1 - b_{fuel}/b_W) + t/c_t\right\} C_2 \qquad (10.38)$$

where:

$$C_2 = \left\{(c_{R_{C_L}} - c_t)(1 - b_{fuel}/b_W)\right\} + c_t$$

$$Y_1 = c_{fuel} \times C_1$$

$$Y_2 = c_{fuel} \times C_2 \qquad (10.39)$$

ρ = fuel density in $\frac{lb/ft^3}{32.174}$

Tip tank variables are illustrated in Figure 10.11.

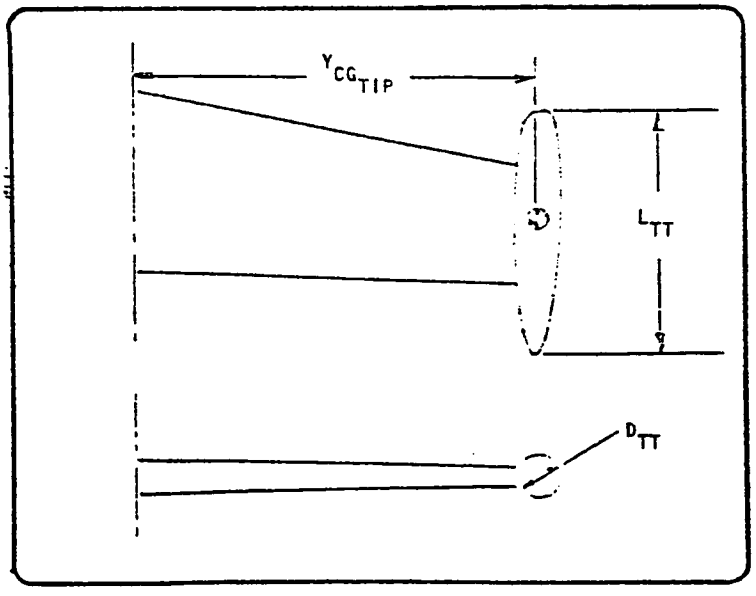

Figure 10.11: Tip tank geometry

The tip tank lateral location variable has a default value of $b_w/2$; using other values drop tanks or nacelle fuel may be simulated.

I_0 inertias are calculated for tip tanks about the pitch and yaw axes by:

$$I_0 = \frac{M_{tip}}{5}\left\{\left(\frac{L_{TT}}{2}\right)^2 + \left(\frac{D_{TT}}{2}\right)^2\right\} \qquad (10.40)$$

using the inertia formula for an elliptical body of revolution. I_0 for the roll axis is considered negligible.

Passenger inertia variables are illustrated in Figure 10.12.

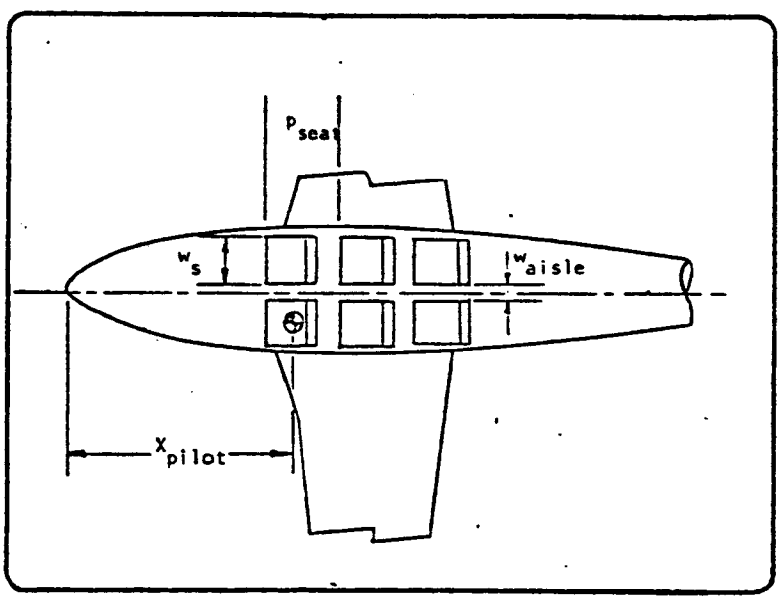

Figure 10.12: Passenger compartment.

Passenger I_0's about the roll axis are found by assuming the passenger's mass to be uniformly distributed over a 4.3 by 1.5 ft. rectangle. I_0's in the pitch and yaw axes are considered negligible.

I_{XZ}'s required for the dynamic stability derivatives are approximated by considering the I_{XZ}'s of the tails, and the wing where applicable.

10.3 CHECK CALCULATIONS

The sample aircraft of Reference 10.1 was used for a check calculation.

a. Wing Pitching Moment of Inertia I_{OY}

$C_a = 8.75$

$C_b = 17.08$

$C_c = 25$

$\rho = 27.98$

(1) = 5908.3

(2) = 88370.4

(3) = 13492.6

$I_{OY} = 9485.3$ slug ft^2

b. Wing Rolling Moment of Inertia I_{OX}

$I_{OX} = 135546$ slug ft^2

c. Wing Yawing Moment of Inertia I_{OZ}

$I_{OZ} = I_{OX} + I_{OY} = 145031$ slug ft^2

d. Fuselage Pitching Moment of Inertia I_{OY}

$I_{OY} = 311319$ slug ft^2

e. Fuselage Rolling Moment of Inertia I_{OX}

K3 = .98

$I_{OX} = 11899.9$ slug ft^2

f. Fuselage Yawing Moment of Inertia I_{OZ}

$I_{OZ} = I_{OY} = 311319$ slug ft^2

g. Horizontal Stabilizer Pitching Moment of Inertia, I_{OY}

$C_a = 3.539$

$C_b = 7.709$

$C_c = 8.33$

$\rho = 4.97$

(1) = 149.61

(2) = 837.4

(3) = 117.2

$I_{OY} = 90.38$

h. Horizontal Stabilizer Rolling Moment of Inertia, I_{OX}

K4 = .72

$I_{OX} = 1723.8$

i. Horizontal Stabilizer Yawing Moment of Inertia, I_{OZ}

$I_{OZ} = I_{OY} + I_{OX} = 1814.2$

j. Vertical Stabilizer Rolling Moment of Inertia, I_{OX}

K5 = .93

$I_{OX} = 188.6$

k. Vertical Stabilizer Yawing Moment of Inertia, I_{OZ}

$C_a = 12.56$

$C_b = 20.8$

$C_c = 20.89$

$\rho = 0.64$

(1) = 122.2

(2) = 1815.17

(3) = 213.6

$I_{OZ} = 164.7$

1. Vertical Stabilizer Pitching Moment of Inertia, I_{OY}

$$I_{OY} = I_{OX} + I_{OZ} = 353.3 \text{ slug ft}^2$$

m. Power Plant Pitching Moment of Inertia, I_{OY}

$$I_{OY} = 2748.8$$

n. Power Plant Rolling Moment of Inertia, I_{OX}

$$I_{OX} = 448.6 \text{ slug ft}^2$$

o. Power Plant Yawing Moment of Inertia, I_{OZ}

$$I_{OZ} = I_{OY} = 2748.8 \text{ slug ft}^2$$

p. Aircraft Cross Product Inertia, I_{XZ}

$$I_{XZ_V} = -Z_{CG_V} (X_{CG_V}) M_V$$

$$I_{XZ_V} = 2892.1$$

$$I_{XZ_V} = Z_{CG_{Wing}} (X_{CG_{Wing}}) M_W$$

$$I_{XZ_W} = 0$$

A comparison of these results with the results of Reference 10.1, as well as with the computer testrun output, will be done in Section 10.4.

10.4 PROGRAM DESCRIPTION

The method described in Section 10.2 was transformed into a FORTRAN computer routine. Table 10.1 shows the computer variables as used in the program. Figure 10.13 shows a flow chart of the program. A listing of the program as well as a sample output is shown in Figure 10.14.

TABLE 10.1 VARIABLE NAMES IN SUBROUTINE "INERTA"

NAME	ENG. SYMBOL	DIMENSION	ORIGIN	REMARKS
AXIS	s	ft	Common	Major axis of tip tank
BENGOB	b_{eng}/b_W	---	Common	
BFUEL	b_{fuel}	ft	Common	
BHT	b_{HT}	ft	Common	
BVT	b_{VT}	ft	Common	
BW	b_W	ft	Common	
BXIS	b	ft	Common	Minor axis of tip tank
CA	C_a	---	---	
CB	C_b	---	---	
CC	C_c	---	---	
CGLG	CG_{LG}	ft	Common	Radial distance from fuselage center line
CFUEL	C_{fuel}	ft	---	

TABLE 10.1 VARIABLE NAMES IN SUBROUTINE "INERTA" (continued)

NAME	ENG. SYMBOL	DIMENSION	ORIGIN	REMARKS
CHORD1	---	---	---	Dummy
CHORD2	---	---	---	Dummy
CON	---	---	---	Dummy
CONST1	---	---	---	Dummy
CONST2	---	---	---	Dummy
CONST3	---	---	---	Dummy
CRCLHT	$C_{R_{HT}}$	ft	Common	
CRCLVT	$C_{R_{VT}}$	ft	Common	
CRCLW	$C_{R_{t_W}}$	ft	Common	
CTHT	$C_{t_{HT}}$	ft	Common	
CTVT	$C_{t_{VT}}$	ft	Common	
CTW	C_{t_W}	ft	Common	
DBARN	$\bar{d}_{nac}$	ft	Common	
ELCG	X_{CG}	ft	Common	
ELCGH	$X_{CG_{HT}}$	ft	Common	
ELCGV	$X_{CG_{VT}}$	ft	Common	
ELF	ℓ_{fus}	ft	Common	
ELN	ℓ_{nac}	ft	Common	

TABLE 10.1 VARIABLE NAMES IN SUBROUTINE "INERTA" (continued)

NAME	ENG. SYMBOL	DIMENSION	ORIGIN	REMARKS
ELTIP	$X_{CG_{Tip}}$	ft	Common	
ELWING	X_{CG_W}	ft	Common	
ENGIOX	$I_{OX_{eng}}$	slug ft^2	---	
ENGIOY	$I_{OY_{eng}}$	slug ft^2	---	
ENGIX	$I_{XX_{eng}}$	slug ft^2	---	
ENGIY	$I_{YY_{eng}}$	slug ft^2	---	
ENGIZ	$I_{ZZ_{eng}}$	slug ft^2	---	
FUELD	ρ_{fuel}	lb/gal	Common	
FUSIOX	$I_{OX_{fus}}$	slug ft^2	---	
FUSIOY	$I_{OY_{fus}}$	slug ft^2	---	
FUSIX	$I_{XX_{fus}}$	slug ft^2	---	
FUSIY	$I_{YY_{fus}}$	slug ft^2	---	
FUSIZ	$I_{ZZ_{fus}}$	slug ft^2	---	
GEARIX	$I_{XX_{LG}}$	slug ft^2	---	
GEARIY	$I_{YY_{LG}}$	slug ft^2	---	
GEARIZ	$I_{ZZ_{LG}}$	slug ft^2	---	

TABLE 10.1 VARIABLE NAMES IN SUBROUTINE "INERTA" (continued)

NAME	ENG. SYMBOL	DIMENSION	ORIGIN	REMARKS
HC	h_c	ft	Common	
HORIOX	$I_{OX_{HT}}$	slug ft^2	---	
HORIOY	$I_{OY_{HT}}$	slug ft^2	---	
HORIX	$I_{XX_{HT}}$	slug ft^2	---	
HORIY	$I_{YY_{HT}}$	slug ft^2	---	
HORIZ	$I_{ZZ_{HT}}$	slug ft^2	---	
INERTX	I_{XX}	slug ft^2	---	
INERTY	I_{YY}	slug ft^2	---	
INERTZ	I_{ZZ}	slug ft^2	---	
IOY	---	---	---	Dummy
IROW	---	---	---	Dummy
IROW2	---	---	---	Dummy
IXXP	$I_{XX_{pax}}$	slug ft^2	---	
IXZ	I_{XZ}	slug ft^2	---	
IXZH	$I_{XZ_{HT}}$	slug ft^2	---	
IXZV	$I_{XZ_{VT}}$	slug ft^2	---	
IXZW	$I_{XZ_{W}}$	slug ft^2	---	
IYYP	$I_{YY_{pax}}$	slug ft^2	---	

TABLE 10.1 VARIABLE NAMES IN SUBROUTINE "INERTA" (continued)

NAME	ENG. SYMBOL	DIMENSION	ORIGIN	REMARKS
IZZP	$I_{ZZ_{pax}}$	slug ft^2	---	
K1	K1	---	---	
K2	K2	---	---	
K3	K3	---	---	
K4	K4	---	---	
K5	K5	---	---	
LENG	ℓ_{eng}	ft	Common	
M	M	lb	---	Dummy
MB	W	lb	Common	
MBT	W_B	slugs	---	
MEP	W_{pe}	slugs	---	
MFTP	$W_{fuel_{tip}}$	slugs	---	
MFW	W_{fuel_W}	slugs	---	
MHT	W_{HT}	slugs	---	
MLG	W_{LG}	slugs	---	
MP	W_p	slugs	---	
MPASS	W_{pax}	slugs	---	
MPLMAX	$W_{pax_{max}}$	slugs	---	
MTIP	W_{tip}	slugs	---	

TABLE 10.1 VARIABLE NAMES IN SUBROUTINE "INERTA" (continued)

NAME	ENG. SYMBOL	DIMENSION	ORIGIN	REMARKS
MVT	W_{VT}	slugs	---	
MW	W_W	slugs	---	
PAX	N_{pax}	---	Common	Excluding pilot
PS	P_{seat}	ft	Common	
R	---	---	---	Dummy
R1	---	---	---	Dummy
RELP	$X_{CG_{eng}}/\ell_{fus}$	---	---	
RELR	$X_{CG_{fus}}/\ell_{fus}$	---	---	.33
RHO	ρ	lb sec^2/ft^4	---	
SAB	---	---	Common	
SAH	---	---	Common	
SF	S_{fus}	ft^2	Common	
SWPLE	Λ_{LE_W}	rad	Common	
SWPLEH	$\Lambda_{LE_{HT}}$	rad	Common	
SWPLEV	$\Lambda_{LE_{VT}}$	rad	Common	
TCR	$t/c\|_R$	---	Common	
TCT	$t/c\|_t$	---	Common	
TIPIOY	$I_{OY_{tip}}$	slug ft^2	---	
UWPAX	W_{pax}	lb	Common	

TABLE 10.1 VARIABLE NAMES IN SUBROUTINE "INERTA" (continued)

NAME	ENG. SYMBOL	DIMENSION	ORIGIN	REMARKS
VERIOX	$I_{OX_{VT}}$	slug ft^2	---	
VERIOY	$I_{OY_{VT}}$	slug ft^2	---	
VERIOZ	$I_{OZ_{VT}}$	slug ft^2	---	
VERIX	$I_{XX_{VT}}$	slug ft^2	---	
VERIY	$I_{YY_{VT}}$	slug ft^2	---	
VERIZ	$I_{ZZ_{VT}}$	slug ft^2	---	
WAS	W_{aisle}	ft	Common	
WB	W_{B_S}	lb	Common	Fuselage structural weight
WBT	W_B	lb	Common	Fuselage weight
WC	W_C	ft	Common	
WEIGHT	W	lb	---	
WEP	W_{pe}	lb	Common	
WFIOX	$I_{OX_{fuel}}$	slug ft^2	---	
WFIX	$I_{XX_{fuel}}$	slug ft^2	---	
WFIY	$I_{YY_{fuel}}$	slug ft^2	---	
WFTP	$W_{fuel_{tip}}$	lb	Common	
WFW	W_{fuel_W}	lb	Common	

TABLE 10.1 VARIABLE NAMES IN SUBROUTINE "INERTA" (continued)

NAME	ENG. SYMBOL	DIMENSION	ORIGIN	REMARKS
WHT	W_{HT}	lb	Common	
WLG	W_{LG}	lb	Common	
WNGIOX	I_{OX_W}	slug ft^2	---	
WNGIOY	I_{OY_W}	slug ft^2	---	
WNGIOZ	I_{OZ_W}	slug ft^2	---	
WNGIX	I_{XX_W}	slug ft^2	---	
WNGIY	I_{YY_W}	slug ft^2	---	
WNGIZ	I_{ZZ_W}	slug ft^2	---	
WP	W_p	lb	Common	
WPLMAX	$W_{pax_{max}}$	lb	Common	
WS	W_{seat}	ft	Common	
WTIP	W_{tip}	lb	Common	
WVT	W_{VT}	lb	Common	
WW	W_w	lb	Common	
XPILOT	X_{pilot}	ft	Common	
Y1	---	---	---	Dummy
Y2	---	---	---	Dummy
YCGENG	$\bar{Y}_{CG_{eng}}$	ft	Common	

TABLE 10.1 VARIABLE NAMES IN SUBROUTINE "INERTA" (continued)

NAME	ENG. SYMBOL	DIMENSION	ORIGIN	REMARKS
YCGHOR	$\bar{Y}_{CG_{HT}}$	ft	Common	.2 b_{HT}
YCGTIP	$\bar{Y}_{CG_{tip}}$	ft	Common	
YCGWNG	$\bar{Y}_{CG_{wing}}$	ft	Common	.18 b_W
Z1	---	---	---	Dummy
Z2	---	---	---	Dummy
ZCGHOR	$\bar{Z}_{CG_{HT}}$	ft	Common	
ZCGVER	$\bar{Z}_{CG_{VT}}$	ft	Common	.6 b_{VT}
ZCGWNG	$\bar{Z}_{CG_W}$	ft	Common	

Table 10.2 illustrates the comparison between the results of the hand calculation, the data of Reference 10.1, and the computer output for the test airplane of Reference 10.1

TABLE 10.2 COMPARISON OF INERTIA COMPUTATIONS

	KU-FRL "INERTA" Hand Calculation	Ref. 10.1	KU-FRL "INERTA" Computer
I_{OY_W}	9,485.3	9,493.2	9,443.9
I_{OX_W}	135,546.0	135,591.5	135,861.6
I_{OZ_W}	145,031.0	145,084.7	143,305.5

TABLE 10.2 COMPARISON OF INERTIA COMPUTATIONS (continued)

	KU-FRL "INERTA" Hand Calculation	Ref. 10.1	KU-FRL "INERTA" Computer
$I_{OY_{fus}}$	311,319.0	311,473.4	311,994.9
$I_{OX_{fus}}$	11,899.9	11,798.5	11,191.9
$I_{OZ_{fus}}$	311,319.0	311,473.4	311,994.9
$I_{OY_{Hoz}}$	90.4	95.7	90.3
$I_{OX_{Hoz}}$	1,723.8	1,774.9	1,724.4
$I_{OZ_{Hoz}}$	1,814.2	1,870.6	1,814.7
$I_{OY_{Vert}}$	353.3	305.2	339.3
$I_{OX_{Vert}}$	188.6	188.4	189.2
$I_{OZ_{Vert}}$	164.7	116.7	150.1
$I_{OY_{eng}}$	2,748.8	2,748.8	2,761.8
$I_{OX_{eng}}$	448.6	447.9	448.6
$I_{OZ_{eng}}$	2,748.8	2,748.8	1,966.8

NOTE: All inertias in slug ft^2.

Table 10.3 gives the results of computer runs to determine the mass properties for several general aviation aircraft. Also given are manufacturers' data.

TABLE 10.3 INERTIA CALCULATIONS, COMPARISON

AIRPLANE TYPE	WEIGHT	SOURCE	I_{XX} slug ft^2	% ERR.	I_{YY} slug ft^2	% ERR.	I_{ZZ} slug ft^2	% ERR.	I_{XZ}
E	MWE	INERTA	650.6	2.9	644.4	2.7	1231.9	6.0	-25.96
		MANF.	631.7		661.5		1157.9		
E	MTOW	INERTA	697.8		645.9		1254.9		
		MANF.	---		---		---		
F	MWE	INERTA	829.6	4.3	1860.2	15.5	2993.7	24.7	-1891.7
		MANF.	794.2		1571.3		2252.4		
F	MTOW	INERTA	1215.2	27.7	1879.8	.1	3334.7	1.0	
		MANF.	1551.4		1878.3		3301.0		
H	MWE	INERTA	9467.5	6.6	13930.9	2.8	22076.5	1.1	-267.5
		MANF.	8846.0		14318.0		21830.0		
H	MTOW	INERTA	17512.7	15.0	21554.0	6.0	37267.6	9.2	
		MANF.	14884.0		20270.0		33836.0		
A	MWE	INERTA	6793.2	11.0	17260.9	13.4	22919.0	14.6	-1320.4
		MANF.	6045.0		14948.0		19572.8		
A	MTOW	INERTA	34319.6		22561.9		52960.9		
		MANF.	---		---		---		

The average error in the computations is as follows:

I_{XX}	I_{YY}	I_{ZZ}
11.3%	6.8%	5.7%

It may be concluded that the subroutine INERTA performs well within the accuracy required for preliminary design work. No data were available for comparison with the I_{XZ} computations.

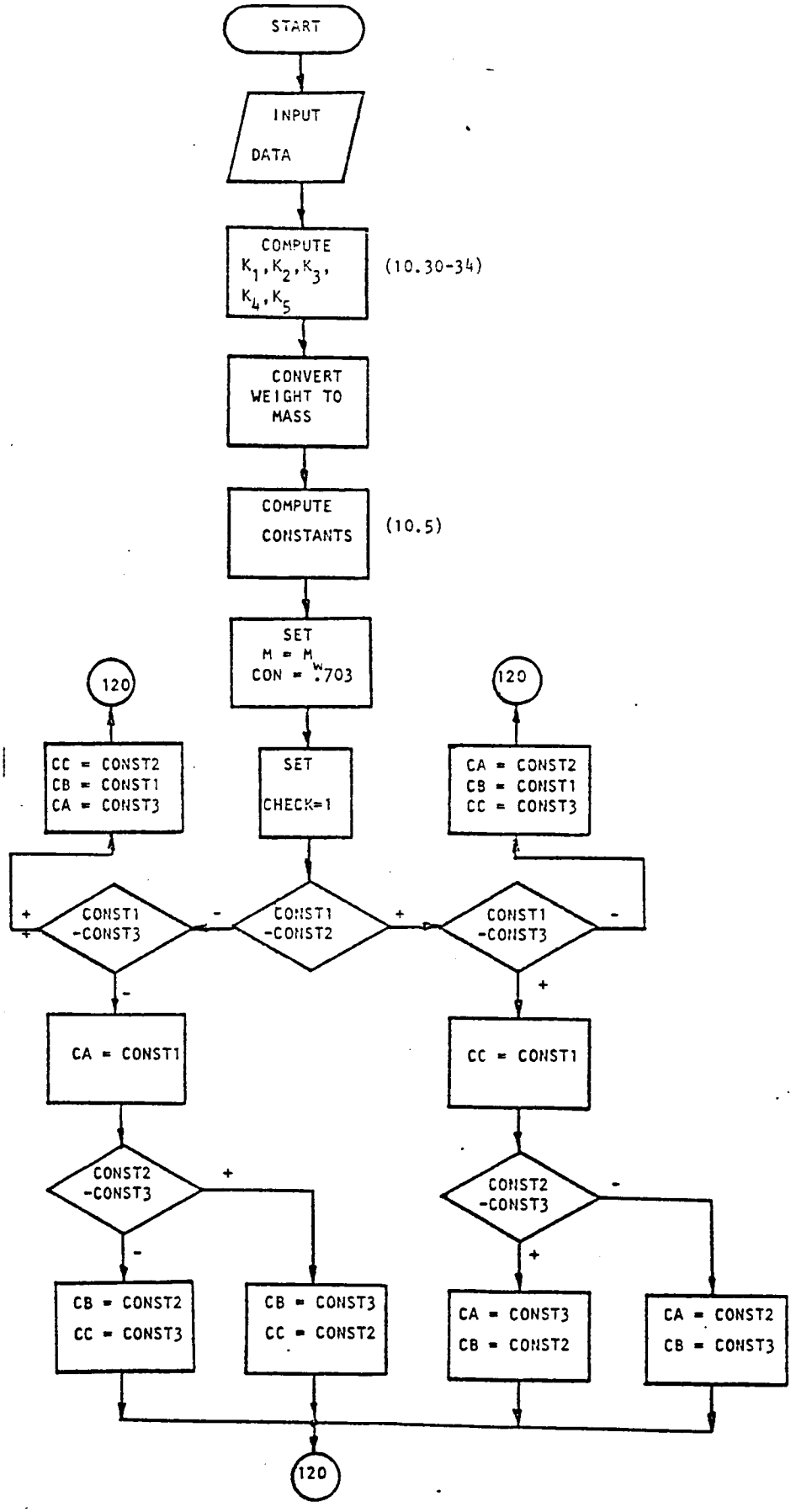

Figure 10.13: Flowchart of subroutine "INERTA"

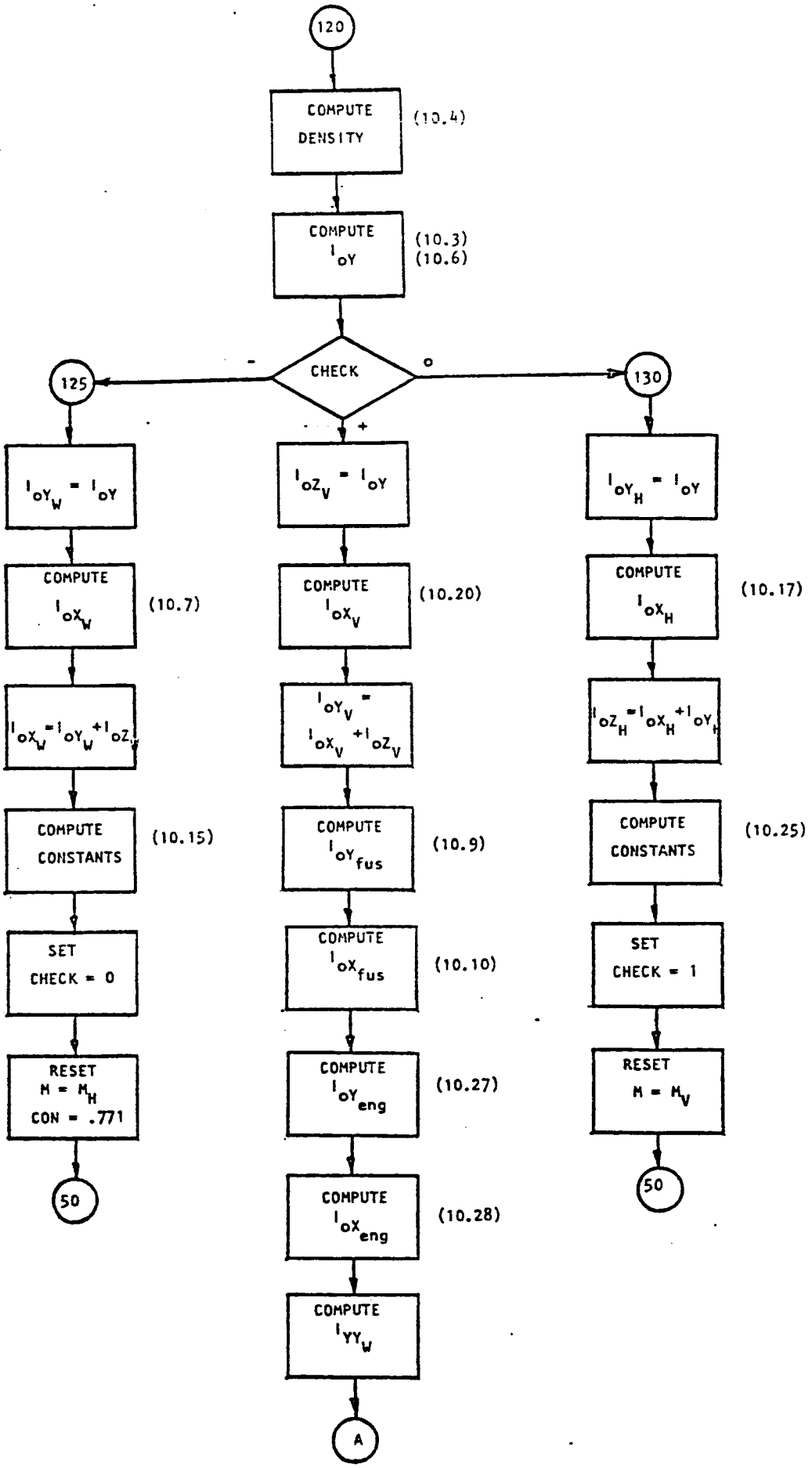

Figure 10.13: continued

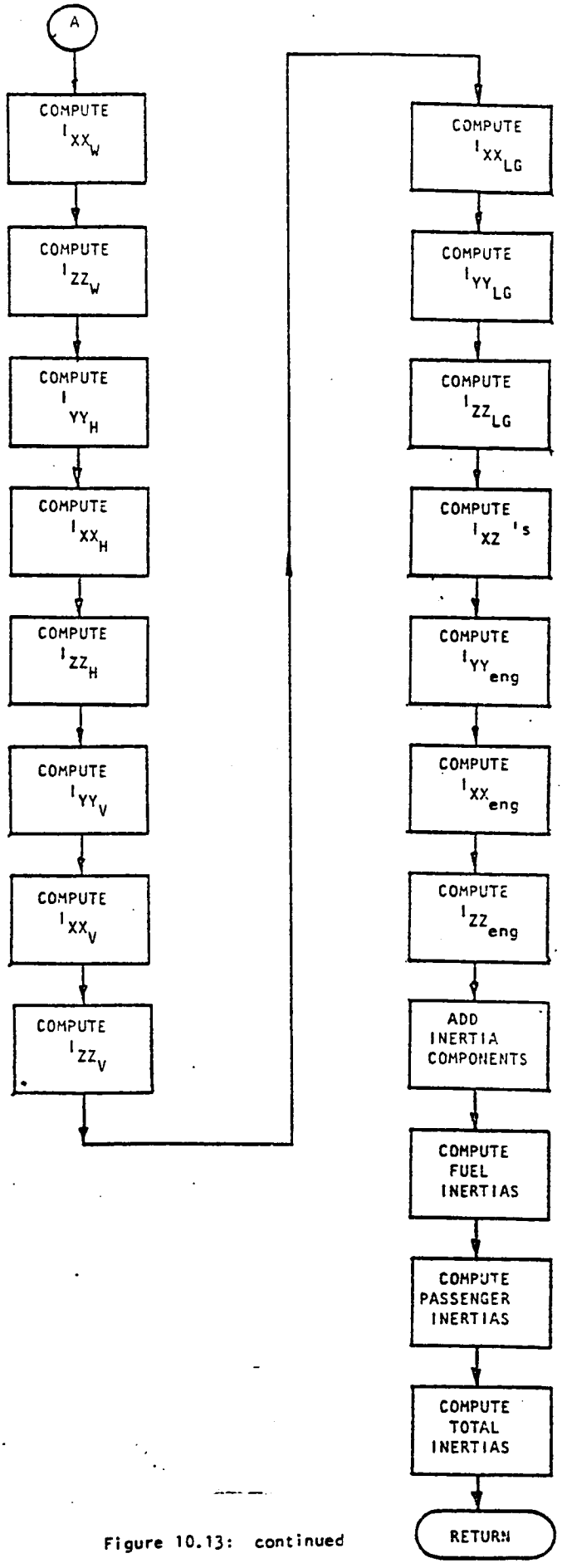

Figure 10.13: continued

```
      SUBROUTINE INERTA (INERTX,INERTY,INERTZ,IXZ,
     &IXXW,IYYW,IZZW)
      REAL K1,K2,K3,K4,K5,MHT,MW,MVT,MP,MB,MLG,
     &MPLMAX,MFW,MFTP,MTIP,MREMN,MPEI,LENG,INERTX,
     &IOY,INERTY,INERTZ,IXZ,IXZW,IXZV,IXZH,LPILOT,IXXP,IYYP,IZZP,MPASS
     &,IXXM,IYYM,IZZM,IOC
      COMMON/WEIGHT/ELCG,WEIGHT
      COMMON/GEOM/DIHD,ZW,SAH,XHMAC,ELINC
      COMMON/WGHT1/WHT,WVT,WW,WP,WEP,WB,WBT,WLG
      COMMON/WGHT2/WTIP,WFW,WFTP,UWPAX,FUELD
      COMMON/WGHT3/WCC,WCFW,WSAS,WFE
      COMMON/WING/DLMC4,AR,SLM,E,CRCLW,CBARW,SW,CLAWP
      COMMON/HORZ/DLMC4H,ARH,SLMH,BHT,CBARHT,SHT,CLAHP,CRCLHT
      COMMON/VERT/DLMC4V,ARV,SLMV,BVT,CBARVT,SVT,CLAVP,CRCLVT
      COMMON/ACCOM/PAX,WAC,WS,PS,SAB,XPILOT
      COMMON/WAC/XWAC,ELN
      COMMON/PRPLS2/BENGCG,DBARN,LENG,BFUEL
      COMMON/WING2/CROOTW,CTIPW,EYEW,TCR,TCT
      COMMON/SHAPE3/YCGWVG,YCGHOR,ZCGVER,CGLG,ZCGWNG,AXIS,BXIS
     &,ELTIP
      COMMON/FUS/ELF,DFUS,HC,WC,LN,ELTH,HH,SO,R2I,LV,ZV
      COMMON/SHAPE4/ELWING,ELCGH,ELCGV,RELP,RELR
      COMMON/FUS3/AFSA,SESRAT,SF
      IF(FUELD.EQ.0) FUELD=6.687
      ZCGHOR=0.0
      CTHT=SLMH*CRCLHT
      CTVT=SLMV*CRCLVT
      YCGTIP=B/2.
      IF(WBT.EQ.0) WBT=WB+WCC+WCFW+WSAS+WFE
      IF(SAH.EQ.1)ZCGHOR= -BVT
      IF(YCGWNG.EQ.0.) YCGWNG=.18*B
      IF(YCGHOR.EQ.0)YCGHOR=0.2*BHT
      IF(ZCGVER.EQ.0)ZCGVER=0.6*BVT
      IF(RELR.EQ.0)RELR=0.33
      X1=YCGWNG/(B*.1667*(CRCLW+2.*CTIPW)/
     &(CRCLW+CTIPW))
      K1=(X1-0.585)**1.8438*1.2454+0.64
      K2=0.95-0.915*(ABS(0.5*ELF-RELR*ELF)/(0.5*ELF))
      K3=0.07+0.186*(HC*12)**0.5*WB/WBT
      K4=1.97*YCGHOR/(BHT*0.1667*(CRCLHT+2*CTHT)
     &/(CRCLHT+CTHT))-1.055
      K5=2.362*ZCGVER/(BVT*0.3333*(CRCLVT+2*CTVT)
     &/(CRCLVT+CTVT))-1.134
      MHT=WHT/32.174
      MLG=WLG/32.174
      MVT=WVT/32.174
      MW=WW/32.174
      MP=WP/32.174
      MEP=WEP/32.174
      WPLMAX=200.
      MPLMAX=WPLMAX/32.174
      MFW=WFW/32.174
      MFTP=WFTP/32.174
```

Figure 10.14: Listing of subroutine "INERTA"

```
      CTIP=CTIP/32.174
      CBT=CBT/32.174
      RLMC4H=DLMC4H*.01745
      RLMC4V=DLMC4V*.01745
      RLMC4=DLMC4*.01745
      SWPLE=ATAN(SIN(RLMC4)/COS(RLMC4)+(1./AR)*((1.-SLM)/(1.+SLM)))
      SWPLEV=ATAN(SIN(RLMC4V)/COS(RLMC4V)+(1./ARV)*((1.-SLMV)/(1.+SLMV
     &))
      SWPLEH=ATAN(SIN(RLMC4H)/COS(RLMC4H)+(1./ARH)*((1.-SLMH)/(1.+SLMH
     %))
      CONST2=B*(SIN(SWPLE)/COS(SWPLE))*.5
       CONST3=CTIP+CONST2
      CON=0.703
      M=MW
      CHECK=-1
   50 IF(CONST1.LE.CONST2)GO TO 90
      IF(CONST1.LE.CONST3)GO TO 70
      CC=CONST1
      IF(CONST2.LE.CONST3)GO TO 60
      CA=CONST3
      CB=CONST2
      GO TO 120
   60 CA = CONST2
      CB=CONST3
      GO TO 120
   70 CA = CONST2
      CB=CONST1
      CC=CONST3
      GO TO 120
   90 IF(CONST1.LT.CONST3)GO TO 100
      CA=CONST3
      CB=CONST1
      CC=CONST2
      GO TO 120
  100 CA=CONST1
      IF(CONST2.LT.CONST3)GO TO 110
      CB=CONST3
      CC=CONST2
      GO TO 120
  110 CB=CONST2
      CC=CONST3
  120 CONTINUE
      RHO=M/(0.5*(-CA+CB+CC))
      IOY=CON*(RHO*0.0833*(-CA**3+CB**3+CC**2*CB+CC*CB**2
     &+CC**3)-((RHO*0.1667*(-CA**2+CB**2+CC*CB+CC**2))**2/M))
      IF(CHECK)125,130,140
  125 WNGIOY=IOY
       WNGIOX=MW*B**2*K1*.0417*((CRCLW+3.*CTIPW)/(CRCLW+CTIPW))
      WNGIOZ=WNGIOY+WNGIOX
      CONST1=CRCLHT
      CONST2=BHT*(SIN(SWPLEH)/COS(SWPLEH))*0.5
      CONST3=CTHT+CON
      CHECK=0
```

Figure 10.14: continued

```
107             M=MHT
108             CON=0.771
109             GO TO 50
110       130   HORIOY=IOY
111             HORIOX=MHT*BHT**2*K4*0.0417*((CRCLHT+3*CTHT)/
112            $(CRCLHT+CTHT))
113             HORIOZ=HORIOY+HORIOY
114             CONST1=CRCLVT
115             CONST2=BVT*(SIN(SWPLEV)/COS(SWPLEV))*0.5
116             CONST3=CTVT+CONST2
117             CHECK=1
118             M=MVT
119             GO TO 50
120       140   VERIOZ=IOY
121             VERIOX=MVT*BVT**2*K5*0.0556*(1+(2*CRCLVT*CTVT)
122            $/((CRCLVT+CTVT)**2))
123             VERIOY=VERIOX+VERIOZ
124             FUSIOY=MBT*SF*K2*0.0265*(3*HC/(2*ELF)+ELF/HC)
125             FUSIOX=MBT*K3*0.25*((SF/(3.142*ELF))**2)
126             ENGIOY=0.061*(0.75*MP*DBARN**2+MEP*LENG**2+
127            $(MP-MEP)*ELN**2)
128             ENGIOX=0.083*MP*DBARN**2
129             WNGIY=WNGIOY+MW*(ELCG-ELWING)**2
130             WNGIX=WNGIOX+MW*YCGWNG**2+MTIP*YCGTIP**2
131             WNGIZ=MW*YCGWNG**2+WNGIOZ+MTIP*YCGTIP**2
132             HORIY=HORIOY+MHT*(ELCGH-ELCG)**2
133             HORIX=HORIOX+MHT*YCGHOR**2
134             HORIZ=HORIOZ+MHT*(ELCGH-ELCG)**2
135             VERIY=VERIOY+MVT*(ELCGV-ELCG)**2
136             VERIX=VERIOX+MVT*ZCGVER**2
137             VERIZ=VERIOZ+MVT*(ELCGV-ELCG)**2
138             FUSIY=FUSIOY+(ELF*RELR-ELCG)**2*MBT
139             FUSIX=FUSIOX
140             FUSIZ=FUSIY
141             GEARIX=MLG*CGLG**2
142             GEARIY=GEARIX
143             GEARIZ=GEARIX
144             IXZW=(ELWING-ELCG)*ZCGWNG*MW
145             IXZH=(ELCGH-ELCG)*ZCGHOR*MHT
146             IXZV=(ELCGV-ELCG)*(-ZCGVER)*MVT
147             IXZ=IXZW+IXZH+IXZV
148            YCGENG=BENGOB*B
149             ENGIY=ENGIOY+MP*(ELF*RELP-ELCG)**2
150              ENGIX=ENGIOX+MP*(BENGOB*B*.5)**2
151             ENGIZ=ENGIOY+MP*(YCGENG**2+(ELF*RELP-ELCG)**2)
152             INERTX=WNGIX+FUSIX+HORIX+VERIX+ENGIX+GEARIX
153             INERTY=WNGIY+FUSIY+HORIY+VERIY+ENGIY+GEARIY
154             INERTZ=WNGIZ+FUSIZ+HORIZ+VERIZ+ENGIZ+GEARIZ
155             WEIGHT=(MW+MHT+MVT+MBT+MP+MTIP+MLG)*32.174
156             IF (WFTP.EQ.0..AND.WFW.EQ.0.) GOTO 275
157             WEIGHT=WEIGHT+WFTP+WFW+UWPAX*(PAX+1)
158             TIPIOY=0.2*(MFTP+MTIP)*((AXIS/2)**2+(BXIS/2)**2)
159              R1=WC/B
```

Figure 10.14: continued

```
160             CHORD1=(CROOT-CTIPW)*(1-R1)+CTIPW
161             CHORD2=(CROOT-CTIPW)*(1.-BFUEL)+CTIPW
162            Z1=((TCR-TCT)*(1-R1)+TCT)*CHORD1
163            Z2=((TCR-TCT)*(1-BFUEL)+TCT)*CHORD2
164            RHO=FUELD*0.2325
165             R=(BFUEL*B-WC)/2
166            CFUEL=(MFW/RHO)/(CHORD1*.0666*RHO*Z1*R+CHORD1*0.1*Z2*R
167           $+CHORD2*0.4*RHO*Z2*R+CHORD2*0.1*RHO*Z1*R)
168            Y1=CFUEL*CHORD1
169            Y2=CFUEL*CHORD2
170            WFIOX=(0.0666*RHO*Z1*Y1+0.1*RHO*Z1*Y2+0.1*RHO*Z2*Y1+
171           $0.4*RHO*Z2*Y2)*R**3
172            WFIY=(ELWING-ELCG)**2*MFW
173            WFIX=WFIOX+MFW*(WC/2)**2
174            MPASS=UWPAX/32.174
175            IXXP=(WAS/24+WS/24)**2*(PAX+1)*MPASS+UWPAX*.0544*(PAX+1)
176            IROW=(PAX+1)/SAB
177            IF((IROW*SAB).LT.(PAX+1))IROW=IROW+1
178            IROW2=IROW + 1
179            DO 250 I=1,IROW2
180            IF(((I-1)*SAB).GT.(PAX+1))SAB=SAB-(IROW*SAB)+PAX+1
181            IYYP=IYYP+(ELCG-XPILOT-((I-1)*PS/12))**2*SAB*MPASS
182       250  CONTINUE
183           IXXM=INERTX+WFIX+(MFTP)*YCGTIP**2+IXXP
184          IYYM=INERTY+WFIY+TIPIOY+(MFTP)*(ELTIP-ELCG)**2+IYYP
185           IZZM=INERTZ+WFIX+(MFTP)*YCGTIP**2+IYYP
186         275 CONTINUE
187           RETURN
188           END
```

Figure 10.14: concluded.

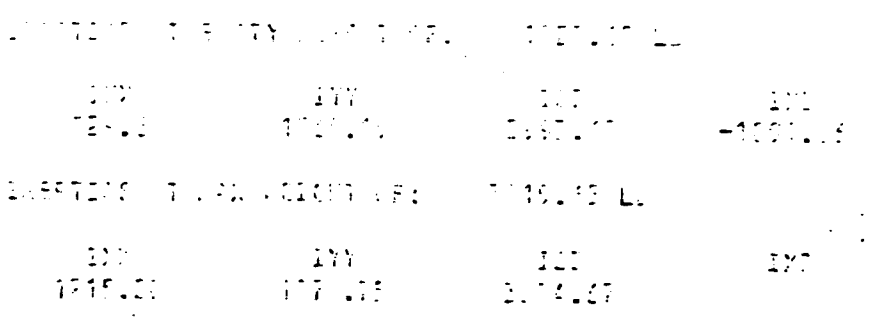

Figure 10.14: Sample printout for subroutine "INERTA"

10.5 REFERENCES

10.1 Marsh, D. Mass Moment of Inertia Estimation Methods, Manned Aircraft, SAWE Technical Paper # 313, 1962

11.1 VARIATION OF DRAG COEFFICIENT WITH ANGLE OF ATTACK, C_{D_α}

11.1.1 INTRODUCTION

This derivative is of importance only for slow speed flight. The computation is according to the method as described in Reference 11.1.1.

11.1.2 DERIVATION OF EQUATIONS

This derivative may be estimated, using the parabolic approximation of the drag polar:

$$C_D = C_{D_0} + \frac{C_L^2}{AR\pi e} \qquad (11.1.1)$$

By differentiation, the derivative C_{D_α} may be found:

$$C_{D_\alpha} = \frac{\partial C_{D_0}}{\partial \alpha} + \frac{2C_L C_{L_\alpha}}{\pi AR\, e} \qquad (11.1.2)$$

The first term in the right hand of the equation is often very small and is also difficult to calculate. Therefore, it will be disregarded.

The lift curve slope, C_{L_α}, may be computed according to Section 11.2.

If the Airplane Efficiency Factor, e, is not explicitly given, it may be approximated using Figure 11.1.1. Note that this Figure yields wing efficiency and therefore is optimistic.

11.1.3 REFERENCES

11.1.1 Roskam, J. Methods for Estimating Stability and Control Derivatives for Conventional Subsonic Airplanes. Roskam Aviation and Engineering Corporation, Lawrence, KS. 1977.

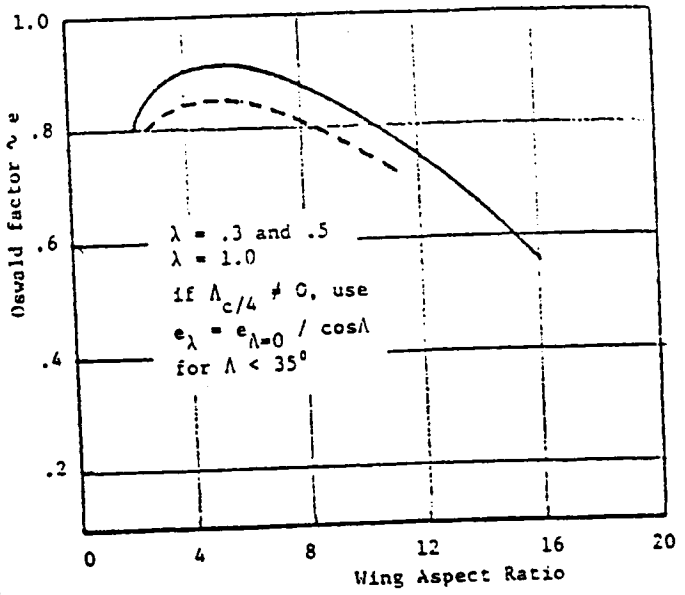

Figure 11.1.1: Method for estimating the Oswald efficiency factor

11.2 LIFT-CURVE SLOPE

11.2.1 DERIVATION OF EQUATIONS

The lift-curve slope of a surface may be computed using the Polhamus Formula (Reference 11.2.1):

$$C_{L_\alpha} = \frac{2\pi AR}{2 + \sqrt{\frac{AR^2 \beta^2}{\kappa^2}\left(1 + \frac{TAN^2 \Lambda_{1/2\bar{c}}}{\beta^2}\right) + 4}} \qquad (11.2.1)$$

This formula calculates the lift-curve slope of the surface without body effects. Using a lifting surface method (Ref. 11.2.2), calculations were made for the lift-curve slope of a wing without body and tail, as a function of aspect ratio and leading-edge sweep angle. These results were compared with the results obtained with the Polhamus Formula. From this comparison an error-function was found. The error thus found is added to the value for the lift-curve slope found with the Polhamus Formula to yield a corrected value for the lift-curve slope. The derivation of the error function is given in Appendix A. The error function is given by:

$AR \leq 4$: $K_{POL} = 1-(1.87- .42399 \cdot \Lambda_{LE}) \cdot AR/100$ (11.2.2a)

$AR > 4$: $K_{POL} = 1-([8.2-2.30 \cdot \Lambda_{LE}]-[.22-.153 \cdot \Lambda_{LE}] \cdot AR)/100$ (11.2.2b)

where: Λ_{LE} in rad.

The corrected lift-curve slope is now given by:

$$C_{L_{\alpha_{CORR}}} = K_{POL} \cdot C_{L_\alpha} \qquad (11.2.3)$$

To convert sweep angles of one chord position to another, use is made of the following formulas (Ref. 11.2.1):

$$TAN\Lambda_{c/2} = TAN\Lambda_{c/4} - \frac{1}{AR}\left(\frac{1-\lambda}{1+\lambda}\right) \quad (11.2.4)$$

$$TAN\Lambda_{LE} = TAN\Lambda_{c/2} + \frac{2}{AR}\left(\frac{1-\lambda}{1+\lambda}\right) \quad (11.2.5)$$

For a ratio of wing span to fuselage diameter, b/d>2, the following approximation may be made:

$$C_{L_{\alpha_{WBH}}} = K_{WB}\, C_{L_{\alpha_W}} + C_{L_{\alpha_H}} \eta_H \frac{S_H}{S}\left(1 - \frac{d\varepsilon}{d\alpha}\right) \quad (11.2.6)$$

where:

$$K_{WB} = 1 - .25\left(\frac{d}{b}\right)^2 + .025\frac{d}{b} \quad (11.2.7)$$

The lift-curve slopes for wing and horizontal tail may be found using Equations (11.2.1) through (11.2.5). The downwash ratio $d\varepsilon/d\alpha$ may be found using Section 11.3.

The effect of flapdeflection on liftcurve slope may be found from:

$$C_{L_\alpha} = \left\{(c'/c - 1)\, S_{W_f}/S_W\right\} C_{L_{\alpha_{WBH}}} + C_{L_{\alpha_{WBH}}} \quad \text{(Ref. 11.2.3)} \quad (11.2.8)$$

where: c'/c is the ratio of wing chord with flap deflected to wing chord with flap retracted.
S_{W_f}/S_W is the ratio of the flap-affected wing area to the wing reference area. The flap affected wing area is a function of flap span and does not include any increase in wing area due to flap extension.

11.2.2 REFERENCES

11.2.1: Dr. Jan Roskam — Methods for Estimating Stability and Control Derivatives of Conventional Subsonic Airplanes. Roskam Aviation & Engineering Corporation, Lawrence, KS. 1977.

11.2.2: Dr. C.E. Lan — Lifting Surface Computer Program, University of Kansas, Aerospace Department.

11.2.3: Hoak, D.E.; Ellison, D.E.; et al. — U.S.A.F. Stability and Control Datcom Flight Control Division, Wright Patterson Air Force Base, Ohio 45433.

11.3 DOWNWASH BEHIND THE WING

11.3.1 INTRODUCTION

The downwash behind the wing is frequently needed for the calculation of other variables. Therefore, it is useful to have a subroutine for its calculation.

11.3.2 DERIVATION OF EQUATIONS

Reference 11.3.1 provides the formulas for this subroutine. The downwash may be found from:

$$\left.\frac{d\varepsilon}{d\alpha}\right|_M = \left.\frac{d\varepsilon}{d\alpha}\right|_{M=0} \left(\frac{C_{L_{\alpha_W}}|_M}{C_{L_{\alpha_W}}|_{M=0}} \right) \tag{11.3.1}$$

For the downwash gradient at low speeds, the following formula is applicable:

$$\left.\frac{d\varepsilon}{d\alpha}\right|_{M=0} = 4.44 \left(K_A K_\lambda K_H \sqrt{\cos\Lambda_{c/4}} \right)^{1.19} \tag{11.3.2}$$

where:

$$K_A = 1/AR - \frac{1}{1 + AR^{1.7}} \quad \text{(Correction factor for aspect ratio)} \tag{11.3.3}$$

$$K_\lambda = \frac{10 - 3\lambda}{7} \quad \text{(Correction factor for taper ratio)} \tag{11.3.4}$$

$$K_H = \frac{1 - \frac{h_H}{b}}{\sqrt[3]{\frac{2\ell_H}{b}}} \quad \text{(Correction factor for geometry)} \tag{11.3.5}$$

The parameters ℓ_H and h_H are defined in Figure 11.3.1.

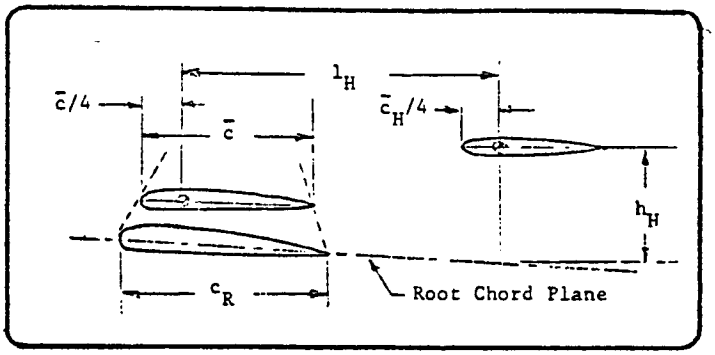

Figure 11.3.1: Geometric parameters for horizontal tail location

11.3.3 REFERENCES

11.3.1 Roskam, J. Methods for Estimating Stability and Conttol Derivatives for Conventional Subsonic Airplanes. Roskam Aviation & Engineering Corporation, Lawrence, KS., 1977.

11.4 VARIATION OF PITCHING MOMENT WITH ANGLE OF ATTACK, C_{M_α}

The computation of this derivative has been discussed in chapter 6, Longitudinal Stability.

11.5 VARIATION OF DRAG COEFFICIENT WITH FORWARD SPEED, C_{D_U}

This derivative is usually negligible in the subsonic Mach range and is not computed in this program. When required, it may be computed from the drag-polars at higher Mach numbers according to Equation 11.5.1:

$$C_{D_U} = \frac{\partial C_D}{\partial M} M \qquad (11.5.1)$$

Where: M is the Mach number in steady state flight, for the condition considered.

$\frac{\partial C_D}{\partial M}$ is the slope of the curve of drag coefficient versus Mach number at the Mach number considered.

11.6 C_{L_u}, VARIATION OF LIFT COEFFICIENT WITH SPEED PERTURBATIONS

11.6.1 DERIVATION OF EQUATIONS

According to Reference 11.6.1, C_{L_u} can be estimated from:

$$C_{L_u} = \left[\frac{M^2}{1 - M^2} \right] C_L \qquad (11.6.1)$$

where: M is the Mach number and C_L is the lift coefficient.

11.6.2 REFERENCES

11.6.1 Roskam, J. Methods for Estimating Stability and Control Derivatives of Conventional Subsonic Airplanes. Roskam Aviation & Engineering Corporation, Lawrence, KS., 1977.

11.7 C_{m_u} ; VARIATION OF PITCHING MOMENT COEFFICIENT DUE TO SPEED PERTURBATIONS, C_{m_u}

11.7.1 DERIVATION OF EQUATIONS

Reference 11.7.1, pp. 4.1, eq. 4.3 gives C_{m_u} as:

$$C_{m_u} = -C_L \frac{\partial \bar{X}_{ac_W}}{\partial M} \qquad (11.7.1)$$

where: C_L is the lift coefficient

$\bar{X}_{ac_W}$ is the non-dimensional aerodynamic center of the wing

M is the Mach number

Because $\partial \bar{X}_{ac_W} / \partial M$ is very hard, if not impossible to determine analytically, reference 11.7.1 suggests plotting $\bar{X}_{ac_W}$ v.s. M for Mach numbers adjacent to the cruise Mach number and drawing a line through the points. The slope of the line is $\partial \bar{X}_{ac_W} / \partial M$.

Figure 3.9, page 3.12 in Reference 11.7.1 presents families of curves for the parameters:

$\frac{\bar{X}_{ac}}{C_R}$ X'_{ac} is the wing a.c. location measured positive aft along the root chord. C_R is the root chord.

L is the wing taper ratio.

A $\tan\Lambda_{LE}$ A is the wing aspect ratio, Λ_{LE} is the leading edge sweep angle

$\frac{\tan \Lambda_{LE}}{\beta}$ $\beta = \sqrt{1 - M^2}$

$\frac{\beta}{\tan \Lambda_{LE}}$ $\beta = \sqrt{1 - M^2}$

The pertinent wing geometry is given below in Figure 11.7.1:

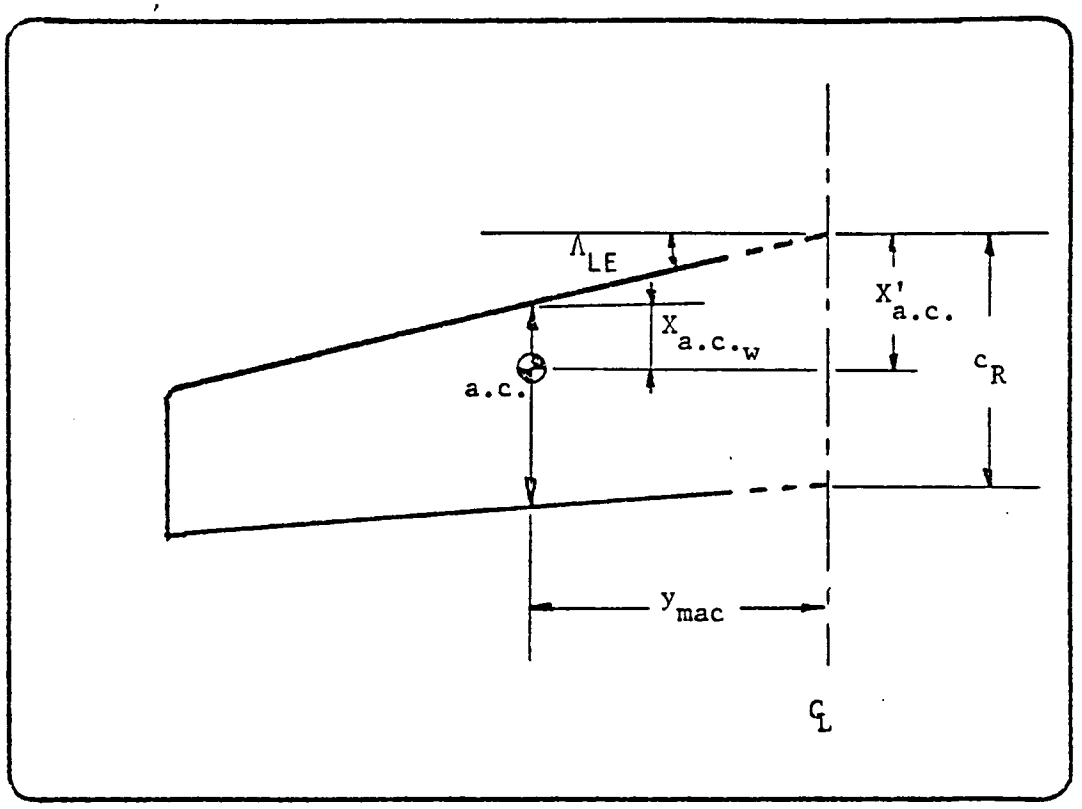

Figure 11.7.1: Wing geometry

From Figure 11.7.1, it is possible to find $\bar{X}_{ac_W}$ in terms of X'_{ac}, Y_{mac}, Λ_{LE}, and $\bar{c}$:

$$X_{ac_W} = X'_{ac} - Y_{mac} \tan\Lambda_{LE}$$

or:

$$\bar{X}_{ac_W} = \frac{X'_{ac} - Y_{mac} \tan\Lambda_{LE}}{\bar{c}} \qquad (11.7.2)$$

The computation of X'_{ac} is done with function "ACEM" and is described in Chapter 6.

11.7.2 REFERENCES

11.7.1 Roskam, J. Methods for Estimating Stability and Control Derivatives for Conventional Subsonic Airplanes. Roskam Aviation & Engineering Corporation, Lawrence, KS., 1977.

11.8 C_{D_q}, VARIATION OF DRAG COEFFICIENT WITH PITCH RATE

This derivative is usually negligible in the subsonic Mach range, and therefore is not computed by the program.

11.9 C_{L_q}, VARIATION OF LIFT COEFFICIENT WITH PITCH RATE

11.9.1 DERIVATION OF EQUATIONS

Reference 11.9.1 presents the method used for calculating C_{L_q}.

C_{L_q} may be considered to be the sum of a wing and tail contribution where the fuselage effect is usually small.

$$C_{L_q} = C_{L_{q_W}} + C_{L_{q_H}} \tag{11.9.1}$$

For the wing contribution:

$$C_{L_{q_{W|M}}} = \left(\frac{A + 2 \cos \Lambda_{c/4}}{AB + 2 \cos \Lambda_{c/4}} \right) C_{L_{q_{W|M=0}}} \quad (\text{rad}^{-1}) \tag{11.9.2}$$

where:

$$C_{L_{q_{W|M=0}}} = \left(\frac{1}{2} + \frac{2X_W}{\bar{c}} \right) C_{L_{\alpha_{W|M=0}}} \quad (\text{rad}^{-1}) \tag{11.9.3}$$

A is the aspect ratio

B is the compressibility factor

$$= \sqrt{1 - M^2 \cos^2 \Lambda_{c/4}} \tag{11.9.4}$$

$\Lambda_{c/4}$ is the quarter chord sweep of the wing

X_W is the distance (positive rearward) from the airplane center of gravity to the aerodynamic center of the wing.

$\bar{c}$ is the wing mean geometric chord

$C_{L_{\alpha_W}}$ is the lift-curve slope of the wing

M is the Mach number

For the horizontal tail contribution:

$$C_{L_{q_{H|M}}} = 2\, C_{L_{\alpha_{H|M}}}\, \eta_H\, \bar{V}_H \quad (\text{rad}^{-1}) \qquad (11.6.5)$$

where:

$C_{L_{\alpha_{H|M}}}$ is the lift-curve slope of the horizontal tail

η_H is the ratio of dynamic pressure at the horizontal tail to the free stream dynamic pressure

$\bar{V}_H$ is the horizontal tail volume coefficient

11.9.2 REFERENCES

11.9.1: Roskam, J. Methods for Estimating Stability and Control Derivatives of Conventional Subsonic Aircplanes. Roskam Aviation & Engineering Corporation, Lawrence, KS. 1977

11.10 C_{m_q}, VARIATION OF PITCHING MOMENT COEFFICIENT WITH PITCH RATE

11.10.1 DERIVATION OF EQUATIONS

Reference 11.10.1 presents the method used for the calculation of the C_{m_q} derivative.

C_{m_q} may be considered to be the sum of a wing and a tail contribution where the contribution of the fuselage are usually small.

$$C_{m_q} = C_{m_{q_W}} + C_{m_{q_H}} \tag{11.10.1}$$

For the wing contribution:

$$C_{m_{q_W}}\Big|_M = \left[\frac{\frac{A^3 \tan^2 \Lambda_{c/4}}{AB + 6\cos\Lambda_{c/4}} + \frac{3}{B}}{\frac{A^3 \tan^2 \Lambda_{c/4}}{A + 6\cos\Lambda_{c/4}} + 3} \right] \quad (\text{rad}^{-1}) \tag{11.10.2}$$

where:

$$C_{m_{q_W}}\Big|_{M=0} = -KC_{\ell_{\alpha_W}} \left(\cos\Lambda_{c/4}\right) \left[\frac{A\left[2\left(\frac{Xw}{\bar{c}}\right)^2 + \frac{1}{2}\left(\frac{Xw}{\bar{c}}\right)\right]}{A + 2\cos\Lambda_{c/4}} + \left(\frac{1}{24}\right) \frac{A^3 \tan^2 \Lambda_{c/4}}{A + 6\cos\Lambda_{c/4}} + \frac{1}{8} \right] \quad (\text{rad}^{-1}) \tag{11.10.3}$$

A is the aspect ratio

B is the compressibility correction factor

$$= \sqrt{1 - M^2 \cos^2 \Lambda_{c/4}} \tag{11.10.4}$$

$\Lambda_{c/4}$ is the quarter-chord sweep angle of the wing

$\bar{c}$ is the mean geometric chord

X_w is the distance from the aircraft center of gravity to the wing aerodynamic center (positive rearward)

$C_{\ell_{\alpha_W}}$ is the spanwise average value of wing section lift-curve slope

K is the correction constant for the wing (Figure 11.10.1)

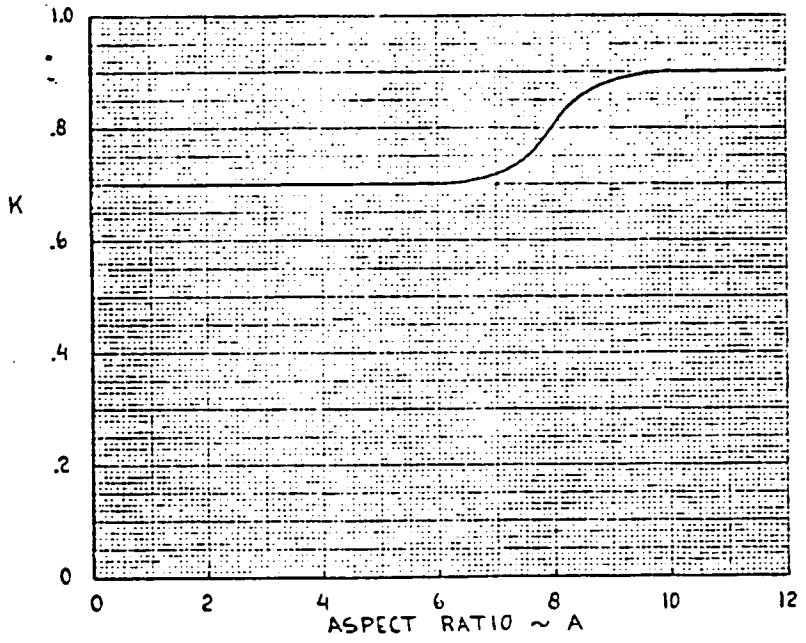

Figure 11.10.1: Correction constant K for wing contribution

For the horizontal tail contribution:

$$C_{m_{q_H}} = -2\, C_{L_{\alpha_H}}\, \eta_H\, \bar{V}_H\, \frac{X_H}{\bar{c}} \quad (\text{rad}^{-1}) \qquad (11.10.5)$$

where:

$C_{L_{\alpha_H}}$ is the horizontal tail lift-curve slope

η_H is the ratio of dynamic pressure at the horizontal tail to free stream dynamic pressure

$\bar{V}_H$ is the horizontal tail volume coefficient

X_H is the distance from the aircraft center of gravity to the aerodynamic center of the horizontal tail

$\bar{c}$ is the mean geometric chord of the wing

11.10.2 REFERENCES

11.10.1 Roskam, J. Methods for Estimating Stability and Control Derivatives of Conventional and Subsonic Airplanes. Lawrence, Ks., 1977.

1.11 $C_{D_{\dot{\alpha}}}$, VARIATION OF DRAG COEFFICIENT WITH ANGLE OF ATTACK RATE

This derivative is usually negligible in the subsonic Mach number range and hence is not calculated by the program.

11.12 $C_{L_{\dot{\alpha}}}$, VARIATION OF LIFT COEFFICIENT WITH ANGLE OF ATTACK RATE

11.12.1 DERIVATION OF EQUATIONS

Reference 11.12.1 suggests that the following relation be used to estimate $C_{L_{\dot{\alpha}}}$:

$$C_{L_{\dot{\alpha}}} = C_{L_{\dot{\alpha}_W}} + C_{L_{\dot{\alpha}_H}} \quad (\text{rad}^{-1}) \tag{11.12.1}$$

where:

$$C_{L_{\dot{\alpha}_W}} = \left[1.5\left(\frac{X_{ac_W}}{C_R}\right) C_{L_{\alpha_W}} + 3\, C_L(g)\right] \quad (\text{rad}^{-1}) \tag{11.12.2}$$

$$C_{L_{\dot{\alpha}_H}} = 2\, C_{L_{\alpha_H}}\, \eta_H\, \bar{V}_H \left(\frac{d\epsilon}{d\alpha}\right) \quad (\text{rad}^{-1}) \tag{11.12.3}$$

Because the major contribution to $C_{L_{\dot{\alpha}}}$ is the $C_{L_{\dot{\alpha}_H}}$ component, it is suggested to use

$$C_{L_{\dot{\alpha}}} = (1.2)\, C_{L_{\dot{\alpha}_H}} \tag{11.12.4}$$

or:

$$C_{L_{\dot{\alpha}}} = (2.4)\, C_{L_{\alpha_H}}\, \eta_H\, \bar{V}_H \left(\frac{d\epsilon}{d\alpha}\right) \quad (\text{rad}^{-1}) \tag{11.12.5}$$

11.12.2 REFERENCES

11.12.1 Roskam, J. Methods for estimating stability and control derivatives of conventional subsonic airplanes. Roskam Aviation & Engineering Corporation, Lawrence, Kansas , 1977.

11.13 $C_{m_{\dot{\alpha}}}$, VARIATION OF PITCHING MOMENT COEFFICIENT WITH ANGLE OF ATTACK RATES

11.13.1 DERIVATION OF EQUATIONS

Reference 11.13.1 gives $C_{m_{\dot{\alpha}}}$ as:

$$C_{m_{\dot{\alpha}}} = C_{m_{\dot{\alpha}_w}} + C_{m_{\dot{\alpha}_H}} \quad (\text{rad}^{-1}) \qquad (11.13.1)$$

Except for triangular wings, no explicit methods are available to estimate $C_{m_{\dot{\alpha}_w}}$. Because $C_{m_{\dot{\alpha}_w}}$ is small, it will not be used.

$$C_{m_{\dot{\alpha}}} = C_{m_{\dot{\alpha}_H}} \quad (\text{rad}^{-1}) \qquad (11.13.2)$$

where:

$$C_{m_{\dot{\alpha}_H}} = -2C_{L_{\alpha_H}} \eta_H \bar{V}_H \frac{\ell_H}{\bar{c}} \left(\frac{d\varepsilon}{d\alpha}\right) \quad (\text{rad}^{-1})$$

so:

$$C_{m_{\dot{\alpha}}} = -2C_{L_{\alpha_H}} \eta_H \bar{V}_H \frac{\ell_H}{\bar{c}} \left(\frac{d\varepsilon}{d\alpha}\right) \quad (\text{rad}^{-1}) \qquad (11.13.3)$$

11.13.2 REFERENCES

11.13.1: Roskam, J. Methods for Estimating Stability and Control Derivatives for Conventional Subsonic Airplanes. Roskam Aviation & Engineering Corporation. Lawrence, KS. 1977

11.14 VARIATION OF SIDE FORCE COEFFICIENT WITH SIDESLIP ANGLE, C_{Y_β}

11.14.1 DERIVATION OF EQUATION

This derivative can be estimated from:

$$C_{Y_\beta} = C_{Y_{\beta_W}} + C_{Y_{\beta_B}} + C_{Y_{\beta_V}} + C_{Y_{\beta_p}} \qquad (11.14.1)$$

The contribution of the wing, $C_{Y_{\beta_W}}$, is only significant in the case where nonzero dihedral angles are considered. For modest values of wing sweep angle (up to 30 deg), the contribution due to wing sweep is negligible (according to Reference 11.14.1). Reference 11.14.2 suggests the following formula for the calculation of the wing effect.

$$C_{Y_{\beta_W}} = -.0001\ |\Gamma|\ 57.3\ (\text{rad}^{-1}) \qquad (11.14.2)$$

where: Γ is the geometric dihedral angle of the wing (in deg)

The fuselage contribution, $C_{Y_{\beta_B}}$, may be estimated from:

$$C_{Y_{\beta_B}} = -2\ K_i \left(\frac{S_0}{S}\right)\ (\text{rad}^{-1}) \qquad (11.14.3)$$

where K_i is a wing-body interference factor, a function of wing position (high-low), maximum body height at wing body intersection, d. This parameter may be obtained from Figure 11.14.1.

S_0 is the cross-sectional area of the fuselage at the point X_0 where the flow

ceases to be potential. The distance X_0 is a function of X_1, the distance from the nose where dS_X/d_X first reaches its maximum negative value. X_1 is usually quickly obtained by inspection when the equivalent fuselage is modeled using straight lines. For cases that are doubtful, the fuselage cross-sectional area distribution should be plotted. X_0 may be calculated according to Reference 11.14.2 as

$$X_0 = \ell_B \left[.378 + .527 \left(\frac{X_1}{\ell_b} \right) \right] \qquad (11.14.4)$$

where ℓ_b is the fuselage length.

NOTE: $\frac{X_1}{\ell_b} = \frac{X_0}{\ell_b}$ when $\frac{X_1}{\ell_b} = .799$

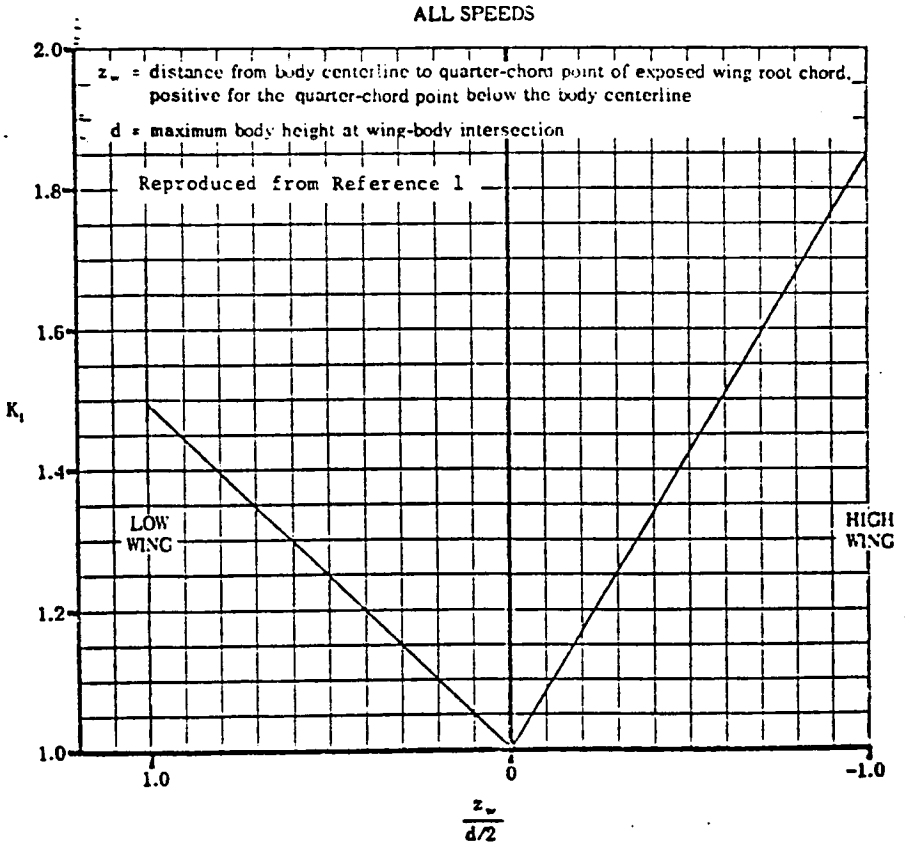

Figure 11.14.1: Wing-body interference factor for wing-body sideslip derivative C_{y_β}

The contribution for the vertical tail ($C_{Y_{\beta_V}}$), in the case of the vertical tail in the plane of symmetry, may be obtained from reference (11.14.1):

$$C_{Y_{\beta_V}} = -k\, C_{L_{\alpha_V}} \left(1 + \frac{d\sigma}{d\beta}\right) \eta_V \frac{S_V}{S} \quad (rad^{-1}) \qquad (11.14.5)$$

where: k is an empirical factor that takes the body influence into account, defined in Figure 11.14.2.

$\left(1 + \frac{d\sigma}{d\beta}\right) \eta_V$ takes the sidewash at the vertical tail into account. This term may be obtained from (Ref. 11.14.1):

$$\left(1 + \frac{d\sigma}{d\beta}\right) \eta_V = .724 + 3.06 \frac{\left(S_V/S\right)}{1 + \cos\Lambda_{c/4}} + .4 \frac{Z_W}{d} + .009\,AR \qquad (11.14.6)$$

where S, $\Lambda_{c/4}$, Z_W, and AR are wing variables. Z_W is measured vertically from the airplane CG to the wing, positive downward. S_V is area of the vertical tail to include the area enclosed within the fuselage to the fuselage centerline.

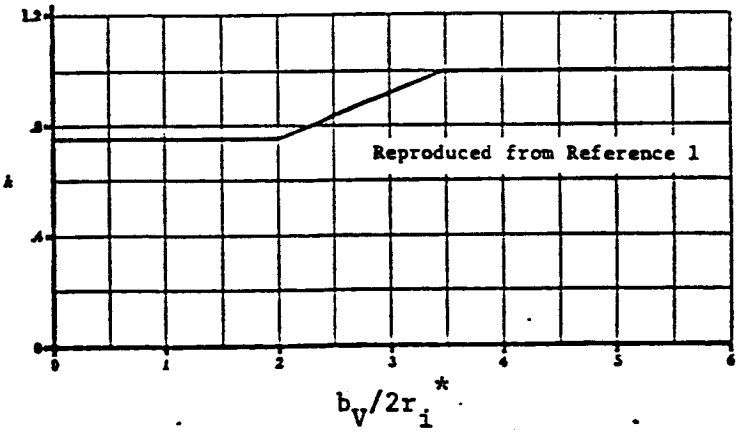

Figure 11.14.2: Empirical factor for estimating sideslip derivative for single vertical tails

*Note: Defined in Figure 11.14.3.

$C_{L_{\alpha_V}}$ is the vertical tail lift-curve slope. This variable may be obtained from the Polhamus equation (see Chapter 11.2), using the effective aspect ratio $AR_{V_{EFF}}$ instead of AR_V. This effective aspect ratio may be obtained from:

$$AR_{V_{EFF}} = \frac{AR_{V(B)}}{AR_V} AR_V \left[1 + K_H \left(\frac{AR_{V(HB)}}{AR_{V(B)}} - 1\right)\right] \qquad (11.14.7)$$

where: $AR_V = b_V^2/S_V$ (11.14.8)

$\frac{AR_{V(B)}}{AR_V}$ is the ratio of the aspect-ratio of the vertical panel in the presence of a body to that of the isolated panel; may be found from Figure 11.14.3.

$\frac{AR_{V(HB)}}{AR_{V(B)}}$ is the ratio of the vertical tail aspect ratio in the presence of the horizontal tail plus body to that of the tail in the presence of the body alone. This ratio is given in Figure 11.14.4.

K_H is a factor that takes the relative sizes of the horizontal and the vertical tail into account; given in Figure 11.14.5.

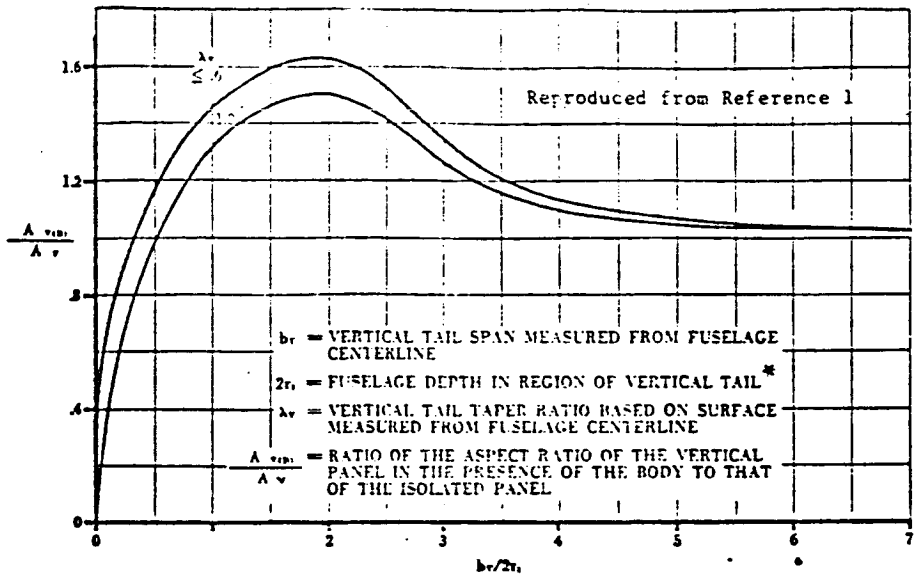

Figure 11.14.3: Effect of body interference on aspect ratio, used for estimating sideslip derivative for single vertical tails

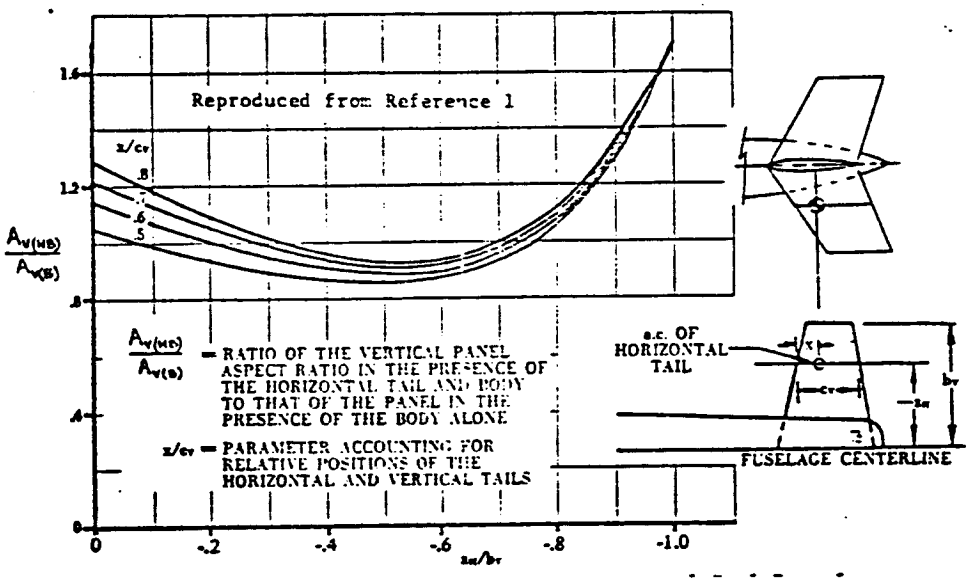

Figure 11.14.4: Effect of horizontal tail interference on aspect ratio, used for estimating the side-slip derivative for single vertical tails

* Note: Use the position of the vertical tail quarter chord line.

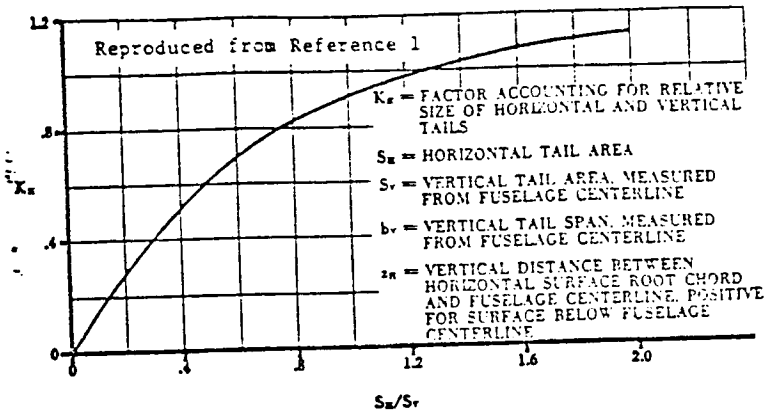

Figure 11.14.5: Factor accouting for relative size of horizontal and vertical tail

The contribution of the propeller, $C_{Y_{\beta_p}}$, may be obtained in a similar way as in Chapter 5 for the normal force of the propeller angle of attack, α_p. Reference is made to this chapter for the derivation of the propeller normal force coefficient. The propeller angle of sideslip, β_p, is assumed to be equal to the sideslip angle β. For tractor propellers this seems to be reasonable. For pusher propellers, however, the exact angle of attack in the X-Y plane is not easy to estimate. It is conservative to assume that $C_{Y_{\beta_p}}$ is zero in this case.

Curve fitting routines produced the following relationships for certain figures as noted:

For the correction factor for wing body interference (Figure 11.14.1):

$$K_i = 1 - .85\left(\frac{Z_W}{d/2}\right) \quad \text{for } \frac{Z_W}{d/2} < 0 \qquad (11.14.9)$$

$$\text{or} \quad K_i = 1 + .495\left(\frac{Z_W}{d/2}\right) \quad \text{for } \frac{Z_W}{d/2} > 0 \qquad (11.14.10)$$

For the influence of body interference on aspect ratio (Figure 11.14.3):*

$$\frac{AR_{V(B)}}{AR_V} = .712 + .9031\left(\frac{b_V}{2r_i}\right) - .2371\left(\frac{b_V}{2r_i}\right)^2 \qquad (11.14.11)$$

$$\text{for} \quad \frac{b_V}{2r_i} < 3$$

or

$$\frac{AR_{V(B)}}{AR_V} = 2.0491 - .344\left(\frac{b_V}{2r_i}\right) + .0287\left(\frac{b_V}{2r_i}\right)^2 \qquad (11.14.12)$$

For the empirical factor of Figure 11.14.2:

$$\kappa = .76 \qquad \text{for } b_V/2r_i < 2 \qquad (11.14.13)$$

$$\kappa = .76 + \left(\frac{b_V}{2r_i} - 2\right).16 \qquad \text{for } 2 < b_V/2r_i < 3.5 \qquad (11.14.14)$$

$$\kappa = 1. \qquad \text{for } b_V/2r_i > 3.5 \qquad (11.14.15)$$

For the horizontal tail interference factor (Figure 11.14.4):

$$\frac{AR_{V(HB)}}{AR_{V(B)}} = \left[1.0429 + .6085\frac{Z_H}{b_V} + .4285\left(\frac{Z_H}{b_V}\right)^2\right] + \left[\left(\frac{X}{c_v} - .5\right)(.73)\left(1 + \frac{Z_H}{b_V}\right)\right] \qquad (11.14.16)$$

$$\text{for} \quad \frac{Z_H}{b_V} \geq -.5$$

or

$$\frac{AR_{V(HB)}}{AR_{V(B)}} = \left[2.4029 + 5.4036\frac{Z_H}{b_V} + 4.6786\left(\frac{Z_H}{b_V}\right)^2\right] \pm \left[\left(\frac{X}{c_v} - .5\right)(.73)\left(1. + \frac{Z_H}{b_V}\right)\right] \qquad (11.14.17)$$

$$\text{for} \quad \frac{Z_H}{b_V} < -.5$$

* Note: An average value of $\lambda_V = .8$ was used.

For the effect of relative size of vertical and horizontal tail:

$$K_H = .0385 + 1.2244 \frac{S_{HT}}{S_{VT}} - .3488 \left(\frac{S_{HT}}{S_{VT}}\right)^2 \qquad (11.14.12)$$

11.14.2 REFERENCES

11.14.1 Roskam, J. Methods for Estimating Stability and Control Characteristics of Conventional Subsonic Airplanes, Roskam Aviation & Engineering Corporation, Lawrence, Ks., 1977.

11.14.2 Hoak, D.E. & Ellison, D.E. USAF Stability and Control DATCOM; Flight Control Division; Air Force Flight Dynamics Laboratory, Wright Patterson Air Force Base, Ohio, 45433.

11.15 C_{ℓ_β}, VARIATION OF ROLLING MOMENT COEFFICIENT WITH SIDESLIP ANGLE

11.15.1 DERIVATION OF EQUATIONS

Reference 11.15.1 presents the method used for calculating C_{ℓ_β}. C_{ℓ_β} may be estimated from three contributions: the wing, the horizontal tail, and the vertical tail.

$$C_{\ell_\beta} = C_{\ell_{\beta_{WB}}} + C_{\ell_{\beta_H}} + C_{\ell_{\beta_V}} \tag{11.15.1}$$

The wing body contribution is found from:

$$C_{\ell_{\beta_{WB}}} = 57.3 \left[C_{L_{WB}} \left\{ \left(\frac{C_{\ell_\beta}}{C_L} \right)_{\Lambda_{c/2}} K_{M_\Lambda} K_F + \left(\frac{C_{\ell_\beta}}{C_L} \right)_A \right\} + \right.$$

$$\Gamma \left(\frac{C_{\ell_\beta}}{\Gamma} K_{M_\Gamma} + \frac{\Delta C_{\ell_\beta}}{\Gamma} \right) + \left(\Delta C_{\ell_\beta} \right)_{z_w} +$$

$$\left. \Theta \tan \Lambda_{c/4} \left(\frac{\Delta C_{\ell_\beta}}{\Theta \tan \Lambda_{c/4}} \right) \right] \quad (\text{rad}^{-1}) \tag{11.15.2}$$

where:

$C_{L_{WB}} = C_L$ is the steady state lift coefficient.

$\left(\frac{C_{\ell_\beta}}{C_L} \right)_{\Lambda_{c/2}}$ is the wing sweep contribution obtained from Figure 11.15.1.

K_{M_Λ} is the compressibility (Mach number) correction to sweep obtained from Figure 11.15.2

K_F is a fuselage correction factor which may be obtained from Figure 11.15.3. An independent

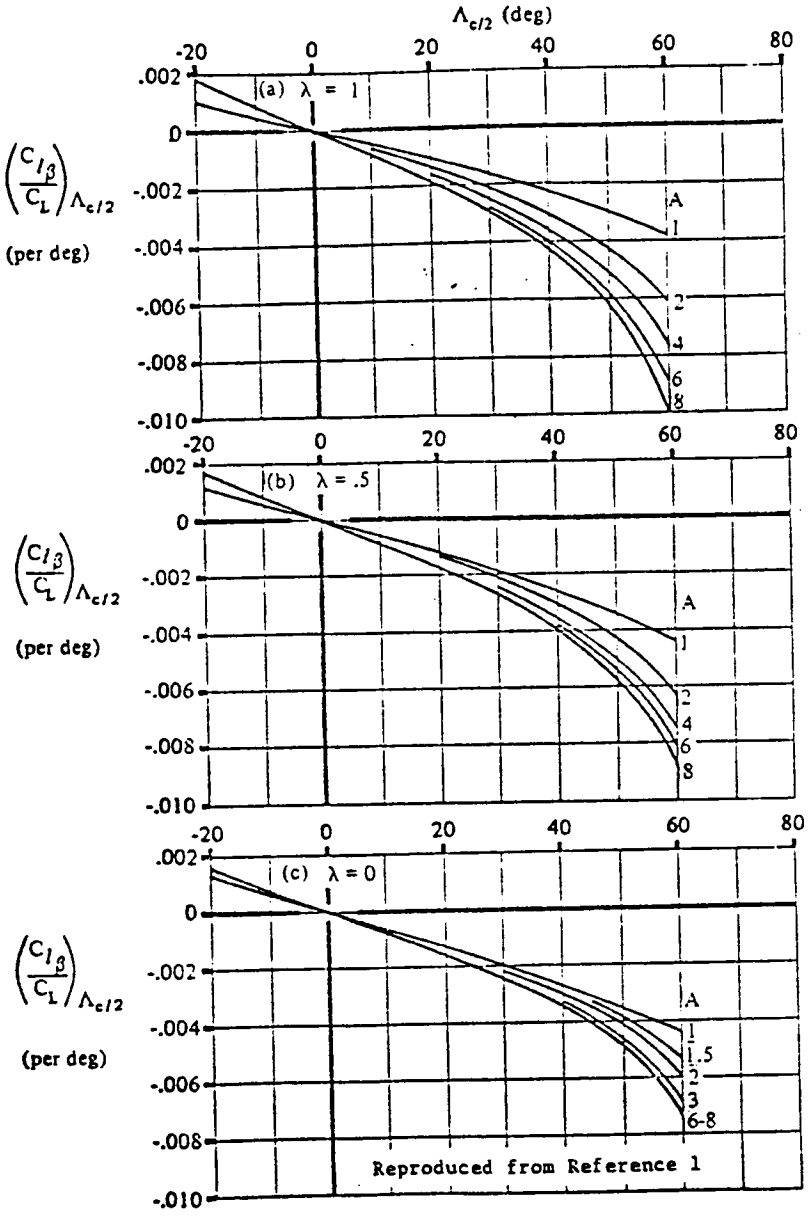

Figure 11.15.1: Wing Sweep Contribution to C_{l_β}

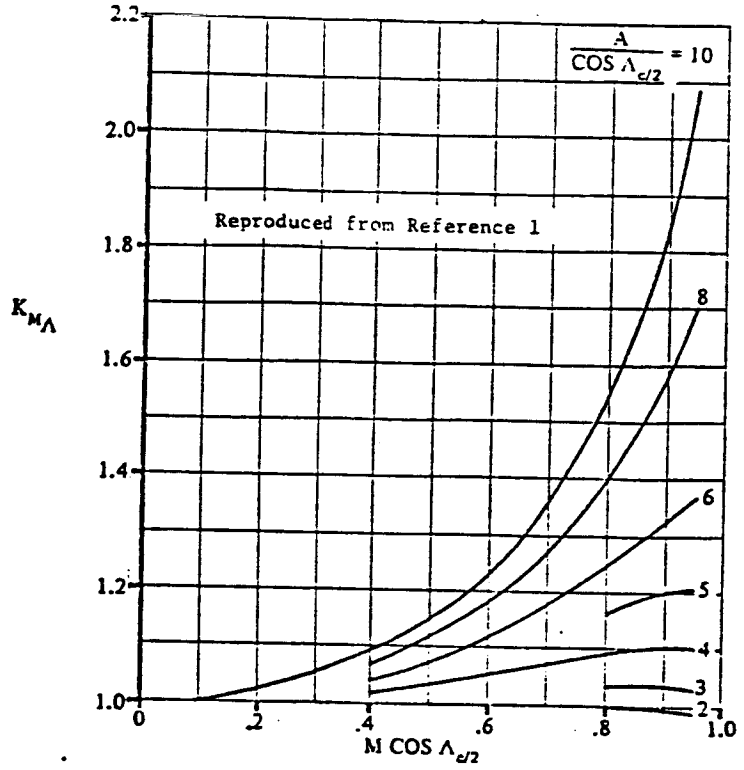

Figure 11.15.2: Compressibility Correction Factor to Sweep Contribution to Wing C_{l_β}

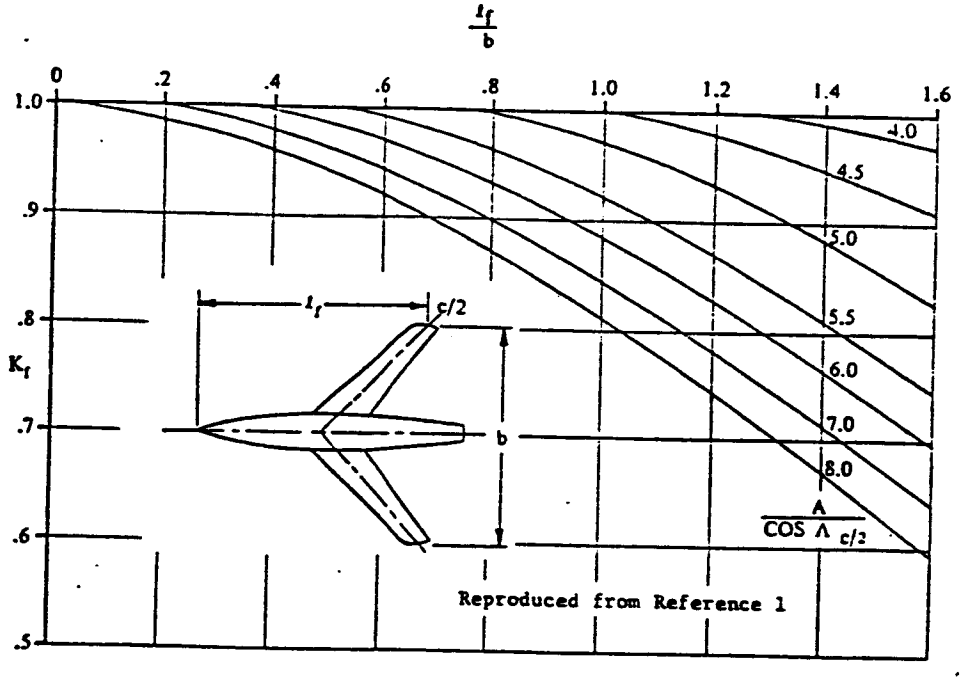

Figure 11.15.3: Fuselage Correction Factor

$\left(\frac{C_{\ell_\beta}}{C_L}\right)_A$ is the aspect ratio contribution obtained from Figure 11.15.4.

Γ is the wing dihedral angle, positive up

$\frac{C_{\ell_\beta}}{\Gamma}$ is the wing dihedral effect obtained from Figure 11.15.5.

K_{M_Γ} is the compressibility correction to dihedral obtained from Figure 11.15.6.

$\frac{\Delta C_{\ell_\beta}}{\Gamma}$ is the body-induced effect on the wing height and is given by:

$$\frac{\Delta C_{\ell_\beta}}{\Gamma} = -.005\ \sqrt{A}\left(\frac{d}{b}\right)^2\ (\text{deg}^{-2}) \qquad (11.15.3)$$

where: b is the wing span, and

d is given by:

$$d = \sqrt{\frac{\text{average fuselage cross sectional area}}{.7854}} \qquad (11.15.4)$$

$\left(\Delta C_{\ell_\beta}\right)_{ZW}$ is another body induced effect on the wing height given by:

$$\left(\Delta C_{\ell_\beta}\right)_{ZW} = -\frac{1.2\sqrt{A}}{57.3}\left(\frac{Z_W}{b}\right)\frac{2d}{b}\ (\text{deg}^{-1}) \qquad (11.15.5)$$

where: Z_W is the vertical distance from the wing root quarter chord point to the fuselage centerline, positive downward.

d is the same as in equation (11.15.4)

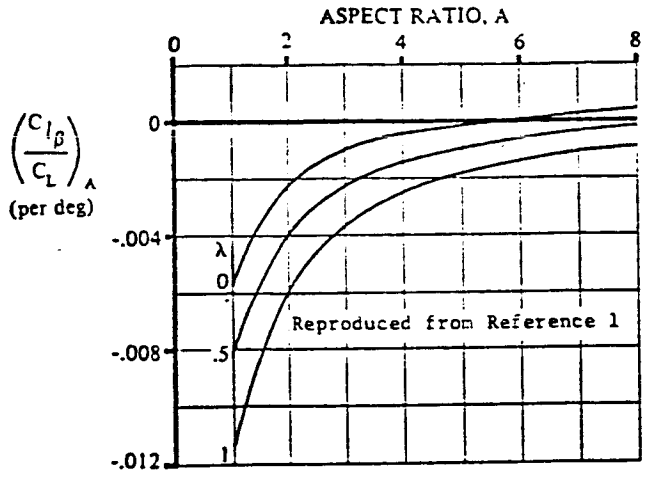

Figure 11.15.4

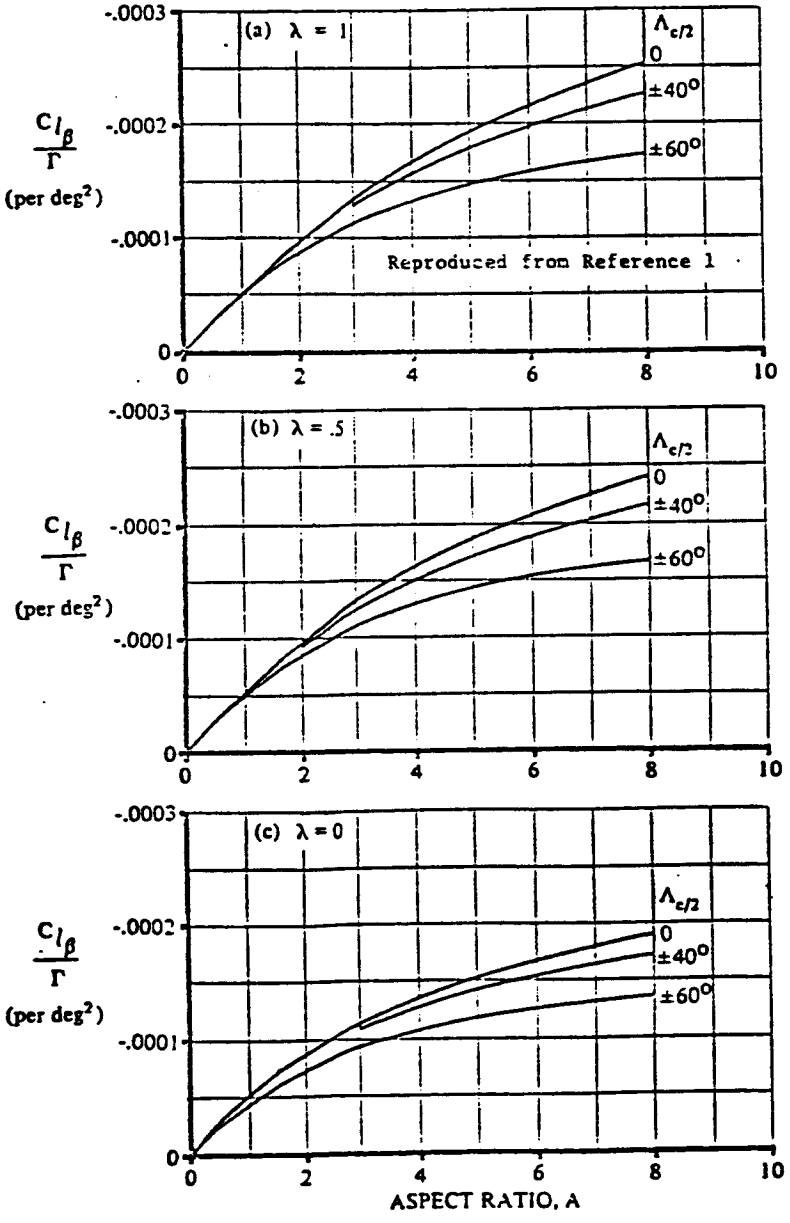

Figure 11.15.5 Effect of Uniform Geometric Dihedral on Wing C_{l_β}

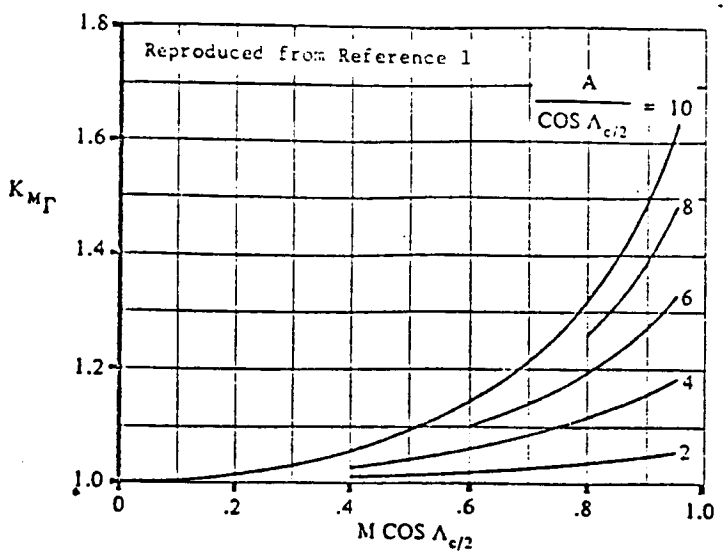

Figure 11.15.6 Compressibility Correction to Dihedral Effect on Wing C_{l_β}

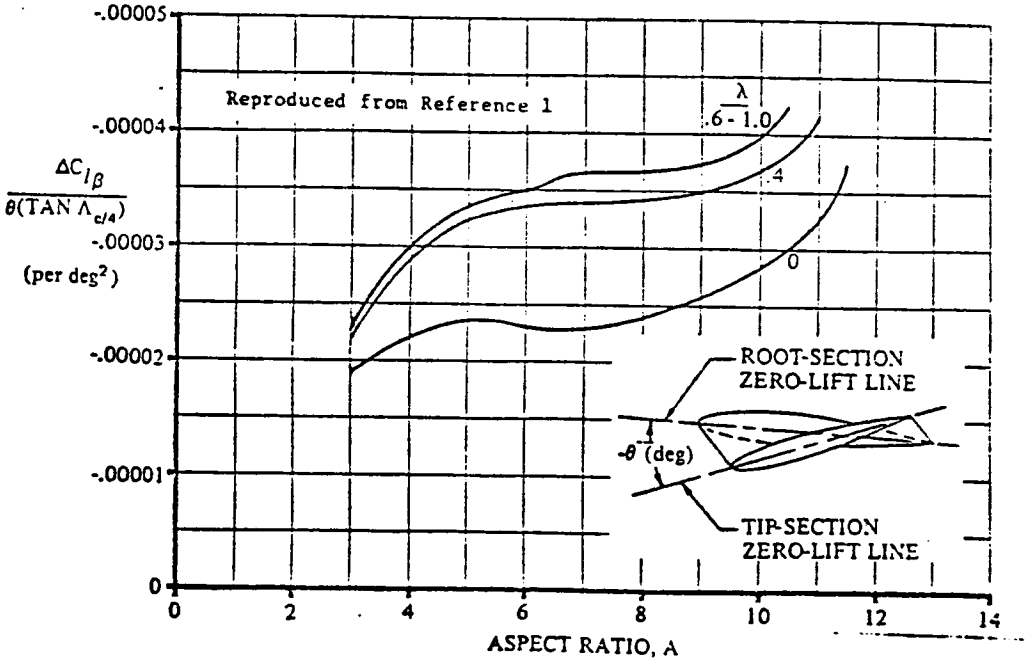

Figure 11.15.7 Effect of Wing Twist on Wing C_{l_β}

study by the author shows $K_F = 1$ is a more accurate assumption. ($K_F = 1$ is reflected in the program.)

$\frac{\Delta C_{\ell_\beta}}{\Theta \tan \Lambda_{c/4}}$ is a wing twist correction factor obtained from Figure 11.15.7.

Θ is the wing twist between root and tip sections, negative for washout.

The contribution of the horizontal tail, $C_{\ell_{\beta_H}}$, can be approximated by:

$$C_{\ell_{\beta_H}} = C_{\ell_{\beta_{HB}}} \frac{S_H \, b_H}{S \, b} \tag{11.15.6}$$

where:

$C_{\ell_{\beta_{HB}}}$ is found from Equation (11.15.2), treating the fuselage-horizontal tail the same way (and using $C_{L_{WB}}$ = the C_{L_H} of the horizontal tail).

The contribution of the vertical tail, $C_{\ell_{\beta_V}}$, can be estimated from:

$$C_{\ell_{\beta_V}} = C_{y_{\beta_V}} \frac{(Z_V \cos\alpha - \ell_V \sin\alpha)}{b} \text{ rad}^{-1} \tag{11.15.7}$$

where:

Z_V and ℓ_V are defined in Figure 11.19.2a, and

$C_{y_{\beta_V}}$ is calculated from the methods of Section 11.14.

11.15.2 REFERENCES

11.15.1 Roskam, J. Methods for Estimating STability and Control Derivatives for Conventional Subsonic Airplanes. Roskam Aviation & Engineering Corporation, Lawrence, KS.1977.

11.16 VARIATION OF YAWING MOMENT COEFFICIENT WITH SIDESLIP ANGLE C_{n_β}

11.16.1 DERIVATION OF EQUATIONS

Reference 11.16.1 provides the following method for the calculation of this variable.

For a tail-aft configuration this derivative may be broken up in the following contributions:

$$C_{n_\beta} = C_{n_{\beta_W}} + C_{n_{\beta_B}} + C_{n_{\beta_V}} + C_{n_{\beta_p}} \qquad (11.16.1)$$

Usually, the wing contribution $C_{n_{\beta_W}}$ is small, except at high angles of attack. In that case it may be calculated using a formula from Reference 11.16.2.

Wing yawing moment derivative at low speeds:

$$\left.\frac{C_{n_{\beta_W}}}{C_L^2}\right|_{M=0} = \left[\frac{1}{4\pi AR} - \frac{\tan\Lambda_{c/4}}{\pi AR(AR + 4\cos\Lambda_{c/4})}\left(\cos\Lambda_{c/4} - \frac{AR}{2} - \frac{AR^2}{8\cos\Lambda_{c/4}} + 6\frac{X}{\bar{c}}\frac{\sin\Lambda_{c/4}}{AR}\right)\right] \quad (\text{rad}^{-1}) \qquad (11.16.2)$$

where: X is the longitudinal distance from the center of gravity to the wing aerodynamic center, positive rearward.

At high sweep angles the above formula is no longer correct. In that case, the Prandtl-Glauert Rule may be applied to yield a correction for the first order three-dimensional effects of compressibility. The resulting expression is:

$$\left.\frac{C_{n_\beta}}{C_L^2}\right|_M = \left(\frac{AR + 4\cos\Lambda_{c/4}}{AR\,B + 4\cos\Lambda_{c/4}}\right)\left(\frac{AR^2B^2 + 4AR\,B\cos\Lambda_{c/4} - 8\cos^2\Lambda_{c/4}}{AR^2 + 4AR\cos\Lambda_{c/4} - 8\cos^2\Lambda_{c/4}}\right)\left.\frac{C_{n_\beta}}{C_L^2}\right|_{M=0} \qquad (11.16.3)$$

where:

$$B = \sqrt{1 - M^2\cos^2\Lambda_{c/4}} \qquad (11.16.4)$$

The body contribution, $C_{n_{\beta_B}}$, including the interference effect of the wing on the body, may be found using:

$$C_{n_{\beta_B}} = -57.3\left[K_N\, K_{R_\ell}\left(\frac{S_{B_S}}{S}\right)\frac{\ell_B}{b}\right](\text{rad}^{-1}) \qquad (11.16.5)$$

where: K_N is an empirical factor for body and body and wing effect, found from Figure 11.16.2.

K_{R_ℓ} is a Reynolds Number correction factor for the fuselage, found from Figure 11.16.3.

S_{B_S} is the projected side area of the body (only).

ℓ_B is the length of the body.

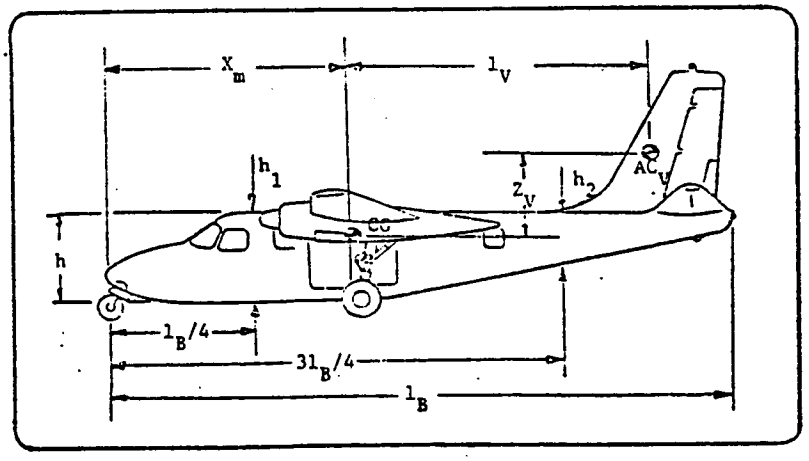

Figure 11.16.1: Definition of geometric parameters.

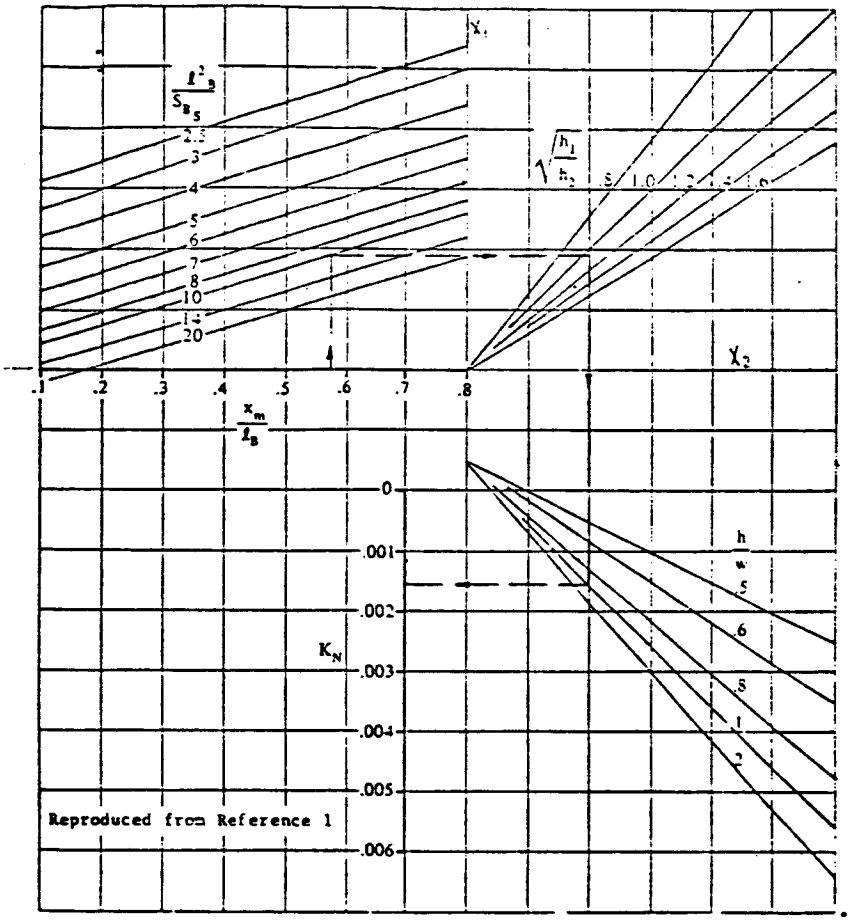

Figure 11.16.2: Empirical Factor for Wing + Wing-Body Interference

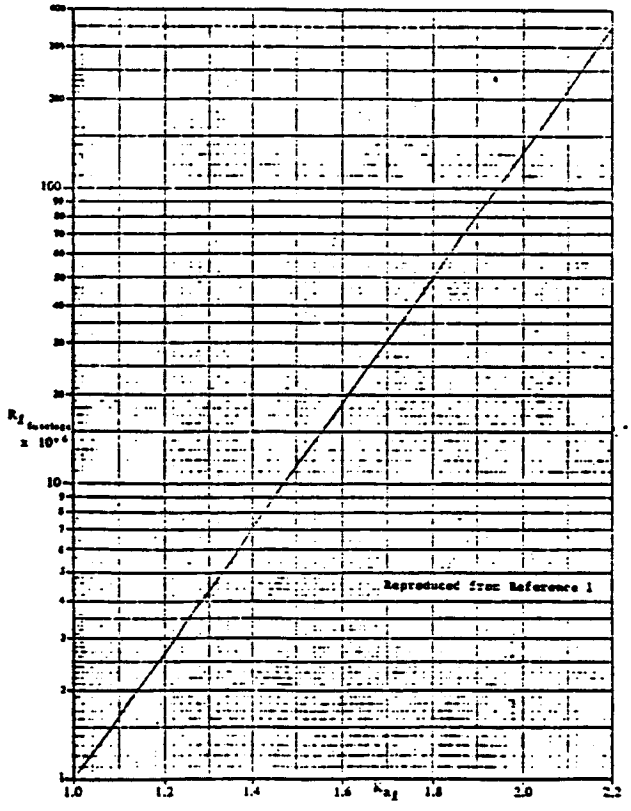

Figure 11.16.3: Effect of Fuselage Reynolds Number on Wing-Body Combinations

The vertical tail contribution, $C_{n_{\beta_V}}$, may be obtained from:

$$C_{n_{\beta_V}} = -C_{Y_{\beta_V}} \left(\frac{\ell_V \cos\alpha + Z_V \sin\alpha}{b} \right) \ (\text{rad}^{-1}) \qquad (11.16.6)$$

where:

ℓ_V and Z_V are defined in Figure 11.16.1.

The side-force derivative $C_{Y_{\beta_V}}$ may be obtained from Section 11.14.

The power term, $C_{n_{\beta_p}}$, is obtained per Equation 5.56 for propellers or Equation 5.68 for jets.

Curve fitting methods yield the following approximations for Figures 11.16.2 and 11.16.3:

$$K_N = \left[-1.0147 + 4.4649\left(\frac{H_C}{W_C}\right) - 3.3626\left(\frac{H_C}{W_C}\right)^2 + 1.0794\left(\frac{H_C}{W_C}\right)^3 - .1217\left(\frac{H_C}{W_C}\right)^4 \right] \frac{Y}{M_1}(.001) - .0005 \qquad (11.16.7)$$

where:

$$M_1 = 3.6497 - 3.5796\sqrt{\frac{H_1}{H_2}} - .39\left(\frac{H_1}{H_2}\right) + 2.0149\left(\frac{H_1}{H_2}\right)^{3/2} - .6946\left(\frac{H_1}{H_2}\right)^2 \qquad (11.16.8)$$

$$Y = 3.01429 \left(\frac{X_{cg}}{\ell_b} - .2\right) + X_1 \qquad (11.16.9)$$

$$X_1 = 3.4 - .7030325 \left(\frac{\ell_b^2}{S_{B_S}} - 2.5\right) + .0539969 \left(\frac{\ell_b^2}{S_{B_S}} - 2.5\right)^2$$

$$- .0014243 \left(\frac{\ell_b^2}{S_{B_S}} - 2.5\right)^3 \qquad (11.16.10)$$

$$K_{R_L} = -1.830754 + .20494 \cdot \text{Ln}\,(R_\ell) \qquad (11.16.11)$$

where: R_ℓ is the Reynolds number of the fuselage $\left(= \frac{\rho V \ell_b}{\mu}\right)$

11.16.2 REFERENCES

11.16.1	Roskam, J.	Methods for Estimating Stability and Control Derivatives of Conventional Subsonic Airplanes, Roskam Aviation & Engineering Corporation, Lawrence, KS, 1977.
11.16.2	Hoak, D.E. & Ellison, D.E.	USAF Stability and Control Datcom; Air Force Flight Dynamics Laboratory, Wright Patterson Air Force Base, Ohio, 45433.

11.17 C_{y_p}, VARIATION OF SIDE FORCE DUE TO ROLL RATE PERTURBATIONS

11.17.1 DERIVATION OF EQUATIONS

Reference 11.7.1, page 8.1 gives C_{y_p} as:

$$C_{y_p} \approx C_{y_{p_v}} \approx 2\left(\frac{Z_v \cos\alpha - \ell_v \sin\alpha}{b}\right) C_{y_{\beta_v}} \quad (\text{rad}^{-1}), \qquad (11.17.1)$$

$C_{y_{\beta_v}}$ is obtained from the C_{y_β} subroutine, section 11.14.

11.17.2 REFERENCES

11.17.1 Roskam, J. Methods for Estimating Stability and Control Derivatives for Conventional Subsonic Airplanes, Roskam Aviation & Engineering Corp. Lawrence, KS, 1977.

11.18 C_{ℓ_p}, VARIATION OF ROLLING MOMENT COEFFICIENT WITH ROLL RATE PERTURBATIONS

11.18.1 DERIVATION OF EQUATIONS

According to Reference 11.8.1, C_{ℓ_p} can be estimated as follows:

$$C_{\ell_p} = C_{\ell_{p_{WB}}} + C_{\ell_{p_H}} + C_{\ell_{p_V}} \tag{11.18.1}$$

and:

$$C_{\ell_{p_{WB}}} \approx C_{\ell_{p_W}} = \left(\frac{\beta\, C_{\ell_p}}{K}\right)\frac{K}{\beta} \tag{11.18.2}$$

where:

$\left(\frac{\beta\, C_{\ell_p}}{K}\right)$ is the roll damping parameter.

$$K = \frac{C_{\ell_{\alpha_W}}\big|_{avg.}}{2\pi} \tag{11.18.2a}$$

$$\beta = \sqrt{1 - M^2} \tag{11.18.2b}$$

$\left(\frac{\beta\, C_{\ell_p}}{K}\right)$ is found from Figure 8.1 of Reference 11.18.1. This figure is reproduced here as Figure 11.18.1, and its use is explained in Section 11.18.2.

$$C_{\ell_{p_H}} = 1/2\left(C_{\ell_p}\right)_H \frac{S_H}{S}\left(\frac{b_H}{b}\right)^2 \tag{11.18.3}$$

where:

$$\left(C_{\ell_p}\right)_H = \left(\frac{\beta\, C_{\ell_p}}{K}\right)\frac{K}{\beta} \tag{11.18.3a}$$

$\left(\frac{\beta\, C_{\ell_p}}{K}\right)$ is found from Figure 11.18.1 using the horizontal tail geometry.

(a) $\lambda = 0$

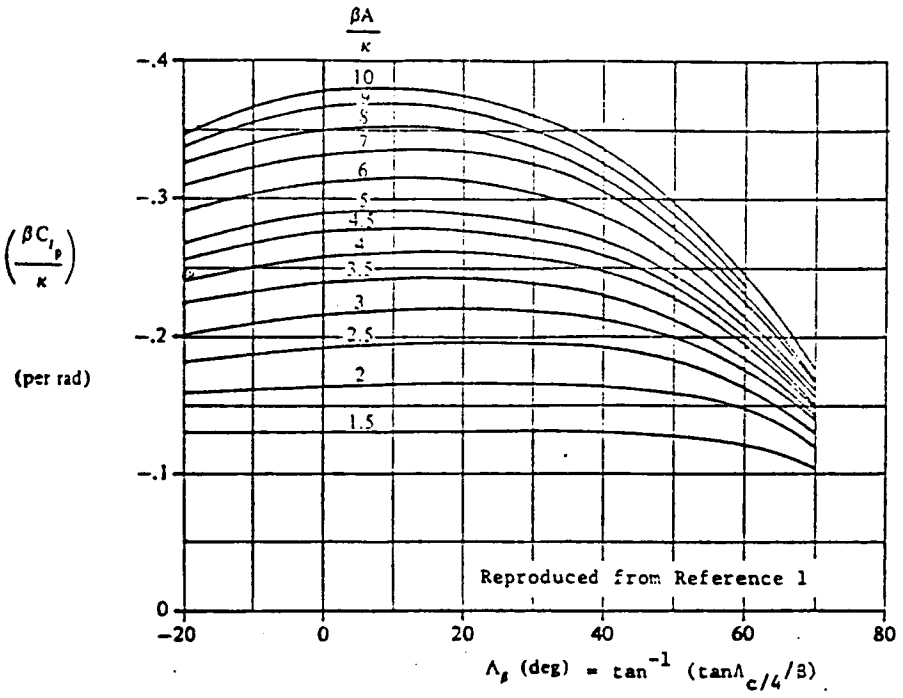

(b) $\lambda = 0.25$

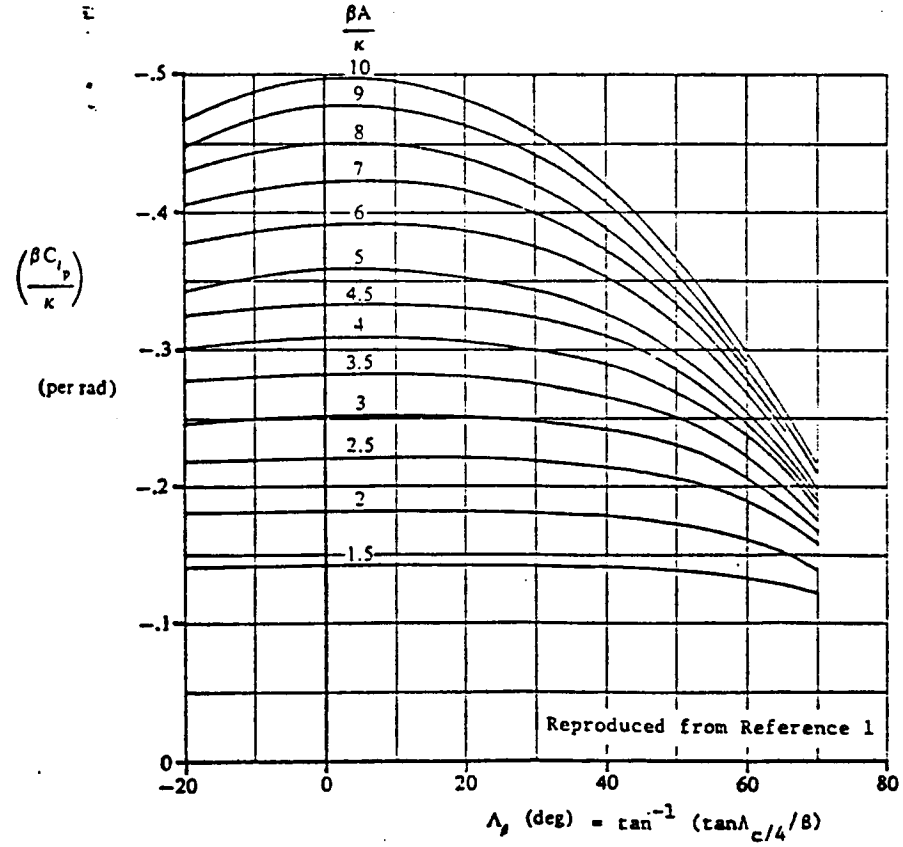

Figure 11.18.1: Roll damping parameter, used for computation of C_{2_p}

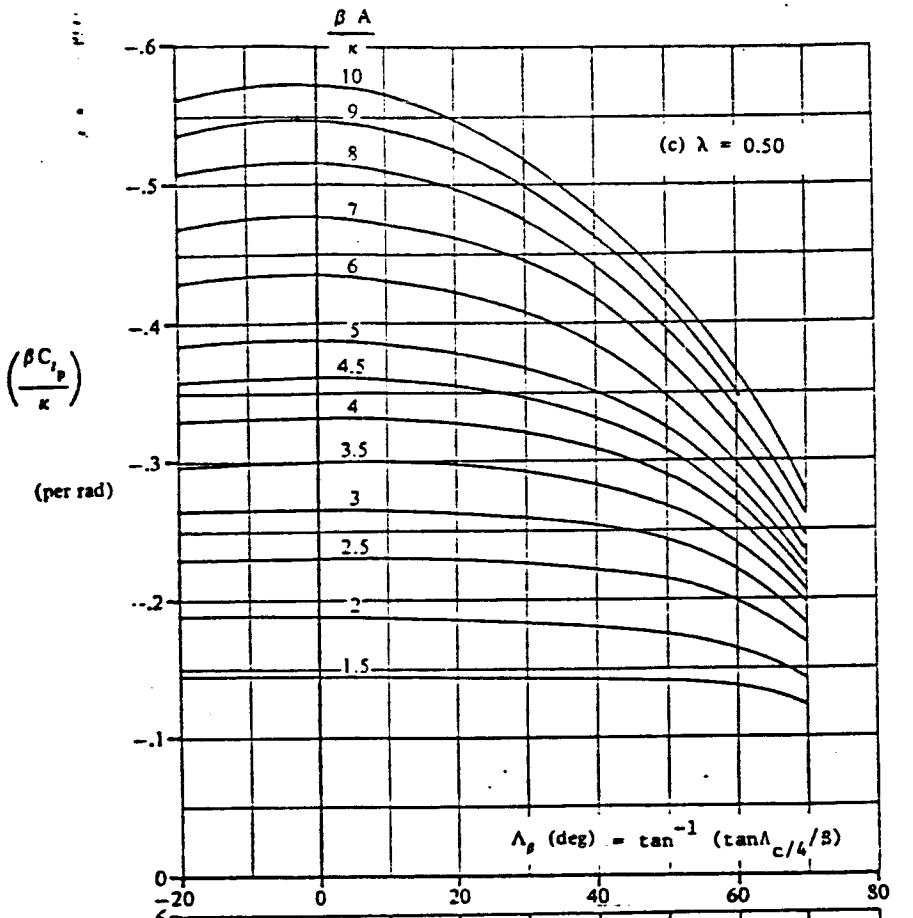

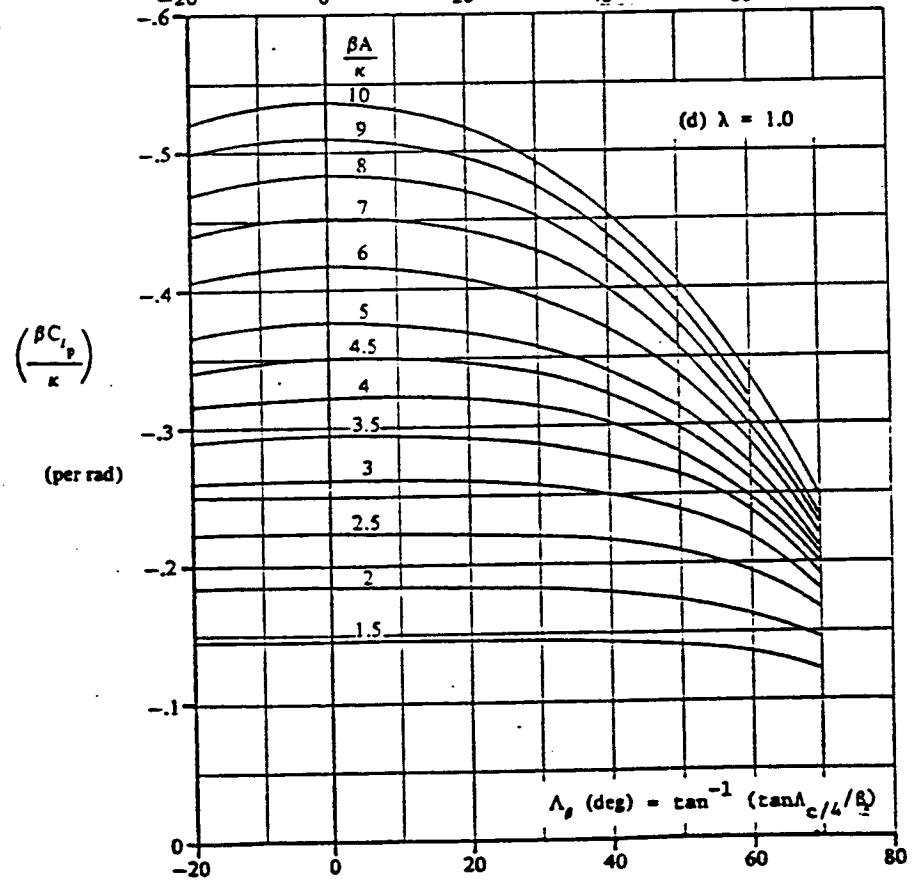

Figure 11.18.1: continued

$$C_{\ell_{p_V}} = 2\left(\frac{Z_V}{b}\right)^2 C_{Y_{\beta_V}} \qquad (11.18.4)$$

where: Z_V is the vertical distance from the body X-axis to the vertical tail aerodynamic center, as shown in Figure 11.18.2.

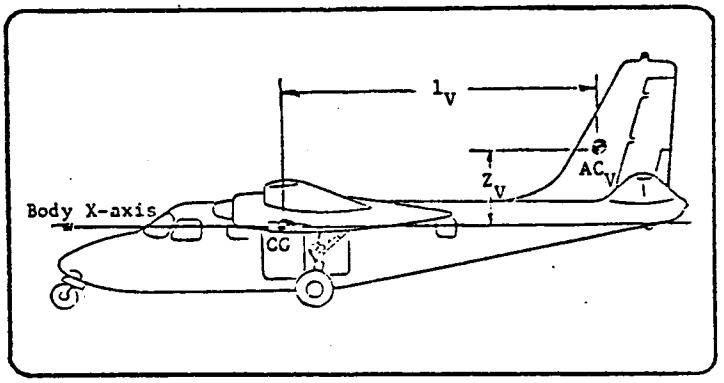

Figure 11.18.2: Geometry for determining distance vertical tail A.C. to body X-axis

11.18.2 DESCRIPTION OF THE METHODOLOGY

The C_{ℓ_p} methodology is straight forward and involves the interpolation of Figure 11.18.1.

The limitations of the subroutine are as follows:

1) $.25 \leq \lambda \leq 1.0$

2) $0° \leq \Lambda_\beta \; 70°$

where: $\Lambda_\beta = \tan^{-1}(\tan\Lambda_{c/4}/\beta)$

$$\beta = \sqrt{1 - M^2}$$

3) $1.5 \leq \frac{\beta A}{\kappa} \leq 10$

where:

$\beta = \sqrt{1 - M^2}$

A = Aspect Ratio

$$\kappa = \frac{C_{\ell_{\alpha_W}}|_{avg}}{2\pi}$$

4) Any limitations in the C_{Y_β} subroutine also apply because the C_{ℓ_p} subroutine obtains $C_{Y_{\beta_V}}$ from the former.

5) $M < 1.0$

11.18.3 REFERENCES

11.18.1 Roskam, J. Methods for Estimating Stability and Control Derivatives of Conventional Subsonic Airplanes. Printed by the author. 519 Boulder, Lawrence, Ks., 1971.

11.19 C_{n_p}; VARIATION OF YAWING MOMENT COEFFICIENT WITH ROLL RATE PERTURBATION

11.19.1 DERIVATION OF EQUATIONS

C_{n_p} is estimated in the conventional manner, as the sum of the wing contribution and the vertical tail contribution:

$$C_{n_p} = C_{n_{p_w}} + C_{n_{p_v}} \tag{11.19.1}$$

The following equations used to determine $C_{n_{p_w}}$ and $C_{n_{p_v}}$ are equations (8.7) through (8.11), pages 8.2 to 8.3 from reference 11.19.1

The wing contribution can be expressed as:

$$C_{n_{p_w}} = - C_{\ell_{p_w}} \text{Tan } \alpha - \left[- C_{\ell_p} \text{Tan } \alpha - \left(\frac{C_{n_p}}{C_L} \right)_{C_L = 0} C_L \right] + \tag{11.19.2}$$

$$+ \frac{\Delta C_{n_p}}{\theta} \theta + \frac{\Delta C_{n_p}}{\alpha_{\delta_F} \delta_F} \alpha_{\delta_F} \delta_F$$

where:

$C_{\ell_{p_w}}$ is the wing contribution to C_{ℓ_p}

α is the wing angle of attack ($\alpha_\omega \approx \alpha_{A/C}$)

C_L is the wing lift coefficient ($C_{L_W} \approx C_{L_{A/C}}$)

$\left(\frac{C_{n_p}}{C_L} \right)_{C_L = 0}$ is the slope of the yawing moment due to rolling at zero lift given by:

$$\left(\frac{C_{n_p}}{C_L} \right)_{C_L = 0} = \left[\frac{A + 4 \cos \Lambda_{c/4}}{AB + 4 \cos \Lambda_{c/4}} \right] \left[\frac{AB + \frac{1}{2}(AB + \cos \Lambda_{c/4}) \tan^2 \Lambda_{c/4}}{A + \frac{1}{2}(A + \cos \Lambda_{c/4}) \tan^2 \Lambda_{c/4}} \right] \left(\frac{C_{n_p}}{C_L} \right)_{\substack{C_L = 0 \\ m = 0}} \tag{11.19.3}$$

where: $B = \sqrt{1 - m^2 \cos^2 \Lambda_{c/4}}$

$\left(\frac{C_{n_p}}{C_L}\right)_{\substack{C_L = 0 \\ m = 0}}$ is the slope of the low-speed yawing moment due to rolling at zero lift given by:

$$\left(\frac{C_{n_p}}{C_L}\right)_{\substack{C_L = 0 \\ m = 0}} = -\frac{1}{6}\left[\frac{A + 6(A + \cos \Lambda_{c/4})\left(\frac{\bar{x}}{\bar{c}} \frac{\tan \Lambda_{c/4}}{A} + \frac{\tan^2 \Lambda_{c/4}}{12}\right)}{A + 4 \cos \Lambda_{c/4}}\right] \qquad (11.19.4)$$

where: $\bar{x}$ is the distance from the center of gravity to the aerodynamic center of the wing, positive when the a.c. is aft of the c.g.

$\bar{c}$ is the wing mean aerodynamic chord.

Referring to eq. 11.19.2 again:

where: $\frac{\Delta C_{n_p}}{\theta}$ is the effect of linear wing twist obtained from Figure 11.19.1

θ is the wing twist in degrees, negative for washout

$\frac{\Delta C_{n_p}}{\alpha_\delta \delta_F}$ is the effect of symmetric flap deflection obtained from Figure 11.19.2

δ_F is the streamwise flap deflection in degrees.

α_{δ_F} is the two-dimensional lift-effectiveness parameter, obtained from Figure 11.23.2 and reproduced here as Figure 11.19.3.

The vertical tail contribution to C_{n_p} can be estimated from:

$$C_{n_{p_v}} = -\frac{2}{b}[\ell_v \cos\alpha + Z_v \sin\alpha]\left[\frac{Z_v \cos\alpha - \ell_v \sin\alpha}{b}\right] C_{y_{\beta_v}} \qquad (11.19.5)$$

where: ℓ_v and Z_v are defined in Figure 11.19.2a.

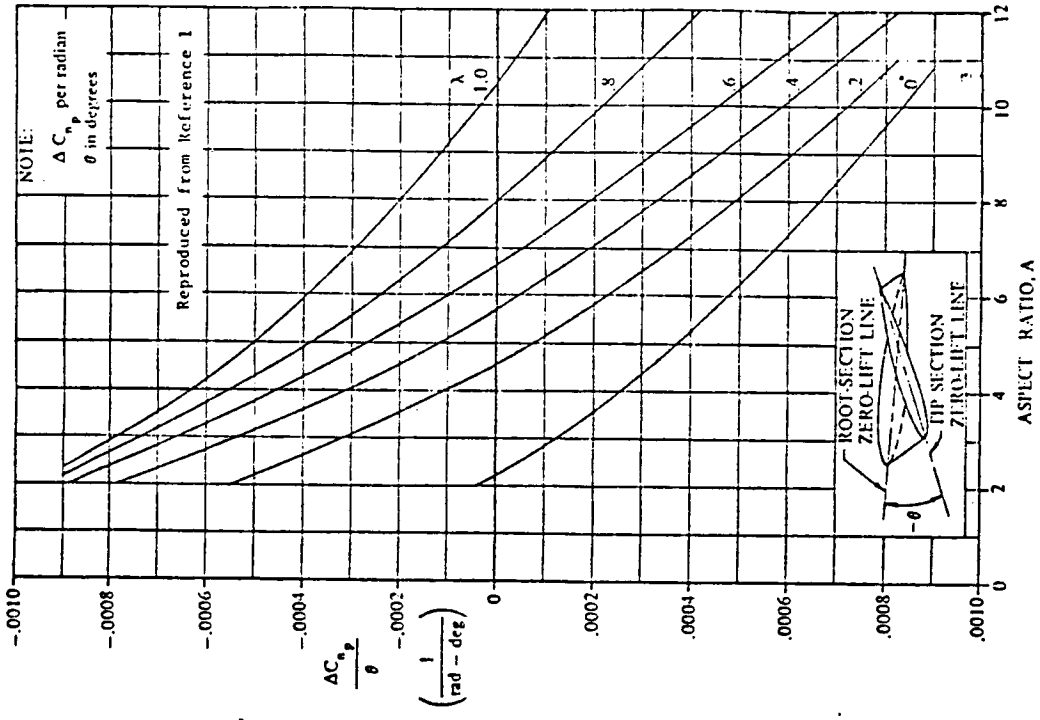

Figure 11.19.1: Effect of wing twist on wing rolling derivative C_{n_p}

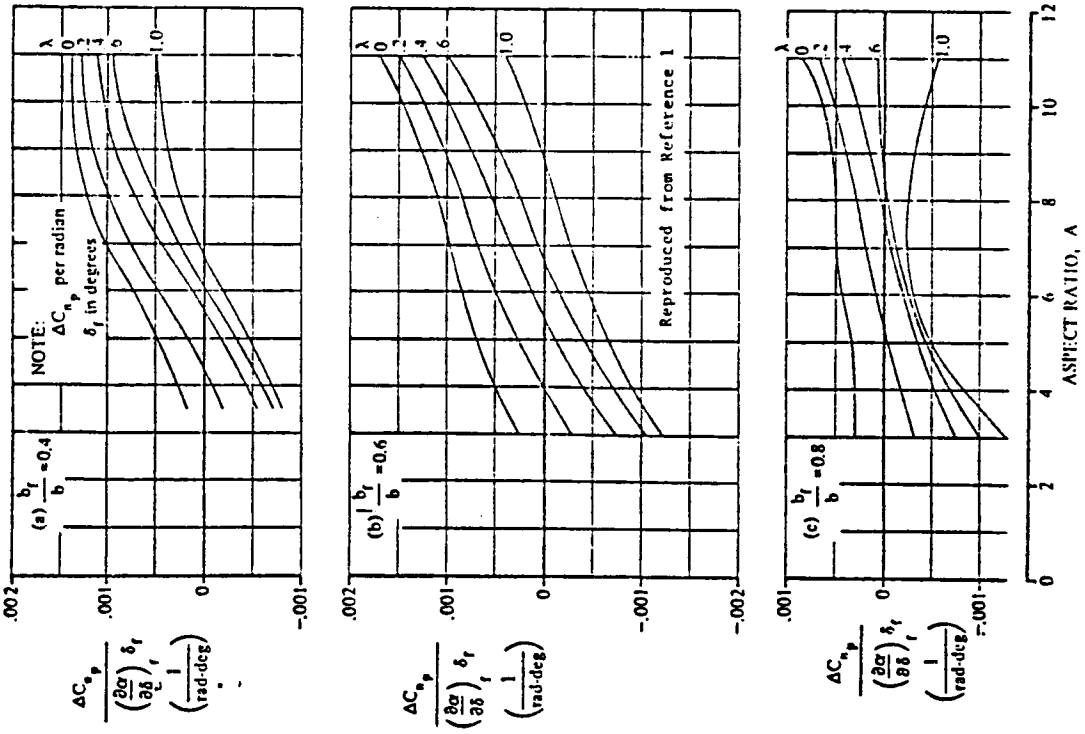

Figure 11.19.2: Effect of flap deflection on wing rolling derivative C_{n_p}

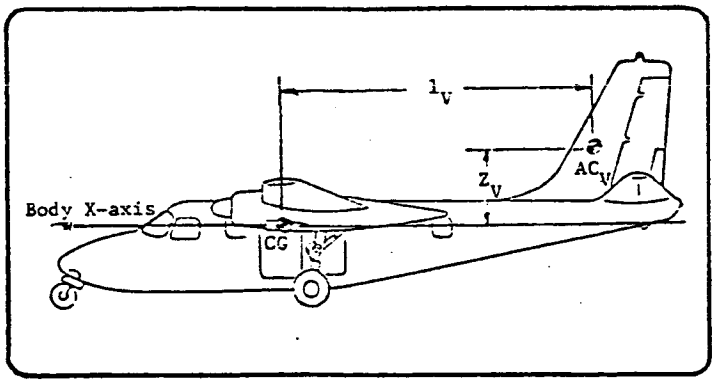

Figure 11.19.2a: Definition of geometric parameters

$C_{y_{\beta_v}}$ is the vertical tail contribution to C_{y_β}.

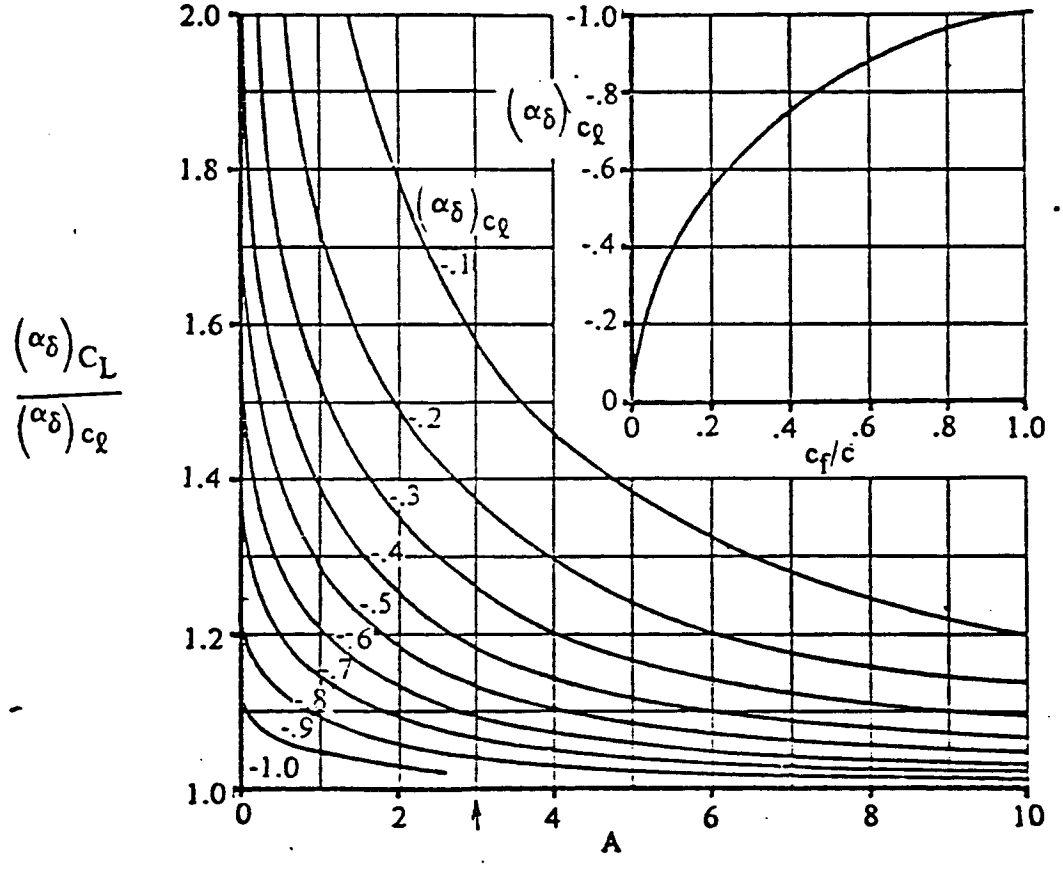

Figure 11.19.3: Influence of flap chord on flap effectiveness

11.19.2 REFERENCES

11.19.1 Roskam, J. Methods for Estimating Stability and Control Derivatives of Conventional Subsonic Airplanes. Dr. Jan Roskam, Published by the author, 519 Boulder, Lawrence, KS, 66044, 1971.

11.20 VARIATION OF SIDE FORCE COEFFICIENT WITH YAW RATE, C_{y_r}

11.20.1 DERIVATION OF EQUATIONS

Usually this derivative is of minor importance. It can be easily calculated however, and Reference 11.20.1 suggests the following formula:

$$C_{y_r} \approx C_{y_{r_V}} = -\frac{2}{b}(\ell_V \cos\alpha + Z_V \sin\alpha) C_{y_{\beta_V}} \qquad (11.20.1)$$

where ℓ_V and Z_V are defined in Figure 11.16.1

$C_{y_{\beta_V}}$ is computed in section 11.14.

11.20.2 REFERENCES

11.20.1 Roskam, J. Methods for Estimating Stability and Control Derivatives for Conventional Subsonic Airplanes. Roskam Aviation & Engineering Corporation. Lawrence, Ks. 1977.

11.21 SUBROUTINE "CLARE" (CLR), VARIATION OF ROLLING MOMENT WITH YAW RATE

11.21.1 DERIVATION OF EQUATIONS

Reference 11.21.1 indicates that C_{ℓ_r} may be estimated from:

$$C_{\ell_r} = C_{\ell_{r_W}} + C_{\ell_{r_V}} \tag{11.21.1}$$

The variation of the wing yawing derivative with lift coefficient is given by:

$$C_{\ell_{r_W}} = C_L\left(\frac{C_{\ell_r}}{C_L}\right)_{\substack{C_L=0\\M}} + \left(\frac{\Delta C_{\ell_r}}{\Gamma}\right)\Gamma + \left(\frac{\Delta C_{\ell_r}}{\Theta}\right)\Theta + \left(\frac{\Delta C_{\ell_r}}{\alpha_{\delta_F}\delta_F}\right)\alpha_{\delta_F}\delta_F \ (\text{rad}^{-1}) \tag{11.21.2}$$

where:

$\left(\frac{C_{\ell_r}}{C_L}\right)_{\substack{C_L=0\\M}}$ is the slope of the rolling moment due to yawing at zero lift given by:

$$\left(\frac{C_{\ell_r}}{C_L}\right)_{\substack{C_L=0\\M}} = \frac{1 + \frac{A(1-B^2)}{2B(AB+2\cos\Lambda_{c/4})} + \frac{AB+2\cos\Lambda_{c/4}}{AB+4\cos\Lambda_{c/4}}\left(\frac{\tan^2\Lambda_{c/4}}{8}\right)}{1 + \frac{A+2\cos\Lambda_{c/4}}{A+4\cos\Lambda_{c/4}}\left(\frac{\tan^2\Lambda_{c/4}}{8}\right)}\left(\frac{C_{\ell_r}}{C_L}\right)_{\substack{C_L=0\\M}} \tag{11.21.3}$$

where:

$$B = \sqrt{1 - M^2\cos^2\Lambda_{c/4}} \tag{11.21.4}$$

$\left(\frac{C_{\ell_r}}{C_L}\right)_{\substack{C_L=0\\M=0}}$ is the slope of the low-speed rolling moment due to yawing at zero lift, obtained from Figure 11.21.1 as a function of aspect ratio, quarter chord sweep, and taper ratio.

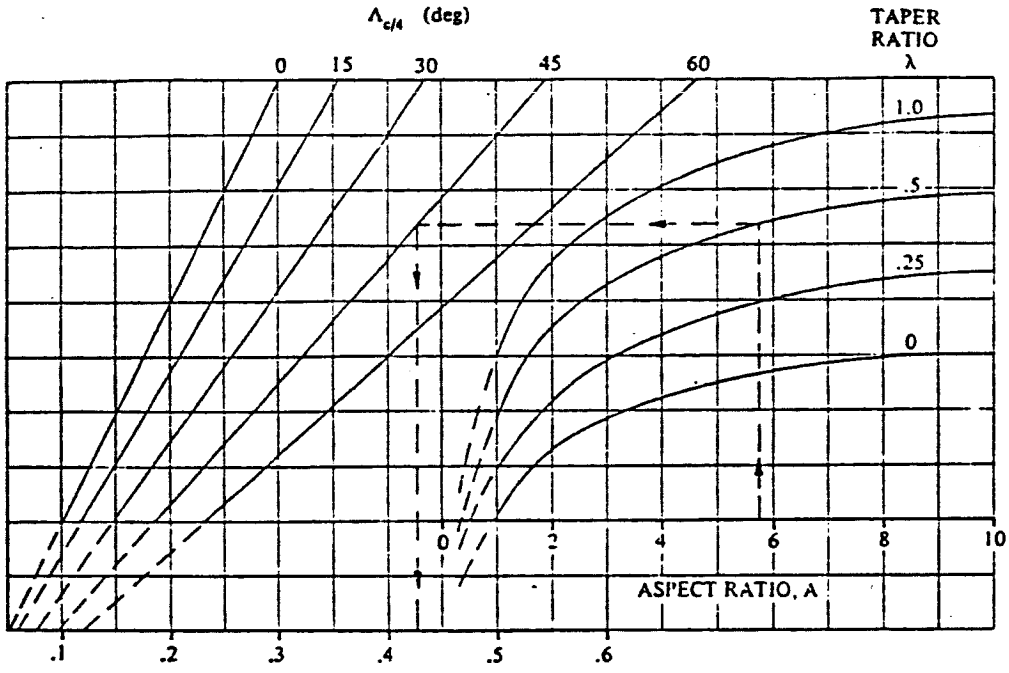

Reproduced from Reference 11.21.1

$$\left(\frac{C_{l_r}}{C_L}\right)_{\substack{C_L = 0 \\ M = 0}} \text{(per rad)}$$

Figure 11.21.1: Wing Yawing Derivative, C_{l_r}

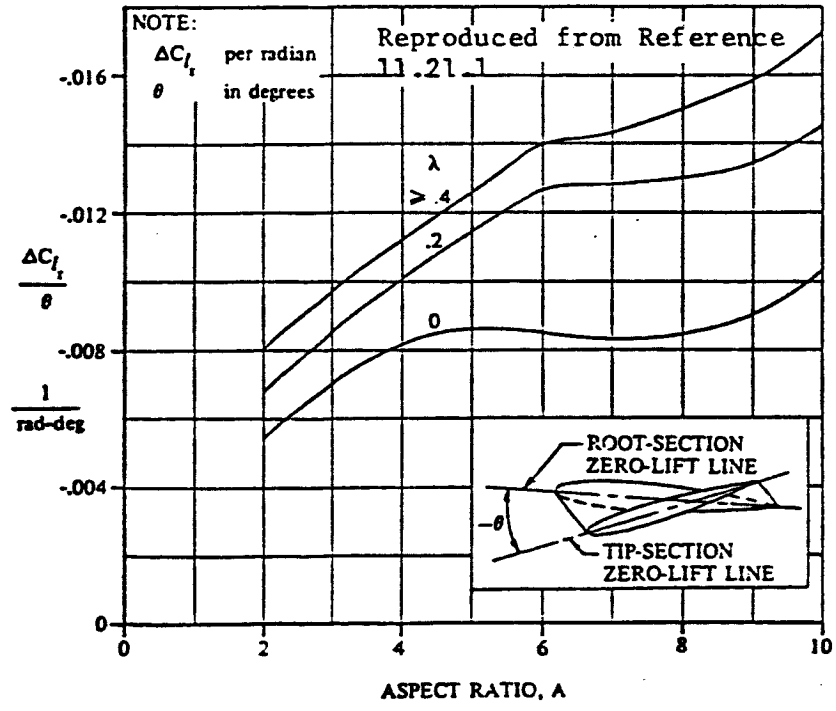

Figure 11.21.2: Effect of Wing Twist on C_{l_r}

C_L is the wing lift coefficient

$\frac{\Delta C_{\ell_r}}{\Gamma}$ is the increment in C_{ℓ_r} due to dihedral, given by:

$$\frac{\Delta C_{\ell_r}}{\Gamma} = \frac{1}{12} \frac{\pi A \sin \Lambda_{c/4}}{A + \cos \Lambda_{c/4}} \text{ (rad}^{-2}\text{)} \qquad (11.21.5)$$

Γ is the geometric dihedral angle, here in radians, positive for the wing tip above the plane of the root chord.

$\frac{\Delta C_{\ell_r}}{\Theta}$ is the increment due to wing twist obtained from Figure 11.21.2.

Θ is the wing twist, negative for washout

$\frac{\Delta C_{\ell_r}}{\alpha_{\delta_F} \delta_F}$ is the effect of symmetric flap deflection obtained from Figure 11.21.3.

δ_F is the streamwise flap deflection in degrees.

$\alpha_{\delta_F} \delta_F$ is the two dimensional lift-effectiveness parameter α_δ obtained from Section 11.23.

The vertical tail contribution is found from

$$C_{\ell_{r_V}} = \frac{-2}{b^2} (\ell_V \cos\alpha + Z_V \sin\alpha)(Z_V \cos\alpha - \ell_V \sin\alpha) C_{y_{\beta_V}}$$

where:

ℓ_V and Z_V are defined in Figure 11.16.1 and

$C_{y_{\beta_V}}$ is determined in Section 11.14.

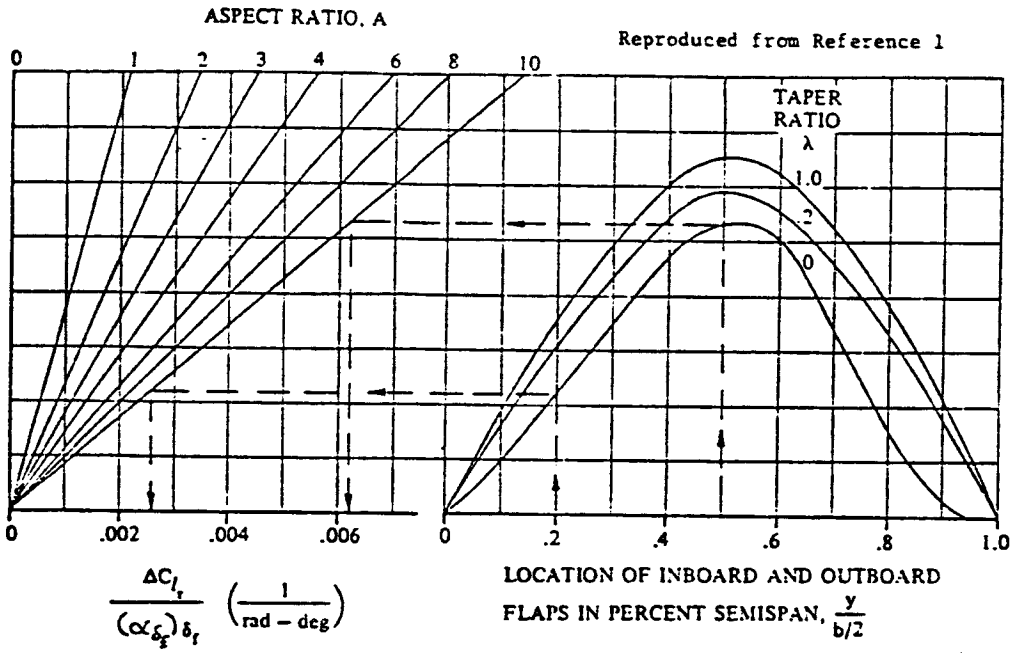

NOTE:
ΔC_{l_r} per radian
δ_f in degrees

NOTE: $\frac{\Delta C_{l_r}}{(\alpha_{\delta_f})\delta_f} = \left[\frac{\Delta C_{l_r}}{(\alpha_{\delta_f})\delta_f}\right]_{\text{outboard}} - \left[\frac{\Delta C_{l_r}}{(\alpha_{\delta_f})\delta_f}\right]_{\text{inboard}}$

Figure 11.21.3: Effect of Flaps on C_{l_r}

11.21.2 REFERENCES

11.21.1 Roskam, J. Methods for Estimating Stability and Control Derivatives of Conventional Subsonic Airplanes. Roskam Aviation & Engineering Corporation. Lawrence, KS.

11.22 VARIATION OF YAWING MOMENT COEFFICIENT WITH YAW RATE, C_{n_r}

11.22.1 DERIVATION OF EQUATIONS

Reference 11.22.1 indicates that this derivative can be estimated from:

$$C_{n_r} = C_{n_{r_W}} + C_{n_{r_V}} \qquad (11.22.1)$$

The contribution of the vertical tail follows from:

$$C_{n_{r_V}} = \frac{2}{B^2} (\ell_V \cos \alpha + Z_V \sin \alpha)^2 \, C_{y_{\beta_V}} \qquad (11.22.2)$$

where: ℓ_V and Z_V are defined in figure 11.16.1,

$C_{y_{\beta_V}}$ follows from section 11.14.

The wing contribution may be estimated from a series of graphs in refence 11.22.1, based on experimental data, as a function of wing sweep, taper ratio, aspect ratio, lift-coefficient and zero-lift drag. A close examination of these graphs revealed that, for the class of airplanes considered in this report, the average contribution of the wing is 7.5 % in the negative sense. Since this is a relatively small value that does not vary very much for different wing planforms, this value was used to adjust the contribution of the vertical tail. The result is:

$$C_{n_r} = 1.075 \frac{2}{B^2} (\ell_V \cos \alpha + Z_V \sin \alpha)^2 C_{y_{\beta_V}} \qquad (11.22.3)$$

11.22.2 REFERENCES

11.22.1 Roskam, J. Methods for Estimating Stability and Control Derivatives of Conventional Subsonic Airplanes, Roskam Aviation & Engineering Corporation, Lawrence, KS, 1977.

11.23 LONGITUDINAL CONTROL DERIVATIVES

11.23.1 INTRODUCTION

This chapter describes the computation of the longitudinal control derivatives. The method that calculates lift increment with flap deflection is valid only for the so-called plain flap type. See Figure 11.23.1. It should be pointed out that this method is equally well suited for the computation of variation of lift coefficient for control surface deflection, and therefore is written in a generalized form.

11.23.2 DERIVATION OF EQUATIONS

11.23.2.1 VARIATION OF LIFT COEFFICIENT WITH FLAP DEFLECTION

The derivation of this derivative is based on Reference 11.23.1, unless otherwise indicated. The layout of the lifting surface and the control surface is as indicated in Figure 11.23.1.

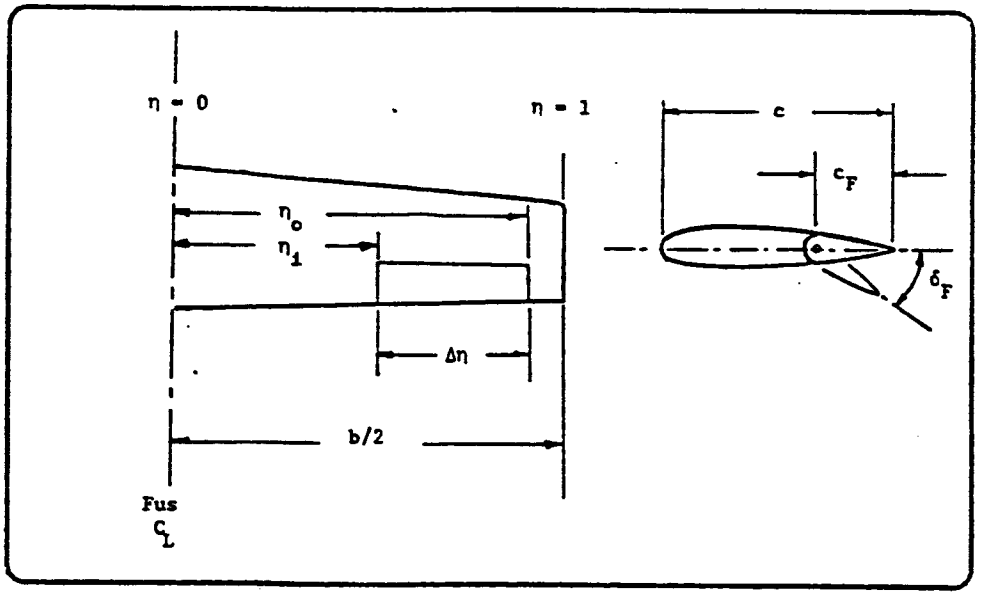

Figure 11.23.1: Geometric Parameters for Control Surface Flap

The derivative $C_{L_{\delta_F}}$ may be estimated from:

$$C_{L_{\delta_F}} = C_{\ell_{\delta_F}} \frac{C_{L_\alpha}|_M}{C_{\ell_\alpha}|_M} \frac{(\alpha_\delta)_{C_L}}{(\alpha_\delta)_{C_\ell}} K_b \qquad (11.23.1)$$

where:

$C_{L_\alpha}|_M$ is the lift-curve slope of the surface without flap deflection, obtained from Section 11.2.

$C_{\ell_\alpha}|_M$ is the section lift-curve slope, corrected for Mach number:

$$C_{\ell_\alpha}|_M = C_{\ell_\alpha} \Big/ \sqrt{1 - M^2} \qquad (11.23.2)$$

$\frac{(\alpha_\delta)_{C_L}}{(\alpha_\delta)_{C_\ell}}$ is the factor that takes three dimensional effects into account. It is given in Figure 11.23.2 as a function of aspect ratio, A_h, and the value of $(\alpha_\delta)_{C_L} = \frac{C_{\ell_{\delta_{flap}}}}{(C_{\ell_\alpha})_{surface}}$, based on experiments. If these data are not available, it may be obtained from the inset of Figure 11.23.2. Average values for c_F/c_w may be used.

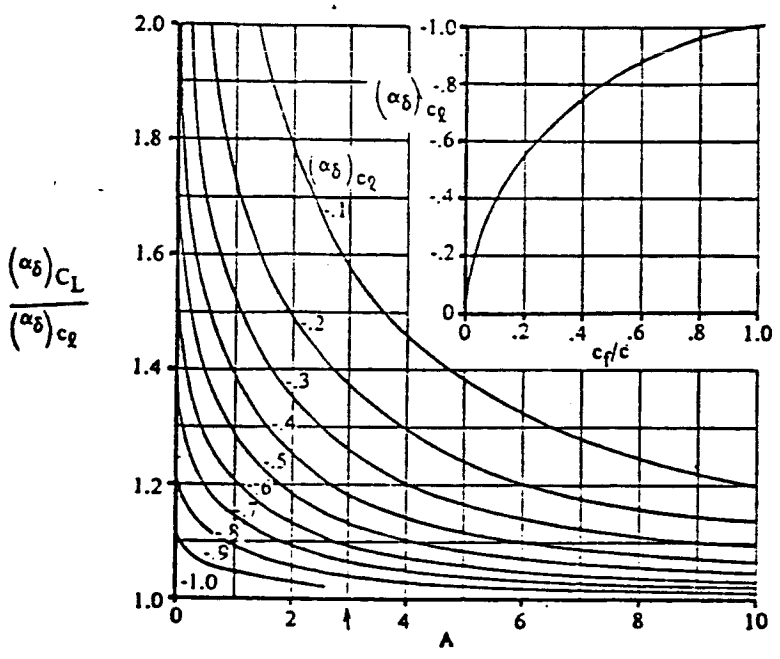

Figure 11.23 2: Influence of flap chord on flap effectiveness

K_b is a factor that takes the spanwise position of the flap into account. It can be obtained from Figure 11.23.3 as a function of taper ratio λ_h and span ratio $\eta = \frac{Y}{b/2}$.

$C_{\ell_{\delta_F}}$ is the section lift effectiveness of the flap, and may be obtained from the following equation:

$$C_{\ell_{\delta_F}} = \frac{1}{\sqrt{1 - M^2}} \left[\frac{C_{\ell_{\delta_F}}}{\left(C_{\ell_{\delta_F}}\right)_{\text{Theory}}} \right] \left(C_{\ell_{\delta_F}}\right)_{\text{Theory}} \left(K'\right) \qquad (11.23.3)$$

where: $\left(C_{\ell_{\delta_F}}\right)_{\text{Theory}}$ is the theoretical lift effectiveness of the flap, obtained from Figure 11.23.4 as a function of c_F/c_w and thickness ratio.

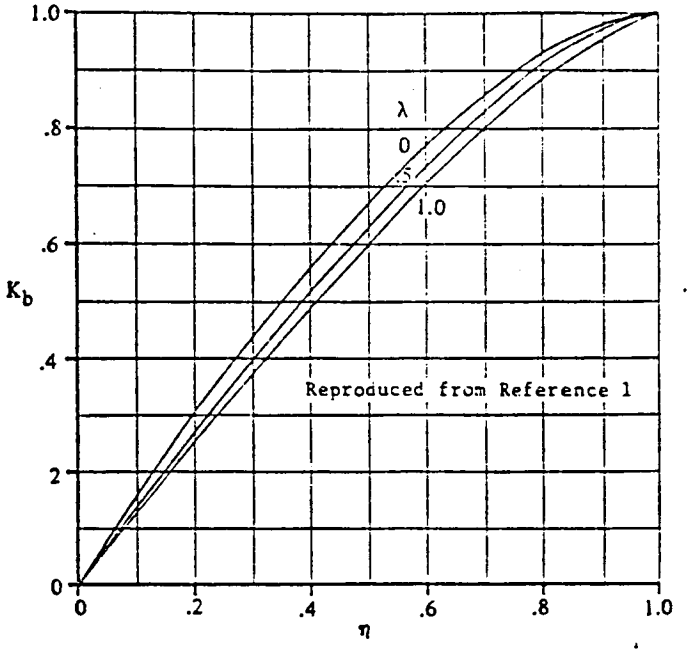

Figure 11.23.3: Span factor for inboard flaps

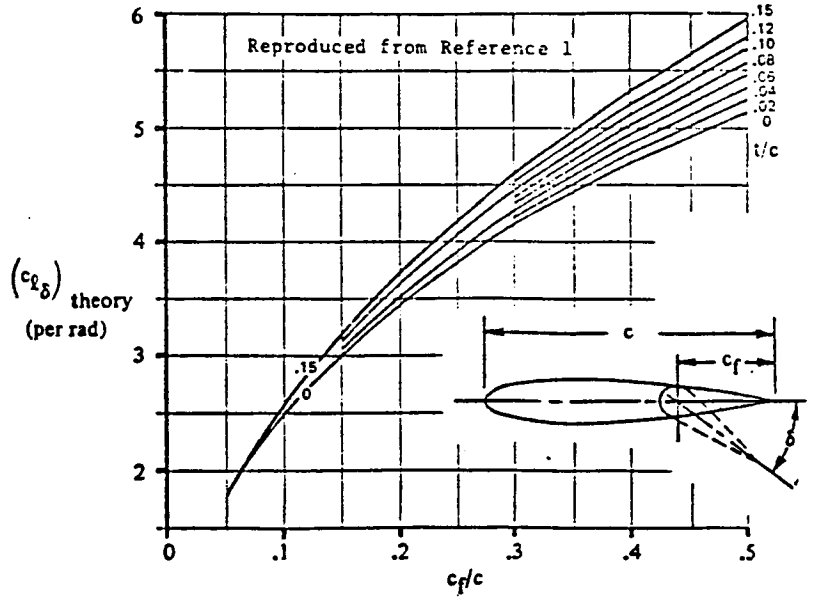

Figure 11.23.4: Theoretical lift effectiveness of plain trailing edge control flap

$\frac{C_{\ell_{\delta_F}}}{C_{\ell_{\delta_F}}_{Theoretical}}$ is an empirical correction factor based on experimental data, and may be obtained from Figure 11.23.5 as a function of c_F/c and $(C_{\ell_\alpha})/(C_{\ell_\alpha})_{Theory}$.

The theoretical section lift curve, $(C_{\ell_\alpha})_{Theory}$ may be obtained from:

$$(C_{\ell_\alpha})_{Theory} = 6.2827 + 5.0442\ t/c \qquad (11.23.4)$$

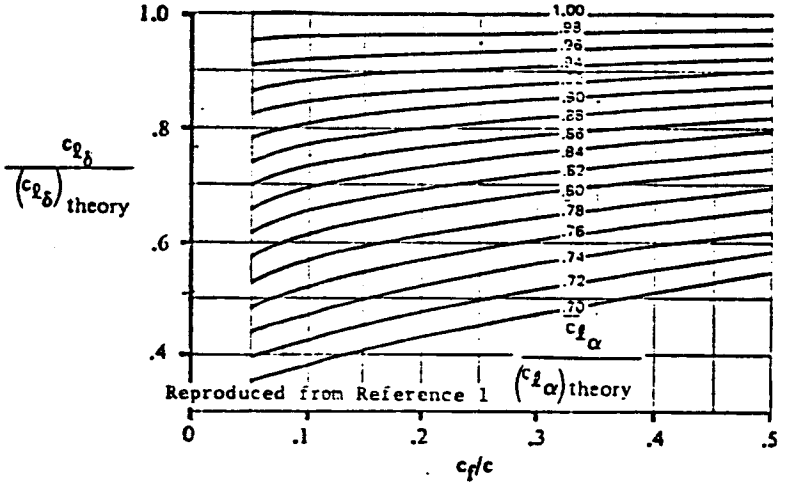

Figure 11.23.5: Empirical correction for lift effectiveness of plain trailing edge control flaps

K' is an empirical correction factor to the lift effectiveness at large deflections of the flap, and may be obtained from Figure 11.23.6.

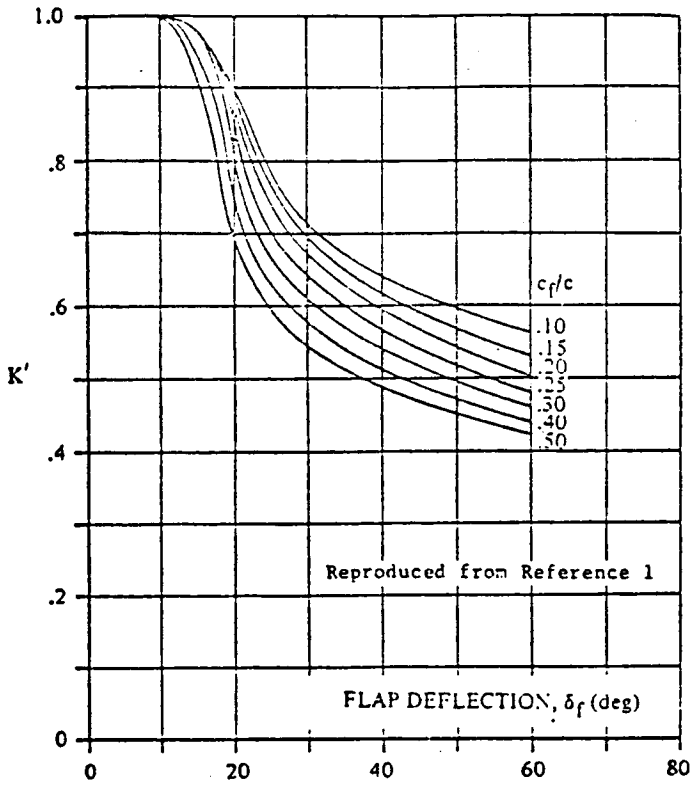

Figure 11.23.6: Empirical correction for lift effectiveness of plain trailing edge control flaps at high control deflections

To implement above method in a computer program, the following curve fittings were derived from the figures.

For the inset of Graph 11.23.2:

$$(\alpha_\delta)_{C_\ell} = -.2747 - 1.4584 \left(\frac{c_F}{c_w}\right) + .7406 \left(\frac{c_F}{c_w}\right)^2 \qquad (11.23.5)$$

For Graph 11.23.3:

$$K_b = -.0091 + 1.5447 \eta - .5175 \eta^2 \qquad (11.23.6)$$

It should be noted that Equation (11.23.5) is accurate for $\lambda = .5$. However, due to the manner in which K_b is calculated, the result will be accurate also for other values of taper ratio.

For graph 11.23.4:

$$(C_{\ell_{\delta_{flap}}})_{theory} = 1.2572 + 12.8356\ c_f/c - 10.3788\ (c_f/c)^2 + A \qquad (11.23.7)$$

where: $A = 12.14\ t/c\ (c_f/c - .05)$ (11.23.8)

For graph 11.23.6:

$\delta_f < 10^0$: $K' = 1$ (11.23.9a)

$10^0 < \delta_f < 20^0$: $K' = .8014 + .01441\ \delta_f - .00246\ \delta_f^2 +$

$$+ (-2.5\ c_f/c + 1.25).(.1672 - .0352\ \delta_f + .0019\ \delta_f^2) \qquad (11.23.9b)$$

$\delta_f > 20^0$: $K' = 1.0356 - .0217\ \delta_f + .000194\ \delta_f -$

$$2.5\ (c_f/c - .5).(-.00154\ \delta_f + .231) \qquad (11.23.9c)$$

11.23.2.2 VARIATION OF PITCHING MOMENT COEFFICIENT WITH FLAP DEFEECTION.

This derivative will not be discussed since the complexity involved in the computation of this derivative is beyond the scope of this report.

11.23.2.3 VARIATION OF LIFT COEFFICIENT WITH STABILIZER INCIDENCE

The derivative $C_{L_{i_H}}$ may be computed from:

$$C_{L_{i_H}} = C_{L_{\alpha_H}}\ S_H/S \qquad (11.23.10)$$

where: $C_{L_{\alpha_H}}$ is computed in section 11.2.

11.23.2.4. VARIATION OF PITCHING MOMENT WITH STABILIZER DEFLECTION

The derivative $C_{m_{i_H}}$ may be computed from:

$$C_{m_{i_H}} = - C_{L_{\alpha_H}} \frac{\ell_H S_H}{S \bar{c}} \qquad (11.23.11)$$

where: $C_{L_{\alpha_H}}$ is obtained from section 11.2.

11.23.2.5. VARIATION OF LIFT COEFFICIENT WITH ELEVATOR DEFLECTION

The derivative $C_{L_{\delta_E}}$ may be computed from:

$$C_{L_{\delta_E}} = C_{L_{\delta_F}} \, S_H/S \qquad (11.23.12)$$

where: $C_{L_{\delta_F}}$ is found from section 11.23.2.1

11.23.2.6. VARIATION OF PITCHING MOMENT WITH ELEVATOR DEFLECTION

The derivative $C_{m_{\delta_E}}$ may be found from:

$$C_{m_{\delta_E}} = - C_{L_{\delta_F}} \frac{\ell_H S_H}{S \bar{c}} \qquad (11.23.13)$$

11.23.3 REFERENCES

11.23.1 Roskam, J. Methods for Estimating Stability and Control Derivatives of Conventional Subsonic Airplanes, Roskam Aviation& Engineering Corp., Lawrence, KS, 1977

11.24 AILERON STABILITY DERIVATIVES $C_{\ell_{\delta_A}}$, $C_{n_{\delta_A}}$, $C_{y_{\delta_A}}$

11.24.1 INTRODUCTION

$C_{\ell_{\delta_A}}$ is the most important of the aileron stability derivatives and it is calculated with a combination of the methods used in References 11.24.1 and 11.24.2. Compressibility effects are taken into account, but the influence of wing taper ratio is neglected.

$C_{n_{\delta_A}}$ is much smaller than $C_{\ell_{\delta_A}}$; preferably it should be positive because this means that there are no adverse yaw effects in making turns. It is calculated with the method used in Reference 11.24.1. The wing taper ratio is an important variable in the determination of $C_{n_{\delta_A}}$, so it is not neglected here.

The value of $C_{y_{\delta_A}}$ is usually so small that it can be ignored. The program does not calculate this derivative.

11.24.2 CALCULATION OF $C_{\ell_{\delta_A}}$

A shortcoming of the method of Reference 11.24.1 is that only moderate wing aspect ratios are allowed in cases with β and κ close to one. With the method of Reference 11.24.2, which basically works the same way, wing aspect ratios from 6 to 16 can be investigated. This method, however, does not take the effect of wing sweep angle into account or the effect of wing taper ratio. This latter influence is a minor one: for taper ratios normally used, the aileron rolling moment parameter is hardly dependent on taper ratio. The effect of sweep angle can be greater, and therefore a mixture of both methods has been used to produce Fig. 11.24.1. According to Reference 11.24.2, it is valid

for aileron deflections up to 20 degrees.

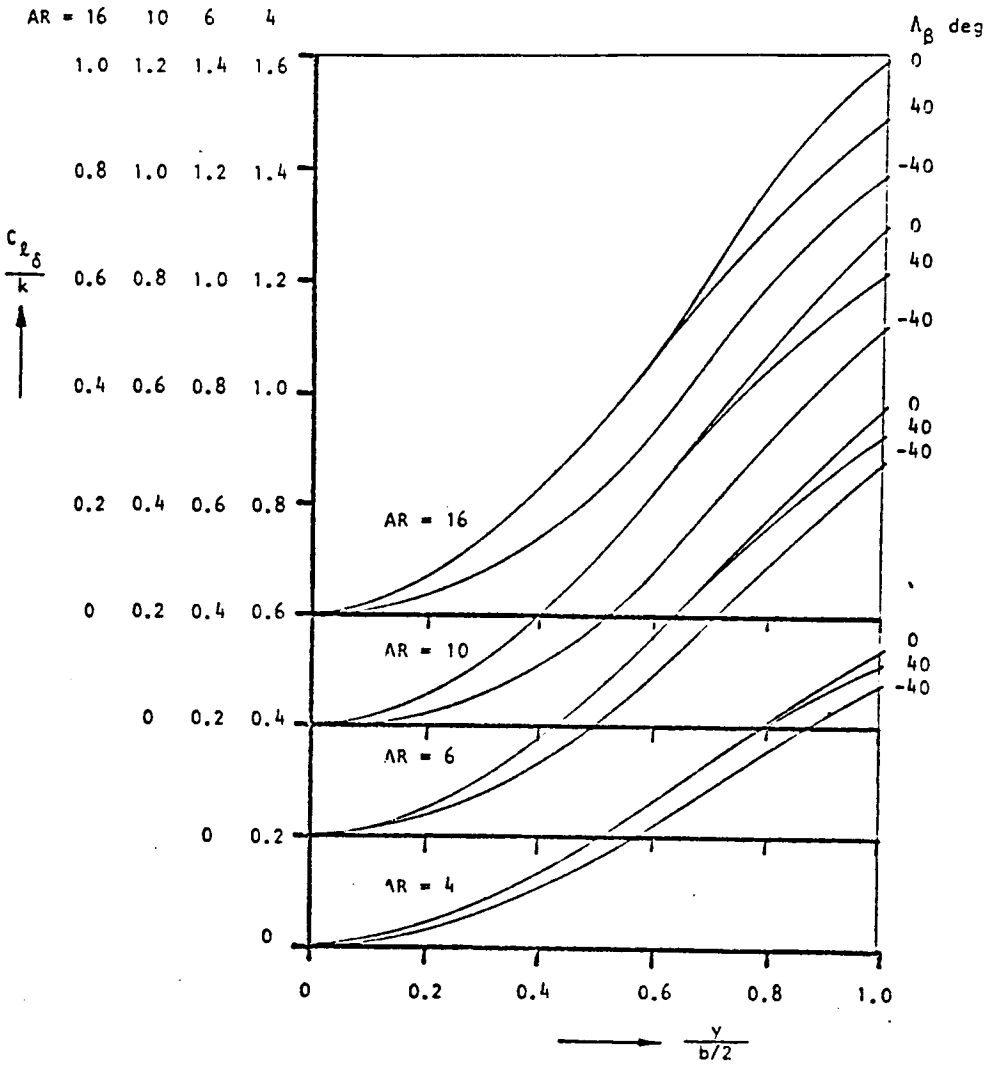

Figure 11.24.1: Determination of C_{ℓ_δ}/k

Fig. 11.24.1 is meant for full-chord controls; for partial-chord controls there is a correction factor, taken from Reference 11.24.2 and presented in Fig. 11.24.2. The variable Λ_β in Fig. 11.24.1 is computed as follows:

$$\Lambda_\beta = \arctan\left(\frac{\tan\Lambda_{c/4}}{\beta}\right) \qquad (11.24.1)$$

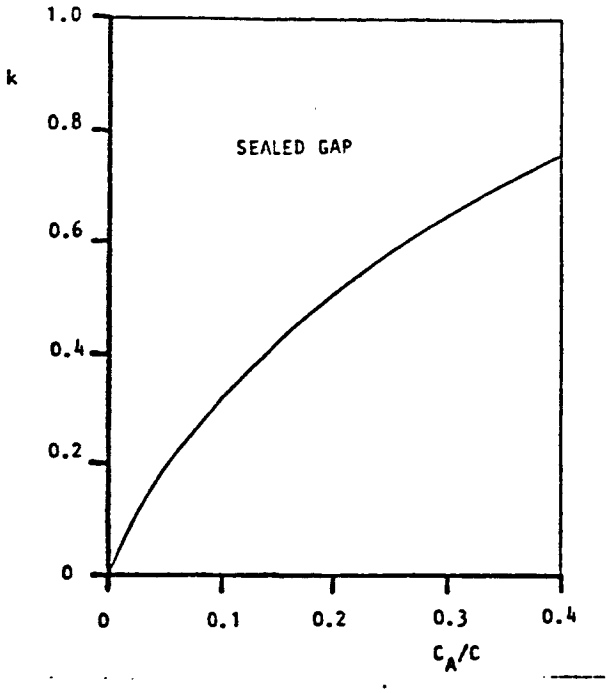

Figure 11.24.2: Correction for Flap-Span Effect

The effect of partial-span controls is taken into account by using Fig. 11.24.1 two times: once for the inboard lateral coordinate of the aileron and again for the outboard lateral coordinate. The difference in the results is then the actual aileron rolling moment parameter.

It is assumed that the effectiveness of the right aileron is equal to that of the left aileron, so Fig. 11.24.1 gives the total aileron rolling moment parameter. The aileron deflection associated with it is defined as:

$$\delta_A = \tfrac{1}{2}(\delta_L - \delta_R) \qquad (11.24.2)$$

in which a positive control deflection is left aileron trailing edge down. $C_{\ell_{\delta_A}}$ is found as the product of $\frac{C_{\ell_\delta}}{k}$ (from Fig. 11.24.1) and k (from Fig. 11.24.2).

11.24.3 CALCULATION OF $C_{n_{\delta_A}}$

This derivative is calculated with the method in Reference 11.24.1, according to:

$$C_{n_{\delta_A}} = K\, C_L\, C_{\ell_{\delta_A}} \qquad (11.24.3)$$

The factor K is a correlation constant which depends on wing aspect ratio, taper ratio and inboard location of the aileron. It is given in Fig. 11.24.3. The lines for A = 12 are the result of extrapolating Fig. 11.3 in Reference 11.24.1.

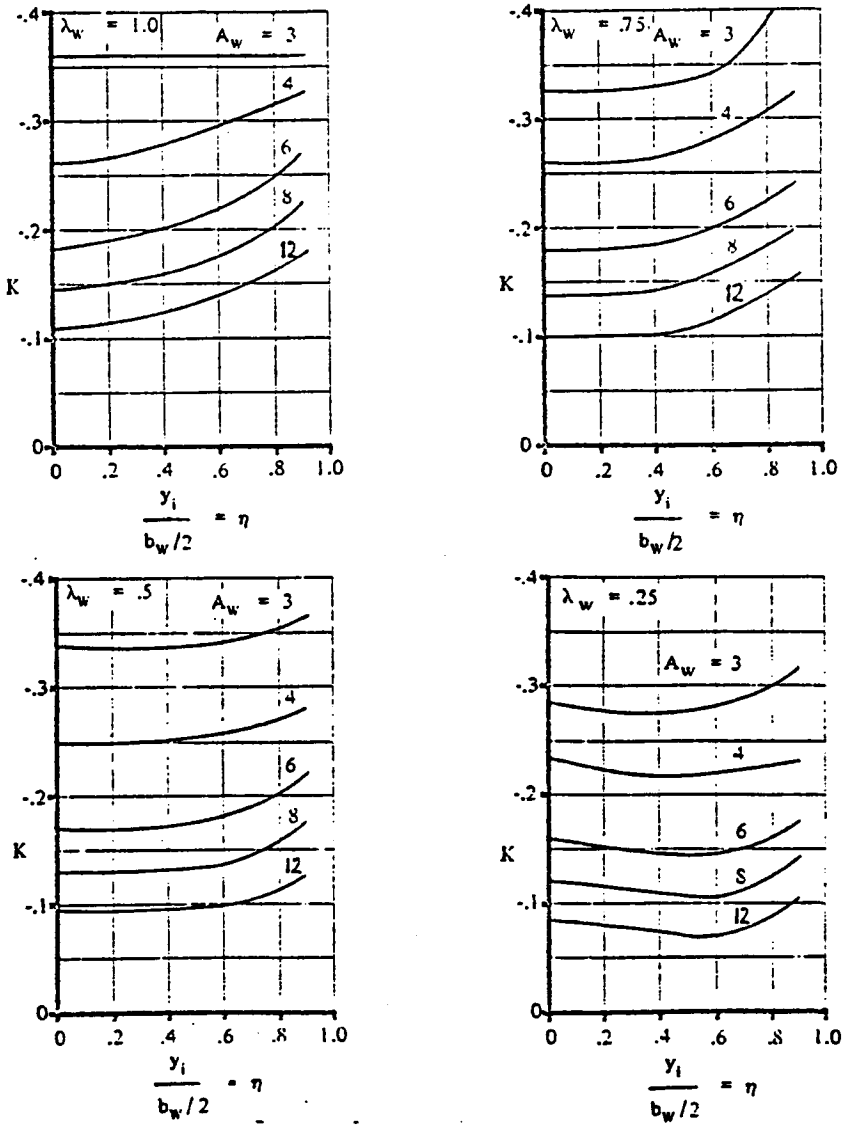

Figure 11.24.3: Correlation Constant for $C_{n_{\delta_A}}$

This figure is only valid for ailerons which extend to the wingtip. To calculate $C_{n_{\delta_A}}$ for ailerons which do not extend to the wingtip, Eqn. (11.24.3) must be used two times: once for an imaginary aileron which extends from the inboard location of the actual aileron to the tip and again for another imaginary aileron which extends from the outboard location of the actual aileron to the tip. Subtracting the $C_{n_{\delta_A}}$ of the second imaginary aileron from that of the first one gives $C_{n_{\delta_A}}$ of the actual aileron. However, it is not enough to take the difference in the correlation constants of the two imaginary ailerons, and $C_{\ell_{\delta_A}}$ must also be calculated for each one.

The value of C_L in Eqn. (11.24.3) follows from:

$$C_L = \frac{W}{\bar{q}S} \qquad (11.24.4)$$

so it is just the steady state lift coefficient.

11.24.4 REFERENCES

11.24.1 Roskam, J. Methods for Estimating Stability and Control Derivatives of Conventional Subsonic Airplanes, Roskam Aviation & Engineering Corporation, Lawrence, KS, 1977.

11.24.2 Dommasch, D.O. Sherby, S.S. Connolly, T.F. Airplane Aerodynamics, Pitman Publishing Corporation, New York, 1967

11.25 DIRECTIONAL CONTROL DERIVATIVES $C_{y_{\delta_R}}$, $C_{\ell_{\delta_R}}$ AND $C_{n_{\delta_R}}$

11.25.1 INTRODUCTION

This chapter describes the computation of the directional control derivatives, and the method presented is taken from Reference 11.25.1. Since it relies on computations in Chapter 11.23 for control-surface effectiveness, it is subject to the limitations of those calculations.

11.25.2 DERIVATION OF EQUATIONS

11.25.2.1 $C_{y_{\delta_R}}$ Variation of sideforce coefficient with rudder deflection. This derivative may be estimated from:

$$C_{y_{\delta_R}} = - C_{L_{\alpha_V}} \left(\frac{(\alpha_\delta)_{C_L}}{(\alpha_\delta)_{C_\ell}} \right) (\alpha_\delta)_{C_\ell} K' K_b \left(\frac{S_v}{S} \right) \eta_v \qquad (11.25.1)$$

Where:

$C_{L_{\alpha_V}}$ is the vertical tail lift curve slope, computed as in Section 11.2.

Note: The effective aspect ratio of the vertical tail, $AR_{V_{EFF}}$, used in the calculation of $C_{L_{\alpha_V}}$ is obtained from Section 11.14.

$\frac{(\alpha_\delta)_{C_L}}{(\alpha_\delta)_{C_\ell}}$ is the ratio of three dimensional flap-effectiveness to two dimensional flap-effectiveness. It may be obtained from Section 11.23.

$(\alpha_\delta)_{C_\ell}$ is the theoretical value of the two-dimensional flap-effectiveness parameter and may be obtained from Section 11.21.

K' is a correction factor for high control-surface angles, obtained from Section 11.21.

K_b is a correction factor for control-surface-span, obtained from Section 11.21.

11.25.2.2 $C_{\ell_{\delta_R}}$ variation of the rolling moment coefficient with rudder deflection.

This derivative may be computed as:

$$C_{\ell_{\delta_R}} = C_{y_{\delta_R}} \left(\frac{Z_V \cos\alpha - \ell_V \sin\alpha}{b} \right) \qquad (11.25.2)$$

Where:

$C_{y_{\delta_R}}$ follows from section 11.25.2.1

Z_V and ℓ_V are defined in Figure 11.16.1

11.25.2.3 $C_{n_{\delta_R}}$ variation of yawing moment coefficient with rudder deflection.

This derivative may be computed as follows:

$$C_{n_{\delta_R}} = - C_{y_{\delta_R}} \left(\frac{\ell_V \cos\alpha + Z_V \sin\alpha}{b} \right) \qquad (11.25.3)$$

Where:

$C_{y_{\delta_R}}$ follows from section 11.25.2.1

Z_V and ℓ_V are defined in Figure 11.16.1.

11.25.3 REFERENCES

11.25.1 Hoak, D.E. & Ellison, D.E. USAF Stability and Control Datcom: . Flight Control Division; Air Force Flight Dynamics Laboratory, Wright Patterson Air Force Base, Ohio, 45433

11.26: HINGE MOMENTS OF CONTROL SURFACES C_{h_α} , C_{h_δ}

11.26.1: INTRODUCTION

This chapter describes the procedure involved in computing the hinge moment derivatives C_{h_α} and C_{h_δ} , where the methods are primarily those of Reference 11.26.1. The data used for the computation of the section hinge moment derivatives are based on the NACA 0009 airfoil. This is a type of airfoil that is used quite often for the horizontal tailplane on general aviation aircraft. The method allows for differences in lifting-surface geometry, control-surface geometry and method of balancing. First the equations for the variation of hinge moment with angle of attack will be derived, followed by the equations for the variation of hinge moment with control surface deflection.

11.26.2.1 DERIVATION OF EQUATIONS FOR C_{h_α}

First the section characteristics for sealed-gap controls will be derived, where a correction will be made to account for open-gap controls. The hinge moment derivative C_{h_α} is based on the control chord squared$(c_F)^2$(see Fig. 11.26.1).

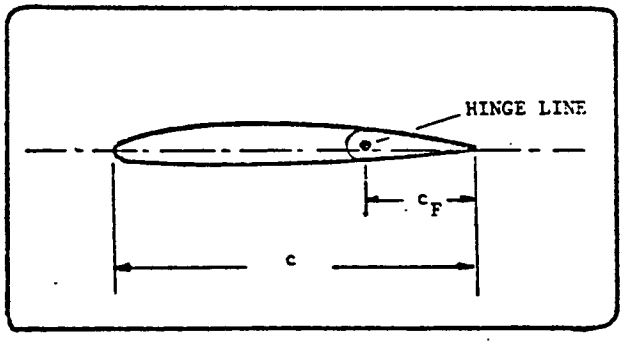

Figure 11.26.1: Geometry of Aileron

The first step requires the computation of the hinge moment derivative C'_{h_α} for a radius-nose, sealed control surface:

$$C'_{h_\alpha} = \left(\frac{C'_{h_\alpha}}{(C_{h_\alpha})_{theory}}\right)(C_{h_\alpha})_{theory} \quad (rad^{-1}) \qquad (11.26.1)$$

Where:

$\frac{C'_{h_\alpha}}{(C_{h_\alpha})_{theory}}$ is the ratio of actual to theoretical hinge moment derivative, obtained from Figure 11.26.2. The parameter $C_{\ell_\alpha}/(C_{\ell_\alpha})_{theory}$ follows from Eqn. 11.23.4

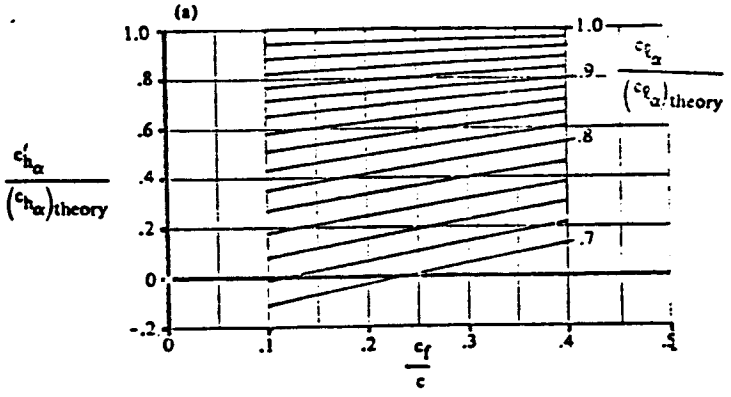

Figure 11.26.2: Rate of Change of Section Hinge Moment C'_{h_α} with Angle of Attack

$(C_{h_\alpha})_{theory}$ is the theoretical hinge moment derivative, and follows from Figure 11.26.3.

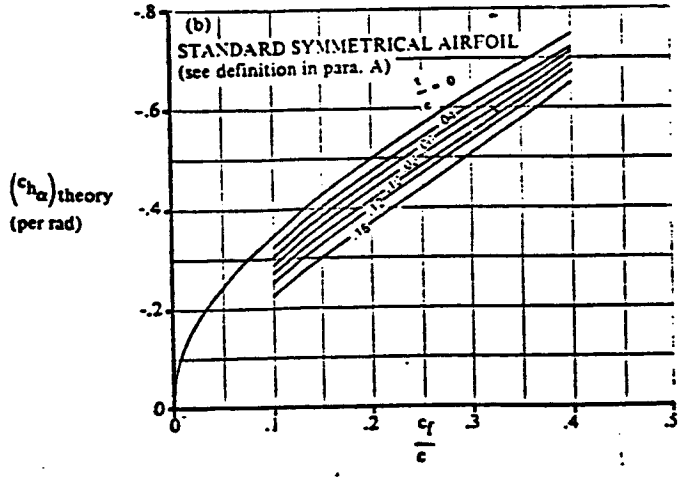

Figure 11.26.3: Theoretical Hinge Moment Derivative

If the trailing edge of the airfoil does not conform to the following condition:

$$\text{TAN}\,\frac{\phi'_{TE}}{2} = \text{TAN}\,\frac{\phi''_{TE}}{2} = \text{TAN}\,\frac{\phi_{TE}}{2} = \frac{t}{c} \qquad (11.26.2)$$

Where: ϕ'_{TE} is the angle between straight lines through 90 and 99 percent of the chord on upper and lower surface

ϕ''_{TE} is the angle between straight lines through 95 and 99 percent of the chord on upper and lower surface*

ϕ_{TE} is the trailing edge angle between tangents to upper and lower surfaces at the trailing edge,

then the following correction has to be applied to equation (11.26.1):

$$C''_{h_\alpha} = C'_{h_\alpha} + 2(C_{\ell_\alpha})_{theory}\left(1 - \frac{C_{\ell_\alpha}}{(C_{\ell_\alpha})_{theory}}\right)\left(\text{TAN}\,\frac{\phi''_{TE}}{2} - \frac{t}{c}\right)\left(\text{rad}^{-1}\right) \qquad (11.26.3)$$

To account for the effect of balancing, the following correction is applied:

$$(C_{h_\alpha})_{balance} = C''_{h_\alpha}\left(\frac{(C_{h_\alpha})_{balance}}{C''_{h_\alpha}}\right)\left(\text{rad}^{-1}\right) \qquad (11.26.4)$$

Where:

C''_{h_α} is obtained from Eqn. (11.26.3), or is equal to C'_{h_α} in Eqn. (11.26.1).

$\dfrac{(C_{h_\alpha})_{balance}}{C''_{h_\alpha}}$ is obtained from Figure 11.26.4.

The definition of the control surface dimensions is given in Figure 11.26.5 while Figure 11.26.6 shows the various nose-shapes.

*Note: For a beveled trailing edge ϕ''_{TE} is equal to the angle of bevel.

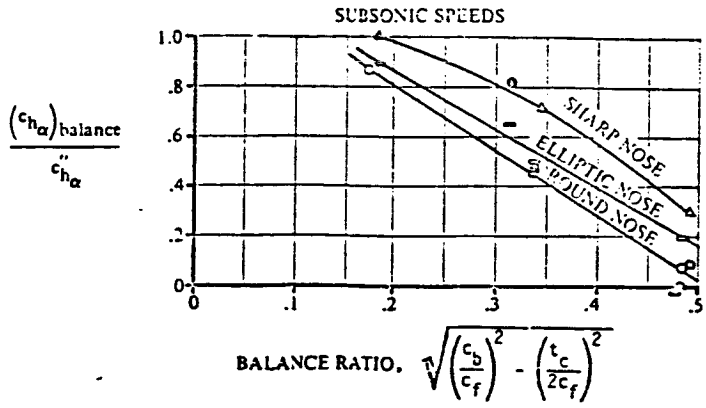

Figure 11.26.4: Effect of Nose Balance on Section Hinge Moment Derivatives

The effect of Mach number may be roughly approximated using the Prandtl-Glauert correction:

$$C_{h_\alpha}\Big|_M = \frac{C_{h_\alpha}\Big|_{\text{Low Speed}}}{\sqrt{1 - M^2}} \qquad (11.26.5)$$

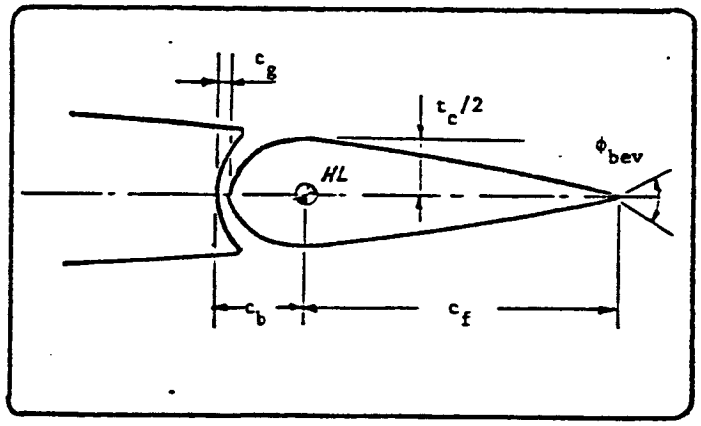

Figure 11.26.5: Geometry of Control Surface

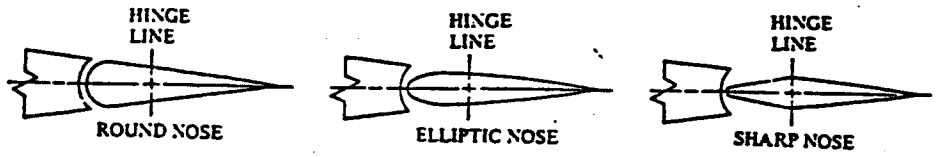

Figure 11.26.6: Various Types of Nose Shapes

*

Using the two dimensional hinge moment computed above, the three dimensional hinge moment coefficient is:

$$C_{h_\alpha} = \frac{AR \cos \Lambda_{c/4}}{AR + 2 \cos \Lambda_{c/4}} (C_{h_\alpha}) + \Delta C_{h_\alpha} \qquad (11.26.6)$$

Where:

C_{h_α} is computed with Eqn. (11.26.5)

ΔC_{h_α} is a correction for induced camber effects, arrived at by using lifting-surface theory. It may be obtained from Figure 11.26.7.

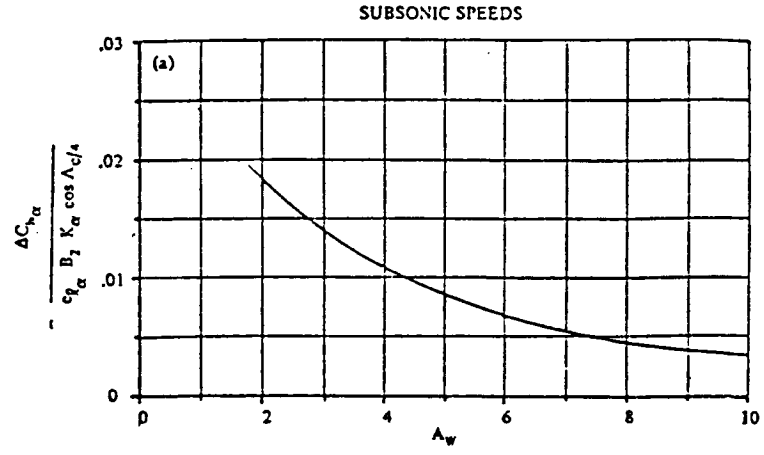

Figure 11.26.7: Correction for Induced Camber

The variables in the y-axis quantity are:

C_{l_α} is section lift curve slope

K_α takes control surface span into account, for outboard controls (see Fig. 11.26.8) if inboard controls are used, then K may be approximated to be equal to $Y_o/(b/2)$, where Y_o and Y_i are defined in Figure 11.26.9.

*The effect of open gap and bevel angle on section characteristics will be determined later.

B_2 accounts for the effect of control surface to balance chord ratios, to be obtained from Figure 11.26.10.

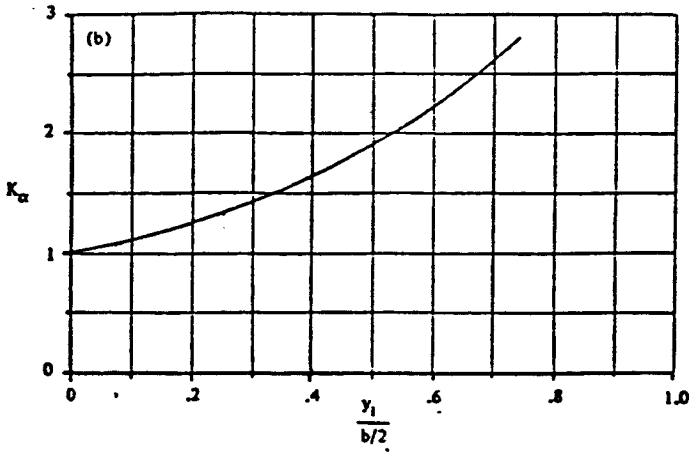

Figure 11.26.8: Effect of Control Surface Span

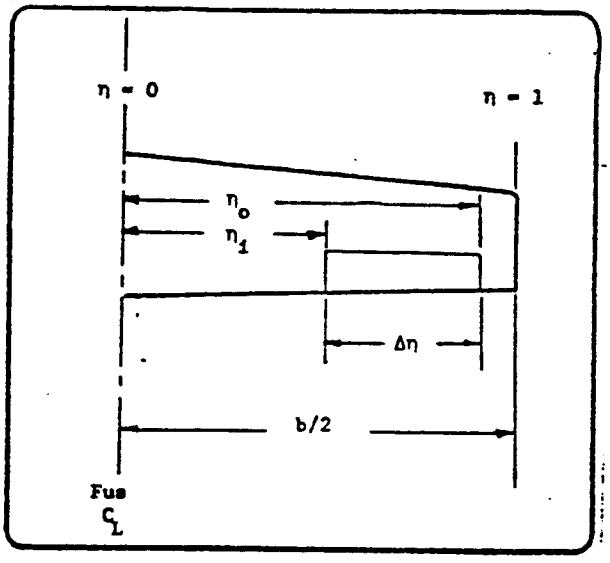

Figure 11.26.9: Control Surface Span Parameters

The primed values in Figure 11.26.10 refer to measurements normal to the wing quarter chord line, and if not explicitly given, they may be approximated by:

$$c_f'/c' = (c_f'' + c_f''')/(c'' - c''' + c_f'' + c_f''') \qquad (11.26.7)$$

and

$$c_b'/c_f' = c_b'/(c_f'' + c_f''') \qquad (11.26.8)$$

Where:

$$c_f'' = c_f \cos \Lambda_{1/4\bar{c}} \tag{11.26.9}$$

$$c_f''' = c_f \sin \Lambda_{1/4\bar{c}} \tan \Lambda_{1/4\bar{c}} \tag{11.26.10}$$

$$c'' = (\bar{c} - c_f) \cos \Lambda_{1/4\bar{c}} \tag{11.26.11}$$

$$c''' = (\bar{c} - c_f) \sin \Lambda_{1/4\bar{c}} \cdot \sin(\Lambda_{LE} - \Lambda_{1/4\bar{c}}) \tag{11.26.12}$$

$$c_b' = c_b \cos \Lambda_{1/4\bar{c}} + c_b \sin \Lambda_{1/4\bar{c}} \tan(\Lambda_{1/4\bar{c}} - \Lambda_{HL}) \tag{11.26.13}$$

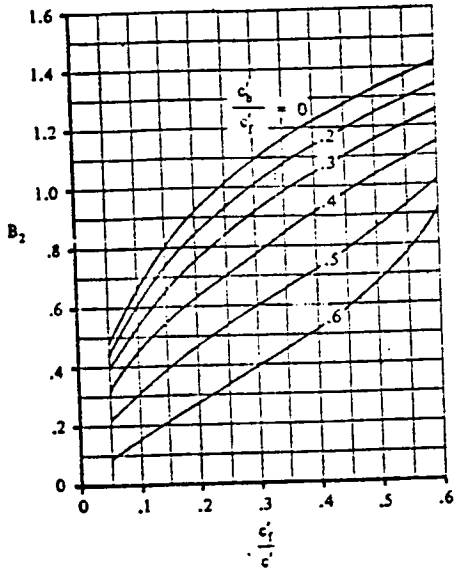

Figure 11.26.10: Correction for Chord Ratio

Corrections for open gap, horn balance and bevel angle may now be made. Reference 11.26.2, Figure 6-8, provides data for the estimation of the effect of open gap. The figure is reproduced as Figure 11.26.11. The definition of the gap may be found in Figure 11.26.5.

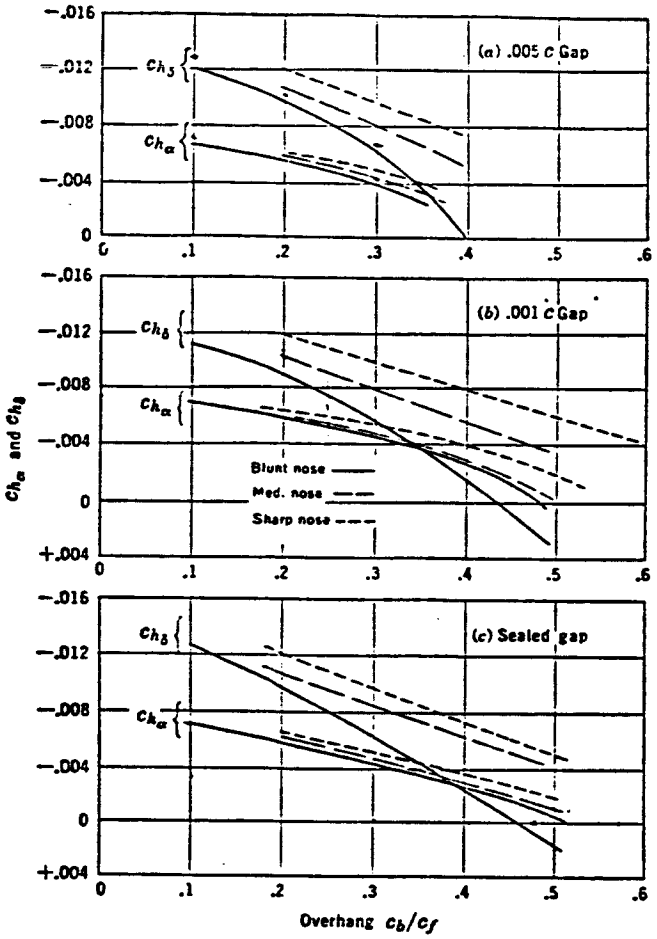

Figure 11.26.11: Effect of Open Gap on Section Hinge Moment Coefficient for a .35$\bar{c}$ Flap

Figure 11.26.11 shows on the average a (positive) increase in C_{h_α} of .0005 for a .005$\bar{c}$ gap. A simple approximation of the effect of open gap, therefore, is:

$$\Delta C_{h_{\alpha_{gap}}} = +.1 \frac{c_{gap}}{c} \quad (\text{deg}^{-1}) \qquad (11.26.14)$$

Reference 11.26.3 provides data for the estimation of the effect of bevel angle. Figure 11.26.12 is a reproduction of Fig. 12:14 of this reference.

This figure is only valid for ailerons which extend to the wingtip. To calculate $C_{n_{\delta_A}}$ for ailerons which do not extend to the wingtip, Eqn. (11.24.3) must be used two times: once for an imaginary aileron which extends from the inboard location of the actual aileron to the tip and again for another imaginary aileron which extends from the outboard location of the actual aileron to the tip. Subtracting the $C_{n_{\delta_A}}$ of the second imaginary aileron from that of the first one gives $C_{n_{\delta_A}}$ of the actual aileron. However, it is not enough to take the difference in the correlation constants of the two imaginary ailerons, and $C_{\ell_{\delta_A}}$ must also be calculated for each one.

The value of C_L in Eqn. (11.24.3) follows from:

$$C_L = \frac{W}{\bar{q}S} \qquad (11.24.4)$$

so it is just the steady state lift coefficient.

11.24.4 REFERENCES

11.24.1 Roskam, J. Methods for Estimating Stability and Control Derivatives of Conventional Subsonic Airplanes, Roskam Aviation & Engineering Corporation, Lawrence, KS, 1977.

11.24.2 Dommasch, D.O. Sherby, S.S. Connolly, T.F. Airplane Aerodynamics, Pitman Publishing Corporation, New York, 1967

11.25 DIRECTIONAL CONTROL DERIVATIVES $C_{y_{\delta_R}}$, $C_{\ell_{\delta_R}}$ AND $C_{n_{\delta_R}}$

11.25.1 INTRODUCTION

This chapter describes the computation of the directional control derivatives, and the method presented is taken from Reference 11.25.1. Since it relies on computations in Chapter 11.23 for control-surface effectiveness, it is subject to the limitations of those calculations.

11.25.2 DERIVATION OF EQUATIONS

11.25.2.1 $C_{y_{\delta_R}}$ Variation of sideforce coefficient with rudder deflection. This derivative may be estimated from:

$$C_{y_{\delta_R}} = - C_{L_{\alpha_V}} \left(\frac{(\alpha_\delta)_{C_L}}{(\alpha_\delta)_{C_\ell}} \right) (\alpha_\delta)_{C_\ell} K' K_b \left(\frac{S_v}{S} \right) \eta_v \qquad (11.25.1)$$

Where:

$C_{L_{\alpha_V}}$ is the vertical tail lift curve slope, computed as in Section 11.2.

Note: The effective aspect ratio of the vertical tail, $AR_{V_{EFF}}$, used in the calculation of $C_{L_{\alpha_V}}$ is obtained from Section 11.14.

$\frac{(\alpha_\delta)_{C_L}}{(\alpha_\delta)_{C_\ell}}$ is the ratio of three dimensional flap-effectiveness to two dimensional flap-effectiveness. It may be obtained from Section 11.23.

$(\alpha_\delta)_{C_\ell}$ is the theoretical value of the two-dimensional flap-effectiveness parameter and may be obtained from Section 11.21.

K' is a correction factor for high control-surface angles, obtained from Section 11.21.

K_b is a correction factor for control-surface-span, obtained from Section 11.21.

11.25.2.2 $C_{\ell_{\delta_R}}$ variation of the rolling moment coefficient with rudder deflection.

This derivative may be computed as:

$$C_{\ell_{\delta_R}} = C_{y_{\delta_R}} \left(\frac{Z_V \cos\alpha - \ell_V \sin\alpha}{b} \right) \qquad (11.25.2)$$

Where:

$C_{y_{\delta_R}}$ follows from section 11.25.2.1

Z_V and ℓ_V are defined in Figure 11.16.1

11.25.2.3 $C_{n_{\delta_R}}$ variation of yawing moment coefficient with rudder deflection.

This derivative may be computed as follows:

$$C_{n_{\delta_R}} = - C_{y_{\delta_R}} \left(\frac{\ell_V \cos\alpha + Z_V \sin\alpha}{b} \right) \qquad (11.25.3)$$

Where:

$C_{y_{\delta_R}}$ follows from section 11.25.2.1

Z_V and ℓ_V are defined in Figure 11.16.1.

11.25.3 REFERENCES

11.25.1 Hoak, D.E. & Ellison, D.E. USAF Stability and Control Datcom: Flight Control Division; Air Force Flight Dynamics Laboratory, Wright Patterson Air Force Base, Ohio, 45433

11.26: HINGE MOMENTS OF CONTROL SURFACES C_{h_α} , C_{h_δ}

11.26.1: INTRODUCTION

This chapter describes the procedure involved in computing the hinge moment derivatives C_{h_α} and C_{h_δ}, where the methods are primarily those of Reference 11.26.1. The data used for the computation of the section hinge moment derivatives are based on the NACA 0009 airfoil. This is a type of airfoil that is used quite often for the horizontal tailplane on general aviation aircraft. The method allows for differences in lifting-surface geometry, control-surface geometry and method of balancing. First the equations for the variation of hinge moment with angle of attack will be derived, followed by the equations for the variation of hinge moment with control surface deflection.

11.26.2.1 DERIVATION OF EQUATIONS FOR C_{h_α}

First the section characteristics for sealed-gap controls will be derived, where a correction will be made to account for open-gap controls. The hinge moment derivative C_{h_α} is based on the control chord squared$(c_F)^2$(see Fig. 11.26.1).

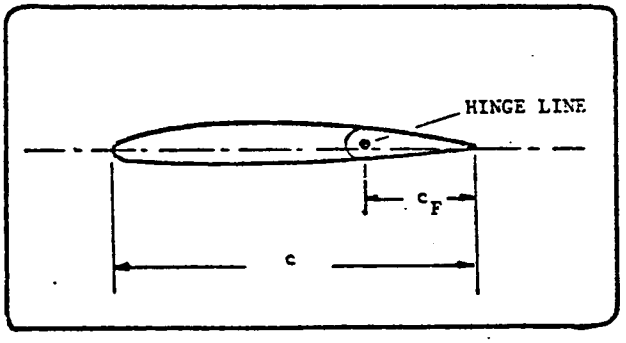

Figure 11.26.1: Geometry of Aileron

The first step requires the computation of the hinge moment derivative C'_{h_α} for a radius-nose, sealed control surface:

$$C'_{h_\alpha} = \left(\frac{C'_{h_\alpha}}{(C_{h_\alpha})_{theory}} \right) (C_{h_\alpha})_{theory} \quad (rad^{-1}) \qquad (11.26.1)$$

Where:

$\frac{C'_{h_\alpha}}{(C_{h_\alpha})_{theory}}$ is the ratio of actual to theoretical hinge moment derivative, obtained from Figure 11.26.2. The parameter $C_{\ell_\alpha} / (C_{\ell_\alpha})_{theory}$ follows from Eqn. 11.23.4

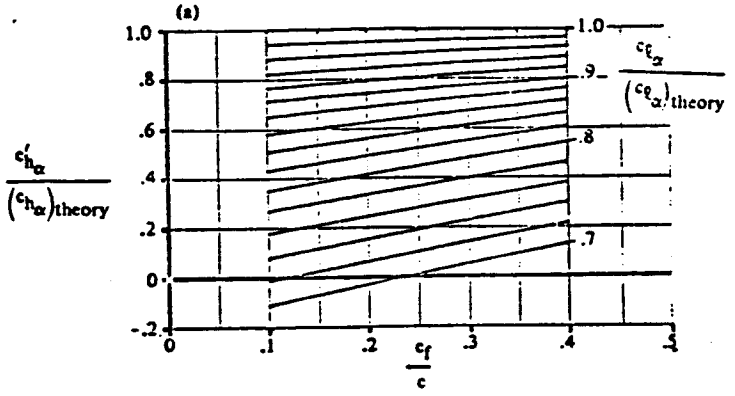

Figure 11.26.2: Rate of Change of Section Hinge Moment C'_{h_α} with Angle of Attack

$(C_{h_\alpha})_{theory}$ is the theoretical hinge moment derivative, and follows from Figure 11.26.3.

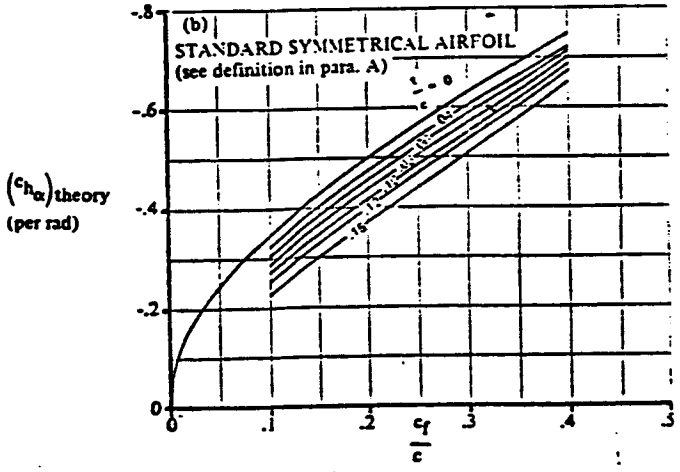

Figure 11.26.3: Theoretical Hinge Moment Derivative

If the trailing edge of the airfoil does not conform to the following condition:

$$\text{TAN}\ \frac{\phi'_{TE}}{2} = \text{TAN}\ \frac{\phi''_{TE}}{2} = \text{TAN}\ \frac{\phi_{TE}}{2} = \frac{t}{c} \qquad (11.26.2)$$

Where: ϕ'_{TE} is the angle between straight lines through 90 and 99 percent of the chord on upper and lower surface

ϕ''_{TE} is the angle between straight lines through 95 and 99 percent of the chord on upper and lower surface*

ϕ_{TE} is the trailing edge angle between tangents to upper and lower surfaces at the trailing edge,

then the following correction has to be applied to equation (11.26.1):

$$C''_{h_\alpha} = C'_{h_\alpha} + 2(C_{\ell_\alpha})_{theory}\left(1 - \frac{C_{\ell_\alpha}}{(C_{\ell_\alpha})_{theory}}\right)\left(\text{TAN}\ \frac{\phi''_{TE}}{2} - \frac{t}{c}\right)\left(\text{rad}^{-1}\right) \qquad (11.26.3)$$

To account for the effect of balancing, the following correction is applied:

$$(C_{h_\alpha})_{balance} = C''_{h_\alpha}\left(\frac{(C_{h_\alpha})_{balance}}{C''_{h_\alpha}}\right)\left(\text{rad}^{-1}\right) \qquad (11.26.4)$$

Where:

C''_{h_α} is obtained from Eqn. (11.26.3), or is equal to C'_{h_α} in Eqn. (11.26.1).

$\frac{(C_{h_\alpha})_{balance}}{C''_{h_\alpha}}$ is obtained from Figure 11.26.4.

The definition of the control surface dimensions is given in Figure 11.26.5 while Figure 11.26.6 shows the various nose-shapes.

*Note: For a beveled trailing edge ϕ''_{TE} is equal to the angle of bevel.

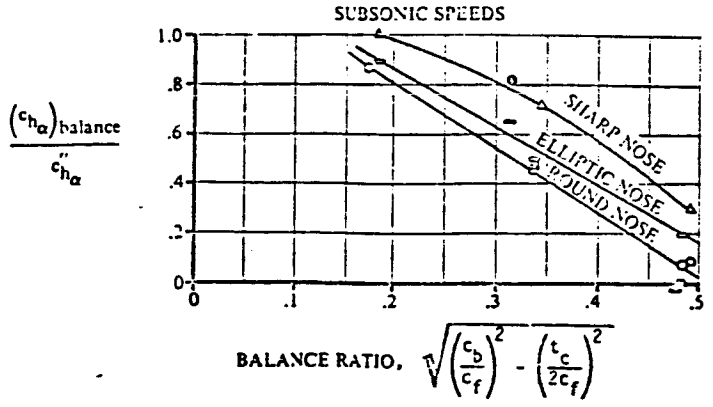

Figure 11.26.4: Effect of Nose Balance on Section Hinge Moment Derivatives

The effect of Mach number may be roughly approximated using the Prandtl-Glauert correction:

$$C_{h_\alpha}\Big|_M = \frac{C_{h_\alpha}\Big|_{\text{Low Speed}}}{\sqrt{1 - M^2}} \qquad (11.26.5)$$

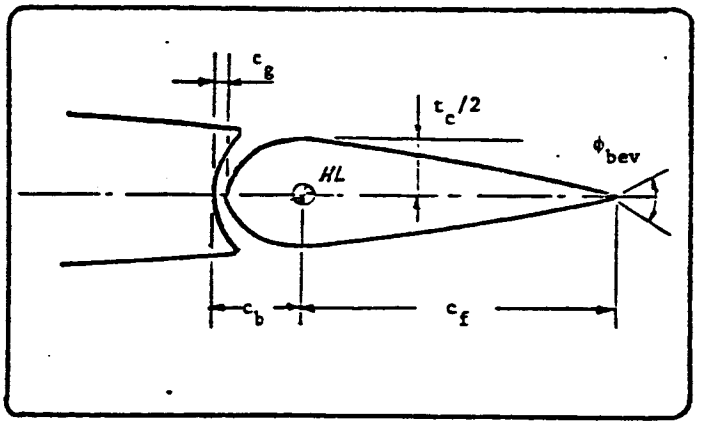

Figure 11.26.5: Geometry of Control Surface

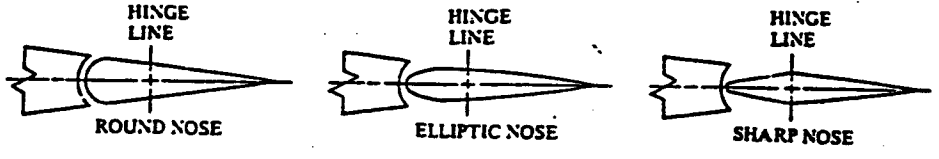

Figure 11.26.6: Various Types of Nose Shapes

*

Using the two dimensional hinge moment computed above, the three dimensional hinge moment coefficient is:

$$C_{h_\alpha} = \frac{AR \cos \Lambda_{c/4}}{AR + 2 \cos \Lambda_{c/4}} (C_{h_\alpha}) + \Delta C_{h_\alpha} \qquad (11.26.6)$$

Where:

C_{h_α} is computed with Eqn. (11.26.5)

ΔC_{h_α} is a correction for induced camber effects, arrived at by using lifting-surface theory. It may be obtained from Figure 11.26.7.

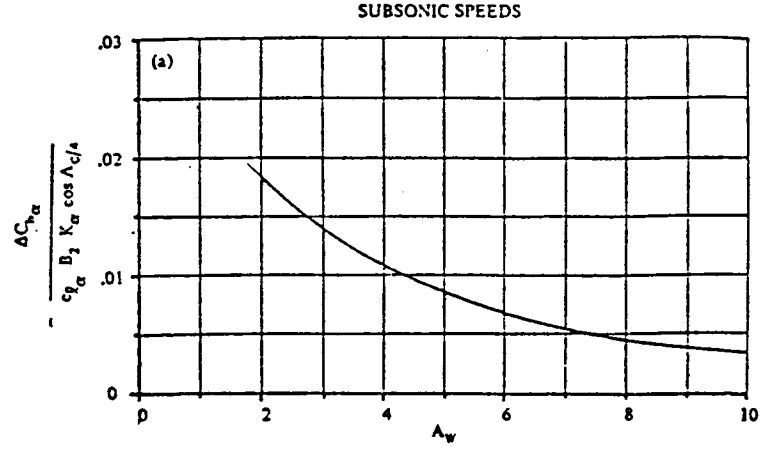

Figure 11.26.7: Correction for Induced Camber

The variables in the y-axis quantity are:

C_{l_α} is section lift curve slope

K_α takes control surface span into account, for outboard controls (see Fig. 11.26.8) if inboard controls are used, then K may be approximated to be equal to $Y_o/(b/2)$, where Y_o and Y_i are defined in Figure 11.26.9.

*The effect of open gap and bevel angle on section characteristics will be determined later.

B_2 accounts for the effect of control surface to balance chord ratios, to be obtained from Figure 11.26.10.

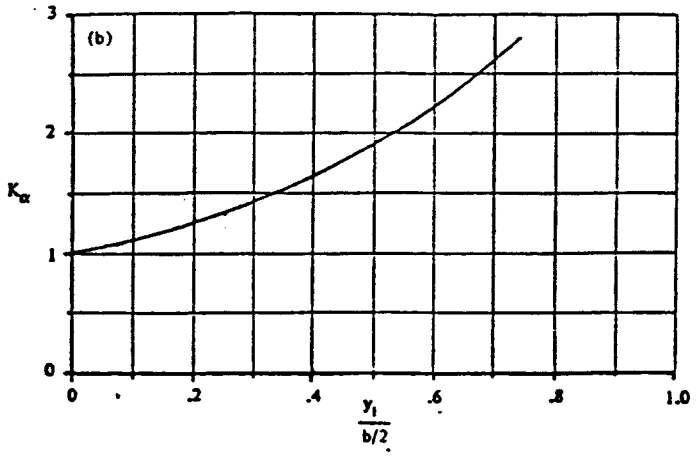

Figure 11.26.8: Effect of Control Surface Span

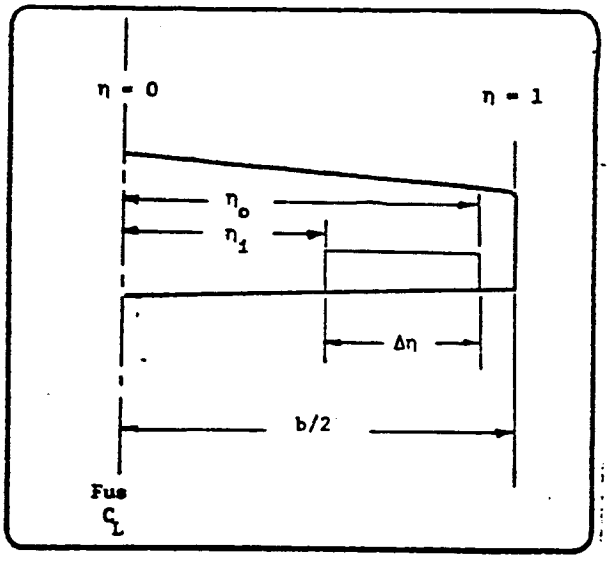

Figure 11.26.9: Control Surface Span Parameters

The primed values in Figure 11.26.10 refer to measurements normal to the wing quarter chord line, and if not explicitly given, they may be approximated by:

$$c_f'/c' = (c_f'' + c_f''')/(c'' - c''' + c_f'' + c_f''') \qquad (11.26.7)$$

and

$$c_b'/c_f' = c_b'/(c_f'' + c_f''') \qquad (11.26.8)$$

Where:

$$c_f'' = c_f \cos \Lambda_{1/4\bar{c}} \tag{11.26.9}$$

$$c_f''' = c_f \sin \Lambda_{1/4\bar{c}} \tan \Lambda_{1/4\bar{c}} \tag{11.26.10}$$

$$c'' = (\bar{c} - c_f) \cos \Lambda_{1/4\bar{c}} \tag{11.26.11}$$

$$c''' = (\bar{c} - c_f) \sin \Lambda_{1/4\bar{c}} \cdot \sin(\Lambda_{LE} - \Lambda_{1/4\bar{c}}) \tag{11.26.12}$$

$$c_b' = c_b \cos \Lambda_{1/4\bar{c}} + c_b \sin \Lambda_{1/4\bar{c}} \tan(\Lambda_{1/4\bar{c}} - \Lambda_{HL}) \tag{11.26.13}$$

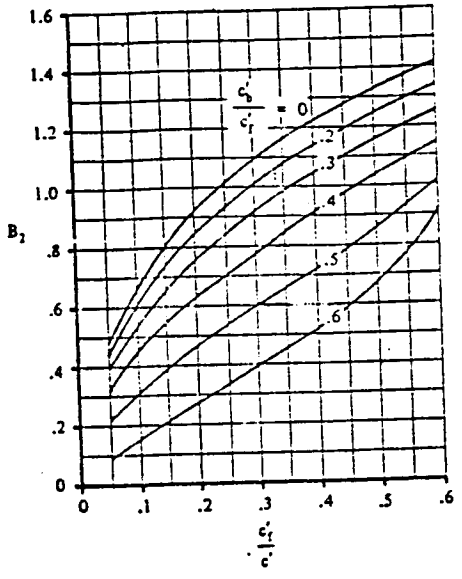

Figure 11.26.10: Correction for Chord Ratio

Corrections for open gap, horn balance and bevel angle may now be made. Reference 11.26.2, Figure 6-8, provides data for the estimation of the effect of open gap. The figure is reproduced as Figure 11.26.11. The definition of the gap may be found in Figure 11.26.5.

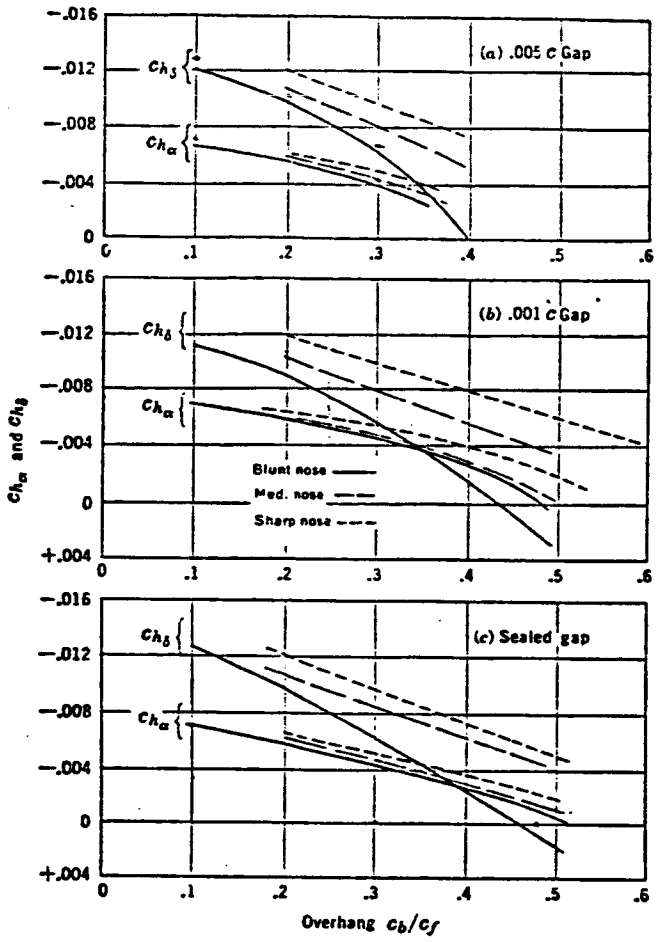

Figure 11.26.11: Effect of Open Gap on Section Hinge Moment Coefficient for a .35c Flap

Figure 11.26.11 shows on the average a (positive) increase in C_{h_α} of .0005 for a .005$\bar{c}$ gap. A simple approximation of the effect of open gap, therefore, is:

$$\Delta C_{h_{\alpha_{gap}}} = +.1 \frac{c_{gap}}{c} \quad (deg^{-1}) \qquad (11.26.14)$$

Reference 11.26.3 provides data for the estimation of the effect of bevel angle. Figure 11.26.12 is a reproduction of Fig. 12:14 of this reference.

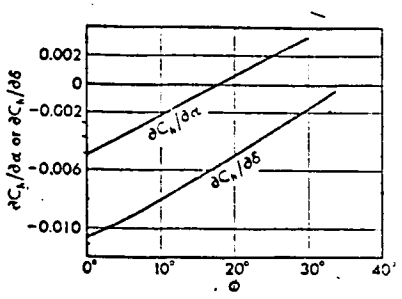

Figure 11.26.12: Effect of bevel Angle on Hinge Moment Coefficient for a .2$\bar{c}$ Flap

The effect of bevel angle may thus be approximated as:

$$\Delta C_{h_\alpha} = .00032\,\phi_{bev} \quad (deg^{-1}) \qquad (11.26.15)$$

Where: ϕ_{bev} in degrees

Both the effect of bevel angle and of open gap have to be corrected for flap-airfoil chord ratio. This can be done by referring to Fig. 11.26.13, which is a reproduction of Figure 12:7 of reference 11.26.3.

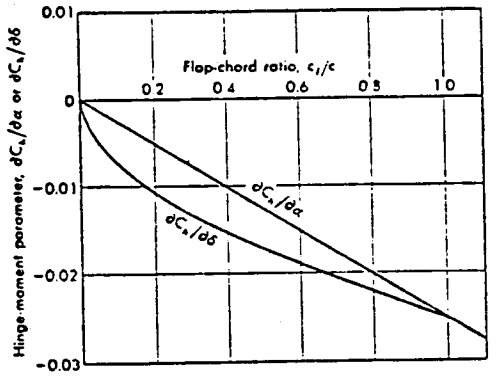

Figure 11.26.13: Correction for Flap-Chord Ratio

The correction for open gap (Eqn. 11.26.14) now becomes:

$$\Delta C_{h_{\alpha_{gap}}} = .1\,\frac{c_{gap}}{c}\left(1. - .025(c_f/c - .35)\right) \quad (deg^{-1}) \qquad (11.26.16)$$

The correction for bevel angle on section hinge moment coefficient now becomes:

$$\Delta C_{h_{\alpha_{bev}}} = .00032 \; \phi_{BEV} \; (1. - .025(c_f/c - .2)) \; (deg^{-1}) \qquad (11.26.17)$$

The corrected three dimensional hinge moment coefficient is based on twice the area moment.

11.26.2.2 Derivation of Equation for C_{H_δ}

The equation for the section characteristics will be derived first, followed by corrections for three dimensional effects. The hinge moment coefficient C_{h_δ} is based on the control chord squared c^2_f. (See Figure 11.26.1). The method is based on closed gap controls where a correction will later be made for open gap.

For a radius-nose, sealed, plain trailing edge control for which the thickness correction as defined on page 11.26.3 is valid, the hinge moment derivative follows from:

$$c'_{h_\delta} = \left(\frac{c'_{h_\delta}}{(c_{h_\delta})_{theory}} \right) (c_{h_\delta})_{theory} \quad (rad^{-1}) \qquad (11.26.18)$$

where:

$\frac{c'_{h_\delta}}{(c_{h_\delta})_{theory}}$ is the ratio of actual to theoretical hinge moment obtained from Figure 11.26.14.

$(c_{h_\delta})_{theory}$ is the theoretical hinge moment derivative, obtained from Figure 11.26.15.

Note: The parameter $c_{\ell_\alpha}/(c_{\ell_\alpha})_{theory}$ in Figure 11.26.14 may be obtained from section 11.23.

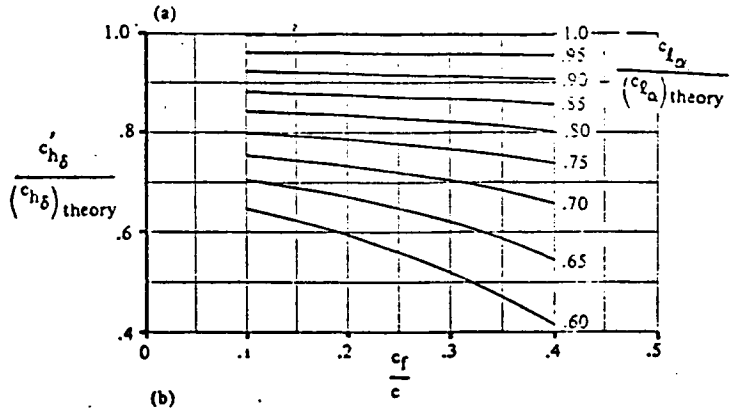

Figure 11.26.14: Ratio of Actual to Theoretical Hinge Moment

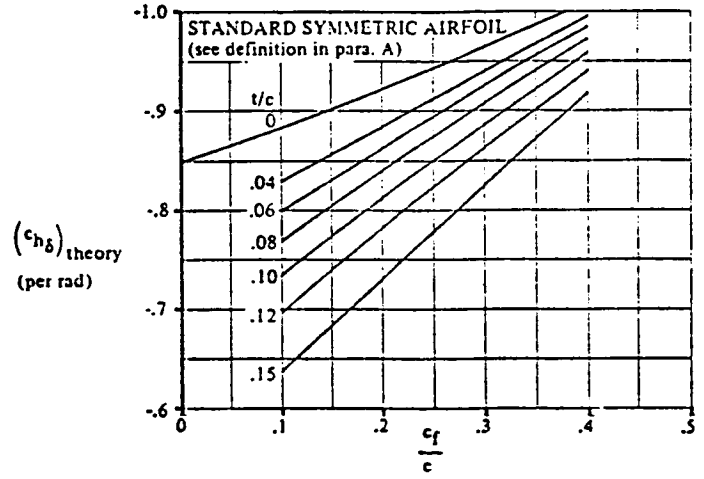

Figure 11.26.15: Theoretical Hinge Moment Derivative

If the thickness condition as defined on page 11.263is not met, then the following correction should be applied.

$$c''_{h_\delta} = c'_{h_\delta} + 2\,(c_{\ell_\delta})_{theory}\left(1 - \frac{c_{\ell_\delta}}{(c_{\ell_\delta})_{theory}}\right)\left(\text{TAN}\,\frac{\phi''_{TE}}{2} - \frac{t}{c}\right)(\text{rad}^{-1}) \qquad (11.26.19)$$

where: c'_{h_δ} is obtained from equation (11.26.18)

$(c_{\ell_\delta})_{theory}$ is the theoretical lift due to flap deflection, obtained from Fig. 11.23.4.

$\frac{c_{\ell_\delta}}{(c_\ell)_{\delta theory}}$ is the ratio of the actual to the theoretical lift due to flap deflection, obtained from Figure 11.23.5.

ϕ''_{TE} is as defined in section 11.26.2.1, for a beveled trailing edge: $\phi''_{TE} = \phi_{BEV}$.

A correction for nose shape can be made as follows:

$$(c_{h_\delta})_{\delta\ balance} = c''_{h_\delta} \left(\frac{(c_{h_\delta})_{\delta\ balance}}{c''_{h_\delta}} \right) \ (rad^{-1}) \qquad (11.26.20)$$

where:

c''_{h_δ} is obtained from eqn. (11.26.19) or assumed equal to c'_{h_δ}.

$\frac{(c_{h_\delta})_{\delta\ balance}}{c''_{h_\delta}}$ is obtained from Figure 11.26.16 for various nose shapes as defined in Figure 11.26.6.

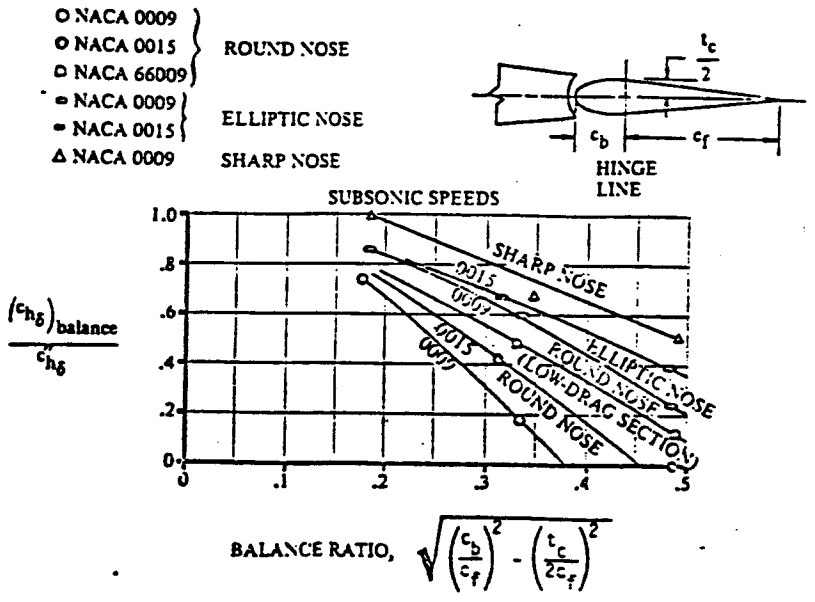

Figure 11.26.16: Effect of Nose Balance on Section Hinge Moment Derivative

The effect of Mach number may be accounted for as follows:

$$(c_{h_\delta})_M = \frac{(c_{h_\delta})_{low\ speed}}{\sqrt{1 - M^2}} \qquad (11.26.21)$$

Now corrections will be made for open gap, horn balance and bevel angle.

From Figure 11.26.11 follows the following correction for open gap:

$$\Delta \left(c_{h_{\delta}}\right)_{gap} = .2 \frac{c_{gap}}{c} \qquad (11.26.22)$$

This has to be corrected for flap-wing chord ratio according to Figure 11.26.13 to provide:

$$\Delta \left(c_{h_{\delta}}\right)_{gap} = .2 \frac{c_{gap}}{c} \left[1+1.25 \left(c_{f/c} - .3\right)\right] (deg^{-1}) \qquad (11.26.23)$$

In the same way a correction factor for the effect of bevel angle is found to be:

$$\Delta \left(C_{h_{\delta}}\right)_{BEV} = .0027\phi_{BEV} \left[1 + 1.25(C_{f}/c - .3)\right] (deg^{-1}) \qquad (11.26.24)$$

The two-dimensional hinge moment coefficient as obtained above may now be corrected for three-dimensional effects. The hinge moment derivative, based on twice the area moment, may be obtained from:

$$C_{h_{\delta}} = \cos\Lambda_{c/4} \cos\Lambda_{HL} \left[C_{h_{\alpha}} + \alpha_{\delta} \frac{2 \cos\Lambda_{c/4}}{AR + 2 \cos\Lambda_{c/4}}\right] + C_{h_{\delta}} \qquad (11.26.25)$$

Where:

$C_{h_{\alpha}}$ is the hinge-moment derivative due to angle of attack, obtained from section 11.26.2.1.

$C_{h_{\delta}}$ is the section hinge moment derivative due to control deflection, obtained from section 11.26.2.1.

α_{δ} is the two dimensional lift effectiveness parameter obtained from section 11.23.

ΔC_{h_δ} is an approximate lifting surface correction which accounts for induced camber. It may be obtained from Figure 11.26.17, where:

B_2 accounts for control surface and balance surface chord ratios, and may be obtained from Figure 11.26.10.

K_δ accounts for control surface span effect for outboard controls per Figure 11.26.18. For inboard controls K_δ can be approximated by using Y_o instead of Y_i.

Note: The values that are primed in Figure 11.26.10 refer to measurements normal to the quarter chord. See Equations 11.26.7 through 11.26.13.

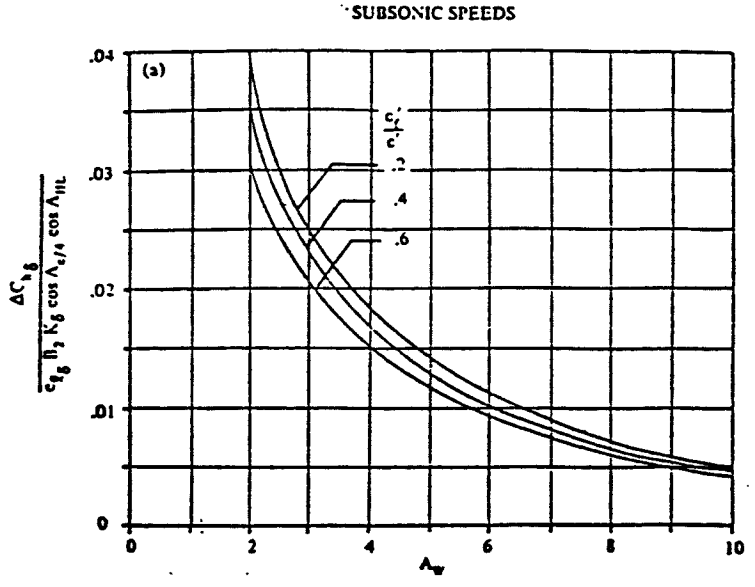

Figure 11.26.17: Lifting Surface Correction for Hinge Moment Derivative

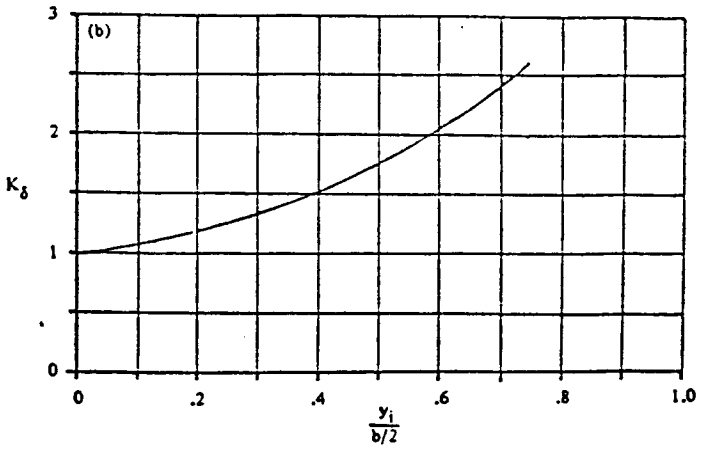

Figure 11.26.18: Correction Factor for Control Surface Span

A last correction that may be applied to the three dimensional values is a correction for the effect of a horn balance. It should be noted that the effect is difficult to estimate. Reference 11.26.3 provides a rough estimation of the effect for the unshielded horn shown in Figure 11.26.19.

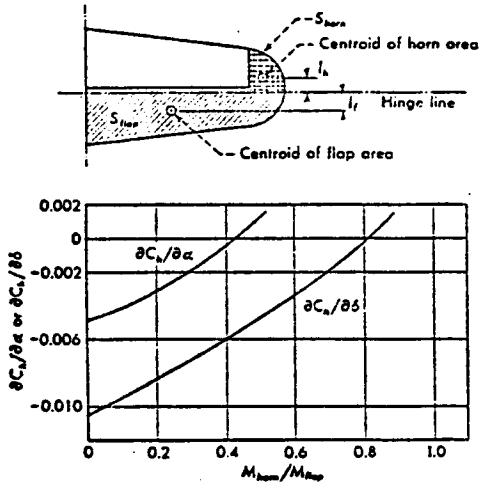

Figure 11.26.19: Effect of Horn Balance

The effectiveness of the horn is determined by the ratio of the moment of the horn area forward of the hinge line to the moment of the flap area aft of the hinge line, where the moment is defined as the area of the flap or horn multiplied by the distance of the respective area centroid from the hinge line. Figure 11.26.19 is for a 0.20 c plain flap on a NACA 0009 airfoil. To correct for different flap-wing chord ratios use can be made of Figure 11.26.13. The effect of horn balance on hinge moment coefficients can be expressed as:

$$\Delta C_{h_\alpha} = (.013125 \frac{M_h}{M_f} (1 - .0025 (\frac{C_f}{c} - .2))) \frac{b_s}{S_{cs}} \qquad (11.26.26)$$

$$\Delta C_{h_\delta} = (.0125 \frac{M_h}{M_f} (1 - .0175(\frac{C_f}{c} - .2))) \frac{b_s}{S_{cs}} \qquad (11.26.27)$$

This concludes the derivation of the equation for the hinge-moment derivatives C_{h_α} and C_{h_δ}.

11.26.3 REFERENCES

11.26.1 Hoak, D.E. & Ellison, D.E. — USAF Stability and Control Datcom: Flight Control Division Air Force Flight Dynamics Laboratory, Wright Patterson Air Force Base, Ohio, 45433.

11.26.2 Perkins, C.D. & Hage, E.H. — Airplane Performance, Stability and Control. New York John Wiley & Sons, 1949.

11.26.3 Dommasch, D.O. Sherby, S.S. Connolly, T.F. — Airplane Aerodynamics, Pitman Publishing Corp. New York, 1967.

11.27 C_{L_o}, C_{m_o} LIFT AND PITCHING MOMENT COEFFICIENTS AT $\alpha = i_H = \delta_E = 0$

11.27.1 INTRODUCTION

The original version of the Stability and Control computer program required C_{L_o} and C_{m_o} to be manually calculated and then included as inputs to the program. Since this was thought to detract from the utility and versatility of the program, the present version of the computer program relies on inputs for $\alpha_{oL_{WB}}$ and the two-dimensional airfoil zero-lift pitching coefficient c_{m_o} as additional inputs to compute C_{L_o} and C_{m_o}. Soubroutine CLOCMO is added to the present computer program to compute C_{L_o} and C_{m_o}.

11.27.2 C_{L_o}

The life coefficient of the total airplane may be represented as: (Reference 11.27.1)

$$C_L = C_{L_o} + C_{L_\alpha}\alpha + C_{L_{i_H}} i_H + C_{L_{\delta_E}} \delta_E \qquad (11.27.1)$$

where C_{L_o} = total airplane lift coefficient when $\alpha = i_H = \delta_E = 0$

C_{L_α} = total airplane lift-curve slope

$C_{L_{i_H}}$ = incremental lift per unit deflection of an all-moving stabilator

$C_{L_{\delta_E}}$ = incremental lift per unit deflection of a stabilizer-elevator arrangement.

C_{L_o} may be computed as

$$C_{L_o} = C_{L_{o_{WB}}} + C_{L_{o_H}} \tag{11.27.2}$$

where $$C_{L_{o_{WB}}} = -C_{L_{\alpha_{WB}}} \alpha_{oL_{WB}} \tag{11.27.3}$$

$$C_{L_{o_H}} = -C_{L_{\alpha_H}} (\varepsilon_o + \alpha_{oL_H}) \frac{S_H}{S} \frac{\bar{q}_H}{\bar{q}_\infty} \tag{11.27.4}$$

Equation 11.27.3 requires an input for $\alpha_{oL_{WB}}$, the zero-lift angle-of-attack for the wing-body combination. $C_{L_{\alpha_{WB}}}$, the wing-body lift-curve slope, is obtained from Subroutine LIFCRV permethods discussed previously.

Equation 11.27.4 requires the computation of ε_o, the downwash at $\alpha = 0$, as

$$\varepsilon_o = -\alpha_{oL_{WB}} \frac{\partial \varepsilon}{\partial \alpha} \tag{11.27.5}$$

Here, α_{oL_H} is an input defined as the zero-lift angle-of-attack for the horizontal tail where the tail is isolated from the downwash of the wing-body. $C_{L_{\alpha_H}}$, the horizontal tail lift-curve slope, is obtained from subroutine LIFCRV per methods discussed previously. It is referenced to S, the reference (wing) area, by the term $\frac{S_H}{S}$ where S_H is the horizontal tail planform area.

11.27.3 C_{m_o}

The steady state pitching moment coefficient for the total airplane may be represented as (Reference 11.27.1):

$$C_m = C_{m_o} + C_{m_\alpha} \alpha + C_{m_{i_H}} i_H + C_{m_{\delta_E}} \delta_E \tag{11.27.6}$$

where C_{m_o} = total airplane pitching moment coefficient when

$\alpha = i_H = \delta_E = 0$

C_{m_α} = change in pitching moment coefficient per unit change in angle of attack

$C_{m_{i_H}}$ = longitudinal control derivative for stabilator deflections

$C_{m_{\delta_E}}$ = longitudinal control derivative for stabilizer-elevator configurations.

C_{m_o} may be computed as

$$C_{m_o} = C_{m_{ac_{WB}}} + C_{L_{o_{WB}}} (\bar{X}_{cg} - \bar{X}_{ac_{WB}}) + C_{L_{\alpha_H}} \frac{\bar{q}_H}{\bar{q}_\infty} \frac{S_H}{S} (\bar{X}_{ac_H} - \bar{X}_{cg}) \varepsilon_o \qquad (11.27.7)$$

where $C_{m_{ac_{WB}}}$ is defined as the wing-body pitching moment coefficient about the wing-body aerodynamic center.

$$C_{m_{ac_{WB}}} = C_{m_{ac_W}} - C_{L_{\alpha_W}} \alpha_{oL_W} \Delta X_{ac_{WB}} \qquad (11.27.8)$$

where the first term on the right side of Equation 11.27.8 is the 3-dimensional pitching moment coefficient of the wing based on an input 2-dimensional C_{m_o}, and corrected for Mach and twist. Reference 11.27.2 describes this development as

$$C_{m_{ac_W}} = \frac{A \cos^2 \Lambda_{c/4}}{A + 2\cos \Lambda_{c/4}} C_{m_o} + \frac{\Delta C_{m_o}}{\theta} \theta \qquad (11.27.9)$$

$M = 0$

where A = planform aspect ratio

$\Lambda_{c/4}$ = sweep of the quarter chord line

C_{m_o} = 2 dimensional pitching moment coefficient

$\frac{\Delta C_{m_o}}{\theta}$ = twist correction per degree

θ = twist in degrees

While Reference 11.27.2 presents graphical data for the twist correction, curve fitting techniques were used to provide the following:

$$\left(\frac{\Delta C_{m_o}}{\theta}\right)_{\lambda = 0} = -.85642 \times 10^{-5} A - .17452 \times 10^{-5} A^2 + .315 \times 10^{-7} A^3 \qquad (11.27.10)$$

$$\left(\frac{\Delta C_{m_o}}{\theta}\right)_{\lambda = .5} = -.90826 \times 10^{-5} A - .28234 \times 10^{-5} A^2 - .68 \times 10^{-8} A^3 \qquad (11.27.11)$$

$$\left(\frac{\Delta C_{m_o}}{\theta}\right)_{\lambda = 1} = -.4986 \times 10^{-5} A - .50556 \times 10^{-5} A^2 + .1554 \times 10^{-6} A^3 \qquad (11.27.12)$$

where λ = planform taper ratio

A = planform aspect ratio

$\frac{\Delta C_{m_o}}{\theta}$ is obtained directly for specific values of λ by interpolating between the values from Equations 11.27.10, 11.27.11, and 11.27.12 as appropriate.

$C_{m_{ac_W}}$ from Equation 11.27.9 is finally corrected for Mach effects using the following relationship which is also developed through curve fitting methods applied to graphical data of Reference 11.27.2:

$$\frac{C_{m_{o_M}}}{C_{m_{o_{M=0}}}} = 1. \text{ for } M \leq .2$$

$$= 1. + .072857143\ (M - .2) + .22(M - .2)^2 + .828571431(M - .2)^3 \quad (11.27.13)$$

for $M > .2$

$$C_{m_{ac_W}}{}_{M>0} = C_{m_{ac_W}}{}_{M=0} \cdot \frac{C_{m_{o_M}}}{C_{m_{o_{M=0}}}} \quad (11.27.14)$$

The remaining terms of Equation 11.27.8 are defined as

$C_{L_{\alpha_W}}$ = wing C_{L_α}, computed per methods discussed earlier (Subroutine LIFCRV).

α_{OL_W} = zero-lift angle-of-attack of the wing, an already-existing input

ΔX_{ac} = fuselage-induced aerodynamic center shift, computed per methods discussed earlier (Subroutine MULTOP).

The remaining terms of Equation 11.27.7 are defined as follows:

$\bar{X}_{cg}$ = the airplane center-of-gravity location measured from the leading edge of the wing mean aerodynamic chord and expressed as a fraction of this chord, positive aft.

$\bar{X}_{ac_{WB}}$ = the wing-body aerodynamic center location measured from the leading edge of the wing mean aerodynamic chord and expressed as a fraction of this chord, positive aft.

$\bar{X}_{ac_H}$ = the horizontal tail aerodynamic center location measured from the leading edge of the wing mean aerodynamic chord and expressed as a fraction of this chord, positive aft.

11.27.4 REFERENCES

11.27.1 Roskam, J. Airplane Flight Dynamics and Automatic Flight Controls, Part I. Roskam Aviation and Engineering Corporation, Lawrence, Ks., 1979.

11.27.2 Hoak, D.E. & Finck, R.D. USAF Stability and Control DATCOM. Flight Control Division, Air Force Flight Dynamics Laboratory, Wright-Patterson Air Force Base, Ohio.

CHAPTER 12

DYNAMIC STABILITY ROUTINE

The Dynamic Longitudinal and Lateral-Directional Stability program that is incorporated in the Stability program described in this report is a modified version of a program developed at the University of Kansas. A full description is presented in Reference 12.1. The program has been tested extensively and produces excellent results.

The major modification consisted of changing the input instructions for this program in such a way that they are performed automatically. The input data for this program consist of the stability derivatives for a particular flight conditon. The stability derivatives are computed in the program described in this report and then transferred automatically to the Dynamic Stability and Control program that computes the Dynamic Stability Characteristics.

Briefly the program computes the following:

I. DYNAMIC STABILITY

- A. Computes dimensional derivatives if non-dimensional derivatives are inputted
- B. Computes coefficients of the characteristic equations
- C. Computes the roots of the characteristic equations
- D. Prints the characteristic equations in factored form and states the root configurations
- E. Longitudinal case computes:
  1. ($\omega_{n_{SP}}$) Short period undamped natural frequency
  2. (ω_{np}) Phugoid undamped natural frequency
  3. (ζ_{SP}) Short period damping ratio
  4. (ζ_{p}) Phugoid damping ratio

5. ($T_{1/2P}$ or T_{2P}) Time to half or double the amplitude of the phugoid mode

6. Short period characteristics

   a. (n/α) Load factor / angle of attack

   b. ($\omega_n^2 / n/\alpha$) Short period undamped natural frequency squared / load factor / angle of attack

F. Lateral directional case computes:

1. (ω_{n_D}) Dutch roll undamped natural frequency
2. (ζ_D) Dutch roll damping ratio
3. (T_S) Spiral time constant
4. (T_R) Roll time constant
5. (T_{2_S}) Time to double the amplitude in the spiral mode
6. ($\zeta_D \omega_{n_D}$) Dutch roll damping ratio x Dutch roll undamped natural frequency
7. ($|\phi/\beta|_D$) Oscillatory bank angle to sideslip ratio
8. ($\omega_{n_D}^2 |\phi/\beta|_D$) Dutch roll undamped natural frequency X oscillatory bank angle to sideslip ratio

G. Sensitivity analysis varies any selected input variable of array DERV and computes for each incremental value:

1. Real and imaginary parts of roots of the characteristic equations
2. Damping ratios and undamped natural frequencies
3. Inverted time constants

II. TRANSFER FUNCTIONS

A. Computes dimensional derivatives if non-dimensional derivatives are inputted

B. For longitudinal case computes:

1. Coefficients of the characteristic equation
2. Numerator coefficients of $U(S)/\delta_E(S)$, $\alpha(S)/\delta_E(S)$, and $\theta(S)/\delta_E(S)$ transfer functions
3. General standard format parameters:
   a. Gain
   b. Numerator time constants, damping ratios, and undamp ed natural frequencies
   c. Denominator damping ratios and undamped natural frequencies

C. For lateral directional case computes:

1. Coefficients of the characteristic equation
2. Numerator coefficients of:
   a. $\beta(S) / \delta_A(S)$, $\phi(S) / \delta_A(S)$, and $\psi(S) / \delta_A(S)$ transfer functions
   b. $\beta(S) / \delta_R(S)$, $\phi(S) / \delta_R(S)$, and $\psi(S) / \delta_R(S)$ transfer functions
3. General standard format parameters for both aileron and rudder forcing functions
   a. Gain
   b. Numerator time constants, damping ratios, and undamped natural frequencies
   c. Denominator damping ratio, undamped natural frequency, and time constants

III. FREQUENCY RESPONSE

A. Computes dimensional derivatives if non-dimensional derivatives are input.

B. For longitudinal case computes:

1. For $U(S) / \delta_E(S)$, $\alpha(S) / \delta_E(S)$, and $\theta(S) / \delta_E(S)$ transfer functions

   a. Magnitude (decibels) as a function of frequency

   b. Phase angle (degrees) as a function of frequency

C. For lateral directional case computes:

1. For $\beta(S) / \delta_A(S)$, $\phi(S) / \delta_A(S)$, and $\psi(S) / \delta_A(S)$ transfer functions

   a. Magnitude (decibels) as a function of frequency

   b. Phase angle (degrees) as a function of frequency

2. For $\beta(S) / \delta_R(S)$, $\phi(S) / \delta_R(S)$, and $\psi(S) / \delta_R(S)$ transfer functions

   a. Magnitude (decibels) as a function of frequency

   b. Phase angle (degrees) as a function of frequency

For a comprehensive, detailed description of this program, the reader is referred to Reference 12.1.

REFERENCE

12.1 Postai, M.: A Computer Program for Determining Open and Closed Loop Dynamic Stability Characteristics of Airplanes and Control Systems. University of Kansas, Lawrence, Kansas, May 1973.

CHAPTER 13

INPUT ROUTINE

13.1 Introduction

A new input methodology has been incorporated into the present Stability and Control computer program in an attempt to increase program versatility and reduce input errors. Essentially, the input format has been changed from one relying on formatted lines or cards of input numbers to one relying on Fortran namelist input. The features of namelist input which make it attractive include:

a. Variables within a namelist may be in any order.

b. Variables are not restricted to particular card columns.

c. Only required variables need be included in a namelist thus avoiding the use of dummy variables.

d. A variable may be included more than once within a namelist where the last value to appear is used.

Other changes which have been incorporated include:

a. The entire input function (except one plain-language identification line) and echo function has been concentrated into an added Subroutine INPUT. Prior to this change many read statements appeared in the main (executive) program as well as in several subroutines.

b. Every input variable is now echoed depending on appropriate (input) control variables. Prior to this change, some input variables could not be verified since they never appeared in the computer output.

c. Vehicle geometric specifications have been reduced to a minimum. Prior to this change, it was possible to overspecify the vehicle's configuration or to input conflicting dimensions.

d. Standard Day atmospheric data may be incorporated by specifying the altitude of interest. Non-Standard Day data is also provided for as user inputs. Prior to this change, the user was required to compute and input values for density, kinematic viscosity, and Mach number based on altitude and true airspeed.

13.2 Input Data File Structure

A detailed description of the input data file structure is included with the User's Manual. In the present version of the computer program, data are input in the following order:

a. Plain-language identification line. This line is read in the main (executive) program and, if an End-Of-File indication is sensed, terminates program execution.

b. Namelists INCTL, INATOI, and INKTOZ are all read (in order) in Subroutine INPUT. All input data are read via these 3 namelists. In order to ease transportability to different computer systems, input pointer controls are not utilized. Hence, users should include the 3 namelists in the order specified with at least one (dummy) variable included in each namelist.

An example of an input deck to include the details of paragraph b above is included in the User's Manual.

13.3 Subroutine INPUT

With the exception of the single, plain language identification line, all data are input and echoed via this subroutine. This routine is called only once and only by the main program for each set of data. Only 3 variables are initialized to zero prior to data input: NANLYS, which is used within the dynamic stability routine to signal a requirement for

a sensitivity analysis (as well as indicate the number of derivatives to be analyzed) is set to zero prior to reading data in order to preclude a conflicting signal to be sensed in the dynamic stability routine. RHO and TEMP, optional inputs which signal nonstandard atmospheric conditions, are set to zero to preclude erroneous flight conditions from being analyzed. When not input, standard day values are computed in Subroutine ATMOS based on the input ALT.

A simplified flowchart of Subroutine INPUT is presented as Figure 11.13.1.

13.4 Subroutine ATMOS

This subroutine was added to the present computer program as part of the input methodology. It is called only once and only by Subroutine INPUT.

Required inputs to this subroutine are altitude in ft (ALT) and true airspeed in ft/sec (TAS). If the density RHO is input greater than .0001 slugs/ft^3, this value is used instead of being computed.

If ALT is input greater than 65,617 ft, the value for pressure (PRESS) is returned equal to -1, and acts as an error signal.

This subroutine computes standard day characteristics for a troposphere from sea level to 36,089 ft and presumes the stratosphere to extend to 65,617 ft. Presumed sea level values are

$$T_o = 518.69°R$$

$$p_o = 2116.2 \text{ lbf/ft}^2$$

$$\rho_o = .0023769 \text{ slug/ft}^3$$

$$a_o = 1116.4 \text{ ft/sec}$$

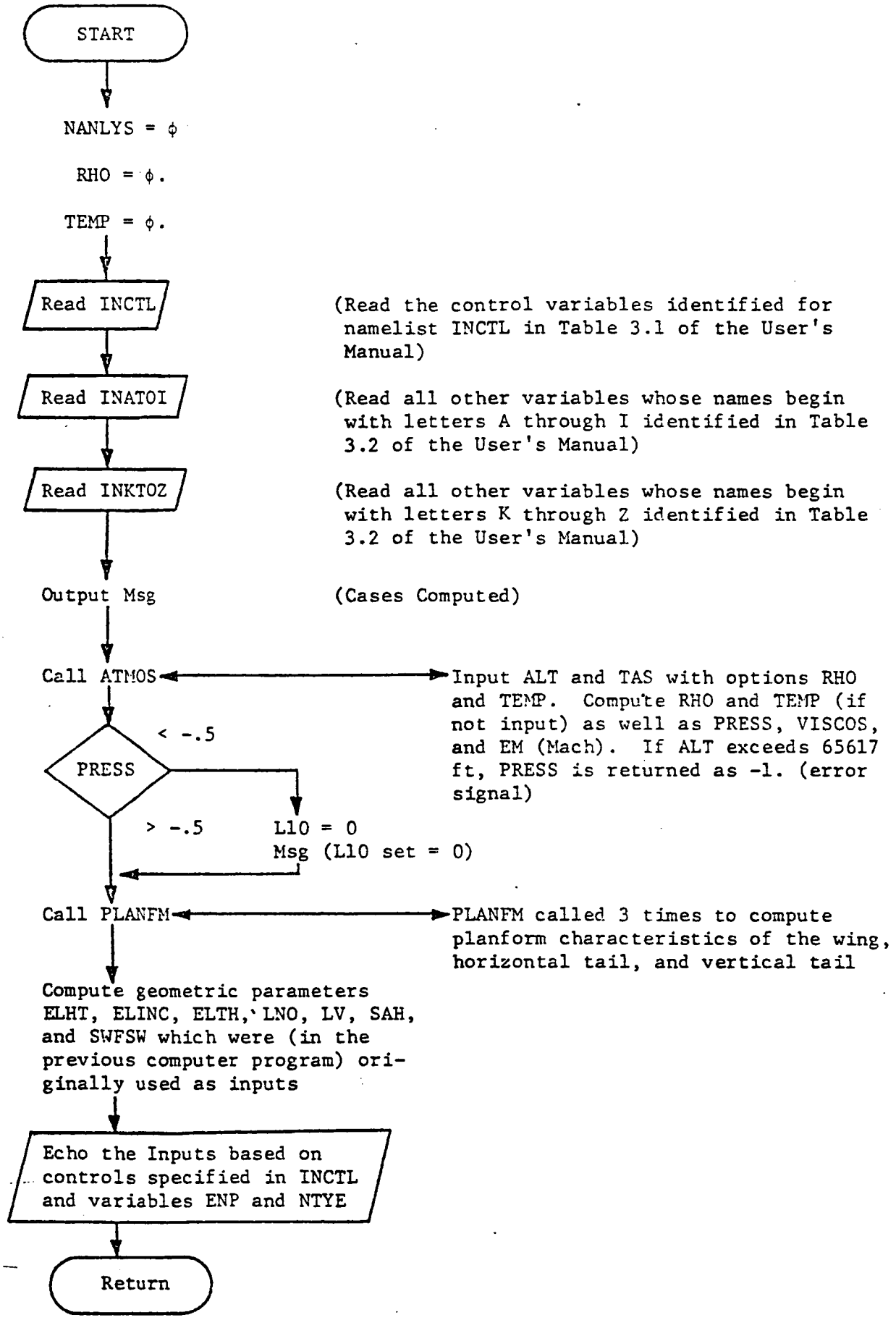

Figure 13.1 Flowchart of Subroutine INPUT

For h (ALT) $\leq$ 36,089 ft,

$$T/T_o = \theta = 1. - (6.87 \times 10^{-6})(h) \tag{13.1}$$

$$p/p_o = \delta = \theta^{5.2559} \tag{13.2}$$

$$\rho/\rho_o = \sigma = \delta/\theta = \theta^{4.2559} \tag{13.3}$$

For 36,089 ft < h $\leq$ 65,617 ft,

$$T = 390°R$$

$$T/T_o = \theta = .7518942 \tag{13.4}$$

$$p/p_o = \delta = .2234\ e^{(4.806 \times 10^{-5})(36,089 - h)} \tag{13.5}$$

$$\rho/\rho_o = \sigma = \delta/\theta \tag{13.6}$$

Once T, ρ, and p have been obtained,

$$a = a_o\sqrt{\theta} \tag{13.7}$$

$$M = V_{TAS}/a \tag{13.8}$$

13.5 Subroutine PLANFM

This subroutine was added to the present computer program as part of the input methodology. It is called three times by Subroutine INPUT to compute planform parameters for the wing, horizontal tail, and vertical tail. It is also called once by Subroutine CYBETA to compute vertical tail planform parameters locally.

Inputs to this routine include 4 independent parameters to specify the planform and one spanwise variable to indicate the position of a wing chord of interest. Figure 13.2 depicts the following input and output parameters:

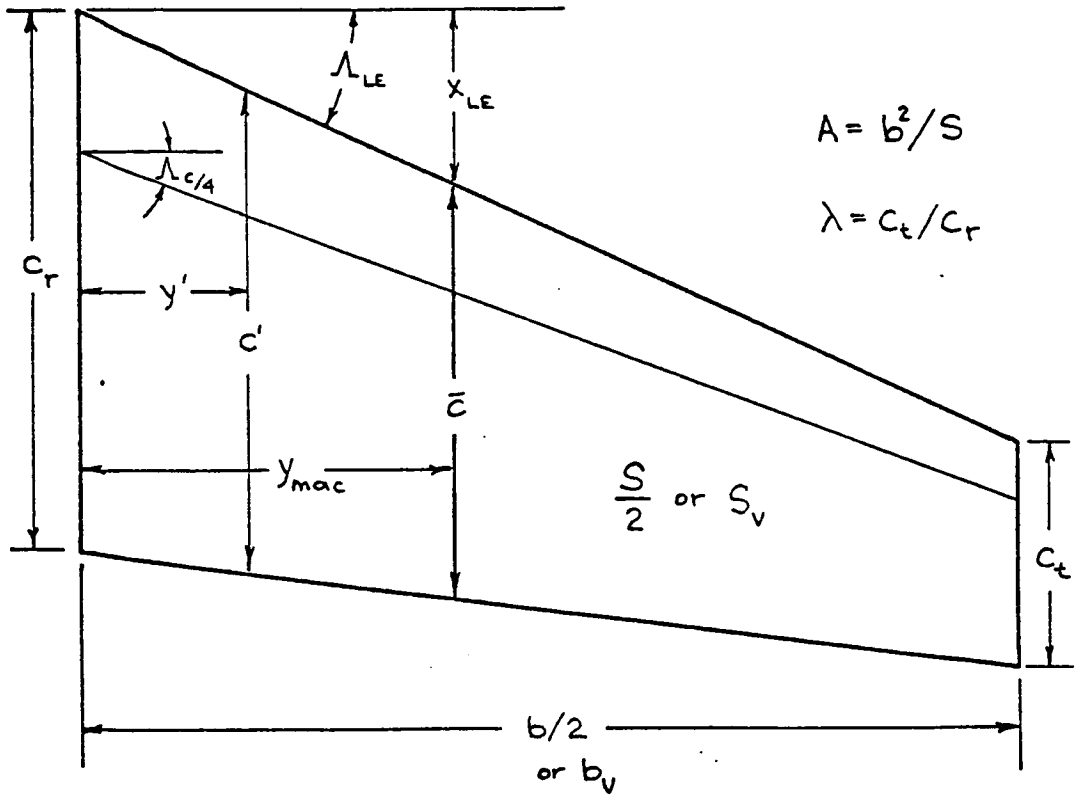

Figure 13.2 Planform Parameters

INPUT: S = total planform area in ft^2

A = aspect ratio

λ = taper ratio

$\Lambda_{c/4}$ = quarter chord sweep angle in degrees

y' = spanwise location of a chord of interest measured from the root chord in ft.

OUTPUT: C_r = root chord in ft

C_t = tip chord in ft

$\bar{c}$ = mean aerodynamic chord in ft

y_{mac} = spanwise location of $\bar{c}$ from the root chord in ft.

x_{LE} = longitudinal distance from the apex to the leading edge of $\bar{c}$ in ft

c' = chord length at a spanwise distance y' from the root chord in ft

b = span of the planform in ft

Λ_{LE} = leading edge sweep angle in radians

The relationships used to derive the output parameters are taken from Reference 13.1 with the exception of c', which is obtained by inspection.

$$\Lambda_{c/4}(\text{rad}) = \Lambda_{c/4}(\text{deg})\ \pi/180 \tag{13.9}$$

$$\Lambda_{LE}(\text{rad}) = \tan^{-1}\left[\tan \Lambda_{c/4} + \frac{1}{A}\left(\frac{1-\lambda}{1+\lambda}\right)\right] \tag{13.10}$$

$$\Lambda_{TE} = \tan^{-1}\left[\tan \Lambda_{LE} - \frac{4}{A}\left(\frac{1-\lambda}{1+\lambda}\right)\right] \tag{13.11}$$

$$b = \sqrt{(S)(A)} \tag{13.12}$$

$$C_r = \frac{2b}{A(1+\lambda)} \tag{13.13}$$

$$C_t = \lambda C_r \tag{13.14}$$

$$\bar{c} = \frac{2}{3} C_r \frac{1 + \lambda + \lambda^2}{1 + \lambda} \tag{13.15}$$

$$y_{mac} = \frac{b}{6} \left(\frac{1 + 2\lambda}{1 + \lambda}\right) \tag{13.16}$$

$$X_{LE} = y_{mac} \tan \Lambda_{LE} \tag{13.17}$$

$$c' = C_r + y'(\tan \Lambda_{TE} - \tan \Lambda_{LE}) \tag{13.18}$$

13.6 REFERENCES

13.1 Hoak, D.E. & Finck, R.D. USAF Stability and Control DATCOM. Flight Control Division, Air Force Flight Dynamics Laboratory, Wright-Patterson Air Force Base, Ohio.

CHAPTER 14

SUMMARY

A considerable amount of effort has been expended to increase the versatility and utility as well as to identify and correct computational errors in a stability and control program originally developed between May 16, 1976 and May 31, 1978 at the University of Kansas under NASA contract NSG-2145. The present effort has resulted in numerous and extensive changes to the computer program.

While most of the program, with the exception of the Inertia routine, has been changed to some extent, the most extensive changes were incorporated in the main (executive) program and those subroutines associated with power effects and static longitudinal stability derivatives. Also, the entire input methodology was changed from one dependent on formatted data cards to one based on Fortran namelist input. A detailed explanation of the new input logic is included in a new User's Manual under separate cover.

In general, it is felt that the present computer program represents a much more versatile tool than its predecessor since it should prove to be significantly easier to implement. This result is achieved by reducing the level of computational complexity required to develop necessary input data such as C_{L_o}, C_{m_o}, redundant planform parameters, and certain configuration-dependent descriptive parameters. Likewise, the characteristics of Fortran namelists eliminates the requirement to duplicate an entire input data deck for each consecutive investigation, and the more complete echo format incorporated into the new Subroutine INPUT allows the user to verify all input data for each computer run.

Furthermore, the corrected documentation reflected in this manual together with the Fortran XREF (cross referenced listing of variables) provided under separate cover should facilitate program implementation considerably. Here, considerable effort was directed toward the verification and correction of equations as they appeared in the original documentation as well as toward the realignment of computer logic to reflect the documentation. This latter task was complicated to some extent since the program listings of the original documentation represented individual (unintegrated) routines which did not reflect the significant amount of data which was transferred between routines via the many common blocks which were added when the individual routines were integrated into one program. The present computer program reflects a significant amount of time dedicated towards tracing individual common block variables throughout the entire program. Typical errors noted were tail volume coefficients computed based on erroneous tail arm lengths, common blocks of varying size in different subroutines, floating point variables changed to integer variables and vice versa, and variables appearing in different order in common blocks of the same name.

The present computer program, this documentation, a User's Manual, and Fortran XREF listing are submitted with a sincere belief that most of the errors of the original program have been detected and corrected. While it is inevitable that other errors will be detected and require correction, it is hoped that the present program represents a significant step forward in providing the general aviation community with a useful and easily implementable tool.

APPENDIX A COMPARISON OF METHODS FOR COMPUTATION OF GROUND EFFECT.

This appendix briefly describes the methods used in the comparison of ground effect calculation methods.

A.1. Corning (Ref. A.1)

A.1.1 Description of Method

Corning defines the ground effect factor as:

$$K_{C_{L_{g_E}}} = \frac{C_L - \Delta C_L}{C_{L_{oge}} - \Delta C_L} \tag{A.1}$$

where: C_L = Lift coefficient including flap and ground effect.

ΔC_L = Lift coefficient increment due to flaps.

$C_{L_{oge}}$ = Lift coefficient out of ground effect (including flap effect).

The lift coefficient in ground effect may then be calculated as:

$$C_{L_{ge}} = K_{C_{L_{ge}}} \left(C_{L_{oge}} - \Delta C_L \right) + \Delta C_L \tag{A.2}$$

According to Corning, the ground effect factor may be calculated as:

$$K_{C_{L_{ge}}} = 1.005 + \left[0.00211 - 0.0003 \, (AR - 3) \right] c_3 \tag{A.3}$$

where: $c_3 = e^{5.2(1 - H_g)}$ (A.4)

H_g = Altitude/wing span (A.5)

A.1.2 Hand Calculation

Following is a hand calculation of the Corning Method for Airplane A, see Appendix C for data.

The computations are for the following flight conditions:

C_L = .96

α = 4.9 (deg)

ΔC_{L_f} = 0.46

δ_f = 38 (deg)

The calculation of the ground effect as a function of height is given in Table A.1.

Height (ft)	H/b	$K_{C_{L_{ge}}}$	$C_{L_{ge}}$	ΔC_L (%)
30	0.787	1.009	0.965	0.5
25	0.656	1.013	0.967	0.7
20	0.525	1.020	0.970	1.0
15	0.393	1.035	0.978	1.9
10	0.262	1.065	0.993	3.4
7.5	0.197	1.089	1.005	4.7
5	0.131	1.123	1.022	6.5
2.5	0.066	1.232	1.076	12.1

Table A.1: Calculation of Ground Effect for Corning Method

A.2 PERKINS AND HAGE METHOD (Ref. A.2)

A.2.1 DESCRIPTION OF METHOD

This change in wing-lift is brought about by a change in the wing lift-curve slope. Figure A.1 shows the effect of ground proximity on wing lift curve slope. The factor k is the ratio of wing lift-curve slope in ground effect to the slope out of ground effect. Height is given by the height of the root quarter chord in semispans.

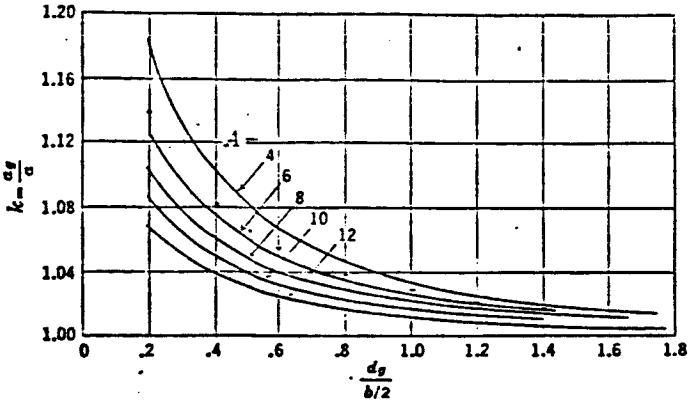

Figure A.1: Effect of Ground Proximity on Wing Lift-Curve Slope

The change in wing angle of attack due to the ground effect may be approximated as:

$$\Delta\alpha = \alpha_g - \alpha_{oge} \tag{A.6}$$

or:

$$\Delta\alpha = \alpha_{oge}\left(\frac{\alpha_g}{\alpha_{oge}} - 1\right) \tag{A.7}$$

Introducing the wing lift curve slope:

$$\Delta\alpha = \left(\frac{C_L}{C_{L_\alpha}}\right)_{oge}\left(\frac{C_{L_{\alpha\ oge}}}{C_{L_{\alpha_g}}} - 1\right) \tag{A.8}$$

or:

$$\Delta\alpha = \left(\frac{C_L}{C_{L_{\alpha\ oge}}}\right) \cdot (1/k - 1) \tag{A.9}$$

where: $k = \dfrac{C_{L_{\alpha_{oge}}}}{C_{L_{\alpha_g}}}$ is given in Figure A.1

Now that the change in angle of attack is known, the revised lift-coefficient may be found as shown in Figure A.2.

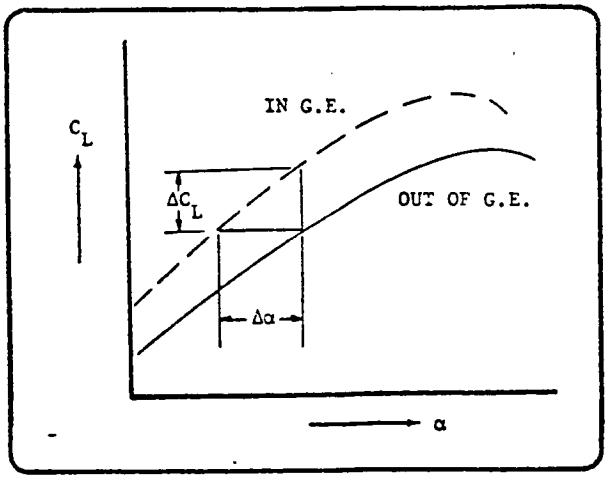

Figure A.2: Ground Effect on Lift-Curve

A.2.2 HAND CALCULATION

The following data are available for Airplane A (see appendix D)

$$C_L = 0.96 \quad (\text{At } V = 1.3\ V_S)$$

$$C_{L_{\alpha_{oge}}} = 4.870 \ \text{rad}^{-1}$$

The factor k is found from Figure A.1. The calculations are given in Table A.2.

Height (ft)	h/(b/2)	k	$\Delta\alpha$(deg)	C_L	ΔC_L (%)
30	1.57	1.014	-0.16	0.974	1.4
25	1.31	1.021	-0.23	0.980	2.0
20	1.05	1.029	-0.32	0.987	2.8
15	0.79	1.040	-0.43	0.997	3.8
10	0.52	1.065	-0.69	1.019	6.1
7.5	0.39	1.082	-0.86	1.033	7.6
5	0.26	1.116	-1.17	1.059	10.4

Table A.2: Calculation by Perkins and Hage Method

A.3. DATCOM METHOD (Reference A.3)

A.3.1 DESCRIPTION OF METHOD

This method takes into account the effect of the image trailing vortex, of the image bound vortex and of the wing flap. The change in wing-body angle of attack at a constant lift coefficient due to ground effect with respect to the out of ground effect lift curve is given by:

$$(\Delta\alpha)_q = -\left\{\left[\frac{9.12}{AR} + 7.16\left(\frac{c_r}{b}\right)\right](C_{L_f})_{WB}\, x\right\} - \left[\frac{AR}{2\,(C_{L_\alpha})_{WB}}\left(\frac{c_r}{b}\right)\left(\frac{L}{L_o} - 1\right)(C_{L_f})_{WB}\, r\right] - \left[\frac{(\delta_{f/50})^2}{(C_{L_\alpha})_{WB}}\left(\Delta\,(\Delta C_L)_{flap}\right)\right] \text{(per deg)} \quad \text{(A.10)}$$

where:

$(C_{L_f})_{WB}$	is the wing-body lift coefficient including flap effects, out of ground effect.
x	accounts for the effect on lift due to the image trailing vortex and is obtained from Figure A.3.
$(C_{L_\alpha})_{WB}$	is the wing-body lift-curve slope, per degree out of ground effect.
$\frac{L}{L_o} - 1$	accounts for the effects on lift due to the image bound vortex, obtained from Figure A.4.
r	accounts for the effect of finite span, is obtained from Figure A.5.
$\Delta\,(\Delta C_L)_{flap}$	is an empirical factor to account for the effect of flaps and is obtained from Figure A.6.

A.3.2 HAND CALCULATION

For Airplane A (See Appendix C) the following flight condition was computed:

$$\delta_f = 38 \text{ deg}$$

For the sake of simplicity, H (Height of quarter chord point of wing mac above ground), $h_{c_r/4}$ (height of quarter chord point of wing root chord above ground and h (average height of quarter chord point at 75% of wing span and of root chord) are assumed to have the same (variable) value.

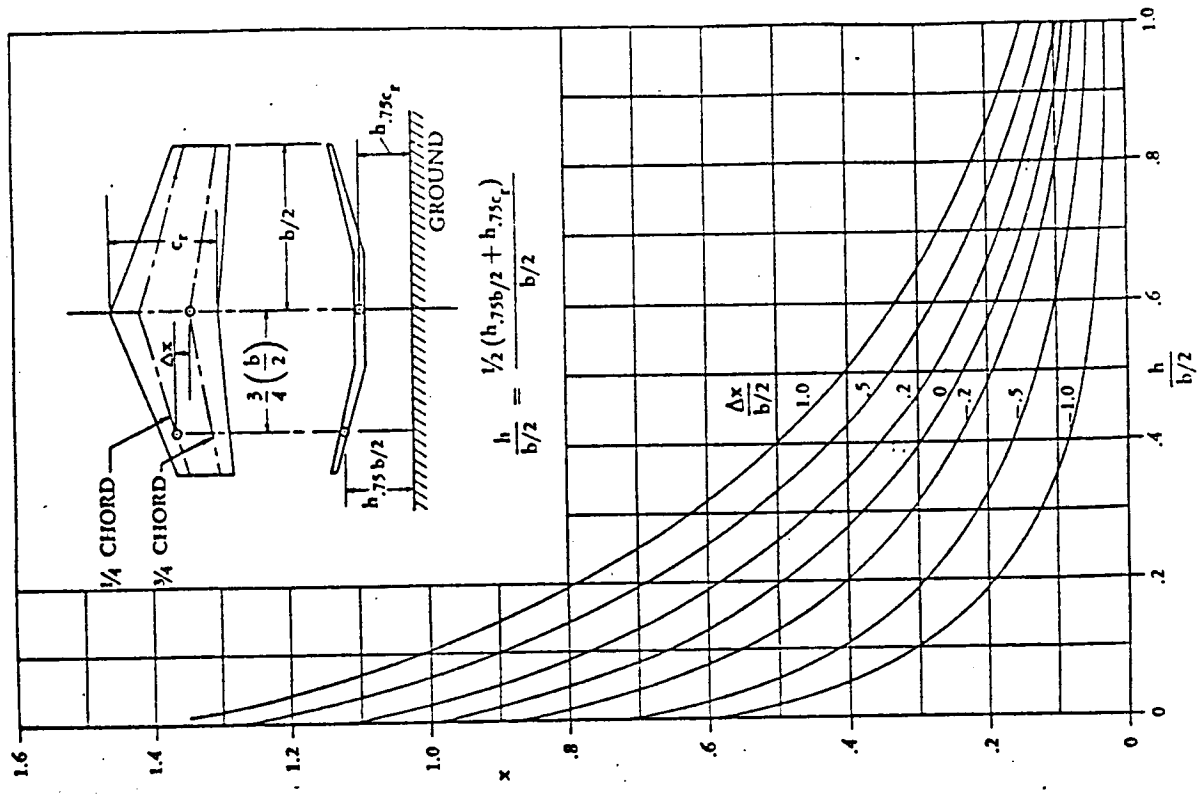

Figure A.3: Effect of Trailing Vortex on Lift in Ground Effect

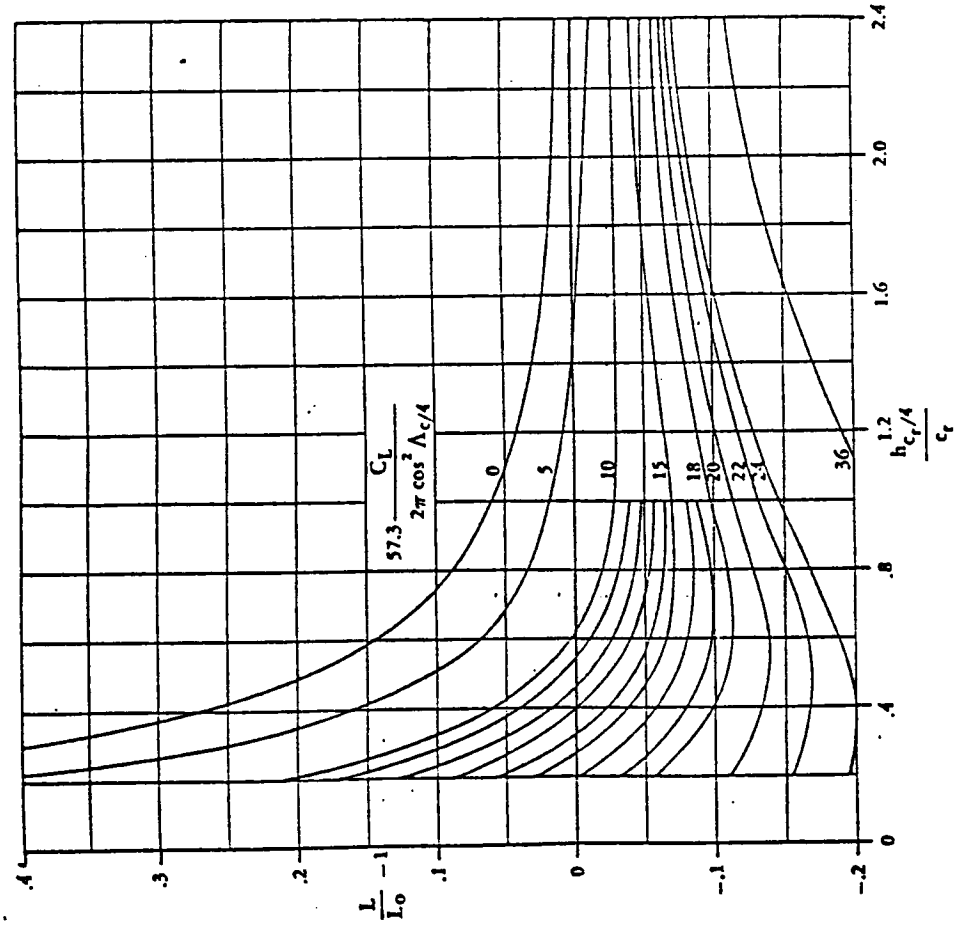

Figure A.4: Effect of Bound Vortex on Lift in Ground Effect

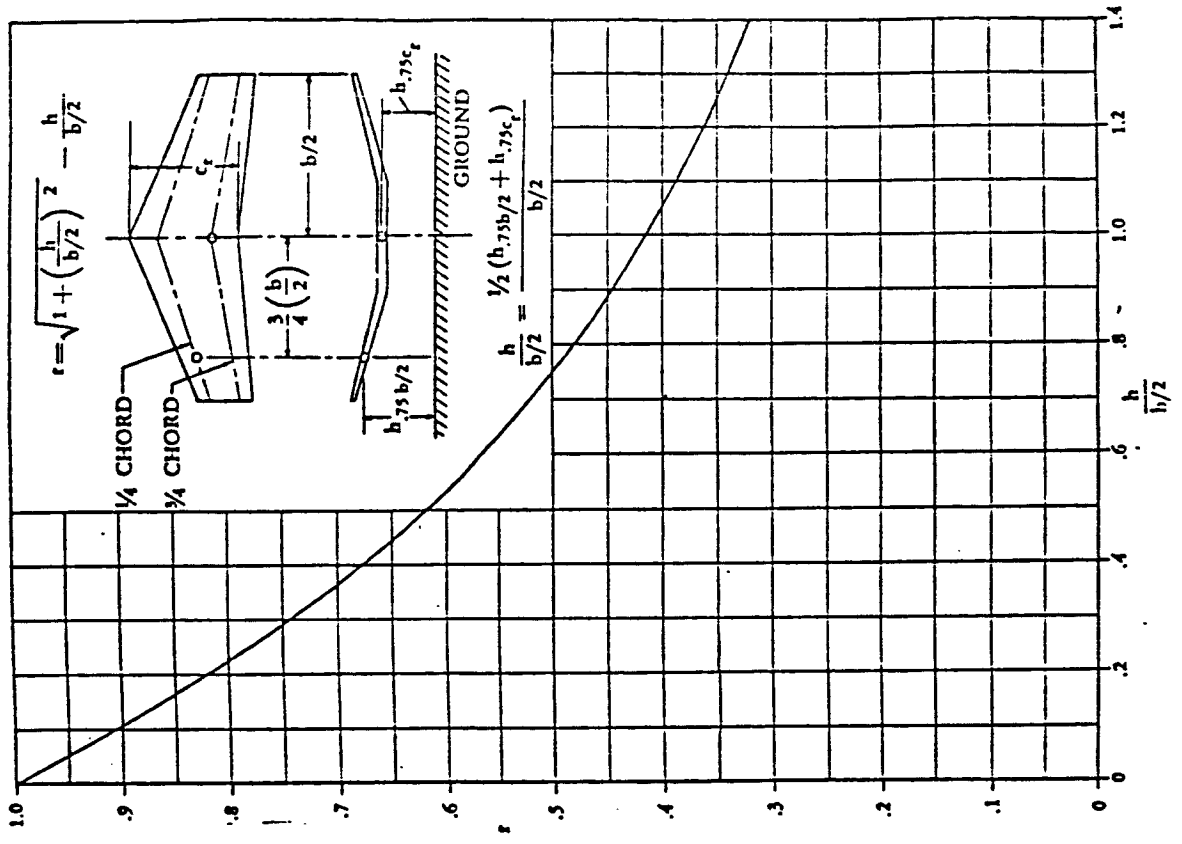

Figure A.5: Effect of Finite Span on Lift in Ground Effect

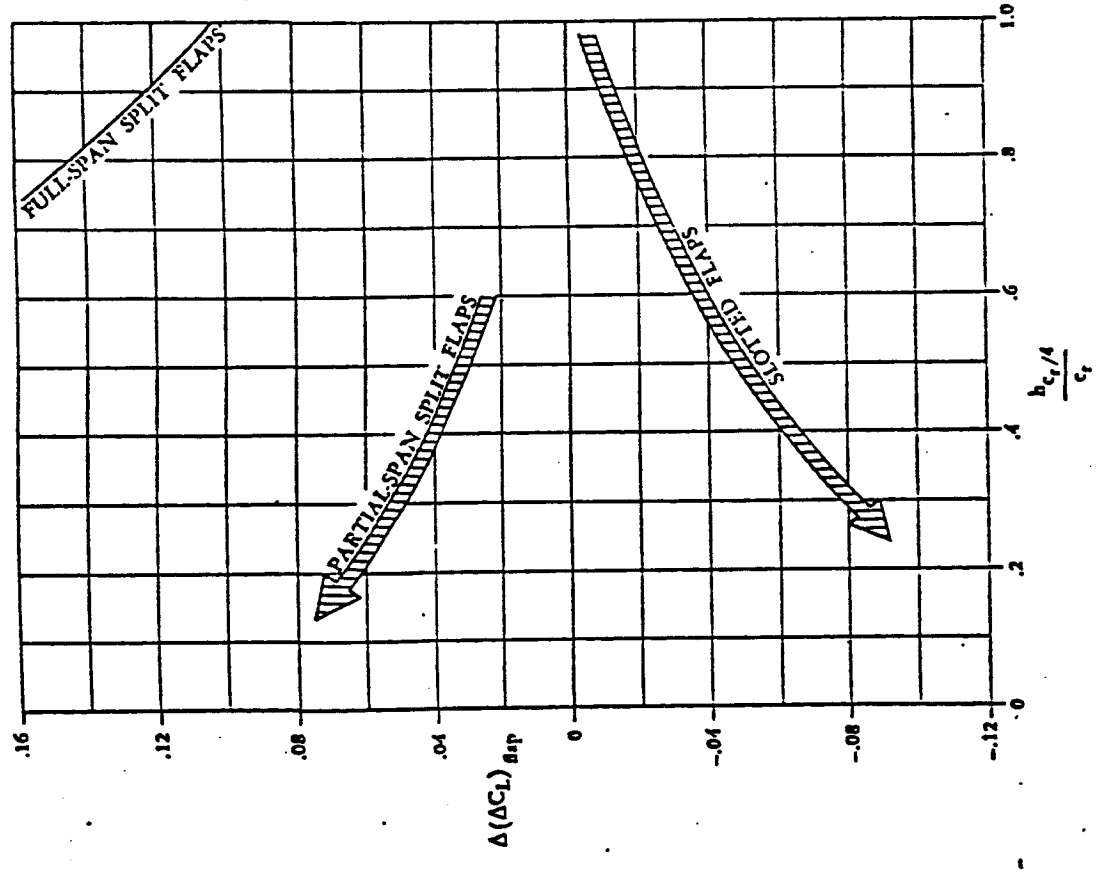

Figure A.6: Effect of Flaps on Lift in Ground Effect

Table A.3 shows the calculations.

Height (ft)	h/c_r	$h/b/2$	x	$\frac{L}{L_o} - 1$	r	$\Delta(\Delta C_L)_f$	$\Delta \alpha_g$	C_L	ΔC_L %
25	2.77	1.31	--	--	--	--	--	0.96	0
20	2.22	1.05	0.08	-0.06	0.40	0	0.5	0.92	-4.2
15	1.66	0.79	0.14	-0.06	0.48	0	-0.22	0.941	-2.0
10	1.11	0.52	0.25	-0.04	0.61	0	-0.60	1.011	5.3
5	0.55	0.26	0.49	+0.03	0.77	-0.045	-1.72	1.106	15.2
3	0.33	0.16	0.64	+0.145	0.86	-0.075	-2.98	1.213	26.4

Table A.3: Calculation of Datcom Method.

A.4. TORENBEEK METHOD (Reference A.4)

A.4.1 DESCRIPTION OF METHOD

A description of this method is given in Chapter 4.

A.4.2 HAND CALCULATION

A hand calculation was done for Airplane A (See Appendix D) for the following conditions:

$$C_{L_{oge}} = 0.96$$

$$C_{flap} = 2.326 \text{ ft.}$$

$$\delta_f = 38 \text{ deg}$$

Calculations are given in Table A.4.

Height ft	$2h_{eff}/b$	h/c_g	β	σ	C_L	ΔC_L %
45	2.32	6.53	0.206	0.0088	0.960	0.03
40	2.06	5.80	0.230	0.0133	0.961	0.11
35	1.80	5.08	0.259	0.0203	0.962	0.24
30	1.54	4.35	0.296	0.0316	0.964	0.46
25	1.27	3.63	0.346	0.0508	0.968	0.84
20	1.01	2.90	0.411	0.0822	0.974	1.48
15	0.75	2.18	0.500	0.1369	0.985	2.57
10	0.49	1.45	0.624	0.2384	1.003	4.51
5	0.22	0.73	0.804	0.4606	1.046	8.92
3	0.12	0.44	0.887	0.6147	1.094	13.94

Table A.4: Calculation of Torenbeek Method.

A.5 CONCLUSIONS

Figure A.7 shows the results of the calculations in this appendix. The general trend for all four methods is the same although the datcom method shows a rather large deviation from the other three. Also the datcom method is the most complicated method, it involves the use of four graphs. The simplest method is the Corning method, as it only involves two formulas. Next comes the Perkins and Hage Method, this involves the use of one graph. Hard data on ground effect for general aviation are rare. Since the method of Torenbeek is based on a sound theoretical principle (an image vortex system) it was decided to use this method.

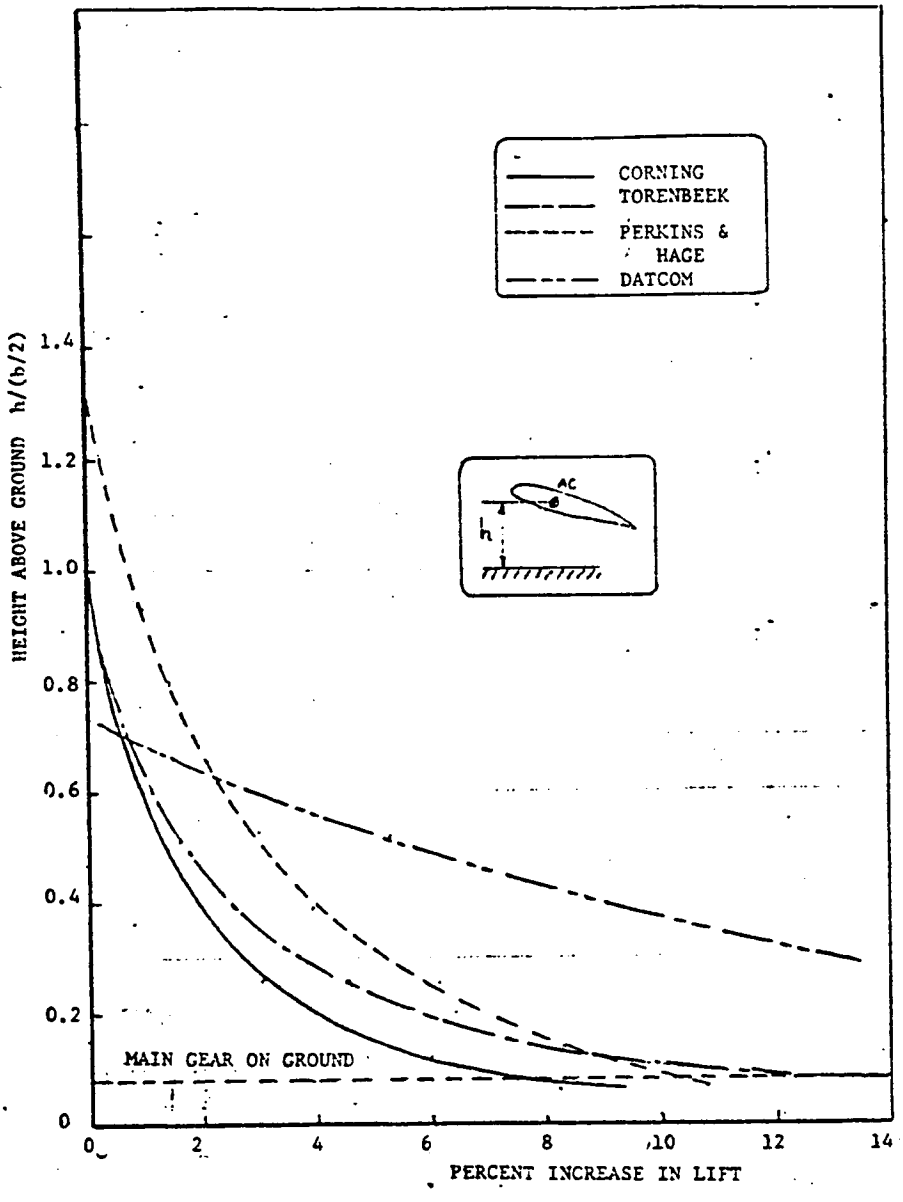

Figure A.7: Comparison of Ground Effect Methods

A.6 REFERENCES

A.1. Corning, G. — Supersonic and Subsonic Airplane Design, published by the Author, 1953.

A.2 Perkins, C.D. Hage, R.E. — Airplane Performance, Stability and Control, New York, John Wiley & Sons, 1949.

A.3. Hoak, D.E. Ellison, D.E. — USAF Stability and Control Datcom, Air Force Flight Dynamics Laboratory, Wright Patterson Air Force Base, Ohio.

A.4. Torenbeek, E. — Synthesis of Subsonic Airplane Design, Delft University Press, Delft, The Netherlands 1976.

APPENDIX B

FUNCTION RDP - A FUNCTION SUB-PROGRAM FOR INTERPOLATING CURVES AND GRAPHS

B.1 INTRODUCTION

Function RDP was written to provide a program which would interpolate along curves, between curves, and between graphs for arbitrary curves and graphs. RDP requires the input of a number of points along the curves; the points are used in conjunction with the Lagrangian interpolating polynomial to interpolate along the curves. RDP interpolates linearly between curves and graphs. If Lagrangian interpolation is needed in interpolating between curves and graphs, RDP can be called more than once, using only the Lagrangian part.

RDP can be used for any number of curves and graphs; from one curve on one graph to "n" curves per graph and "m" graphs.

RDP was checked out quite extensively. The initial checks and those done when RDP was called in a subroutine indicate that RDP works quite well.

B.2 DESCRIPTION OF THE PROGRAM AND LISTING

RDP is a Function, called in the form:

B = RDP (U, V, W, JK, IJ, KL, LM. UU, VV, WW, DD)

where:

U is the numerical value of graph parameter

V is the numerical value of curve parameter

W is the numerical value of X-coordinate parameter

* JK is the number of graphs

IJ is the number of curves per graph

KL is the number of data points (X,Y pairs) input per curve

LM is the number of rows in the DD array

UU is the array of actual graph parameters

VV is the array of actual curve parameters

WW is the array of X-coordinates at which Y-values were taken

DD is the array of Y-values in the form:

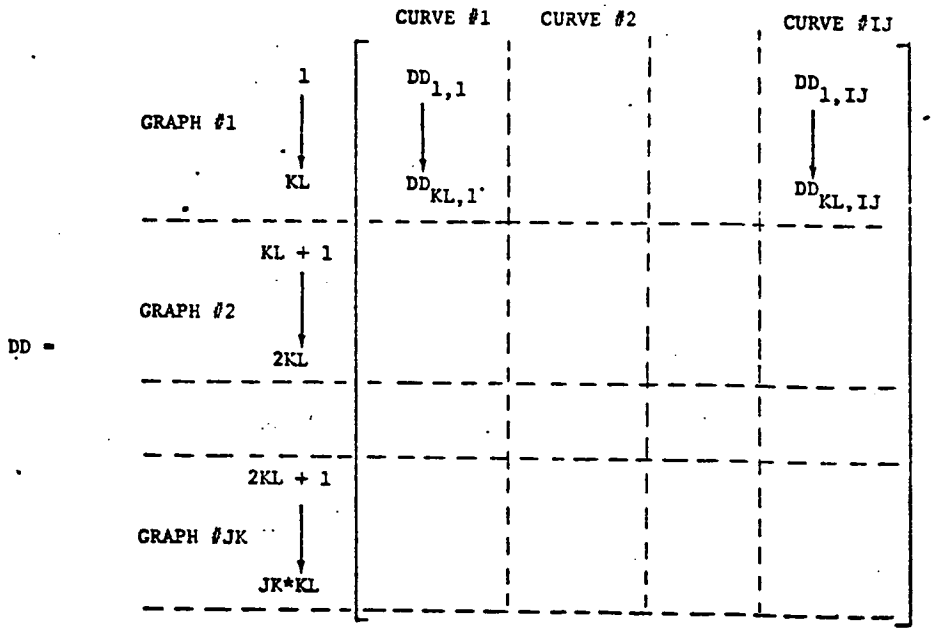

---

* NOTE: These are listed in the calling statement as numbers.

Example: B = RDP (U, V, W, 1, 1, 4, 4, UU, VV, WW)

where: JK = IJ = 1

KL = LM = 4

The other variables are initialized by data statements in the main program.

APPENDIX C

DATA FOR TEST-AIRPLANES

This Appendix presents data for a variety of airplanes that were used for checking the subroutines discussed in the foregoing chapters. The example airplanes range from a small single engine high-wing propeller-driven trainer airplane to a twin jet-engine business airplane. The data were assembled from a variety of sources. Also included in this Appendix are three-views of the aircraft considered.

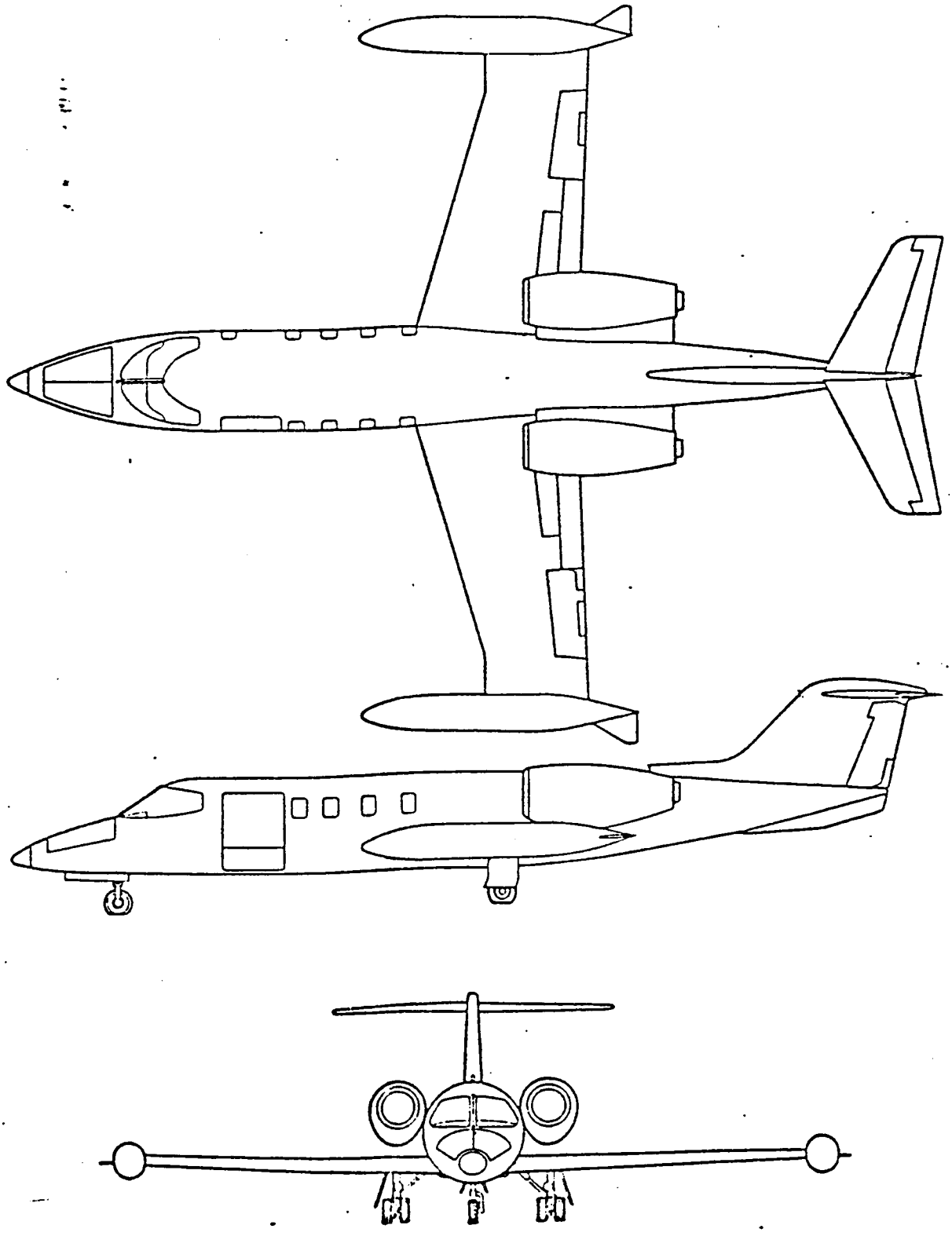

Figure C.1: Threeview of Airplane A

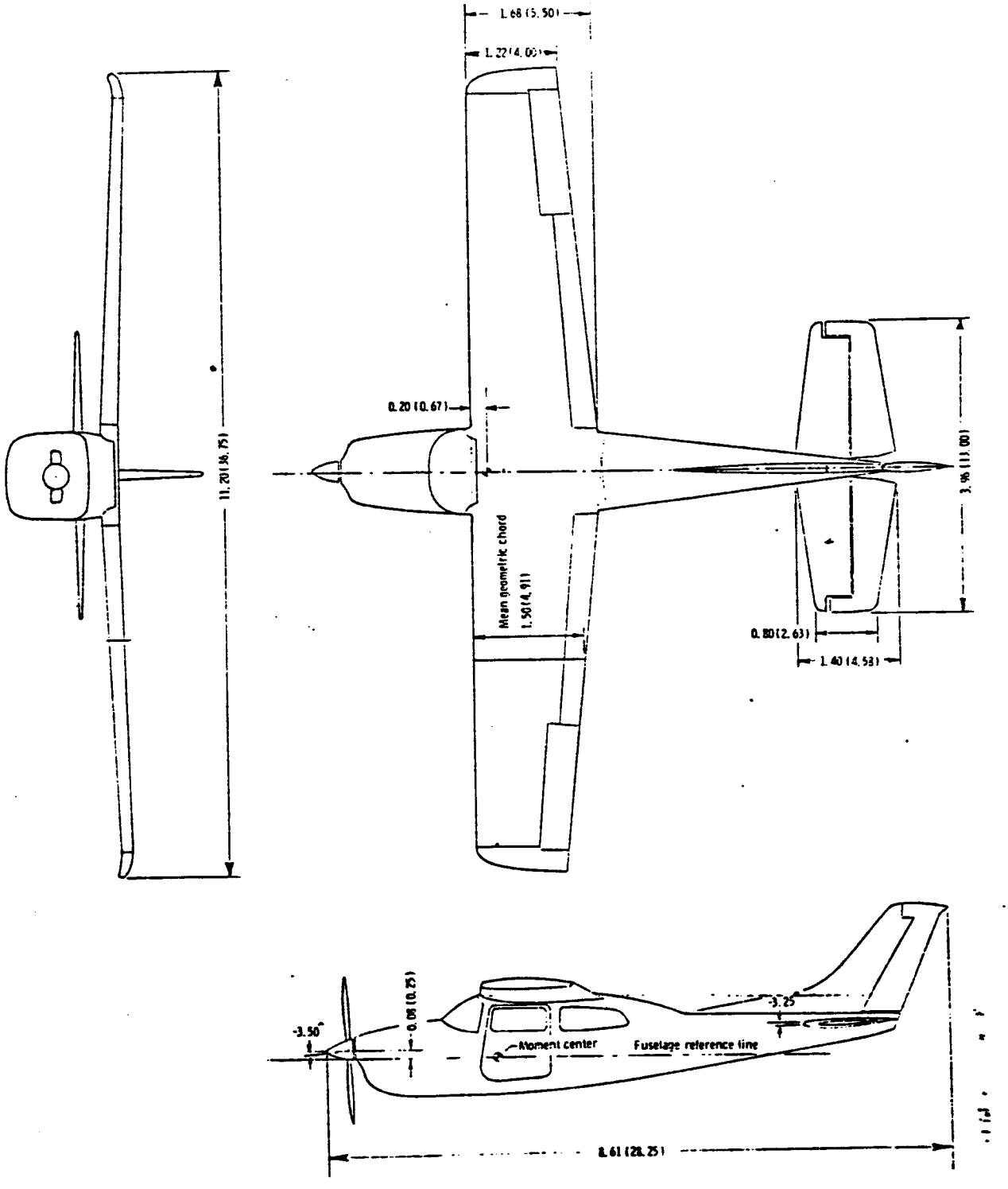

Figure C.2: Threeview of Airplane B

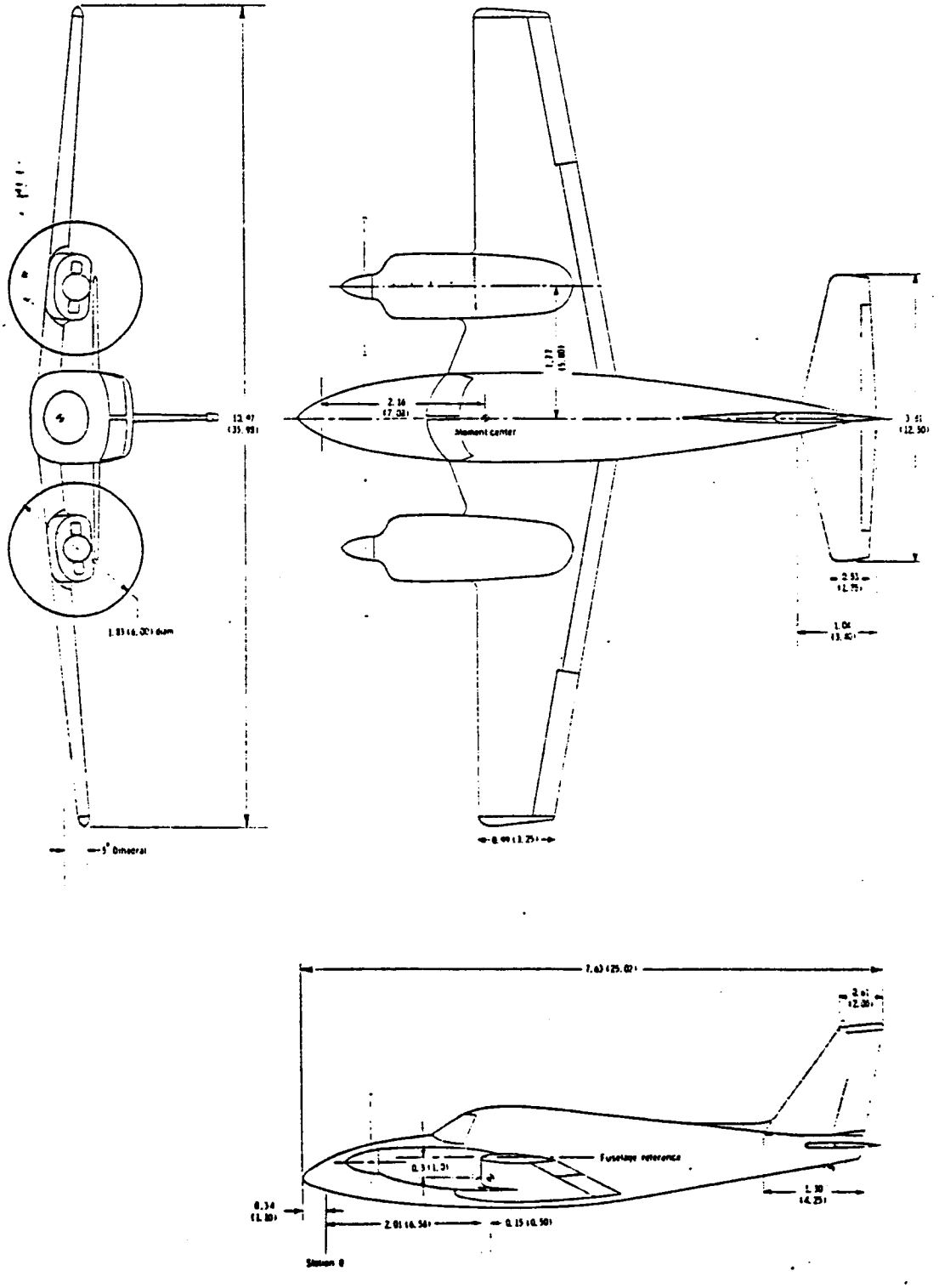

Figure C.3: Threeview of Airplane C

TABLE C.1. AIRPLANE DATA

WING	A	B	C	D	Dimension
AR_w	5.74	7.72	7.27	5.08	
b_w	38.13	36.75	35.98	26.25	ft
$C_{\ell_{\alpha_w}}$	6.131	5.443	5.44	6.709	rad^{-1}
$\bar{c}_w$	6.896	4.91	4.96	5.4	ft
c_τ		5.58	6.0		ft
c_t		4	3.32		ft
$(c_\tau)_{C.L.}$	9.02	5.81	6.39	7.06	ft
i_w		1.5	2		deg
$\ell_{\bar{c}/4_w}$		8.66	9.13	9.37	ft
S_w	253.3	175	178	135.62	ft^2
Z_w	1.61	-2.9	-.02	4.44	ft
α_{o_w}	-1	-1.8	-3.1		deg
Γ_w	2.5		5	-6.4	deg
$\Lambda_{\bar{c}/4_w}$	13	-3	-2.5	15.5	deg
λ_w	.564	.727	.513	.465	

HOR. TAIL	A	B	C	D	Dimension
AR_H	4	3.61	4.8	4.64	
b_H	14.7	13	12.5	12.99	ft
$C_{\ell_{\alpha_H}}$	6.303	6.254	6.25	6.245	rad^{-1}

TABLE C.1. AIRPLANE DATA

HOR. TAIL (Cont'd)	A	B	C	D	Dimension
$\bar{c}_H$	3.83	3.605	2.7	2.94	ft
$(c_{\tau_H})_{C.L.}$	5	4.58	3.4	3.88	ft
h_H	8.12		2.34		ft
ℓ'_H		14.42	13.76		ft
S_H	54	46.8	32.55	36.36	ft^2
$(t/c)_H$		.09			
$x_{H_{mac}}$	1.61			.95	ft
Z_H		-1.4			ft
α_{o_H}	0	0	0		deg
$\Lambda_{\bar{c}/4_w}$	25	0	8	14.33	deg
λ_H	.469	.574	.514	.442	
ϕ_{TE}		6			deg

VERT. TAIL	A	B	C	D	Dimension
AR_V	.782			1.32	
b_V	5.48			5.25	ft
$C_{\ell_{\alpha_V}}$	6.303			6.245	rad^{-1}
$\bar{c}_V$	7.17			4.34	ft

TABLE C.1. AIRPLANE DATA

VERT. TAIL (Cont'd)	A	B	C	D	Dimension
$(c_{\tau_V})_{C.L.}$	8.88			6.07	ft
ℓ_{HV}	1.07			3.96	ft
S_V	38.35			20.84	ft^2
$(t/c)_V$	.1				
Z_V	5.21			4.3	ft
$\Lambda_{\bar{c}/4_V}$	35.63			38.65	deg
λ_V	.577			.308	

CONTRL. SURF.	A	B	C	D	Dimension
$\delta_{A_{max}}$	18 up 18 down	22 up 14 down	18 up 14 down		deg
$\delta_{R_{max}}$	30 right 30 left	25 right 25 left	22 right 20 left		deg
$c_A/\bar{c}_w$	.22				
$c_R/\bar{c}_V$	.20				
η_{i_V}	0				
η_{o_V}	.778				
η_{i_A}	.544				
η_{o_A}	.792				

TABLE C.1. AIRPLANE DATA

CNTRL. SURF. (Cont'd).	A	B	C	D	Dimension
i_H	-8.1 to 1	-3.25	N.A.		deg
$\delta_{E_{min}}$	-15				deg
$\delta_{E_{max}}$	15				deg
$c_E/\bar{c}_H$	.262				
$c_{gap}/\bar{c}_H$		.005			
c_b/c_f		.054			
$c_h/\bar{c}_H$		.754			
η_{i_E}		0			
η_{o_E}		1			
$c_F/\bar{c}_w$	.268				

POWER PLANT	A	B	C	D	Dimension
b/0.3	N.A.	.0693	.0693	N.A.	
b/0.6	N.A.	.0820	.082	N.A.	
b/0.6	N.A.	.0682	.0682	N.A.	
D_p	N.A.	6.75	6.0		ft
i_T		-3.5	0		deg
N	2	1	2	1	

TABLE C.1. AIRPLANE DATA

POWER PLANT (Cont'd)	A	B	C	D	Dimension
N_b	N.A.	2	2	N.A.	
y_T		0	5.61		ft
Z_T		-.25	-.869		ft
$\beta_{.75}$		20	21.5		deg
X'_p		7.68	6.0		ft
x_{nac}		0	2.6		ft
X_p			5.26		
T			965.0		

FUSELAGE	A	B	C	D	Dimension
ℓ_B	46.19	26.11	24.16	30.44	ft
D_f	5.1	4.7	4.08	5.56	ft
h_c	5.1	4.7	4.08		ft
w_c	5.1	4.7	4.08		ft
ℓ_n	10.02		9.13		ft
b_c			4		

TABLE C.1. AIRPLANE DATA

MISCELLANEOUS	A	B	C	D	Dimension
W_g	17,000	3100	3600		lbs
Z_s			-.8		ft
Z_{HT}			-1.67		
C_{L_α}	5.114				rad^{-1}
$C_{L_{max}}$	1.35				

APPENDIX D DERIVATION OF CORRECTION FOR THE POLHAMUS FORMULA

The results of a comparison between the lift-curve slope as calculated with the Polhamus Formula (11.2.1) and the Lifting Surface Method is shown in Figure D1. To find an approximation for the error, the graph is split up into two parts, one for aspect ratio lower than 4 and one for aspect ratios higher than 4.

For aspect ratios lower than 4 a linear curve fit was applied with the following result:

$$\text{Error} = (1.87 - .42399 \quad \Lambda_{LE})\ AR \sim \% \qquad \text{where } \Lambda_{LE} \text{ in rad} \tag{D1}$$

For aspect ratios greater than 4 also a linear curve fit was applied, yielding:

$$\text{Error} = (8.2 - 2.30\ \Lambda_{LE}) - (.22 - .153\ \Lambda_{LE})\ AR \sim \% \tag{D2}$$

Using Formulas (D1) and (D2), the correction factor for the Polhamus Formula was found to be:

$$AR < 4 \quad K_{pol} = 1. + (1.87 - .42399 \quad \Lambda_{LE})\ AR/100 \tag{D3}$$

$$AR > 4 \quad K_{pol} = 1. + \{(8.2 - 2.30\Lambda_{LE}) - (.22 - .153\Lambda_{LE})AR\}/100 \tag{D4}$$

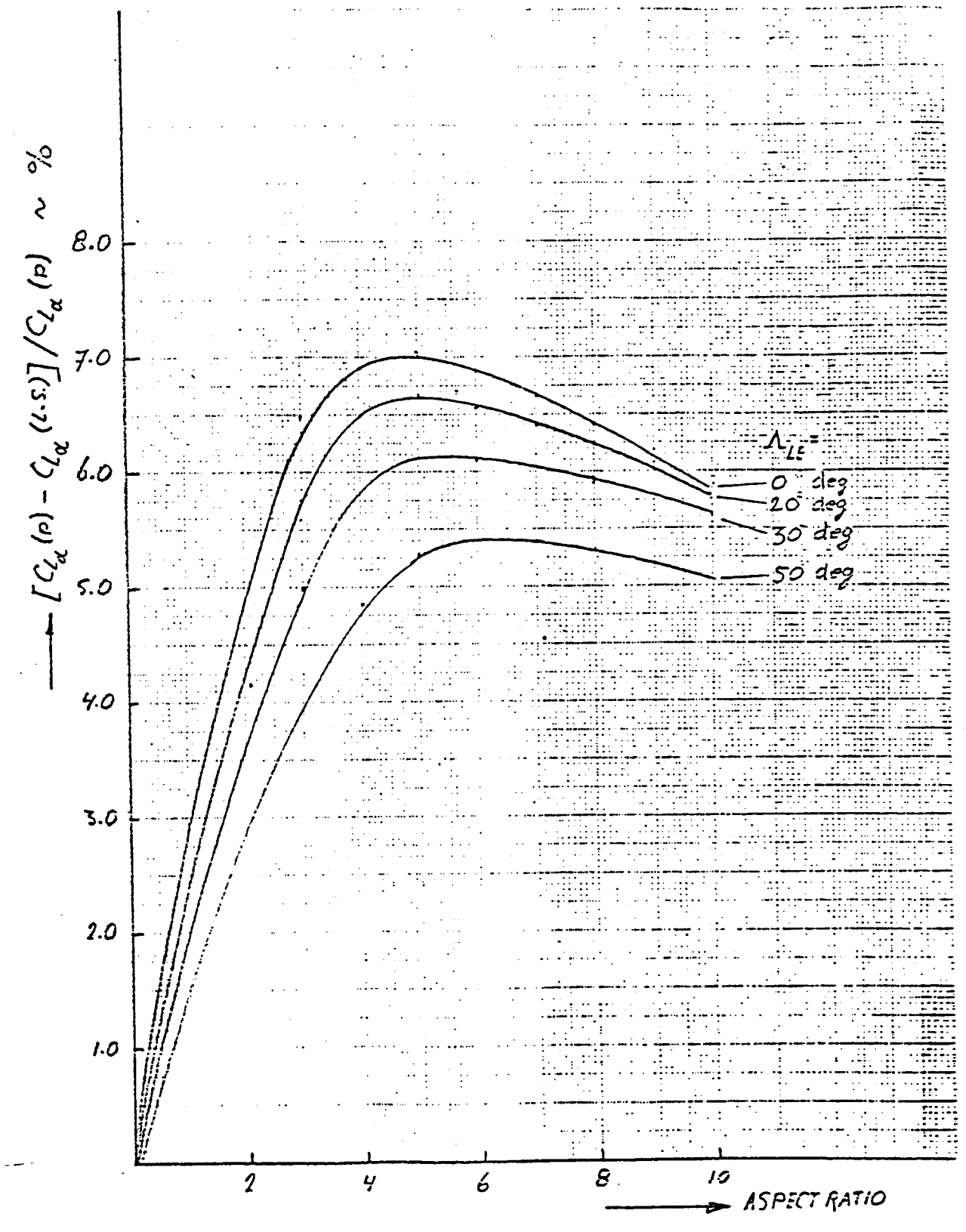

Figure D.1: Correction Factor for Liftcurve Slope.

SUMMARY

This report presents the documentation of a computer program for the analysis of the dynamic stability and control characteristics of airplanes. The program is specifically written for conventional configuration subsonic airplanes. This report describes in detail the theoretical methods used in the program and the implementation of the methods into a computer program ~~[and the results of testruns for a variety of aircraft.]~~ This report is not a user's manual for the program. The reader who wishes to utilize the program to analyze a specific design is referred to "User's Manual for KSTAB, A Computer Program to Analyze the Dynamic Stability Characteristics of Conventionally Configured Subsonic Airplanes," Kohlman Aviation Corporation, Lawrence, Kansas 66044, February 1982.

Summary page
delete sentence
pull
summary page
for CR page
Abstract
3rd sent
This report... [add and]
[and do a the results of
test ... aircraft]